
NICOLÒ ALVISI
A STICKY TALE
BIOMATERIAL COATINGS FROM MODULAR PROTEINS

Propositions

1. The superior biocompatibility and ease-of-use of adsorption-driven protein-based coatings makes synthetic coatings obsolete.
   (this thesis)

2. Molecular self-assembly is a deceivingly reliable principle in the bottom-up design of protein-based materials.
   (this thesis)

3. Copyright laws for scientific publications weaponize the protection of attribution while threatening derivative work and, therefore, scientific progress.

4. The rise of conspiratorial thought and anti-scientific movements is exacerbated by academia's subservience to industrial needs over laypeople's problems.

5. Following the precautionary principle, the use of social media should be severely limited in both professional and private contexts.

6. The meritocracy ideal is a mere justification of social and economic inequalities.

7. The institution of a Universal Basic Income is the only scientifically proven way to combat poverty.

Propositions belonging to the thesis, entitled

"A Sticky Tale - Biomaterial coatings from modular proteins"

Nicolò Alvisi
Wageningen, 24 February 2023

A STICKY TALE

BIOMATERIAL COATINGS FROM MODULAR PROTEINS

Nicolò Alvisi

Thesis committee

Promotor
Dr R.J. de Vries
Associate Professor, Physical Chemistry and Soft Matter
Wageningen University & Research

Co-promotor
Dr Ing. H.B. Albada
Associate Professor, Organic Chemistry
Wageningen University & Research

Other members
Prof. Dr A.H. Velders, Wageningen University & Research
Dr A. van Amerongen, Wageningen University & Research
Dr P. Zijlstra, Eindhoven University of Technology
Prof. Dr L. Hall, University of Cambridge, United Kingdom

This research was conducted under the auspices of VLAG Graduate School (Biobased, Biomolecular, Chemical, Food and Nutrition Sciences).

A Sticky Tale

Biomaterial coatings from modular proteins

Nicolò Alvisi

Thesis

submitted in fulfilment of the requirements for the degree of doctor
at Wageningen University,
by the authority of the Rector Magnificus,
Prof. Dr A.P.J. Mol,
in the presence of the
Thesis Committee appointed by the Academic Board
to be defended in public
on Friday 24 February 2023
at 11 a.m. in the Omnia Auditorium.

Nicolò Alvisi
A Sticky Tale - Biomaterial coatings from modular proteins
208 pages.

PhD thesis, Wageningen University, Wageningen, The Netherlands (2023)
With references, with summary in English

ISBN: 978-94-6447-483-1
DOI: https://doi.org/10.18174/580537

To my family.

In loving memory of Gino Strada and Piero Angela,
models of empathy and curiosity.

“We live in capitalism. Its power seems inescapable.
So did the divine right of kings.”
Ursula K. Le Guin

Contents

CHAPTER 1

Introduction

In this thesis, we explore the potential of polypeptide-based coatings as molecular tools for the design of novel biomaterial surfaces, focusing on biosensing applications. This chapter serves as a broad introduction to surface biofunctionalization strategies for biomaterials, focusing on the currently available techniques. We also discuss the versatility of genetically engineered protein materials, with an eye on the advantages of protein polymers compared to their synthetic counterparts. We then highlight the requirements of our strategy, describing our “bottom-up” approach for the synthesis of modular and multifunctional protein coatings. We conclude this chapter giving an outline of the thesis.

A long hike surrounded by nature is one of the most effective ways to combat stress.[1] Aside from the obvious benefits of physical activity, the fascination created by natural settings on the human mind is a known psychological factor which impacts our mental health.[2] A pleasant and relaxing experience can, however, be brought to a quick but temporary halt upon coming into contact with a specimen of *Urtica dioica*, the stinging nettle. This inconvenience should not distract us from the wonders of nature. On the contrary, it gives our minds enough time to briefly dwell on the fascinating mechanism that caused the unpleasant itch. The stinging hairs of the nettle, also known as secretory trichomes, have fascinated scientists for centuries. It should not surprise us that Robert Hooke outlined the basic morphology of stinging hairs as early as 1665 in one of the first books about microscopy.[3] These highly specialized defensive structures are composed of a multicellular pedestal supporting a long and hollow stinging cell. When brought in contact with the skin of a carefree hiker, the trichomes act as hypodermic needles, injecting inflammatory compounds such as histamine, acetylcholine, and formic acid.[4] The specific mechanical requirements for the creation of a microscopic syringe are achieved thanks to the addition of silica, calcium carbonate, and calcium phosphate to the cell wall of the stinging cell, in a process known as biomineralization (Figure 1-1a).[5] The relatively simple morphology of the stinging hair is in stark contrast with the complex geometry and patterning of the biomineral distribution. The small and sharp tip must be hard and brittle to easily break off, while the shaft is stiff and sturdy. On the contrary, the base is flexible and thin, allowing for its compression and the subsequent expulsion of the irritating liquid.[6] The layering and the distinctive deposition of silica and calcium minerals responsible for these features enable the synthesis of an array of exquisite defensive structures (Figure 1-1b).[7] Although the exact mechanisms involved in trichome mineralization are still not completely understood, this remarkable example of microengineering reminds us that living organisms can precisely control and interact with minerals around them to create a plethora of biomaterials. We gently rub our sore skin and quickly recover from the pain, maybe in a less relaxed mood but surely fascinated by the precision and resourcefulness of this minute weaponry. How can we design materials capable of such microscopic deeds?

Let us continue, then, with our hike.

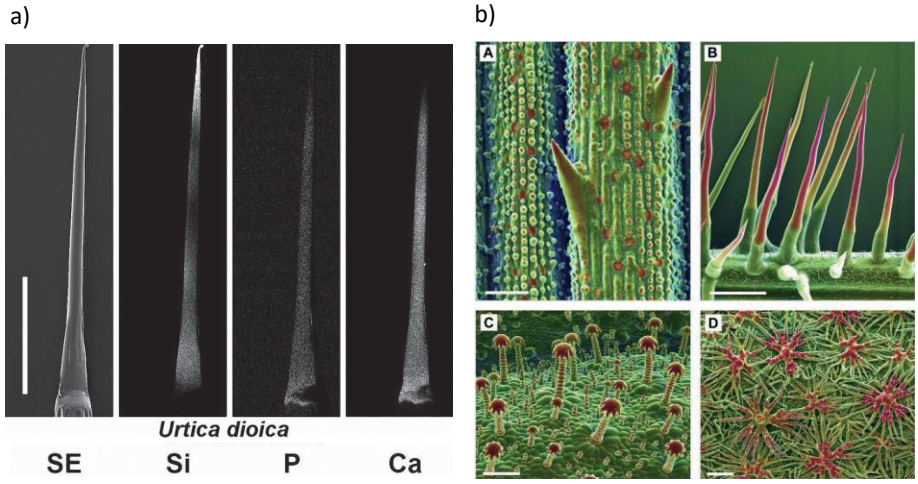

Figure 1-1. **(a)** Energy-dispersive X-ray element mapping micrograph of full-length stinging hair of *Urtica dioica*. The tip of the hair is heavily mineralized with silica (Si), phosphorus (P) is present only in traces, while calcium (Ca) is present in all parts except regions with high Si concentrations. Scale bar = 500 µm. Adapted with permission from Mustafa *et al*.[6] **(b)** Biomineralized plant surface structures. Combined topographic and compositional contrast scanning electron microscopy images showing mineralized structures in color. **(A)** Abrasive epidermis inclusions in the grass *Spartina pectinata.* **(B)** Stinging hairs of stinging nettle *Urtica mairei*. **(C)** Barbed trichomes of the electric shock plant *Blumenbachia insignis*. **(D)** Dense cover of stiff, branched trichomes on the mustard *Phyllolepidum cyclocarpum*. Adapted from Ensikat *et al*.[7]

In this thesis, we drew inspiration from two aspects of nature for the design of a novel protein-based coating. Firstly, we harnessed surface-binding peptides and proteins to strategically place molecules of interest on biomaterial surfaces. Secondly, we used proteins as molecular building blocks to impart more functionalities to our biomaterial coating. In this chapter, we will discuss how we applied these inspirations in our final designs. In the following section, we will briefly introduce biomaterials and how surface functionalization is a requirement for next-generation biomaterials. We will then focus on polypeptides and the design of protein-based coatings. Finally, we will outline our strategy for the synthesis of a protein-based, multifunctional, and modular coating for biosensing applications.

1.1. Surface functionalization is the keystone of biomaterials

Nature is an unmatched source of inspiration for engineers and scientists: plant leaves, gecko toes, butterfly wings, shark skin, spider silk, and moth antennae are but a fraction of the most studied designs.[8] Few scientific fields have been influenced by nature as much as biomaterials science. A biomaterial is defined as any nonviable, organic or inorganic material intended to interact with biological systems. This definition is very broad, spanning from implants and artificial organs to drug-delivery platforms and biosensors. Historically, naturally derived materials such as wood were adopted for the creation of prosthetic devices, usually as structural replacements of damaged tissues.[9] Since the beginning of the 20th century, synthetic materials such as metal alloys, polymers, and ceramics have started to replace their natural counterparts, providing higher stability and reliability.[9] These materials are appreciated mostly for their mechanical properties, considering that they largely perform mechanical functions. Bioinertness, described as the lack of toxic leachable compounds, is the only mechanism used to avoid biological rejection.[10] Although prosthetics continue to improve and save countless lives, their rudimentary level of structural complexity often results in stochastic and unplanned responses from the host. The next generation of biomaterials should therefore strive to combine desirable macroscopic properties with higher precision and control at the microscopic level.

Since the 1970s, the advancements in molecular biology, medical engineering, and proteomics have provided us with the knowledge and the tools necessary for the improvement of biomaterials. Firstly, the chemical composition of biomaterials has become as relevant as the interface between solid biomaterials and biological systems. Secondly, the appreciation of the complexity of biological systems revealed the need to design multifunctional and dynamic materials, adopting a “bottom-up” approach inspired by natural functionalities. The incorporation of bioactive components on the surface of new materials has greatly increased the number of possible applications, resulting in the expansion from implantable devices to therapeutic and diagnostic tools. Bioinspired information-rich materials could tackle new needs: low-cost and early diagnosis of human diseases, better *in vitro* screening of drug toxicity, food and water contamination, and controlled growth of stem cells. The goal of surface engineering has shifted from “bioinertness” to “biocompatibility”: instead of simply avoiding negative

interactions, biomaterials should actively participate and improve the interplay between living elements and man-made components.

The modification of solid surfaces with biocompatible functionalities has greatly benefited both *in vivo* and *in vitro* applications. In many instances, these functionalities have become the gold standard in laboratory and diagnostic practice. For example, cell-adhesive oligopeptides such as arginine-glycine-aspartic acid (RGD) are used for surface modification in tissue engineering and regenerative medicine, while poly(ethylene glycol) (PEG) is commonly immobilized on solid surfaces to avoid the nonspecific adsorption of proteins and cells (anti-fouling).[11–13] Antimicrobial peptides are being evaluated as coating agents for medical devices, and antibodies have monopolized immune-based assay systems.[14,15] However, tethering bioactive molecules onto solid surfaces introduces two challenges: the coating must be able to deal with unwanted biofouling, and biomolecules must be correctly and integrally presented to maintain their desired function.

Unwanted biofouling is a well-recognized issue affecting both *in vivo* and *in vitro* applications. In a living organism, all physiological processes are governed by specific molecular interactions between ligands and receptors. A solid surface lacking any topological cue is recognized as a foreign body since it allows for the adsorption of many different proteins, in native form or denatured.[16] Thus, preventing biofouling is as critical as decorating surfaces with the appropriate signaling moieties. Biological media can also compromise the functionality of non-implantable biomaterials. In biosensing, for example, biofouling is responsible for high background noise and device contamination, ultimately causing a reduction in the sensitivity and in the lifespan of the biosensor.[17–19] In this case, antifouling surfaces are necessary to guarantee the correct and prolonged functionality of the biosensing device. To address this issue, various types of antifouling substrates have been developed in recent years. Aside from the aforementioned PEG, other hydrophilic materials have been explored, such as zwitterionic polymers, polysaccharides, and peptides.[20–23] In general, these antifouling materials act by creating a densely packed hydration layer at the interface.[13] In addition, they can be tailored as molecular spacers to tether additional functionalities on substrate surfaces.[24,25]

The development of suitable immobilization techniques represents the second major hurdle in biomaterial synthesis. An ideal immobilization technique should warrant the correct presentation of the desired biomolecules without interfering with their native structure.[26,27] Random orientation and

denaturation of displayed antibodies, for example, can strongly reduce the sensitivity of immunosensors.[28] Furthermore, aqueous-based chemistry is preferable, since most biomolecules do not tolerate the presence of organic solvents.[26,29] Additionally, the availability of reactive groups on the solid surface has to be considered when choosing an appropriate strategy. Overall, these requirements reduce the number of applicable strategies, while simultaneously guaranteeing and enhancing the biocompatibility of a biomaterial.

Surface biofunctionalization strategies can be broadly divided into two categories: non-covalent immobilization based on physical adsorption, and covalent immobilization based on the formation of chemical bonds. Physical adsorption is a simple, mild, and quick method, resulting from the incubation of the substrate material with a solution of the biomolecules of interest. The biomolecules can be attached directly thanks to multiple weak interactions (van der Waals interactions, hydrophobic interactions, etc.).[30] However, the direct non-specific adsorption of biomolecules can result in their unfolding or misorientation. In the case of antibody immobilization for immunoassays, for example, the majority of adsorbed antibodies is functionally inactivated.[31] Moreover, the stability of the resulting coating is generally not comparable to covalent immobilization.

In covalent bonding, the biomolecules of interest are chemically bound to the biomaterial surface. As previously mentioned, covalent bonding results in irreversible coatings, with a higher control on the retention, orientation, and distribution of bioactive molecules. Unfortunately, the process usually consists of multiple steps, where occasional harsh conditions and toxic compounds can drastically reduce the biocompatibility of the resulting coating.[26] In fact, if the material surface does not display any relevant functional groups (amines and carboxyl groups), chemical or physical treatments are necessary for surface activation.[32] Similarly to non-covalent strategies, the nonspecific covalent immobilization of certain biomolecules can result in the loss of bioactivity.[33] Furthermore, the procedures are usually too complex and expensive for bulk, low-cost applications. For these reasons, the development of simple, adsorption-based strategies has garnered continuous interest.

In both non-covalent and covalent approaches, the direct attachment of biomolecules to solid surfaces results in misfolding, misorientation, steric hindrance, and poor coverage, with obvious effects on the biocompatibility of the resulting biomaterial.[34] To overcome these problems, intermediate

molecules capable of binding both the solid surface and the biomolecule can provide a more flexible approach.[32] As mentioned earlier, antifouling spacers can additionally be used as linker molecules, providing a multifunctional molecular architecture capable of simultaneously tackling the two major hurdles of surface functionalization. To summarize, a combined technique featuring physically adsorbed antifouling linkers would favor the facile and oriented immobilization of biomolecules in mild reaction conditions.

1.2. Protein design, the benefits of nature's toolbox

Polypeptides are among the most well-studied and versatile biologically derived macromolecules. Proteins are polymeric materials synthesized inside every living cell, in a multi-step process where DNA is first converted into messenger RNA and ultimately into a precise string of amino acids. After having properly folded and assembled into a functional structure, these macromolecules participate and regulate all biological processes, including mechanical support, motion, enzymatic catalysis, storage, transport, immune mechanisms, and cell division and death.[35] Given their fundamental role, proteins display a wealth of diverse properties, making them the ideal building blocks for many biomaterials.

Over the past decades, protein engineering has enhanced the design of novel molecular architectures. In fact, protein-based materials offer many relevant features, making them an appealing alternative to synthetic polymers. For example, proteins can undergo conformational changes in response to external stimuli such as variations of pH, temperature, and ionic strength. Most importantly, polypeptides are capable of self-assembling into hierarchical and ordered structures ranging from nanocages to macroscopic three-dimensional gels.[36,37] These structures assemble in a predictable and orderly fashion, with clearly demarcated interfaces and surfaces. Furthermore, protein materials can be highly robust and resistant to both mechanical and chemical stresses (i.e., silks, keratin, and collagen).

In the design of surface functionalization strategies, protein materials present two major advantages compared to their synthetic counterparts: biocompatibility and tunability. The biocompatibility of biologically derived molecules is an obvious feature, especially when comparing synthetic polymers like PEG and peptide-based polymers. Firstly, synthetic polymers are known to activate immune responses.[38,39] In the case of PEG, a sizeable fraction of the human population already produces anti-PEG antibodies due to

previous exposure to the polymer.[40] Additionally, synthetic polymers do not degrade in the human body and the effects of their long-term accumulation are still unclear.[41–43] On the contrary, proteins are fully biodegradable and, unless they are derived from pathogenic organisms, highly biocompatible.[44]

Polypeptides are tunable in many aspects, from design to synthesis and functionality. While polydispersity, limited yields, and poorly controlled stoichiometry can severely limit the application of synthetic polymers, proteins can be designed and produced in a facile manner with a high degree of control over their size, sequence, and chemistry.[45,46] Furthermore, different protein sequences can be fused and combined for the creation of novel multidomain systems, in which each block theoretically preserves its ability to self-assemble and its molecular function.[47] The exquisite precision of protein engineering is

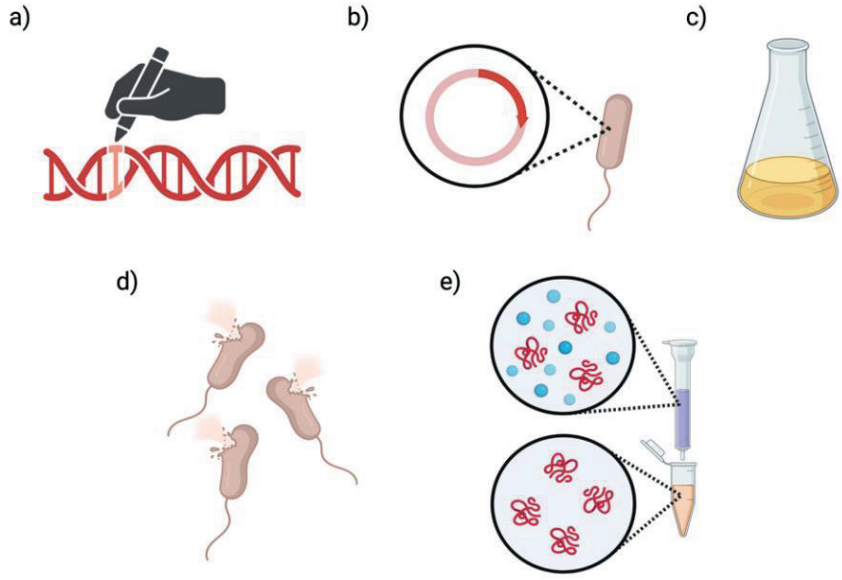

Figure 1-2. Schematic representation of the recombinant production of proteins. **(a)** New DNA sequences are identified in living organisms or designed *in silico*. **(b)** The gene of interest is assembled into a circular vector called plasmid and introduced into a suitable host such as *Escherichia coli*. **(c)** The bacterial host is grown in the appropriate medium; the host produces the protein of interest following the genetic instructions contained in the plasmid. **(d)** The chemical or physical lysis of the bacterial cells releases the expressed protein contained in the cell cytoplasm. **(e)** After the extraction, the protein is purified from the cell lysate with chromatographic techniques.

made possible by the advancements of genetic manipulation techniques and recombinant technology.

The blueprint of every protein design is encoded in a genetic sequence. Genes of interest can be identified in a living organism or rationally designed *in silico*, thanks to the recent improvements in the synthetic production of new DNA molecules (Figure 1-2a). Then, recombinant DNA technology provides the biotechnological tools for the correct assembly and replication of the genetic fragments. Restriction enzymes recognize and cut specific sites within the DNA molecule, while ligases "glue" compatible fragments into expression vectors. The most common expression vectors are circular molecules of DNA known as plasmids, which can be easily introduced into hosts organisms such as bacteria, fungi, and mammalian cells (Figure 1-2b). The host organism will then produce the designed protein following the genetic instructions contained in the expression vector (Figure 1-2c). Finally, the protein is extracted from the host organism via cell lysis and usually purified with chromatographic techniques (Figure 1-2d-e). Thanks to the skyrocketing success of biotechnology in the past 40 years, recombinant technology is a reliable method for the scalable production of newly designed proteins.[48]

Aside from their use as highly lucrative medical and pharmaceutical products, recombinant polypeptides have unsurprisingly found numerous applications in the synthesis of biomaterials.[49] Protein polymers such as elastin-like polypeptides, for example, have reached clinical trials as drug conjugates or as scaffolds for tissue engineering.[50] Furthermore, the vast majority of surface functionalization strategies relies on recombinant polypeptides, especially for *in vivo* applications.[32] However, as mentioned in Section 1.1, proteins are particularly sensitive to the harsh conditions sometimes necessary for their covalent immobilization. Their direct adsorption is also undesirable, often resulting in misfolding, unstable coatings, and loss of bioactivity. It is therefore clear that the main challenge of biofunctionalization still lies in the development of appropriate strategies to interface solid inorganic surfaces and bioactive molecules.

1.3. Coatings for solid surfaces: towards a protein-based molecular architecture

In the previous sections, we have outlined the relevance of surface functionalization for the design of new biomaterials. We have highlighted that adsorption-based immobilization methods are preferrable to covalent

immobilization methods, given the mild reaction conditions and the simplicity of the process. Furthermore, the adoption of antifouling linkers is a necessary step for the biocompatibility of the resulting coating. Finally, we have shown that proteins in general, and recombinant proteins in particular, can provide a biocompatible, highly tunable, and scalable alternative to synthetic polymers for the functionalization of biomaterial surfaces. We will now argue that multifunctional protein-based coatings can be developed for surface functionalization strategies.

To begin with, we must define the requirements for a biocompatible self-assembling polypeptide-based coating.

Firstly, an ideal surface functionalization strategy should allow for the immobilization of a wide variety of bioactive molecules (Figure 1-3a). Thus, a suitable molecular architecture for a surface coating should accommodate this need. In particular, the polypeptide coating should not negatively impact the functionality of the immobilized molecules, acting as an antifouling spacer between the solid substrate and the biomolecule.

Secondly, the polypeptide coating should correctly self-assemble on the solid surface, maintaining the expected orientation on the interface. The polypeptide should therefore feature a block with high affinity for the solid substrate, enabling directed assembly (Figure 1-3b).

Thirdly, surface functionalization with a polypeptide-based coating should be a simple and fast process, without pre-treatment of the solid substrate. This requirement includes a series of implications that heavily influences further design choices. The absence of surface pre-treatment implies that our polypeptide coating must rely on physical adsorption for its own immobilization. The coating should also be modular, so that surface-affine blocks can be easily replaced to adapt the polypeptide coating to various solid surfaces (Figure 1-3c). Additionally, biomolecules should be quickly and easily attached to the polypeptide, either in the bulk or on coated surfaces (Figure 1-3d).

Finally, the synthesis of the polypeptide should be scalable and sustainable within the current technical limitations. It must be possible to design the polypeptide with current biotechnological tools and to produce it within standard expression hosts.

The aim of this thesis is to develop a novel protein-based coating following the four requirements that we have previously listed. With the help of biotechnological tools, we aim for the design of a modular multifunctional

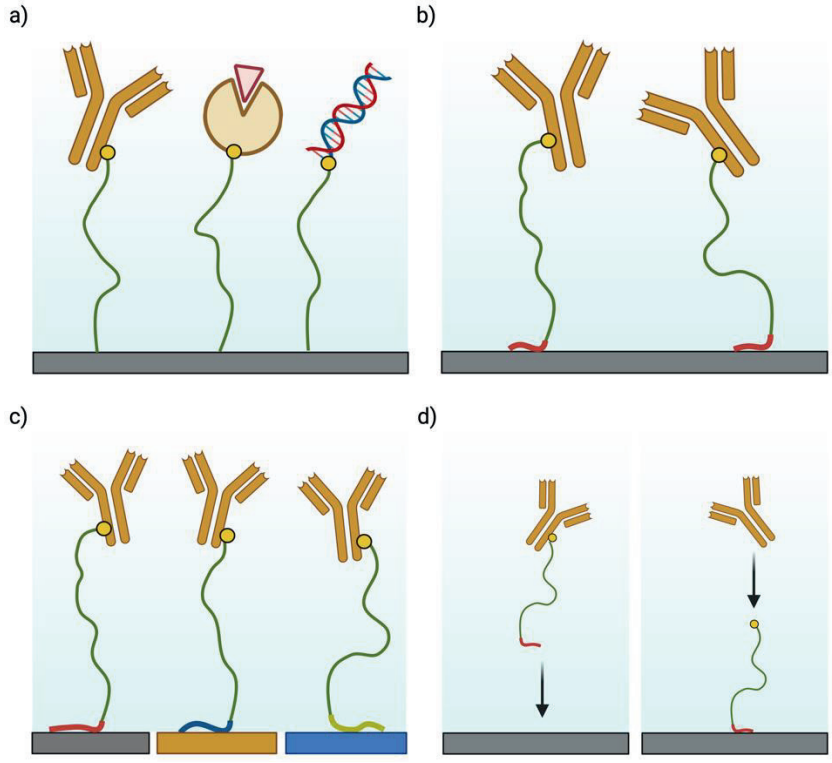

Figure 1-3. Requirements of a self-assembling polypeptide coating: **(a)** the coating should allow for the immobilization of a wide variety of bioactive molecules (i.e. antibodies, enzymes, nucleic acids), acting as antifouling spacer between the molecule and the solid surface; **(b)** a polypeptide block with high affinity for the solid surface should guarantee the correct and oriented assembly of the coating; **(c)** the coating should be based on physical adsorption, and surface-affine blocks should be easily replaceable to adapt the polypeptide for different solid surfaces; **(d)** the biomolecules of interest should easily attach to the polypeptide, either in bulk before adsorption or directly on the adsorbed coating.

coating that can physically adsorb to biomedically relevant solid surfaces. With a "bottom-up" approach, the combination of functional polypeptide blocks should allow us to develop an antifouling molecular architecture that can quickly and stably adsorb on solid surfaces in a controlled and oriented manner. In our designs, we will explore both naturally derived and *de novo* computationally designed protein blocks. For the non-covalent immobilization

of our protein coating, we will rely on a class of material-specific polypeptides called solid-binding peptides. We will also explore elastin-like polypeptides as biocompatible antifouling polymers. The addition of reactive amino acids should provide unique moieties for the conjugation of bioactive molecules of interest (antibodies, probes, DNA, cell-adhesive peptides, drugs). In conclusion, we hope to prove the feasibility of such concept design for biosensing applications, by conjugating a model antibody to our protein coating. The design can then later be adapted for different surfaces and tested both *in vitro* and *in vivo* for various biomedical applications.

1.4. Thesis outline

In Chapter 2, we provide an extensive overview of the state of the art in the use of solid-binding peptides for biomedical applications. We first describe how solid-binding peptides are developed and how they bind to solid surfaces. We then analyze a selection of successfully implemented molecular architectures for the functionalization of both naturally occurring (calcium phosphate, silicates, and ice crystals) and synthetic surfaces (metals, plastics, and graphene). We conclude the chapter with an outlook on possible advancements and new applications.

In Chapter 3, we assess in detail the silica binding ability of a series of solid-binding peptides. We then explore the recombinant production of simple polypeptide diblocks named *B*-*E*, where the *B* block is a series of silica-binding peptides, and the *E* block is a hydrophilic elastin-like polypeptide. We show that the microbial production platform *Escherichia coli* can be used for the recombinant production of the designed protein diblocks. We focus on one *B*-*E* diblock and demonstrate that it can form dense polymer brushes on silica surfaces and stabilize silica nanoparticles. With the help of a quartz crystal microbalance, we show that the polypeptide brush can withstand prolonged rinsing, but that high ionic strength buffers quickly displace the protein diblocks. Finally, we show that the *B*-*E* diblock can prevent the non-specific interaction between functionalized particles and polypeptide-coated glass slides.

In Chapter 4, we explore the concept of multivalent binding for the physical attachment of self-assembling polypeptide brushes. To increase the resistance to displacement in a wider range of solvent conditions, we evaluated the introduction of multiple silica-binding *B* blocks both as tandem repeats and in star-like architectures via an oligomerizing domain *M*. We find

that a trimer-forming *M* domain satisfies our production and purification requisites, while tandem repeats show cytotoxic effects in *E. coli*. We then proceed with the characterization of the trimer-forming triblock polypeptide *B-M-E*. We show that this protein can self-assemble in stable and homogenous coatings both on flat silica surfaces and on silica nanoparticles. Finally, we demonstrate the improved salt resistance and antifouling properties of the resulting polypeptide brush via quartz crystal microbalance.

In Chapter 5, we expand our work on the silica-binding *B-M-E* polypeptide by testing the modularity of the design for the functionalization of gold surfaces. Thanks to recombinant DNA technology, we engineer new *B-M-E* polypeptides featuring a gold-binding peptide as *B* block and a zwitterionic, antifouling *E* block. We find that both polypeptides can be produced and purified similarly to our previous silica-binding *B-M-E* design. A preliminary characterization of the triblock reveals that both polypeptides can stably coat gold surfaces while maintaining excellent antifouling properties in the tested setting.

In Chapter 6, we present an overview of the findings of this work in relation to the criteria expressed in this Introduction. We first evaluate the potential of our multifunctional and modular design as antifoulant agent, suggesting further improvements. We then discuss our strategy for the bioconjugation of antibodies to diblock polypeptides, with a focus on alternative recombinant methods for future applications. Successively, we highlight the features of our production strategy that can warrant the possible scalability of the process. We conclude by giving a broader overview on the role of biotechnology in materials science.

1.5. References

[1] J. Pretty, J. Peacock, M. Sellens, M. Griffin. The mental and physical health outcomes of green exercise. *International Journal of Environmental Health Research* 15, 319–337 (2005).

[2] G. N. Bratman, J. P. Hamilton, G. C. Daily. The impacts of nature experience on human cognitive function and mental health. *Annals of the New York Academy of Sciences* 1249, 118–136 (2012).

[3] R. Hooke, J. Allestry, J. Allestry. *Micrographia, or, Some physiological descriptions of minute bodies made by magnifying glasses : with observations and inquiries thereupon /*. (Printed for James Allestry, printer to the Royal Society, and to be sold at his shop, at the Rose and Crown in Duck-Lane, 1667). doi:10.5962/bhl.title.113984.

[4] H.-Y. Fu, S.-J. Chen, R.-F. Chen, L.-L. Kuo-Huang, R.-N. Huang. Why do Nettles Sting? About Stinging Hairs Looking Simple but Acting Complex. *Functional Plant Science and Biotecnology* 1, 46–55 (2007).

[5] M. Weigend, A. Mustafa, H. J. Ensikat. Calcium phosphate in plant trichomes: the overlooked biomineral. *Planta* 247, 277–285 (2018).

[6] A. Mustafa, H. J. Ensikat, M. Weigend. Stinging hair morphology and wall biomineralization across five plant families: Conserved morphology versus divergent cell wall composition. *American Journal of Botany* 105, 1109–1122 (2018).

[7] H. J. Ensikat, M. Weigend. Distribution of Biominerals and Mineral-Organic Composites in Plant Trichomes. *Frontiers in Bioengineering and Biotechnology* 9, 1–12 (2021).

[8] K. Liu, L. Jiang. Bio-inspired design of multiscale structures for function integration. *Nano Today* 6, 155–175 (2011).

[9] N. Huebsch, D. J. Mooney. Inspiration and application in the evolution of biomaterials. *Nature* 462, 426–432 (2009).

[10] B. D. Ratner, S. J. Bryant. Biomaterials: Where we have been and where we are going. *Annual Review of Biomedical Engineering* 6, 41–75 (2004).

[11] F. Wang, Y. Li, Y. Shen *et al.* The functions and applications of RGD in tumor therapy and tissue engineering. *International journal of molecular sciences* 14, 13447–13462 (2013).

[12] U. Hersel, C. Dahmen, H. Kessler. RGD modified polymers: Biomaterials for stimulated cell adhesion and beyond. *Biomaterials* 24, 4385–4415 (2003).

[13] Q. Chen, D. Zhang, J. Gu *et al.* The impact of antifouling layers in fabricating bioactive surfaces. *Acta Biomaterialia* 126, 45–62 (2021).

[14] J. Hasan, R. J. Crawford, E. P. Ivanova. Antibacterial surfaces: The quest for a new generation of biomaterials. *Trends in Biotechnology* 31, 295–304 (2013).

[15] P. J. Conroy, S. Hearty, P. Leonard, R. J. O'Kennedy. Antibody production, design and use for biosensor-based applications. *Seminars in Cell and Developmental Biology* 20, 10–26 (2009).

[16] J. M. Anderson. Biological Responses to Materials. *Annual Review of Materials Research* 31, 81–110 (2001).

[17] M. J. Russo, M. Han, P. E. Desroches *et al.* Antifouling Strategies for Electrochemical Biosensing: Mechanisms and Performance toward Point of

Care Based Diagnostic Applications. *ACS Sensors* 6, 1482–1507 (2021).

[18] R. D'AGATA, N. BELLASSAI, V. JUNGBLUTH, G. SPOTO. Recent advances in antifouling materials for surface plasmon resonance biosensing in clinical diagnostics and food safety. *Polymers* 13, 1–24 (2021).

[19] G. ROCCHITTA, A. SPANU, S. BABUDIERI *ET AL.* Enzyme biosensors for biomedical applications: Strategies for safeguarding analytical performances in biological fluids. *Sensors (Switzerland)* 16, (2016).

[20] J. A. BURDICK, G. D. PRESTWICH. Hyaluronic acid hydrogels for biomedical applications. *Advanced Materials* 23, 41–56 (2011).

[21] S. JIANG, Z. CAO. Ultralow-fouling, functionalizable, and hydrolyzable zwitterionic materials and their derivatives for biological applications. *Advanced Materials* 22, 920–932 (2010).

[22] C. LI, C. LIU, M. LI *ET AL.* Structures and Antifouling Properties of Self-Assembled Zwitterionic Peptide Monolayers: Effects of Peptide Charge Distributions and Divalent Cations. *Biomacromolecules* 21, 2087–2095 (2020).

[23] D. ZHANG, Q. CHEN, W. ZHANG *ET AL.* Silk-Inspired β-Peptide Materials Resist Fouling and the Foreign-Body Response. *Angewandte Chemie - International Edition* 59, 9586–9593 (2020).

[24] M. SUN, J. DENG, Z. TANG *ET AL.* A correlation study of protein adsorption and cell behaviors on substrates with different densities of PEG chains. *Colloids and Surfaces B: Biointerfaces* 122, 134–142 (2014).

[25] Q. CHEN, S. YU, D. ZHANG *ET AL.* Impact of Antifouling PEG Layer on the Performance of Functional Peptides in Regulating Cell Behaviors. *Journal of the American Chemical Society* 141, 16772–16780 (2019).

[26] K. S. MASTERS. Covalent Growth Factor Immobilization Strategies for Tissue Repair and Regeneration. *Macromolecular Bioscience* 11, 1149–1163 (2011).

[27] Q. WEI, T. BECHERER, S. ANGIOLETTI-UBERTI *ET AL.* Protein interactions with polymer coatings and biomaterials. *Angewandte Chemie - International Edition* 53, 8004–8031 (2014).

[28] Y. JUNG, J. Y. JEONG, B. H. CHUNG. Recent advances in immobilization methods of antibodies on solid supports. *Analyst* 133, 697–701 (2008).

[29] D. C. FERREIRA SOARES, C. M. R. ODA, L. O. F. MONTEIRO, A. L. B. DE BARROS, M. L. TEBALDI. Responsive polymer conjugates for drug delivery applications: recent advances in bioconjugation methodologies. *Journal of Drug Targeting* 27, 355–366 (2019).

[30] C. NICOSIA, J. HUSKENS. Reactive self-assembled monolayers: From surface functionalization to gradient formation. *Materials Horizons* 1, 32–45 (2014).

[31] J. E. BUTLER, L. NI, W. R. BROWN *ET AL.* The immunochemistry of sandwich elisas-VI. Greater than 90% of monoclonal and 75% of polyclonal anti-fluorescyl capture antibodies (CAbs) are denatured by passive adsorption. *Molecular Immunology* 30, 1165–1175 (1993).

[32] M. R. CASANOVA, R. L. REIS, A. MARTINS, N. M. NEVES. Surface biofunctionalization to improve the efficacy of biomaterial substrates to be used in regenerative medicine. *Materials Horizons* 7, 2258–2275 (2020).

[33] B. SAHA, P. SONGE, T. H. EVERS, M. W. J. PRINS. The influence of covalent immobilization conditions on antibody accessibility on nanoparticles. *Analyst* 142, 4247–4256 (2017).

[34] W. R. Algar, D. E. Prasuhn, M. H. Stewart *et al.* The controlled display of biomolecules on nanoparticles: A challenge suited to bioorthogonal chemistry. *Bioconjugate Chemistry* 22, 825–858 (2011).

[35] N. H. C. S. Silva, C. Vilela, I. M. Marrucho *et al.* Protein-based materials: From sources to innovative sustainable materials for biomedical applications. *Journal of Materials Chemistry B* 2, 3715–3740 (2014).

[36] C. Lv, X. Zhang, Y. Liu *et al.* Redesign of protein nanocages: The way from 0D, 1D, 2D to 3D assembly. *Chemical Society Reviews* 50, 3957–3989 (2021).

[37] J. Zhu, N. Avakyan, A. Kakkis *et al.* Protein Assembly by Design. *Chemical Reviews* 121, 13701–13796 (2021).

[38] Y. Qi, A. Simakova, N. J. Ganson *et al.* A brush-polymer/exendin-4 conjugate reduces blood glucose levels for up to five days and eliminates poly(ethylene glycol) antigenicity. *Nature Biomedical Engineering* 1, 1–12 (2017).

[39] K. Knop, R. Hoogenboom, D. Fischer, U. S. Schubert. Poly(ethylene glycol) in drug delivery: Pros and cons as well as potential alternatives. *Angewandte Chemie - International Edition* 49, 6288–6308 (2010).

[40] R. P. Garay, R. El-Gewely, J. K. Armstrong, G. Garratty, P. Richette. Antibodies against polyethylene glycol in healthy subjects and in patients treated with PEG-conjugated agents. *Expert Opinion on Drug Delivery* 9, 1319–1323 (2012).

[41] D. G. Rudmann, J. T. Alston, J. C. Hanson, S. Heidel. High molecular weight polyethylene glycol cellular distribution and PEG-associated cytoplasmic vacuolation is molecular weight dependent and does not require conjugation to proteins. *Toxicologic Pathology* 41, 970–983 (2013).

[42] V. Delplace, J. Nicolas. Degradable vinyl polymers for biomedical applications. *Nature Chemistry* 7, 771–784 (2015).

[43] P. Zhang, P. Jain, C. Tsao *et al.* Polypeptides with High Zwitterion Density for Safe and Effective Therapeutics. *Angewandte Chemie - International Edition* 57, 7743–7747 (2018).

[44] S. Banskota, P. Yousefpour, N. Kirmani, X. Li, A. Chilkoti. Long circulating genetically encoded intrinsically disordered zwitterionic polypeptides for drug delivery. *Biomaterials* 192, 475–485 (2019).

[45] M. F. Maitz. Applications of synthetic polymers in clinical medicine. *Biosurface and Biotribology* 1, 161–176 (2015).

[46] F. M. Veronese, G. Pasut. m10. PEGylation, successful approach. *Drug discovery today* 10, 1451–1458 (2005).

[47] Y. Wang, P. Katyal, J. K. Montclare. Protein-Engineered Functional Materials. *Advanced Healthcare Materials* 8, 1–33 (2019).

[48] N. K. Tripathi. Production and purification of recombinant proteins from Escherichia coli. *ChemBioEng Reviews* 3, 116–133 (2016).

[49] P. V. Pham. Medical biotechnology: Techniques and applications. *Omics Technologies and Bio-engineering: Towards Improving Quality of Life* 1, 449–469 (2018).

[50] S. R. Macewan, A. Chilkoti. Applications of elastin-like polypeptides in drug delivery. *Journal of Controlled Release* 190, 314–330 (2014).

CHAPTER 2

Biomedical applications of solid-binding peptides and proteins

Over the past decades, solid-binding peptides (SBPs) have found multiple applications in materials science. In non-covalent surface modification strategies, solid-binding peptides are a simple and versatile tool for the immobilization of biomolecules on a vast variety of solid surfaces. Especially in physiological environments, SBPs can increase the biocompatibility of hybrid materials and offer tunable properties for the display of biomolecules with minimal impact on their functionality. All these features make SBPs attractive for the manufacturing of bioinspired materials in diagnostic and therapeutic applications. In particular, biomedical applications such as drug delivery, biosensing, and regenerative therapies have benefited from the introduction of SBPs. Here, we review recent literature on the use of solid-binding peptides and solid-binding proteins in biomedical applications. We focus on applications where modulating the interactions between solid materials and biomolecules is crucial. In this chapter, we describe solid-binding peptides and proteins, providing background on sequence design and binding mechanism. We then discuss their application on naturally occurring surfaces (calcium phosphates, silicates, and ice crystals) and on surfaces of artificial materials (metals, plastics, and graphene). Although the limited characterization of SBPs still represents a challenge for their design and widespread application, our review shows that SBP-mediated bioconjugation can be easily introduced into complex designs and on nanomaterials with very different surface chemistries.

This chapter is based on:
Nicolò Alvisi & Renko de Vries, Biomedical Applications of Solid-Binding Peptides and Proteins, (*submitted*) **2022**.

2.1. Introduction

For over 3.7 billion years, living organisms have evolved strategies to survive in challenging environments.[1] One of the earliest strategies that organisms adopted for survival was the manipulation of inorganic solids in their environment. In particular, the incorporation of inorganic solid materials in organized extracellular architectures allowed for the creation of solid structures for defense, support, and spatial organization.[2] Early in the evolution of multicellular organisms, silica and calcium carbonate were already harvested and organized in spicules by sponges or mother-of-pearl by mollusks, in a process known as biomineralization.[3] Next to biomineralization, living organisms have also evolved strategies for interacting with solid surfaces in their surroundings, for example as a means of colonizing specific environments such as rocks or ice.[4,5]

Organisms have at their disposal a plethora of mechanisms for the recognition and binding of inorganic surfaces. Specifically, proteins and peptides prominently feature among the biomolecules that mediate these interactions. Many proteins involved in solid-binding and biomineralization have been described in recent years, providing insights in the interfacial mechanisms of solid recognition. Notable examples are lustrin A, responsible for binding the matrix of shell and pearl nacre,[6] silaffin-2, produced by diatoms in the matrix of biosilica,[7] and the proteins involved in the self-assembly of magnetite crystals inside magnetosensitive bacteria.[8]

The synthesis of novel biomaterials has taken much inspiration from natural proteins that interact with solid surfaces. The integration of inorganic solids in a biological environment is essential in the development of effective medical devices such as implants, catheters, and prosthetic joints.[9] Furthermore, bioanalytical devices rely on the controlled integration of surface-bound receptors. Aside from silicates and hydroxyapatite, new materials such as titanium, gold, silver, and plastics have been utilized for the development of biomedical devices. While these materials can be used without further modifications, undesired interactions with biomolecules, cells, and tissues can hinder their successful and long-term use.[10] It is therefore clear that novel biomaterials must precisely control the interactions of biomolecules with solid surfaces.

The most common functionalization approaches are based on the physical and chemical modification of biomaterial surfaces, like grit-blasting and acid etching of titanium implants.[11] These methods are widely applied

given their scalability and robustness, although they are still lacking with regards to biocompatibility. Alternatively, biofunctionalization is achieved via the immobilization of synthetic coatings such as self-assembled monolayers (SAMs) or the multilayer deposition of various polymeric materials.[12,13] These strategies are robust and versatile since they rely on the covalent immobilization of selected biomolecules.[14] Nevertheless, there is increasing interest in employing nature's toolkit by using solid-binding peptides and proteins. As previously mentioned, the recognition and binding of solid surfaces via non-covalent interactions is an effective strategy adopted by many organisms. The use of solid-binding peptides (SBPs) can improve the biocompatibility of surface functionalization strategies, allowing for the display of a wide range of biologically active macromolecules while retaining their function, with high surface specificity and ease of use.

In general, SBPs bind to solid surfaces via multiple non-covalent interactions. Various factors can define the binding strength of SBPs, such as surface topography and solution conditions. However, a key aspect of binding solid surfaces resides in the amino acid composition and the structural variety of SBPs. The term "solid-binding peptide" is usually reserved for short and unstructured peptides, typically with disordered conformations both in solution and when adsorbed on flat surfaces (Figure 2-1a). For the purpose of this review, we distinguish these SBPs from longer solid-binding domains or solid-binding proteins that may adopt ordered three-dimensional structures (Figure 2-1b).[15,16] Ice-binding proteins (IBPs) are a notable example of the natural variability of interfacial recognition structures. IBPs have independently evolved in several biological kingdoms, resulting in a large size range (3-180 kDa) and different physiological roles.[17] Most importantly, they present a remarkable variety of structural organization, from short glycosylated peptides to three-dimensional rigid structures like parallel α-helices, four helix bundles, and β-solenoids.[18,19] These examples highlight how the lack of a precise secondary or tertiary structure is not necessary for binding solid surfaces, both in crystalline and amorphous solids.

Over the years, the increasing amount of evidence surrounding the application of SBPs has brought attention to the topic. Given the broad spectrum of possible applications within materials science, SBPs have created many opportunities for novel bioinspired materials. In this chapter, we provide an overview of recent literature on the use of solid-binding peptides, solid-binding domains, and solid-binding proteins in biomedical applications. We

focus on applications where modulating the interactions between solid materials and biomolecules is crucial. While we include few examples relevant for biomineralization, we mainly concentrate on applications featuring pre-existing, untreated solid surfaces. Furthermore, we find that most applied work makes use of short and unstructured SBPs rather than large and folded solid-binding proteins, presumably due to the ease of obtaining and including short

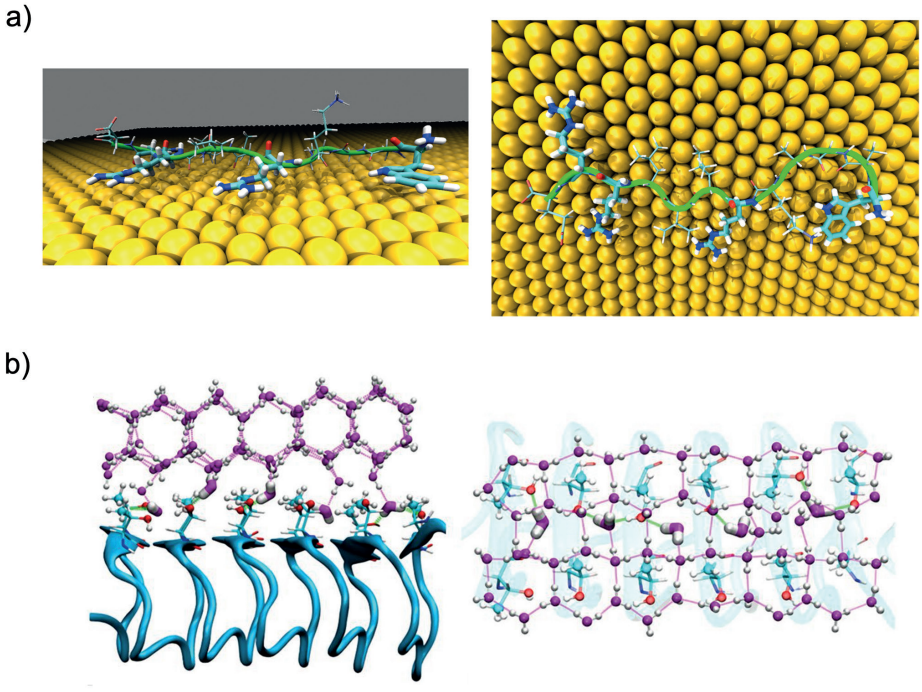

Figure 2-1. Molecular dynamics simulations of solid-binding peptide and solid-binding protein. **(a)** Typical disordered structure for the surface adsorbed conformations of the gold-binding peptide *AuBP1*. Side view on the left, top view on the right. The amino acid residues interacting with the gold surface are highlighted with thicker bonds. Water molecules are not shown for clarity. Reprinted with permission from Bialowska *et al*., copyright 2013 American Chemical Society.[20] **(b)** Simulation results for the structured antifreeze protein *MpdAFP* of the beetle *Microdera punctipennis dzungarica*. Side view (left) and top view (right) of the hexagonal ice-like water molecules atop the ice-binding site of the protein. The ice-binding site consists of an ordered array of β-sheets (blue arrows). Reprinted with permission from Liu *et al.,* copyright 2016 National Academy of Sciences.[21]

peptides in larger molecular architectures. Reflecting this difference, we mainly focus on SBPs, while briefly addressing globular solid-binding domains and proteins.

In recent years, other comprehensive reviews on SBPs have been published. On the one hand, most of them have a broad focus and only incidentally discuss biomedical applications among the other possible application areas.[22,23] Pushpavanam *et al.*, for example, explored the application of SBPs as molecular linkers and material synthesizers.[24] On the other hand, other authors reviewed biofunctionalization techniques for specific biomedically-relevant surfaces, without a clear focus on SBPs.[25–28] Only Care *et al.* provided a brief overview on the use of SBPs as tools for medically-relevant solid interfaces and biomaterials.[29] With our review, we hope to provide a more extensive and updated analysis.

In the first part of this chapter, we provide theoretical background on SBP sequences and on the molecular mechanisms of their binding to solid surfaces. Next, we review the biomedical applications of SBPs to both naturally occurring solid surfaces (calcium phosphate minerals, silica, and ice) and surfaces of artificial materials (metals and metal oxides, plastics, and graphene). In each case, we focus on studies that describe how SBPs are successfully integrated in larger designs with biomedical applications. In the outlook, we provide suggestions for future work and opportunities in this area.

2.2. Background

2.2.1. Design of solid-binding peptides and proteins

Natural adhesion peptides and proteins are products of the evolutionary process. Consequently, these peptides may not have suitable properties for biomedical applications. Moreover, the complex and clouded sequence-to-structure relationship within folded peptides makes systematic engineering difficult. Besides this, no specific binders have evolved for some crucially important synthetic biomaterials, such as titanium and plastics. Hence, design of new adhesion peptides and proteins is an important issue in materials science.[30]

Three main strategies have been used to identify and design functional peptide sequences for material binding: bioabstraction, de novo computational design and combinatorial design. While bioabstraction and combinatorial design have typically led to sequences for SBPs, de novo

computational design has so far been successful for the design of solid-binding proteins. The three strategies are illustrated in Figure 2-2.

First, bioabstraction involves the isolation of solid-binding regions, usually from natural multi-domain proteins (Figure 2-2a). The increasing availability of three-dimensional protein structures has allowed the discovery of minimal functional domains that were successfully adapted for surface functionalization. The unexpected discovery of micro-organisms capable of binding and degrading synthetic polymers has expanded the pool of possible surfaces.[31,32] Nonetheless, although this technique has proven to work in some specific examples, its success is not guaranteed.[33–35] In fact, the evolutionary pressure on organisms to select efficient binders for synthetic surfaces has obviously been very limited. For this reason, bioabstraction is mostly limited to surfaces with which organisms naturally interact.

Next, de novo computational design entails the generation of synthetic proteins with amino acid sequences that are not found in nature, based on biophysical and biochemical principles (Figure 2-2b).[36] Considerable advancements can be attributed to improved computational methods and computing power, as well as synthetic manufacturing of new DNA sequences. De novo design through computational engineering is a popular method and significant progress has been made with folded binders for single crystalline surfaces.[37–42] More recently, first principles computational design was attempted for the synthesis of new disordered SBPs.[43] However, it remains difficult to rationally design binders for materials with no clearly defined structure due to, for example, variations in local curvature, crystal plane morphology, topology, and crystal defects.[44] Despite recent successes, these methods have so far been mainly employed towards small molecule binders and not solid materials.[45]

Finally, the most used and successful method is combinatorial design. Combinatorial design involves the synthesis of peptide libraries and the subsequent screening and selection for binding to the surface of a specific solid material. This technique was introduced by George Smith as phage display, for which a library of bacteriophage viral particles is used for the screening of the peptides.[46] In phage display, random peptide sequences are fused on specific viral coat proteins, so that each viral particle displays several copies of the same peptide (Figure 2-2c). With multiple rounds of “biopanning” and multiplication, the phage library is enriched in peptides with the desired binding properties: after incubating phages with the material of interest, the

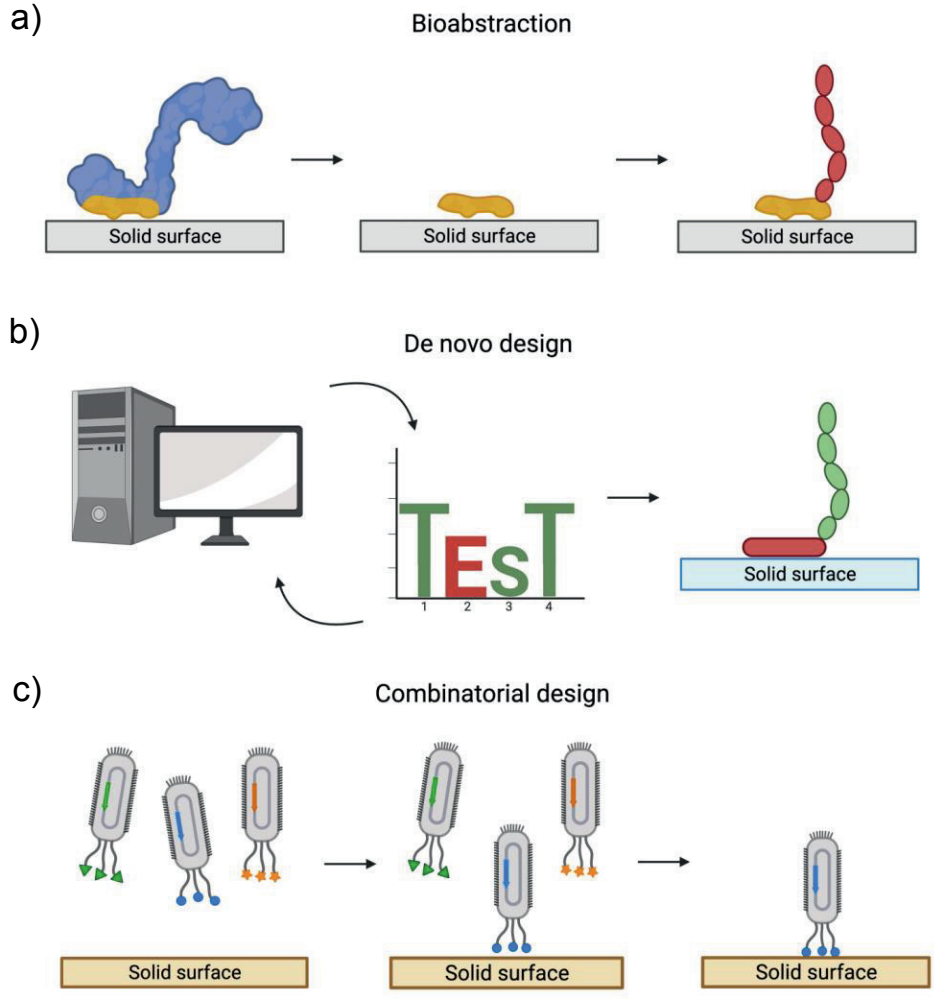

Figure 2-2. Examples of different peptide identification and design strategies. **(a)** In bioabstraction, functional domains are isolated from naturally occurring proteins. **(b)** Rational and computational methods can be applied, also to existing sequences, for the design of de novo peptides with the desired binding characteristic. **(c)** Phage display is one of the many combinatorial methods used for the discovery of functional peptides. A library of bacteriophages, which display a certain peptide sequence, is used for "biopanning" and enrichment on a surface of interest. Strongly bound bacteriophages contain the genetic information for the synthesis of high affinity peptide sequences.

weakly bound phages are washed away while the strongly bound phages are eluted separately. The eluted phages can be replicated and sequenced to identify the peptide. With this method, multiple solid-binding peptides can be identified, with high affinity for a wide variety of surfaces of interest.

Other methods of surface display have been developed, which use bacteria and yeast for cell surface display.[47,48] Phage display, however, shows fewer technical limitations and has been applied for the development of new drugs[49] and vaccines.[50] Furthermore, phage display is not limited to naturally occurring surfaces: strong binders have been identified for, among others, cellulose surfaces,[51] metal oxides,[52,53] titanium,[54] hydroxyapatite,[55,56] noble metals,[57,58] and polymeric materials.[59–62] In a few cases, phage display has also allowed for the identification of solid-binding peptides capable of discriminating between different surfaces and even crystal planes of the same material.[55,63–66] Unlike the previous design strategies, phage display can probe a very large chemical space and address defects and curvature of the solid surface. The resulting interactions generally yield more robust binding at different environmental conditions. Phage display, however, shows a clear bias for electrostatic bonds, generally resulting in low selectivity for the tested surface. For this reason, the sequences found via phage display often have little resemblance with known peptide motifs and are difficult to translate to empirical design strategies. Furthermore, since strongly bound phages display multiple copies of the same peptide sequence, surface functionalization strategies relying on a single peptide can be unsatisfactory. For an extensive overview of the use of phage display in materials science, we refer to Seker *et al.*[67]

In combinatorial design, peptide libraries can also be created synthetically and subsequently tested for the identification of SBPs. For example, in split-and-mix and SPOT libraries, peptides are synthesized on a solid support and then incubated with particles of the material of interest to identify sequences with strong binding.[30,68] Both split-and-mix and SPOT libraries allow to test fewer peptide combinations compared to phage display, but they provide more reliable results. A last promising alternative is directed protein evolution. This combinatorial technique is aimed at tailoring protein properties to specific application conditions. Starting from a known peptide with suboptimal properties, directed evolution iterates cycles of random mutagenesis and screening for improved protein variants with the desired

characteristics.[69] Although directed evolution has been explored for a wide range of applications, its use in materials science is still in its infancy.[70–73]

2.2.2. Techniques for analysis of binding

The screening of combinatorial libraries is an effective way to find sequences for SBPs with high affinity for materials of interest, but it provides little information regarding binding mechanisms and strengths. Binding of peptides and proteins to solid surfaces is a complex physical-chemical process depending on various conditions, such as the chemistry of the surface, the composition of the solvent, the concentration of solutes, and temperature. Furthermore, only few methods are available for experimentally elucidating the atomic structures of peptides and proteins at solid interfaces, especially if they are disordered. Unsurprisingly, the analysis of protein-surface interactions is a broad field of study, and we suggest the review by Bansal *et al.* for a more detailed discussion.[74]

A straightforward characterization of SBPs can be performed by measuring the kinetics of adsorption and desorption of the peptides under a representative set of conditions. Many instruments are available for this type of analysis. For example, quartz crystal microbalance with dissipation monitoring (QCM-D) is becoming increasingly popular, since many solid surfaces are commercially available for testing and sensors can be easily modified. QCM-D uses a piezoelectric sensor that monitors mass changes on its surface. These data are often analyzed in terms of simple equilibrium models where peptides independently adsorb and desorb from the surface. However, this assumption is not always applicable, since some SBPs have been shown to assemble cooperatively on solid surfaces.[75,76] The recording of dissipation energy can provide additional information on the density and packing of the adsorber layers, especially in relation to changes in the surrounding solution (pH, ionic strength).[77]

Atomic force microscopy (AFM) in air is an imaging technique with nm resolution used for the visualization of SBP-coated surfaces. AFM imaging is an effective tool to study conformation, surface coverage, aggregation, and selectivity. This technique can therefore help establish if SBPs adsorb independently forming uniform coatings, or if they cooperatively assemble on the surface creating fibers and aggregates.[75,76,78] The formation of peptide layers can also be followed in real-time and in solution via AFM imaging, although the setup optimization is more laborious.[37,79,80] AFM can also be used

for single-molecule force spectroscopy (SMFS) in order to measure the adhesion forces of a single SBP molecule to a solid substrate with pN accuracy.[81] A combination of these techniques can provide a reasonably thorough characterization of SBP binding. For example, a recent publication by our group showed how contrasting results from SMFS and QCM-D can be rationalized using AFM imaging.[75] In addition, our results highlighted the risk of characterizing SBPs in terms of a single equilibrium binding constant, since independent adsorption and full equilibrium cannot be assumed for all SBPs.

Finally, nuclear magnetic resonance (NMR) spectroscopy and solid-state NMR allow to study the structure and surface arrangement of SBPs both in solution and adsorbed on a surface, highlighting which side chains interact with the surface. Solid-state NMR is one of the few techniques providing structural information at the atomic level on the conformation of peptides adsorbed on solid surfaces. Unfortunately, these analyses are difficult and rarely applied for SBP characterization.[74]

2.2.3. Molecular features determining binding of SBPs to solid surfaces

We wish to point out three molecular features that determine the binding of solid-binding peptides and proteins to solid surfaces: the amino acid composition of the binding region, the orientation of the amino acids in contact with the surface, and the number of amino acids in contact with the surface. A schematic illustration of these molecular features is presented in Figure 2-3.

First, the amino acid composition can influence the binding strength, since the amino acid side chains contain chemical groups with affinity for certain solid surfaces (Figure 2-3). For example, metal-binding SBPs are enriched in hydrophobic and polar residues, while positively charged amino acids significantly contribute to silica binding, and aromatic residues preferentially bind carbon-based materials.[20,75,82,83] Furthermore, threonine is crucial in most ice-binding proteins, and acidic amino acids strongly interact with calcium phosphate minerals, while peptides binding to plastic materials are enriched in hydrophobic residues.[72,84,85] Single-residue mutants can provide insightful information on which amino acid residues contribute to the binding affinity of solid-binding peptides and proteins.[86,87] Each amino acid is systematically substituted with a “non-functional” amino acid like alanine, and the resulting peptides are tested with respect to their surface binding

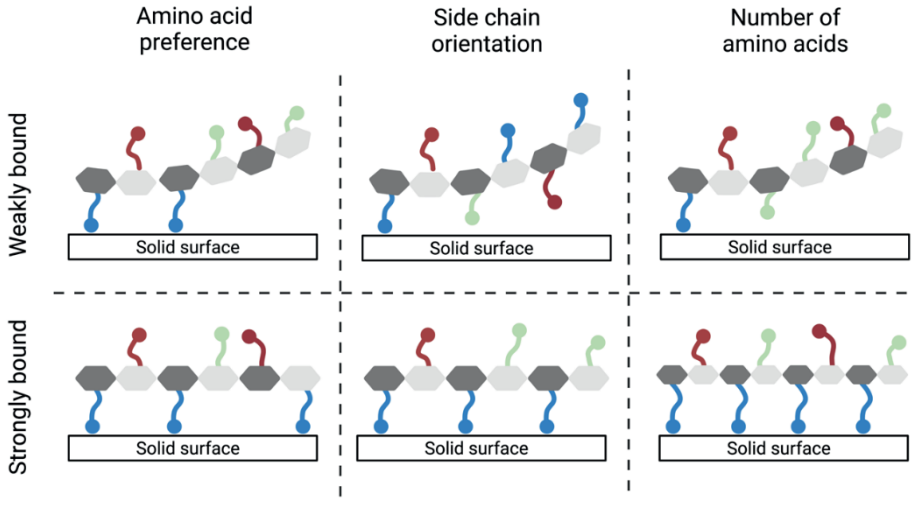

Figure 2-3. Schematic representation of the molecular features that determine surface binding. Amino acids interact with solid surfaces via their side chain (in color). Enrichment in amino acids with desirable chemical properties (charge, polarity, and hydrophobicity) can highly influence the binding strength of a peptide sequence. The relative position and orientation of the side chains is also responsible for stronger binding. Finally, increasing the number of binding moieties can result in improved binding affinity.

capabilities. Furthermore, these mutants show that the position of an amino acid within an SBP can highly affect the overall binding ability.[88,89]

Second, the possible orientations of each residue with respect to the surface is a fundamental factor determining the binding strength of solid-binding peptides, domains, and proteins (Figure 2-3).[90] Short SBPs usually lack a stable three-dimensional structure, and their inherent flexibility allows them to adopt multiple conformations upon adsorption. In some cases, molecular simulations have shown that the orientation of anchor residues plays a key role in determining the overall binding strength.[20,77] In fact, the anchor residues typically bind strongly to the surface, while the remaining residues are either weakly bound or not bound in most configurations. In addition, given their reduced size, SBPs can experience structural confinement caused by intramolecular steric repulsions and misorientation of relevant side chains.[91] These observations lead to the hypothesis that non-binding residues in SBPs might allow for the optimal orientation of the anchor amino acids with respect to the surface.

The orientation of key residues is equally relevant in solid-binding proteins and solid-binding domains. For example, the rigid structure of IBPs is necessary for the binding of ice crystals. These proteins feature precisely arranged one- or two-dimensional arrays of threonines.[84] These residues are all projected away from the ice-binding site with the same orientation, maximizing their possible interactions with matching crystal planes. Conversely, some solid-binding domains, like the silica-binding protein Si-tag, lack a stable three-dimensional structure and can remain partially or totally unfolded under physiological conditions.[92] These intrinsically disordered proteins can assume an optimal conformation upon binding with a solid surface, adapting their structure to maximize the intermolecular interface.[93–95] Since the majority of proteins involved in biomineralization appears to be intrinsically disordered,[96] structural flexibility seems to be preferrable to rigidity when interacting with solid surfaces at leats for this application.

Third, the binding strength is determined by the number of amino acids involved in surface-binding: changing the number of amino acids or domains can be used to tune the strength of binding to the solid surface.[97] For example, the affinity of an SBP can be increased by repeating in tandem the sequences of interest. This approach was successfully applied to many inorganic surfaces,[98,99] but satisfactory results are not always guaranteed.[100,101] In these cases, the connections between SBPs presumably introduced steric constraints, preventing optimal orientation of key residues. Alternatively, multiple copies of an SBPs can be displayed on suitable molecular scaffolds to engineer multivalent binding.[102] This approach has been applied successfully in various cases, leading to dramatically enhanced affinities using both synthetic[103–105] and protein-based scaffold structures.[106,107]

2.3. Biomedical applications of solid-binding peptides

In the following section, we will outline a selection of successful biomedical applications of solid-binding peptides and proteins, both for naturally occurring surfaces (calcium phosphate minerals, silicates, and ice) and artificial surfaces (metals and metal oxides, plastics, and graphene). All *in vivo* results were obtained in animal models, unless stated otherwise. A list of the solid-binding peptides and proteins discussed can be found in Table 2-1 at the end of this section.

2.3.1. Naturally occurring surfaces

2.3.1.1. Calcium phosphate minerals

Calcium phosphate (CaP) minerals are the main inorganic components of human bones and teeth. Hydroxyapatite (HA) crystals are the prevalent mineral constituent found in native bone, while phosphate and calcium ions are used for synthetic bone replacements such as β-tricalcium phosphate (β-TCP). Calcium phosphates are therefore highly biocompatible and osteoconductive, making them ideal biomaterials for regenerative therapies, as bone fillers or as coatings for metal implants.[108] Calcium phosphates present good mechanical and physical properties, but they lack the ability to recruit immature cells and induce their differentiation (osteoinductivity). For this reason, considerable research efforts have been dedicated to the functionalization of CaP-based materials with therapeutic growth factors.

Since many proteins and peptides are involved in the formation of hard tissues, SBPs are a popular choice for the immobilization of bioactive molecules on CaP surfaces. A particularly attractive feature of SBP-mediated functionalization is the reversibility and tunability of the binding strength. Localized delivery and sustained release of growth factors, for example, can effectively mimic the physiological chemotactic gradient required for tissue growth.[109,110] Furthermore, HA surfaces include only few functional groups for covalent bonding, making adsorption-based methods an attractive option.[111] In the current section, we will discuss the application of CaP-binding peptides in implant coatings and remineralization therapies, material synthesis, drug delivery, and vaccine development.

The extracellular matrix of bone is rich in acidic non-collagenous proteins, involved in cell migration and differentiation.[85] These proteins can bind to HA crystals and regulate bone formation. Unsurprisingly, the simplest HA-binding peptides consist of repetitive acidic amino acids. One of the first successful attempts at cell attachment onto HA using acidic binding peptides was reported by Fujizawa *et al.*, featuring a poly-glutamate heptapeptide (E7) for HA binding.[112] The fusion protein also contained an RGD peptide for cell binding, resulting in improved *in vitro* osteoblast attachment and mineralization.[113] The same HA-binding peptide was then adopted in similar designs with the three other cell-binding peptides, showing that not all cell-binding motifs elicit the desired response.[114,115] Promising results were reported for fusions with the collagen-derived motif DGEA: the peptide coating

was stable *in vivo* for at least 2 months when used on HA, allograft bone, β-TCP, and Ca-containing cement.[116,117] Interestingly, the authors showed that varying the length of the poly-glutamate peptide is an effective method to tune the release rate of the adsorbed biomolecules.[114,116]

In the same series of experiments, Culpepper *et al*. showed similar results when using a peptide derived from the bone morphogenic protein 2 (BMP-2) fused to the HA-binding peptide E7.[117] The same modular protein was extensively researched in subsequent studies, proving its remarkable osteoinductivity both *in vitro* and *in vivo* on allograft bone, bone scaffolds, bone substitutes, mineralized silk fibres, and hybrid aerogels.[118–122] Tests performed with different osteogenic peptide motifs yielded similarly positive results.[123] For example, a vascular endothelial growth factor (VEGF)-derived peptide fused to the HA-binding peptide E7 could be slowly released from AH disks to stimulate neovascularization *in vitro*.[124,125] Finally, the poly-glutamate octapeptide E8 was reported to effectively anchor recombinant BMP2 to HA disks.[126]

More recently, the poly-aspartate heptapeptide D7 was investigated in combination with a BMP-2-derived peptide. The fusion protein showed higher affinity for HA-surfaces compared to the E7-labeled peptide, exerting excellent bone regeneration capabilities *in vitro* and *in vivo* on synthetic bone scaffolds.[127–129] Shorter poly(D) peptides have been successfully applied for the sustained release of osteogenic hormones.[130]

Non-repetitive HA-binding peptides have also been extensively studied for cell adhesion and bone factor delivery strategies.[131] For example, an osteocalcin-derived HA-binding peptide was fused to a BMP-2-derived peptide.[132] Follow up studies revealed that the fusion protein could target bone tissues, while promoting stem cell differentiation *in vitro* and bone healing *in vivo* on HA-coated surfaces.[132–135] A fusion protein with a VEGF-derived peptide was tested *in vitro* on HA and β-TCP surfaces, confirming the ability to induce endothelial cell proliferation.[136,137]

Ramaraju *et al*. reported the use of an HA-binding peptide derived from phage display.[138] Interestingly, the peptide was shown to inhibit cell mineralization *in vitro*, possibly by sequestering calcium ions and delaying their deposition.[139] Nonetheless, when the peptide was fused to other cell-binding domains, the resulting protein could effectively coat 2D and 3D mineralized scaffolds and induce osteogenesis both *in vitro* and *in vivo*.[140–142] In these instances, the phosphorylation of the serines in the HA-binding

peptide has been related to an increase in its binding strength.[143] Consequently, a lack of phosphorylation resulted in weaker binding without adverse effects. These seemingly contradictory results highlight the importance of understanding the binding mechanisms of SBPs to better tailor their usage.

HA-binding peptides have found several applications in the design of tooth remineralization therapies. Peptides used for these applications are usually derived from the enamel matrix, a protein-rich mixture that forms the hard and highly mineralized tooth tissue. In a few recent examples, remineralization of damaged teeth was achieved both *in vivo* and *in vitro* thanks to four HA-binding peptides derived from the enamel matrix proteins amelogenin and tuftelin.[144–147] Positive results were also achieved with acidic peptides derived from the dental epithelium protein copine 7 or the salivary protein statherin.[148,149] Notably, three of these HA-binding peptides improved remineralization without being fused to other functional peptides. This finding indicates that these HA-binding peptides can exert a physiological function other than surface binding.

The interactions of SBPs and CaP minerals have found limited but noteworthy applications in the improvement of CaP-based biomaterials.[150] A straightforward yet effective approach involved the synthesis of a protein-mineral nanocomposite. The poly-glutamate octapeptide E8 was fused to charged elastin-like polypeptides (ELPs) and mixed with calcium-based fillers.[151–153] The resulting materials showed increased stability in fluids and improved binding to teeth, without impacting their biocompatibility *in vitro*.[152,154] Other proof-of-principle examples relied on more exotic materials, like spider silk fibres, polyetherimide films, methacrylate antibacterial adhesives, and shape memory polymer gels.[155–158] Finally, a notable example was recently reported by Lauria and co-authors.[159,160] Potato virus X nanoparticles were engineered to expose both cell-binding and HA-binding peptide on their surface, then subsequently loaded into hydrogels, mimicking the extracellular matrix. Remarkably, the viral nanoparticles initiated mineralization inside the hydrogel and sustained osteogenesis *in vitro*, showing good potential as an innovative composite for bone tissue engineering.

Next, various proof-of-concept studies have addressed the use of HA-binding peptides for the immobilization of antimicrobial peptides (AMPs) against oral pathogens. In most instances, a HA-binding peptide was fused to

an AMP, directly or via a short flexible linker. Huang *et al*. showed how the fusion protein could effectively disrupt *S. mutans* biofilms *in vitro*, although less effectively than conventional antibiotics.[161] The fusion protein could retain cytocompatibility and stability in human saliva. Comparable results were obtained with similar designs against *Escherichia coli*.[162,163] Finally, using an amelogenin-derived HA-binding peptide fused to an AMP is an effective strategy to achieve both antimicrobial activity and carious tissue remineralization.[164]

Bone-specific drug delivery via HA-binding peptides has also been explored in the past decade. Effective delivery of drugs to bone tissues is complicated by the limited blood supply and the bone marrow-blood barrier.[165] Nonetheless, bones are a unique solid material within the human body and peptide-mediated delivery has proved effective and with limited off-target effects. In a first proof-of-concept, a repetitive acidic oligopeptide (poly(E)) was directly tethered to an estrogen and tested *in vivo* as possible therapy against osteoporosis.[166] These promising results stimulated the testing of other osteotropic drugs fused to acidic HA-binding tags.[167,168] Repetitive acidic tags were successfully used for the targeted delivery of enzymes, lyposomes, and nanoparticles to bone tissue, showing in all cases highly promising results both *in vitro* and *in vivo* in animal models.[169–175] Poly(D) peptides have also been applied in gene delivery therapies targeted to bone tissue. For example, the adeno-associated virus 2 vector used for gene delivery was modified to expose HA-binding peptides, with clear improvements.[176,177] Finally, Ren *et al.* reported an elegant strategy for the delivery of drugs to specific cells in the bone tissue: the authors combined an HA-binding peptide derived from amelogenin and an osteoblast-specific aptamer to develop a nanocarrier with improved specificity both *in vitro* and *in vivo*.[178]

Targeted delivery to HA surfaces furthermore finds promising applications in the field of bioimaging, especially for *in vivo* bone imaging, although only proof-of-concept studies have so far been reported. In a first attempt, an HA-binding peptide derived from phage display was fused to a green fluorescent protein derivative.[179] The resulting fusion protein was tested *in vitro* on acellular cementum of human teeth, giving positive results with fluorescence microscopy. In another example, Bang *et al.* identified a supposedly highly specific HA-binding peptide via phage display and combined it with the fluorescent Cy5.5 dye.[180] During *in vivo* real-time whole-body imaging, the conjugate showed preferential binding for bone tissues. The

development of probes for nuclear imaging was also attempted, but with unsatisfactory results.[181]

Lastly, CaP minerals have found applications in vaccine engineering. For example, biomimetic mineralization of viral particles was proven to increase their efficacy as vaccine vectors. CaP mineral shells have been shown to provide physical and chemical protection to the viral particle, resulting in enhanced infectivity, circumvention of neutralizing antibodies, avoidance of pre-existing immunity, and improved thermal stability.[182–185] CaP-binding peptides have therefore found an application in this field. A relevant example of biomineralized vaccine vectors is reported in Figure 2-4. In this study, viral particles have been engineered to expose CaP-binding peptides on their surface (Figure 2-4.1).[186] The resulting mineralized particles showed increased thermostability compared to uncoated particles, while improving their ability to induce an immune response (Figure 2-4.2,3). Furthermore, CaP nanoparticles have been successfully administered as biocompatible vaccine adjuvants.[187] In this regard, CaP-binding peptides can both guide the synthesis of the nanoparticles and allow the exposition of antigens on their outer shell.[188,189]

In conclusion, CaP-binding peptides have been extensively applied to a vast range of biomedical applications, often yielding promising results in animal model experiments. This success lies in the flexibility of peptide-based functionalization strategies, given the reversibility and tunability of binding and the inherent biocompatibility. It is also worth noting that peptides derived from extracellular matrix proteins have provided the most promising results.

2.3.1.2. Silicates

Silica is the most abundant biomineral found in the Earth's lithosphere, making up almost a third of its crust.[190] Given the abundancy of this material, it is not surprising that silica mineralization is extensively used by many organisms, such as diatoms and sponges, for the creation of complex extracellular structures. The unique properties of silica make it an ideal material for biotechnological and biomedical applications. Not only are silica-based materials generally biocompatible and non-toxic, they also present excellent thermal and pH stability, chemical inertness, and mechanical resistance.[191] For these reasons, silica is widely used for the fabrication of implantable devices, nanoparticle-mediated drug delivery, biosensing, and bioencapsulation

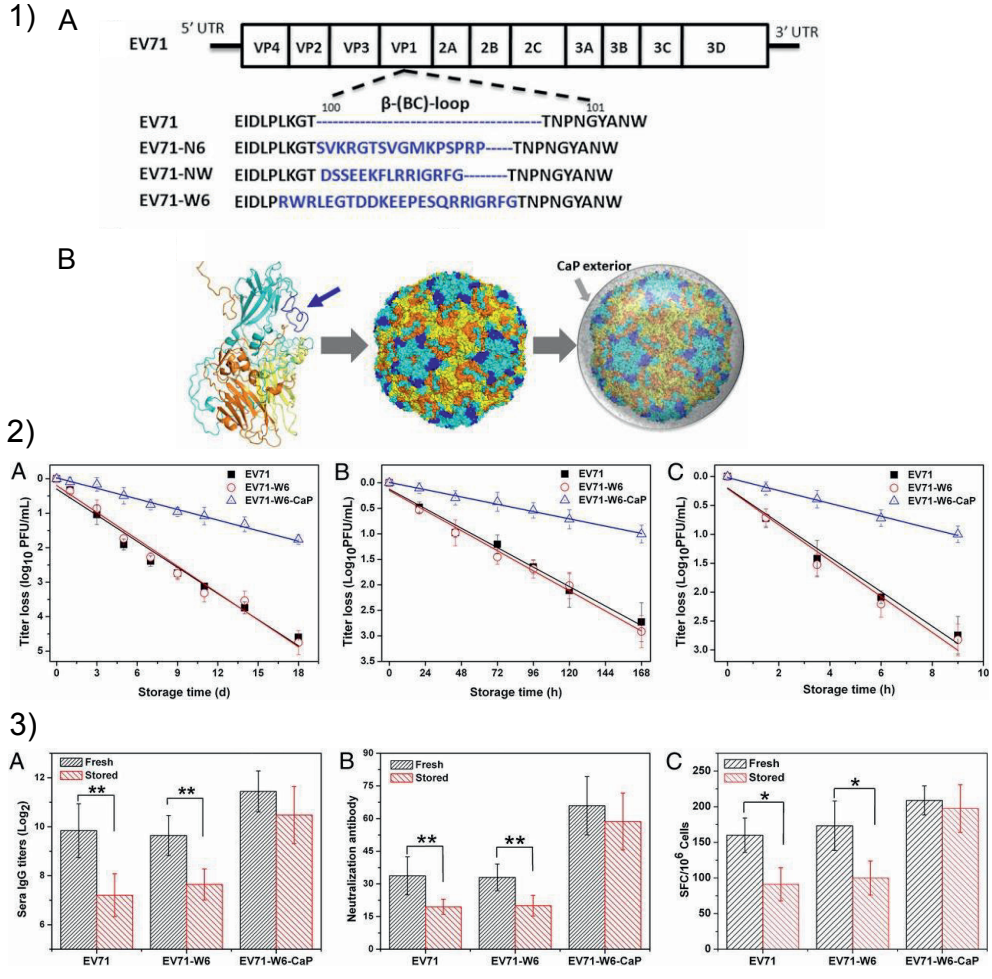

Figure 2-4. CaP-binding peptides can be used in the design of biomineralized vaccine carriers. **(1) (A)** The CaP-binding sequence was inserted in a capsid protein of human enterovirus type 71 (EV71) **(B)** to achieve a uniform distribution on the virion surface (dark blue) and induce in situ mineralization. **(2)** In vitro test of virus thermostability at **(A)** 26 °C, **(B)** 37 °C, and **(C)** 42 °C. After incubation, the infectivity was evaluated by plaque assay. The percentage of infectivity is shown in logarithmic scale as a function of storage time. **(3) (A)** Testing of vaccines, either fresh or stored at 37 °C for 5 days, on animal models. EV71-specific IgG titres and **(B)** neutralizing antibodies induced by uncoated (EV71 and EV71-W6) and CaP-coated viral particles (EV71-W6-CaP), 4 weeks after immunization. **(C)** Frequency of EV71-specific splenocytes in immunized mice 2 weeks. Adapted from Wang *et al*.[186]

strategies.[192] Although silica surfaces present moieties for covalent modification, there is growing interest in simpler adsorption-based strategies. Fortunately, the increasing understanding of biological silicification has made silica-binding peptides an attractive alternative for the modification of silica surfaces. For example, peptides derived from natural proteins such as silaffin R5 have been shown to mediate the formation of nanoparticles *in vitro*, allowing for the facile immobilization of biomolecules on newly synthesized particles.[193–195] In general, peptides enriched in positively charged residues have been shown to preferentially bind to silica surfaces.[88] This finding suggests that electrostatic interactions are a major contributor to the binding affinity on negatively charged silica surfaces. In this section, we will provide an overview of suggested biomedical applications of silica-binding peptides as part of coatings for implants, for drug delivery, and in biosensing.

Silicon and silicate ions have a direct influence on the formation and repair of bone tissue, and in recent years, bioactive glasses have been extensively evaluated as possible bone graft materials.[196,197] Silica-binding peptides have therefore been used for the synthesis and functionalization of silica-based biomaterials, such as biomimetic silk films and hydrogel layers.[198–200] Guo *et al*. reported the use of a peptide solution as ink for the inkjet printing of silica micropatterns on a hydrogel.[201] The printed silica-binding peptide mediated the silicification of the micropatterns and allowed the alignment of mesenchymal stem cells on the surface *in vitro*. In a different approach, a bifunctional peptide was used for the multi-layer silicification of titanium implantable surfaces, resulting in improved bone formation *in vitro* and *in vivo*.[202] Finally, Yun *et al*. prepared a porous biomineral composite material with the help of a bifunctional peptide and marine phytoplankton.[203] The porous calcium carbonate shell of coccolithophores (coccolith) was mixed with the peptide solution, resulting in a silicified material with high *in vitro* cytocompatibility and osteoinductivity *in vivo*.

The antibacterial activity of biomaterial surfaces is an important functionality of implantable materials. Implantable silica surfaces have been modified to reduce the chance of bacterial colonization. In two recent publications, two bacteriolytic enzymes were adsorbed on silica and silicone surfaces via silica-binding peptides.[204,205] In one case, the coating showed good antibacterial properties against *Staphylococcus aureus* both in static and dynamic biofilms, providing a proof-of-concept for its usage in clinically relevant applications.[205] Interestingly, AMPs were not successfully included in

similar bifunctional designs, to the authors' knowledge. We speculate that the cationic nature of most AMPs might compete with the silica-binding peptides for the adhesion to negatively charged silica surfaces, resulting in reduced and misoriented peptide immobilization. Interestingly, the positive charge of AMPs can be advantageously used for the direct adsorption on mesoporous silica particles, providing sufficient adsorption strength for delivery, release and functionality.[206]

The targeted delivery of bioactive molecules has extensively relied on silica nanoparticles, both porous and non-porous, as inert and biocompatible carriers. In this context, silica-binding peptides have found many applications. For example, Lu *et al.* reported the synthesis of a bi-functional peptide binding both silica and RNA. The peptide was used for the nanoparticle-mediated delivery of miRNA, resulting in effective gene silencing in *in vitro* cell cultures.[207] More recently, a silica-binding peptide linked to bioactive polyphenols was used for the functionalization of silica nanoparticles and the delivery to the nucleus of cancerous cells *in vitro*.[208] Silica nanoparticles coated via silica-binding peptides have also been used for cell targeting. For example, a silica-binding peptide was fused to an antibody-binding domain, providing a flexible platform for the conjugation of different IgG antibodies to the surface of nanoparticles for photodynamic therapy and cancerous cell targeting.[209,210]

Silica-binding peptides have been shown to induce local growth of silica. For this reason, they have been used to explore alternative methods for drug delivery, like particle encapsulation to increase the loading of poorly soluble drugs. Since silicification was proved to increase the thermal and chemical stability of fluorescent proteins, enzymes, viruses, and eukaryotic cells, this approach was tested with therapeutical compounds.[211–214] For example, the use of a bifunctional polypeptide allowed to stabilize a model hydrophobic drug into polypeptide assemblies and induce the formation of a silica shell around the polypeptide/drug core, with positive results both *in vitro* and *in vivo*.[215,216] More recently, other molecular scaffolds were combined with silicification. After showing that the transport protein ferritin can be modified with a silica-binding peptide to create a silica-enveloped drug carrier, Ki *et al.* proved that a second drug can be loaded into the outer silica shell.[217,218] The resulting dual delivery system was tested *in vitro*, revealing that the two drugs can be released at different rates after cellular intake. Modified ferritin was also used for the controlled synthesis of silica nanoparticles with an encapsuled

anticancer drug.[219] Finally, an elegant delivery method was proposed by Delalat *et al.*, via live diatom silica immobilization.[220] In this method, diatoms are genetically modified with a synthetic gene encoding the protein of interest fused to silaffin-derived peptides. Since these peptides are a natural component of diatom biosilica, they can direct the permanent immobilization of the protein of interest on the newly formed extracellular surface. In this way, the authors could functionalize diatom biosilica with an antibody-binding peptide. The antibody-labelled biosilica was then loaded with micelles containing an anticancer drug and successfully tested both *in vitro* and on animal models.

In the past decades, the increasing request for plastic-free and low cost materials for *in vitro* diagnostic devices has brought attention to silica surfaces as a reliable substrate.[221] Since surface modification is a key aspect in any biosensor design, silica-binding peptides have provided a valuable tool for the oriented immobilization of bioactive detection elements. In a first proof-of-principle experiment, antibodies were immobilized on silica surfaces via a fusion peptide and used for the detection of allergens on an optical ring resonators device.[222–224] A similar approach was explored for the detection of pathogens, both on flat surfaces and on silica nanoparticles.[225–227] Silica-binding peptides were also tested for the bioencapsulation of enzymes for the detection of glucose, for immunoprecipitation essays, but also for the detection of antibiotics and the detection of asbestos in live cells *in vitro*.[228–231]

An elegant series of recent publications has highlighted how silica-binding peptides can be adapted for the design of cheap biosensing platforms. Henderson *et al.* designed a fusion protein featuring a silica-binding peptide, the fluorescent protein mCherry and the enzyme sarcosine oxidase (SOx).[232] The biosensing system is illustrated in Figure 2-5. In their design, the silica-binding peptide functions as immobilization and purification tag, the mCherry marker provides a visual reference for the monitoring of protein production, while SOx is used to generate H_2O_2 in the presence of the prostate cancer biomarker sarcosine (Figure 2-5a-b). A second fusion protein, containing the enzyme horseradish peroxidase instead of SOx, can convert the H2O2 produced by SOx into a fluorescent product and ultimately allow the colorimetric detection of sarcosine.[233] Silica particles extracted from sand have been employed for the purification of the recombinant protein directly from bacterial crude extract. The functionalized particles were then inserted in a flat, hourglass shaped device (Figure 2-5c). The device was used for the

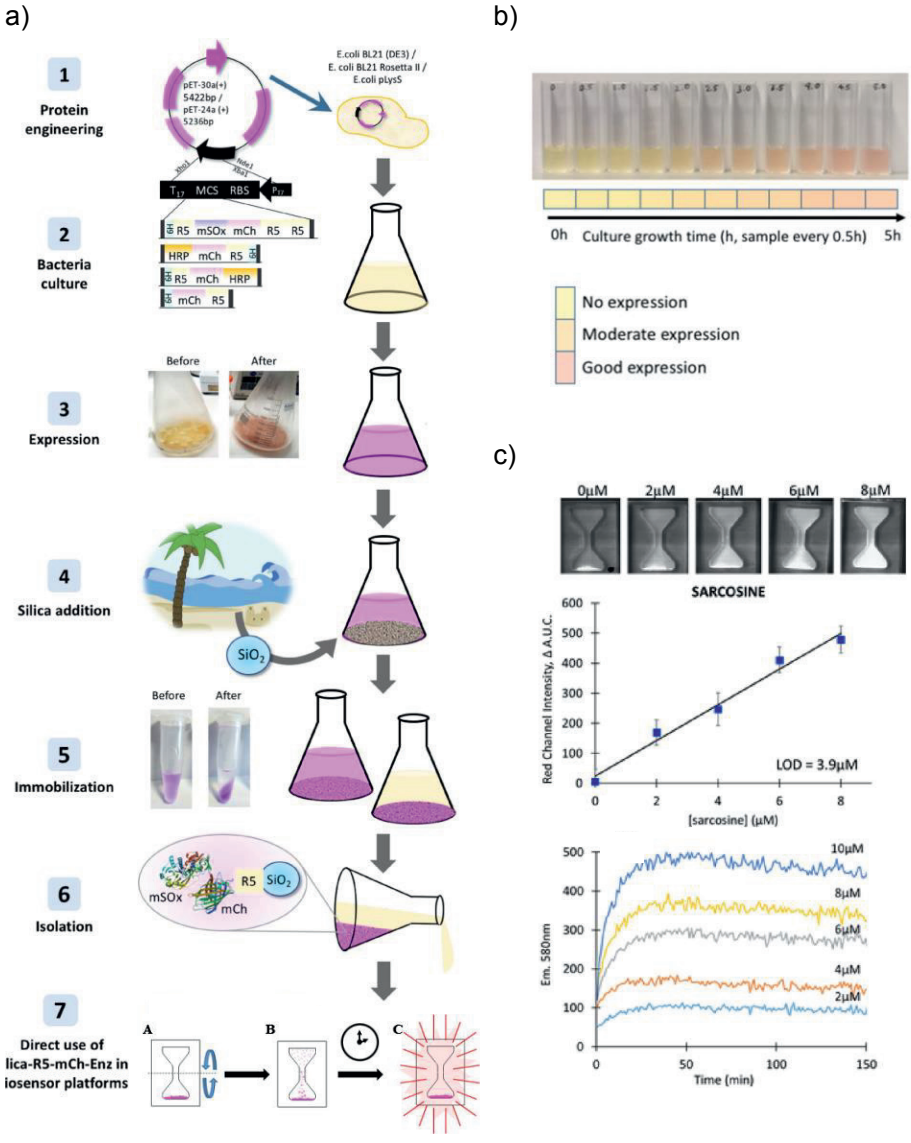

Figure 2-5. Silica-binding peptides are used for the immobilization of protein on silica particles in sarcosine detection biosensor. **(a)** Schematic illustration of production and purification steps in the "gene to device" strategy. **(b)** Visual change in color of induced bacterial cultures allows semi-quantitative detection of protein expression levels with the help of a color card. **(c)** Hourglass biosensing device can detect sarcosine in solution, providing a quantitative output. The device can be reliably used for end-point essays. Adapted from Henderson *et al.*[232], Henderson *et al.*[234], with permission from Elsevier.

detection of sarcosine by inverting the hourglass, allowing the particles to sediment and come into contact with the whole sample volume.[234] This "falling particle" biosensor was recently adapted for the DNA polymerase-based clinical diagnosis of malaria infections in Ghana, proving how solid-binding peptides are invaluable tools for the design of cheap, simple and effective biosensing devices.[235]

In conclusion, silica-binding peptides are versatile tools for many *in vitro* applications, from drug delivery to biosensing. Given the natural abundance and cheapness of silicates, peptide-based surface functionalization will likely become increasingly relevant in the synthesis of silicon-based biomaterials. Furthermore, given the importance of silicates in bone remineralization, *in vivo* applications might be explored more extensively.

2.3.1.3. Ice crystals

Although liquid water is fundamental for the survival of any organism, the formation of ice crystals can have lethal consequences for cells and tissues. Life at sub-zero temperatures is made possible by cryoprotective molecules like ice-binding proteins (IBPs), thanks to their ability to bind ice crystals and modulate their growth.[17] As mentioned in the introduction, the natural variety of IBP structures and sequences seems to demonstrate that there is no preferred way to bind a crystalline solid surface. Both disordered glycosylated peptides and highly ordered proteins with molecularly flat binding interfaces are effective IBPs.

Since their discovery in 1969, IBPs have drawn substantial attention for their potential application in agriculture, food technology, and biomedicine.[236] A particularly promising biomedical application is the cryopreservation of cells, embryos, organs, and other tissues. While widespread research on IBPs and IBP analogues is still ongoing, it should be emphasized that research on the use of IBPs in cryopreservation is still in its early stages. Considering the wealth of excellent and comprehensive reviews on the topic, we refer the reader to recent general reviews on cryopreservation,[237] the possible role of IBPs in cryopreservation in general,[18,238,239] and their use in the preservation of organs and tissues[240] and in reproductive medicine in particular.[241]

2.3.2. Artificial surfaces

2.3.2.1. Metals and metal oxides

Metals have played a paramount role in the history of medicine since ancient times: the Greek physician Hippocrates employed silver for the treatment of wounds, while gold was already used in ancient China 4 millennia ago. In the last decades, metals have found new biomedical applications especially in the field of nanomedicine, due to their unique physical and chemical properties.[242] Next to gold and silver, titanium is a key metal used as biomaterial. In the following sections, we will focus on biomedical applications of gold-, silver-, and titanium/titanium oxide-binding peptides. In the case of gold and silver, we will mainly review therapeutic and biosensing applications, with a focus on nanoparticle functionalization. In the case of titanium, we will instead review the application of titanium-binding peptides in coatings for implants.

Among the noble metals, gold (Au) has found practical applications in medical treatments.[243,244] For example, one of the clinical uses of gold dates back to the late 1920s, in the form of gold salts for the treatment of rheumatoid arthritis.[245] In the past decades, gold nanoparticles (AuNPs or GNPs) and gold nanoclusters (AuNCs) have been extensively researched, showing a vast range of potential biomedical applications.[246–249] The success of gold nanostructures is due to their unique physical and chemical properties, including biocompatibility, bioinertness, tunable morphologies and optical properties, and resistance to corrosion and oxidation.[246] Furthermore, since AuNPs present a simple surface chemistry, various conjugation strategies have been developed for their functionalization. Many synthesis and functionalization strategies rely on the covalent attachment of bioactive molecules, which grants chemical stability at the expense of flexibility of use. For this reason, gold-binding peptides have been explored for the facile and efficient functionalization of AuNPs, both in therapeutic and biosensing applications. In the case of Au-binding peptides, various amino acids have been reported to recognize the Au lattice: aromatic amino acids (Y, F, W), basic amino acids (R, K), and polar hydroxyl-containing amino acids (S, Y) appear to have a high affinity for the gold-water interface.[250] It should also be remembered that cysteine (C) residues covalently bind to gold surfaces via their thiol side group.

Au-binding peptides have found limited but noteworthy applications in photothermal therapy. For example, Oh *et al.* designed a modified T7 phage

displaying both an Au-binding peptide and a prostate cancer cell-binding peptide.[251] The modified phages could assemble a thin AuNP shell and act as nanocarriers for cancer-targeted photothermal therapy *in vitro*. Similar results were achieved more recently with nucleus-targeting AuNPs by Gao *et al.*[252] In their article, the authors speculate that the aggregation of AuNPs in the cancer cell nucleus could produce more heat during photothermal therapy, resulting in a reduced cell viability. Furthermore, the recent report of the intracellular synthesis of AuNPs thanks to a fusion peptide shows promising future applications in nanomaterial synthesis and, possibly, theranostics and bioimaging.[253]

Gold is a key material in the biosensing field, in both plasmon-based sensing and electrochemical sensing. In biosensing platforms, the detection of analytes relies on the precise, homogeneous, and oriented immobilization of a biological sensitive element. In this regard, Au-binding peptides provide a simple and fast method for the functionalization of gold surfaces. For example, an Au-binding peptide has been successfully implemented in many electrochemical biosensors.[254,255] In a recent publication, Lee *et al*. fabricated an enzyme-based electrochemical sensor by fusing an Au-binding peptide to a glucose dehydrogenase.[256] The fusion protein was then adsorbed on a gold electrode surface and used for the detection and quantification of glucose in whole blood samples. The sensor showed high sensitivity and could be stored for over a month. It is important to remark that the fusion site (C-terminal or N-terminal) and the amino acid sequence of the Au-binding peptides are crucial parameters in the design of direct electron transfer-based biosensors. Both factors directly influence the orientation, the proximity and ultimately the interface between the enzyme and the electrode surface.[257,258] Other explored biosensor designs include ELISA-based approaches, optical biosensors or lab-on-a-chip microfluidic biosensors.[259–264] Au-binding peptides have also been tethered to DNA for the detection of nucleic acid targets.[265] In their recent reports, Kim and co-authors described the use of an Au-binding peptide in a biosensor based on fluorescence resonance energy transfer (FRET) and a colorimetric biosensor for the detection of *Mycobacterium tuberculosis*. Both of these examples highlight how both Au-binding peptides and silica-binding peptides can be included in biosensor designs with different rationales.[266,267]

Similarly to gold, the medical properties of silver (Ag) are long known: starting from 1500 BCE, silver-containing compounds have been used as wide-spectrum antimicrobials for topical applications.[268] Silver ions appear to

interfere with several intracellular processes and bind the negatively charged bacterial cell wall, increasing its permeability.[268] Nowadays, silver is generating an increasing interest as an alternative to conventional antibiotics, and the adsorption of silver ions onto medical devices is one of the proposed strategies in the fight against antibiotic resistance.[268] In this context, silver-binding peptides have provided help in the synthesis of silver-containing hybrid materials such as silk-silver fibers and antimicrobial hydrogels.[269,270]

The number of Ag-binding peptides is low compared to other SBPs. In fact, only few combinatorial studies have attempted to identify Ag-binding sequences.[271–273] The systematic characterization of Ag-binding is less developed compared to other metals, both in experimental quantification and in molecular simulations.[43,274] Given the structural and physical similarities between silver and gold surfaces, however, the materials selectivity of SBPs has been investigated for these two metals. Interestingly, peptides initially selected for Ag surfaces could bind Au surfaces and vice versa, showing comparable binding affinities.[20,275,276] These results highlight how combinatorial techniques alone might be insufficient to select materials-specific sequences. Despite recent advancements, achieving preferential binding to Ag surfaces in the presence of gold still represents a substantial obstacle.[43]

Silver nanoparticles (AgNPs) have gained popularity for cosmetics, surgical coatings, medical implants, and as bactericidal compounds, due to their large surface to volume ratio, small size, and chemical stability.[277] Since small AgNPs show the highest antimicrobial effect, silver-binding peptides have been used for the size-constrained synthesis of homogeneous AgNP populations.[278,279] The resulting AgNPs showed increased cytotoxicity against *E. coli*, *Pseudomonas aeruginosa*, *Salmonella typhimurium*, *Shigella flexneri* and *Bacillus subtilis* compared to chemically synthesized AgNPs. Bifunctional peptides have been employed to facilitate the synthesis of AgNPs and reduce their cytotoxicity towards fibroblast cells.[280,281] The growth of bacterial biofilm can be effectively tackled by biofunctionalized AgNPs. Chen *et al*. fused a Ag-binding peptide with the enzyme dispersin B and adsorbed the protein on silver nanoparticles.[282] After the treatment, AgNPs could dissolve *S. epidermidis* biofilm and kill the released bacterial cells. Further efforts have been taken to make AgNPs pathogen selective. Kim *et al.*, for example, tested two multifunctional proteins featuring a Ag-binding peptide and two cell wall binding domains.[283] The two proteins were adsorbed on AgNPs and subsequently incubated with mixtures of either *B. subtilis* and *Bacillus*

anthracis, or *S. aureus* and *B. anthracis*. This approach resulted in the selective decontamination of only one pathogenic species from each mixture, proving the specificity of coated AgNPs in pathogen detection and killing.

Yet another application for Ag-binding peptides was recently explored by Woolfolk *et al.* The authors reported the synthesis of a bifunctional peptide for the coating of silver diamine fluoride-treated tooth tissue.[284] Silver diamine fluoride is applied to effectively slow the progression of dental caries. In an *in vitro* experiment, an Ag-binding peptide fused to a remineralization-inducing peptide promoted the remineralization of the affected area.

Titanium (Ti) and titanium alloys are the standard inert materials for the manufacturing of dental and orthopedic implants. The mechanical properties of titanium, alongside its biocompatibility and resistance to corrosion, make it ideal for implantable devices.[285] The lack of recognizable moieties on the implant, however, does not allow for the regulation of bone cell processes and can can induce a foreign body reaction to the implant. For this reason, SBPs have been suggested as an easy and efficient approach for the functionalization of Ti surfaces to modulate the interactions of the implant with the surrounding tissue. The interfacial interactions of Ti and TiO_2 in aqueous solutions and amino acids or peptides have hardly been investigated in detail.[286] However, recent studies have highlighted the role of charged and aromatic amino acids in the binding affinity of Ti-binding peptides.[82,286]

Kang *et al*. effectively immobilized the epidermal growth factor on Ti surfaces via a phosphorylated Ti-binding peptide, confirming that the promotion of cell growth is correlated to the prolonged activation of cell signal transduction.[287] A similarly designed bifunctional peptide, featuring the cell attachment peptide RGDS, improved the adhesion and proliferation of osteoblasts and fibroblasts on implant-grade Ti.[288] A follow up study confirmed that the elicited cell signal transduction is needed for improved mineral deposition and osteogenesis.[289] A recent and thorough study by Liu *et al*. confirmed this finding using implants *in vivo*.[290] As shown in Figure 2-6, the designed fusion peptide could anchor oral epithelial cells, sustain epithelial sealing *in vitro* and *in vivo* and promote the expression of key genes involved in wound healing. In a more articulated architecture, silk fibroin protein was grafted with both a Ti-binding peptide and an RGD peptide in equal ratio. The obtained silk was grafted onto a Ti surface, resulting in improved fibroblast adhesion and strongly bound endothelium.[291] In another example, an *in vivo* study showed that a fusion protein between a Ti-binding peptide and the bone

1)

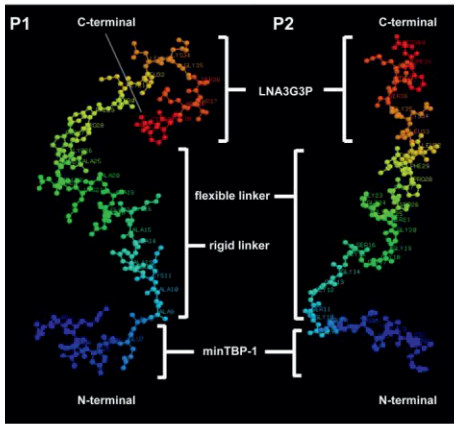
P1
C-terminal
P2
C-terminal
LNA3G3P
flexible linker
rigid linker
minTBP-1
N-terminal
N-terminal

2)

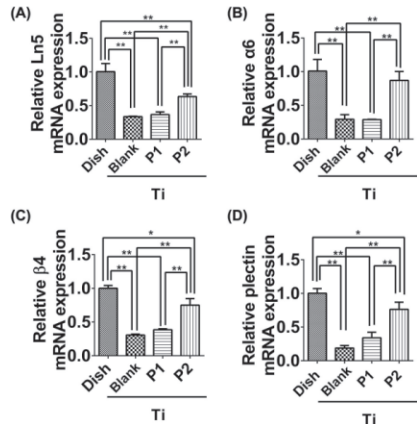
(A)
Relative Ln5 mRNA expression
(B)
Relative α6 mRNA expression
(C)
Relative β4 mRNA expression
(D)
Relative plectin mRNA expression
Dish
Blank
P1
P2
Ti

3)

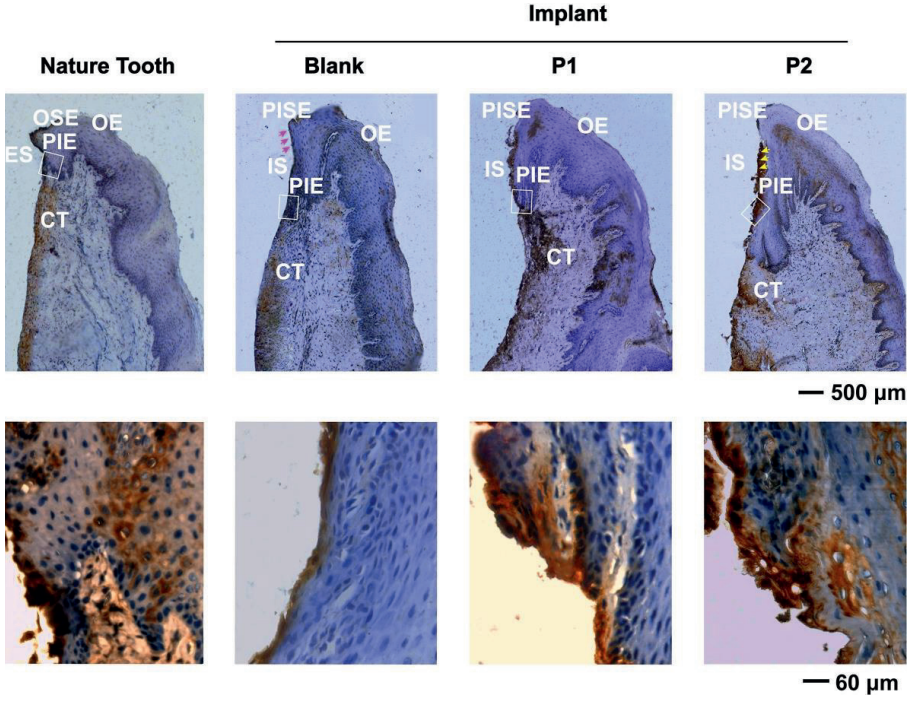
Implant
Nature Tooth
Blank
P1
P2
OSE
OE
PIE
ES
CT
PISE
IS
— 500 μm
— 60 μm

Figure 2-6 (previous page). Example of a Ti-binding peptide used for the functionalization of dental titanium implants. **(1)** Pseudo-3D representation of fusion peptides P1 and P2. While the blue fragment at the N-terminal bins to the Ti surface, the peptide at the C-terminal binds to oral epithelial cells and activates soft tissue sealing around the implant. **(2)** Relative mRNA expression levels of *Ln-5*, *Integrin α6*, *Integrin β4*, and *Plectin* genes in human oral epithelial cells. The cells were cultured for 10 days on a culturing dish, uncoated titanium surfaces (bare) and peptide-coated titanium surfaces (P1 and P2). qRT-PCR analysis revealed that P2 strongly upregulates the expression of key genes involved in soft tissue sealing. **(3)** Immuno-histochemical analysis of Ln-5 distribution. In the top row, the images show the gingival mucosa around the tooth and around implanted titanium abutments, either blank or coated with P1 and P2 peptides. The bottom row shows a magnification of selected areas (white square) indicated in the images above. For a complete interpretation of the figure, we refer the reader to the original publication. Reprinted from Liu *et al.*[290] with permission from Elsevier.

morphogenic protein BMP-2 can stabilize collagen gels around implanted Ti, affecting osteoinduction in the surrounding tissue.[292] More recently, 3D printed Ti implants were coated with a Ti-binding fusion protein, promoting angiogenesis and osteointegration both *in vitro* and *in vivo*.[293]

Growth of pathogenic bacteria on the surface of an implant leads to inflammation and infection. Therefore, to increase the chance of successful integration of an implanted device, bacterial growth must be minimized. For this reason, biofunctionalization mediated by SBPs has largely focused on the mitigation of bacterial biofilm formation using AMPs. In a first attempt, four known AMPs were fused with a Ti-binding peptide. The resulting fusion peptides could effectively coat a Ti surface, while reducing the attachment of the oral pathogen *Porphyromonas gingivalis.*[294] In a follow-up study, a rigid linker was introduced between the two peptides, improving the adsorption onto Ti surfaces and reducing the growth of *Streptococcus gordonii* and *Streptococcus sanguinis*.[295] A similar approach was explored in two related studies, where a Ti-binding peptide was fused to sequences derived from human β-defensin-3 via flexible linkers. Peptide-coated Ti substrates showed resistance to biofilm formation from *Streptococcus oralis*, *S. gordonii*, and *S. sanguinis*.[296,297] Furthermore, the addition of an RGD peptide to the design allowed for the proliferation of osteoblasts *in vitro*.[297] The efficacy of similar bifunctional designs was tested *in vitro* against *E. coli*, *Streptococcus mutans* and *Streptococcus epidermidis*.[298,299] Although the antimicrobial activity of these peptides was never tested on *in vivo* models, Wisdom *et al*. recently

proved that such peptides can efficiently bind to Ti implantable surfaces in the presence of serum proteins and resists brushing with a commercially available electric toothbrush.[300,301]

Finally, for the sake of completeness, we refer the interested reader to other successful biomedical applications of SBPs on other metal surfaces such as zinc,[99,302] stainless steel,[303] and iron.[304]

2.3.2.2. Plastics

In the last decades, plastics have become ubiquitous materials for packaging, construction, clothing, and many more applications. Synthetic polymers are exceptional materials, showing durability, chemical and physical resistance, flexibility, ease of use, and low production costs. Although most plastics are petroleum-based and non-biodegradable, they are widely used for the manufacturing of laboratory and medical equipment like catheters, membranes, surgical sutures, and implants.[305] Especially for these applications, surface biofunctionalization is needed to adequately modulate the interactions of plastic materials with biological fluids, cells, and tissues.[69,306] After the identification of multiple plastic-binding peptides mostly via phage display, many plastic surfaces have been successfully functionalized in recent years.[69,307–309] Not surprisingly, plastic-binding peptides are usually enriched in hydrophobic amino acids, while polystyrene preferably binds to peptides enriched in aromatic residues such as tryptophan (W).[72] In the current section, we will review the application of plastic-binding peptides in *in vitro* cell culturing and in the synthesis of smart materials.

A few simple designs have been developed to enhance the biocompatibility of plastic surfaces. For example, the epidermal growth factor was anchored to polystyrene dishes via a polystyrene-binding peptide.[310] The obtained surface was used for the adhesion and selective expansion of neural stem cells for neurosphere culture. In a similar approach, Waku *et al*. coated isotactic poly(methyl methacrylate) (it-PMMA) surfaces with a fusion protein featuring two plastic-binding peptides and an RGD motif for cell adhesion.[311] The protein could uniformly adsorb on it-PMMA, resulting in the effective attachment and spreading of mouse fibroblasts on the surface. In another example, polydimethylsiloxane surfaces were functionalized with an anchor peptide fused to the cell-adhesive GRGDS motif.[312] This one-step coating strategy allowed for the adhesion and proliferation of mouse fibroblasts and endothelial cells on polydimethylsiloxane. Finally, Carson *et al*. showed how

these bifunctional peptides can be harnessed to mimic the myocardial structure *in vitro*.[313] A nanopatterned polyurethane acrylate (PUA) surface was functionalized with a polypeptide featuring a PUA-binding peptide and an RGD motif. Subsequently, human stem cell-derived cardiomyocytes were cultured on the nanogrid, resulting in mature and aligned sarcomere structures.

In more recent studies, plastic-binding peptides have been included in more sophisticated designs, providing promising results for future *in vivo* applications. For example, Garay-Sarmiento *et al*. exploited a plastic-binding peptide to develop a coating for wound dressings.[314] The coating consists of two hybrid constructs adsorbed on polycaprolactone (PCL) surfaces via a PCL-binding peptide: while the first construct exhibits antifouling properties thanks to a grafted polymer block, the second construct features the bactericidal enzyme endolysin. Tests conducted *in vitro* showed that the coating could effectively repel and kill *E. coli* and *Streptococcus agalactiae*, both on flat surfaces and electrospun PCL meshes. Furthermore, the coating showed antifouling properties against fibroblasts and blood plasma proteins.
Another application was developed by Hosseinnejad *et al.* for the immobilization of an antifouling, nitric oxide-producing hydrogel for extracorporeal membrane oxygenation, as shown in Figure 2-7.[315] A plastic-binding peptide acted as anchor, allowing the facile and stable connection of the hydrogel to a hydrophobic poly(4-methylpentene) (PMP) membrane (Figure 2-7.1). Thanks to the catalytic activity of the hydrogel, the membrane inhibited platelet activation and reduced clot formation when in contact with human whole blood. A follow up study from the same authors confirmed the *in vitro* functionality of the microgel coating in a PMP catheter challenged with a blood flow (Figure 2-7.2).[316]

Finally, an extensive study by Hintzen *et al.* evaluated different plastic-binding peptides for the development of a bioadhesive coating.[317] Multifunctional fusion proteins were screened for simultaneous binding to poly(chloro-p-xylylene) (Parylene C) surfaces and the extracellular matrix of the retina. Subsequently, cytotoxicity tests with retinal progenitor cells indicated that a candidate protein showed good biocompatibility. An *ex vivo* proof-of-concept experiment with rabbit eyes proved the efficacy of the bioadhesive coating on Parylene C retinal stimulating arrays.

The examples featured in this section clearly show that plastic-binding peptides can be included in complex designs, with promising results for *in vivo*

1)

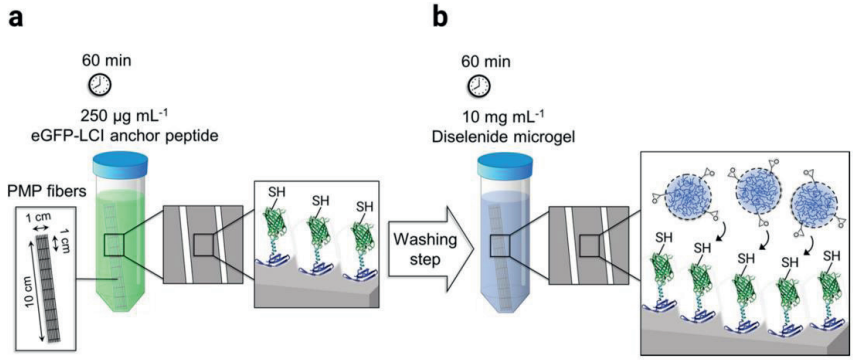
a
b
60 min
250 µg mL-1
eGFP-LCI anchor peptide
PMP fibers
1 cm
1 cm
10 cm
SH
SH
SH
Washing step
60 min
10 mg mL-1
Diselenide microgel
SH
SH
SH
SH
SH

2)

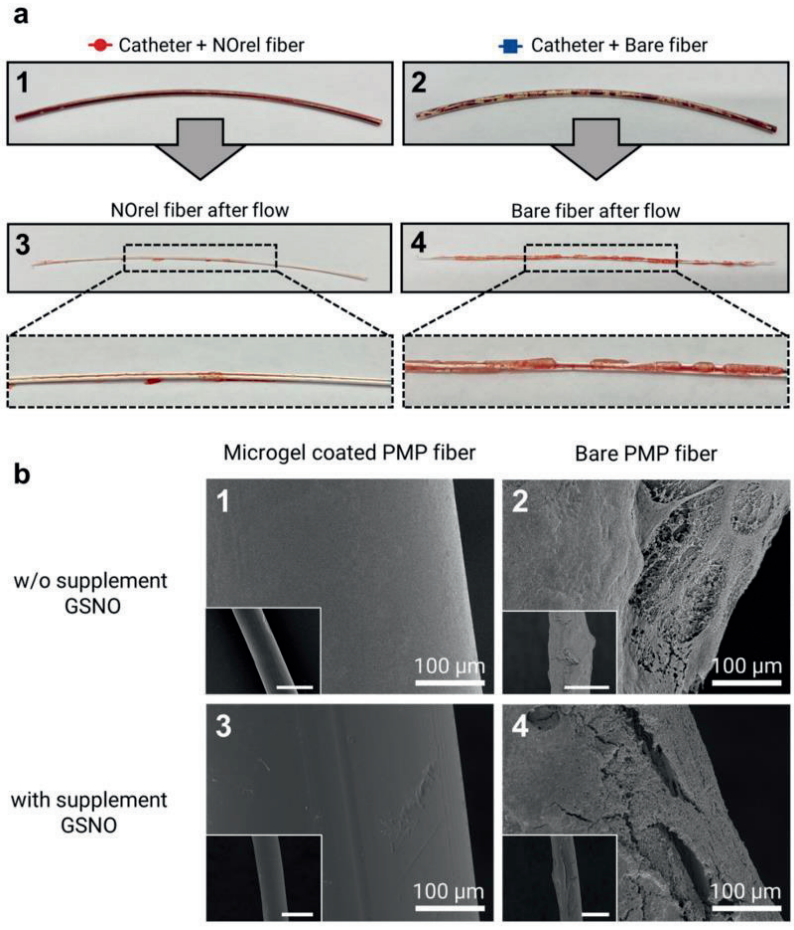
a
Catheter + NOrel fiber
Catheter + Bare fiber
1
2
NOrel fiber after flow
Bare fiber after flow
3
4
b
Microgel coated PMP fiber
Bare PMP fiber
w/o supplement GSNO
with supplement GSNO
1
2
3
4
100 µm
100 µm
100 µm
100 µm

Figure 2-7 (previous page). Plastic-binding peptides have been included in sophisticated designs. **(1)** Schematic procedure for the coating of poly(4-methylpentene) (PMP) fibers with nitric oxide-releasing microgel (NOrel). **(a)** The polymer-binding fusion protein is incubated with PMP fibers, **(b)** the microgels are immobilized to the adsorbed support via a click reaction. **(2)** The fibers were tested in blood flow experiments: **(a)** while coagulated blood can be seen in non-coated fibers, **(b)** SEM analysis showed that NOrel coated fibers can prevent the deposition of fibrin networks and platelet aggregation. Adapted from Winnersbach *et al.*[316]

applications. These examples highlight how SBPs can be effectively paired to various other functionalities, warranting biocompatibility, flexibility, and control of surface chemistry.

2.3.2.3. Graphene

Due to their unique mechanical and electrical properties, two-dimensional carbon materials such as graphene are attractive for biological and chemical sensing applications. Graphene is a metallic and fully conducting two-dimensional crystal that has justifiably received attention in recent years. Extensive research on graphene has revealed that covalent functionalization of its surface results in defects and loss of electronic properties, making non-covalent techniques largely preferred.[318] It is therefore unsurprising that many graphene-binding peptides have been isolated and characterized for a wide variety of applications.[319] Similarly to other carbon-based materials, graphene-binding peptides are enriched in aromatic amino acids.[319] The side chains of these residues most likely interact with the graphene surface through π- π stacking. Interestingly, the position of aromatic residues within the peptide seems to increase the binding affinity for certain regions of graphene sheets.[320] In the current section, we will mostly focus on biosensing applications.

In a first sensing approach, Mannoor *et al.* developed a graphene field-effect transistor (GFET) biosensor for the detection of bacterial cells.[321] At first, a graphene-binding peptide was fused to the frog-derived antimicrobial peptide odorranin-HP. The fusion protein was then adsorbed onto a graphene surface and subsequently printed onto biodegradable silk fibroin. As proof-of-concept, the resulting flexible biosensor was implanted on a bovine tooth and used for the real-time remote sensing of the pathogen *Helicobacter pylori* in human saliva. Furthermore, the sensor was interfaced with an intravenous (IV) bag to simulate its usage for biohazard monitoring in hospital sanitation.

Consequently, the sensor could detect *S. aureus* in the IV liquid at a reported concentration of 1 bacterium μL^{-1}.

Another GFET biosensor was developed by Khatayevich *et al*. for the detection of biomolecules at low concentrations.[322] More recently, Kim *et al.* developed a GFET biosensor for the detection of the neurotransmitter neuropeptide Y (NPY).[323] Via phage display, the authors identified an NPY-binding peptide and fused it to a graphene-binding peptide. The resulting protein was then adsorbed onto graphene and the sensor was analyzed using liquid-cell TEM. This technique allowed for the simultaneous testing of the sensor and the *in operando* observation of the sensor surface. As a result, the GFET device could detect NPY with pM sensitivity, even in presence of a competing molecule. A more recent study by the same authors reported a reduction of the sensor's sensitivity when used with artificial sweat, revealing a common hurdle of potentiometric sensing.[324]

Finally, Wang *et al.* explored the use of graphene-binding peptides as biocompatible material synthesizers.[325] A graphene-binding peptide was connected to the cell-binding RGD peptide via a hydrophilic elastin-like polypeptide (ELP) and used to coat reduced graphene oxide (rGO). Since ELPs show interesting stimuli-responsive properties, their adsorption onto the surface was shown to modulate the hydrophobicity and aggregation of rGO. Furthermore, the resulting surface showed improved osteoblast cell attachment compared to unmodified rGO.

In conclusion, graphene-binding peptides have been successfully explored as a facile approach for modifying graphene for biomedical applications. Despite the promising proof-of-concept experiments, it appears that more research is needed for the widespread adoption of graphene in the biomedical field.

Table 2-1. List of solid-binding peptides featured in this chapter, listed per surface in alphabetical order. We report the amino acid sequences of short peptides (<30 residues); longer peptides and domains are reported with their original nomenclature. Continued on next pages.

Target	Sequence	Application	Reference
Gold	MHGKTQATSGTIQS	Photothermal therapy, biosensing	[251,254,255,259–264], first described in [47]
	WALRRSIRRQSY	Theranostics	[252], first described in [326]
	LKAHLPPSRLPS	Biosensing	[256], first described in [327]
	WAGAKRLVLRRE	Biosensing	[265], first described in [326]
	AYSSGAPPMPPF	Material synthesis	[253], first described in [272]
Graphene	HSSYWYAFNNKT	Biosensing	[321,323,324], first described in [328]
	IMVTESSDYSSY	Biosensing	[322]
	HNWYHWWPH	Biocompatibility	[325], first described in [329]
Hydroxyapatite	Poly(E)	Osteoinductivity, material synthesis, drug delivery	[112,113,122–126,149,151–154,114,160,167,170,174,115–121]
	Poly(D)	Osteoinductivity, drug delivery	[127,128,175–177,129,130,166–169,172,173]
	γEPRRγEVAγEL	Osteoinductivity	[132–137], first described in [330]
	VTKHLNQISQSY	Osteoinductivity	[138–142], first described in [331]
	TKREEVD	Remineralization	[144,164]
	SYENSHSQAINVDRT	Remineralization	[145]

Table 2-1, continued.

Target	Sequence	Application	Reference
Hydroxyapatite (continued)	TKRQQVV	Remineralization	[146]
	DRNLGDSLHRQEI	Remineralization	[147]
	KYKQKRRSYK	Remineralization	[148]
	DpSpSEEK	Remineralization	[149]
	CMLPHHGAC	Multi-material synthesis, biocompatibility, imaging	[150,156–158,160,162,179]
	MSESDSSDSDSKS	Multi-material synthesis	[155,159]
	NNHYLPR	Biocompatibility	[161], first described in [332]
	SVSVGMKPSPRP	Biocompatibility	[163]
	$(DSS)_6$	Drug delivery	[171], first described in [333]
	STDKTKREEVD	Drug delivery	[178], first described in [334]
	KNFQSRSH	Imaging	[180]
Polycaprolactone	LCI peptide (47 amino acids)	Material synthesis	[303,314], first described in [335,336]
Poly(chloro-*p*-xylylene) (Parylene C)	LCI peptide	Material synthesis	[317]
	CecA peptide (37 amino acids)	Material synthesis	[317], first described in [337]
Polydimethylsiloxane	LCI peptide	Biocompatibility	[312,338]

Table 2-1, continued.

Target	Sequence	Application	Reference
Poly(methyl methacrylate) (PMMA)	ELWRPTR	Biocompatibility	[311], first described in [339]
Poly(4-methylpentene) (PMP)	LCI peptide	Multi-material synthesis	[315,316,338]
Polystyrene	RIIIRRIRR	Biocompatibility	[310], first described in [340]
	LCI peptide	Biocompatibility	[338]
Polyurethane acrylate (PUA)	AIRGIRGIRGIR	Biocompatibility	[313]
Silica	RGRRRRLSCRLL	Drug delivery	[207], first described in [341]
	SSKKSGSYSGSKGSKRRIL	Drug delivery, material synthesis, biosensing, biocompatibility	[198,199,228,229,232–235,200,202,205,208,211,215,217,218], first described in [342]
	L-linker (95 amino acids	Drug delivery, biosensing	[209,210,225–227], first described in [343]
	RKKRKKRKKRKKGGGY	Drug delivery	[216], first described in [344,345]
	KPTHHHHHHDG	Material synthesis, drug delivery	[219], first described in [341]
	Si-tag (273 amino acids)	Biosensing,	[222–224], first described in [16]
	SSRSSSHRRHDHHDHRRGS	Biosensing, material synthesis, biocompatibility	[203,229], first described in [346]
	DSARGFKKPGKRGGGC	Biosensing	[230], first described in [347]
	MSPHPHPRHHHT	Biocompatibility	[204,205], first described in [341]

Table 2-1, continued.

Target	Sequence	Application	Reference
Silver	NPSSLFRYLPSD	Nanoparticle synthesis, material synthesis	[269,279], first described in [272]
	Ac-(3′-PyA)LRLRLRL(3′-PyA)-$CONH_2$	Material synthesis	[270]
	AYSSGAPPMPPF	Nanoparticle synthesis	[280], first described in [272]
	EQLGVRKELRGV	Biocompatibility, material synthesis	[281,282,284], first described in [348]
	WSWRSPTPHVVT	Antimicrobial material synthesis	[283], first described in [271]
Titanium	DSSEE	Biocompatibility	[287], first described in [349]
	RPRENRGRERGL	Biocompatibility	[288,289,298–301]
	SRPNGYGGSESS	Biocompatibility	[288,298,299]
	CGHTHYHAVRTQT	Biocompatibility	[291], first described in [345]
	DYFSSPYYEQLF	Biocompatibility	[292], first described in [106,350]
	RKLPDA	Biocompatibility	[290,293–295] , first described in [54]
	RKLPDAPGMHTW	Biocompatibility	[296,297], first described in [54]
	HAYKQPVLSTPF	Biocompatibility	[298]

2.4. Outlook

In this chapter, we have collected and reviewed numerous successful applications of solid-binding peptides and proteins on biomedically relevant surfaces. We have shown that SBP-mediated bioconjugation can be easily introduced into complex designs and on nanomaterials with very different surface chemistries. The examples collected in this chapter show that SBPs can be adapted for use under various conditions, with good binding strength for the materials under consideration.

The use of material specific SBPs, however, does not always guarantee a direct translation from *in vitro* to *in vivo* applications. Like in all physical adsorption processes, the competitive replacement from proteins contained in biological fluids (Vroman effect) can compromise the functionality of SBP coatings in physiological environments.[351] The susceptibility of protein-based coatings to protease degradation is yet another factor to evaluate, especially in long term applications.[352] As a first step, exploring various molecular architectures and testing more than one SBP can provide valuable indications on which protein design is more suitable. For example, increasing the multivalency via the oriented display of multiple SBPs might be a sufficient strategy to reduce competitive displacement. Secondly, as suggested earlier by Care *et al.*, the isolation and selection conditions of a suitable SBP should appropriately mimic the physiological environment in which the SBP will have to operate.[29] Fortunately, combinatorial design strategies are flexible regarding the working conditions and they have been successfully introduced in alternative biopanning systems.[30,353–355] Moreover, the application of directed protein evolution to solid-binding peptides can compensate the shortcomings of phage display (sequence and interaction biases) and should be explored also with existing peptides.

The discovery and design of solid-binding sequences has experienced sizeable developments in the past decades. As we described in Section 2.1, many techniques are available for finding functional peptide and protein sequences, leading to large data sets that we partially collected in Table 2-1. Nevertheless, systematic engineering of new peptides and proteins is still difficult, for the following reason. As our review shows, smaller SBPs are used in biomedical applications more often than larger SBPs. Computational tools for de novo design are most successful at designing large, folded solid-binding domains and proteins. By contrast, better tools are still needed for the computational design of shorter sequences that are disordered both in solution and at solid interfaces. In these regards, the disparity between experimental quantification and molecular simulations can highly vary for different surfaces: gold and silicates, for example, are much better understood than

titanium and silver. Thus, for de novo design of SBPs for medical applications, the available methods do not align with demand.

The limited characterization of surface binding is a major constraint in the design and tailoring of solid-binding sequences. In general, only a selection of known SBPs is characterized using more than one technique, while in most cases SBP binding is described only with one technique such as QCM-D or SPR. A more thorough characterization should combine different techniques. In addition, simple adsorption models are not always the correct choice for calculating affinity constants. Since SBPs often do not bind independently and can form surface assemblies, a quantitative and qualitative estimate of surface coverage is necessary to better elucidate the binding process.[75,276,356]

Unfortunately, there is little work performing detailed physical characterization of larger sets of SBPs, which would allow for a fair comparison between the performance of different SBP sequences. Instead, for each material, a few well-characterized and validated sequences are used in many studies. This approach can obviously yield positive results, but it simultaneously creates a bias in favor of previously used sequences. Although a recent report on gold-binding peptides suggests that the binding affinity of many sequences is comparable, performing a screening might provide a practical advantage to better tailor the design to the application conditions, either *in vitro* or *in vivo*.[20]

In conclusion, solid-binding peptides, domains, and proteins are useful surface functionalization tools for the design of novel biomaterials and in the construction of new biomedical devices. Despite the theoretical and technological challenges, the promising results highlighted in this chapter clearly show that SBPs can provide a convenient alternative to covalent functionalization strategies. Moreover, the ease of use of SBPs is a major advantage for their application to new or underexplored materials that might benefit from the flexibility offered by non-covalent functionalization. Although we could not include all biomedically relevant surfaces in our review, application-driven designs could and should explore materials such as biodegradable plastics, absorbable polymers, 2D nanostructures, and gold and silver nanoclusters.

2.5. List of abbreviations

Abbreviation	Meaning
AFM	atomic force microscopy
AMP	antimicrobial peptides
AuNP	gold nanoparticles
BMP-2	bone morphogenic protein 2
CaP	calcium phosphate
ELP	elastin-like polypeptide
GFET	graphene field-effect transistor
HA	hydroxyapatite
IBP	ice-binding protein
NMR	nuclear magnetic resonance
NPY	neurotransmitter neuropeptide Y
PCL	polycaprolactone
PMP	poly(4-methylpentene)
PUA	polyurethane acrylate
QCM-D	quartz crystal microbalance with dissipation monitoring
SBP	solid-binding peptide
SMFS	single molecule force spectroscopy
SOx	sarcosine oxidase
VEGF	vascular endothelial growth factor
β-TCP	β-tricalcium phosphate

2.6. References

[1] M. S. DODD, D. PAPINEAU, T. GRENNE *ET AL.* Evidence for early life in Earth's oldest hydrothermal vent precipitates. *Nature* 543, 60–64 (2017).

[2] M. B. DICKERSON, K. H. SANDHAGE, R. R. NAIK. Protein- and peptide-directed syntheses of inorganic materials. *Chemical Reviews* 108, 4935–4978 (2008).

[3] G. K. HUNTER, J. OYOUNG, B. GROHE, M. KARTTUNEN, H. A. GOLDBERG. The flexible polyelectrolyte hypothesis of protein-biomineral interaction. *Langmuir* 26, 18639–18646 (2010).

[4] H. G. SILVERMAN, F. F. ROBERTO. Understanding marine mussel adhesion. *Marine Biotechnology* 9, 661–681 (2007).

[5] J. A. RAYMOND, C. FRITSEN, K. SHEN. An ice-binding protein from an Antarctic sea ice bacterium. *FEMS Microbiology Ecology* 61, 214–221 (2007).

[6] X. SHEN, A. M. BELCHER, P. K. HANSMA, G. D. STUCKY, D. E. MORSE. Molecular cloning and characterization of Lustrin A, a matrix protein from shell and pearl nacre of Haliotis rufescens. *Journal of Biological Chemistry* 272, 32472–32481 (1997).

[7] N. POULSEN, M. SUMPER, N. KRÖGER. Biosilica formation in diatoms: Characterization of native silaffin-2 and its role in silica morphogenesis. *Proceedings of the National Academy of Sciences of the United States of America* 100, 12075–12080 (2003).

[8] T. MATSUNAGA, T. SUZUKI, M. TANAKA, A. ARAKAKI. Molecular analysis of magnetotactic bacteria and development of functional bacterial magnetic particles for nano-biotechnology. *Trends in Biotechnology* 25, 182–188 (2007).

[9] M. RIOOL, A. DE BREIJ, J. W. DRIJFHOUT, P. H. NIBBERING, S. A. J. ZAAT. Antimicrobial peptides in biomedical device manufacturing. *Frontiers in Chemistry* AUG, 1–13 (2017).

[10] D. KHATAYEVICH, M. GUNGORMUS, H. YAZICI *ET AL.* Biofunctionalization of materials for implants using engineered peptides. *Acta Biomaterialia* 6, 4634–4641 (2010).

[11] J. C. M. SOUZA, M. B. SORDI, M. KANAZAWA *ET AL.* Nano-scale modification of titanium implant surfaces to enhance osseointegration. *Acta Biomaterialia* 94, 112–131 (2019).

[12] J. T. KOEPSEL, W. L. MURPHY. Patterned Self-Assembled Monolayers: Efficient, Chemically Defined Tools for Cell Biology. *ChemBioChem* 13, 1717–1724 (2012).

[13] J. BAGGERMAN, M. M. J. SMULDERS, H. ZUILHOF. Romantic Surfaces: A Systematic Overview of Stable, Biospecific, and Antifouling Zwitterionic Surfaces. *Langmuir* 35, 1072–1084 (2019).

[14] V. BIJU. Chemical modifications and bioconjugate reactions of nanomaterials for sensing, imaging, drug delivery and therapy. *Chemical Society Reviews* 43, 744–764 (2014).

[15] J. M. BOLIVAR, B. NIDETZKY. Positively charged mini-protein Z basic2 as a highly efficient silica binding module: Opportunities for enzyme immobilization on unmodified silica supports. *Langmuir* 28, 10040–10049 (2012).

[16] K. TANIGUCHI, K. NOMURA, Y. HATA *ET AL.* The Si-tag for immobilizing proteins on a silica surface. *Biotechnology and Bioengineering* 96, 1023–1029 (2007).

[17] P. L. DAVIES. Ice-binding proteins: a remarkable diversity of structures for stopping and starting ice growth. *Trends in Biochemical Sciences* 39, 548–555 (2014).

[18] I. K. VOETS. From ice-binding proteins to bio-inspired antifreeze materials. *Soft Matter* vol. 13 4808–4823 at https://doi.org/10.1039/c6sm02867e (2017).

[19] A. BIAŁKOWSKA, E. MAJEWSKA, A. OLCZAK, A. TWARDA-CLAPA. Ice binding proteins: Diverse biological roles and applications in different types of industry. *Biomolecules* vol. 10 at https://doi.org/10.3390/biom10020274 (2020).

[20] Z. TANG, J. P. PALAFOX-HERNANDEZ, W. C. LAW *ET AL.* Biomolecular recognition principles for bionanocombinatorics: An integrated approach to elucidate enthalpic and entropic factors. *ACS Nano* 7, 9632–9646 (2013).

[21] K. LIU, C. WANG, J. MA *ET AL.* Janus effect of antifreeze proteins on ice nucleation. *Proceedings of the National Academy of Sciences of the United States of America* 113, 14739–14744 (2016).

[22] A. CARE, P. L. BERGQUIST, A. SUNNA. Solid-binding peptides: Smart tools for nanobiotechnology. *Trends in Biotechnology* 33, 259–268 (2015).

[23] D. T. YUCESOY, D. KHATAYEVICH, C. TAMERLER, M. SARIKAYA. Rationally designed chimeric solid-binding peptides for tailoring solid interfaces. *Medical Devices & Sensors* 3, 1–12 (2020).

[24] K. PUSHPAVANAM, J. MA, Y. CAI, N. Y. NASER, F. BANEYX. Solid-Binding Proteins: Bridging Synthesis, Assembly, and Function in Hybrid and Hierarchical Materials Fabrication. *Annual Review of Chemical and Biomolecular Engineering* 12, 333–357 (2021).

[25] N. G. FISCHER, E. A. MÜNCHOW, C. TAMERLER, M. C. BOTTINO, C. APARICIO. Harnessing biomolecules for bioinspired dental biomaterials. *Journal of Materials Chemistry B* 8, 8713–8747 (2020).

[26] X. REN, Y. FENG, J. GUO *ET AL.* Surface modification and endothelialization of biomaterials as potential scaffolds for vascular tissue engineering applications. *Chemical Society Reviews* 44, 5680–5742 (2015).

[27] K. E. SAPSFORD, W. R. ALGAR, L. BERTI *ET AL.* Functionalizing nanoparticles with biological molecules: Developing chemistries that facilitate nanotechnology. *Chemical Reviews* 113, 1904–2074 (2013).

[28] Y. WANG, K. XIA, L. WANG *ET AL.* Peptide-Engineered Fluorescent Nanomaterials: Structure Design, Function Tailoring, and Biomedical Applications. *Small* 17, 1–29 (2021).

[29] A. CARE, P. L. BERGQUIST, A. SUNNA. Solid-binding peptides in biomedicine. *Advances in Experimental Medicine and Biology* 1030, 21–36 (2017).

[30] N. TEN BRUMMELHUIS, P. WILKE, H. G. BÖRNER. Identification of Functional Peptide Sequences to Lead the Design of Precision Polymers. *Macromolecular Rapid Communications* 38, 1–17 (2017).

[31] R. MOR, A. SIVAN. Biofilm formation and partial biodegradation of polystyrene by the actinomycete Rhodococcus ruber: Biodegradation of polystyrene. *Biodegradation* 19, 851–858 (2008).

[32] I. CACCIARI, P. QUATRINI, G. ZIRLETTA *ET AL.* Isotactic polypropylene biodegradation by a microbial community: Physicochemical characterization of metabolites produced. *Applied and Environmental Microbiology* 59, 3695–3700 (1993).

[33] Y. P. DU, H. H. CHANG, S. Y. YANG *ET AL.* Study of binding interaction between Pif80 protein fragment and aragonite. *Scientific Reports* 6, 1–10 (2016).

[34] P. WILKE, H. G. BÖRNER. Mussel-glue derived peptide-polymer conjugates to realize enzyme-activated antifouling coatings. *ACS Macro Letters* 1, 871–875 (2012).

[35] N. HOLTEN-ANDERSEN, J. H. WAITE. Mussel-designed protective coatings for compliant substrates. *Journal of Dental Research* 87, 701–709 (2008).

[36] P. S. HUANG, S. E. BOYKEN, D. BAKER. The coming of age of de novo protein design.

Nature 537, 320–327 (2016).

[37] H. PYLES, S. ZHANG, J. J. DE YOREO, D. BAKER. Controlling protein assembly on inorganic crystals through designed protein interfaces. *Nature* 571, 251–256 (2019).

[38] M. S. PACELLA, J. J. GRAY. A Benchmarking Study of Peptide-Biomineral Interactions. *Crystal Growth and Design* 18, 607–616 (2018).

[39] Z. XU, Q. WEI, W. ZHAO, Q. CUI, N. SAHAI. Essence of Small Molecule-Mediated Control of Hydroxyapatite Growth: Free Energy Calculations of Amino Acid Side Chain Analogues. *Journal of Physical Chemistry C* 122, 4372–4380 (2018).

[40] M. S. PACELLA, D. C. E. KOO, R. A. THOTTUNGAL, J. J. GRAY. *Using the Rosetta surface algorithm to predict protein structure at mineral surfaces*. *Methods in Enzymology* vol. 532 (Elsevier Inc., 2013).

[41] D. L. MASICA, J. J. GRAY. Solution- and adsorbed-state structural ensembles predicted for the statherin-hydroxyapatite system. *Biophysical Journal* 96, 3082–3091 (2009).

[42] K. MAKRODIMITRIS, D. L. MASICA, E. T. KIM, J. J. GRAY. Structure prediction of protein-solid surface interactions reveals a molecular recognition motif of statherin for hydroxyapatite. *Journal of the American Chemical Society* 129, 13713–13722 (2007).

[43] Z. E. HUGHES, M. A. NGUYEN, J. WANG *ET AL.* Tuning Materials-Binding Peptide Sequences toward Gold- And Silver-Binding Selectivity with Bayesian Optimization. *ACS Nano* 15, 18260–18269 (2021).

[44] T. R. WALSH. Pathways to Structure-Property Relationships of Peptide-Materials Interfaces: Challenges in Predicting Molecular Structures. *Accounts of Chemical Research* 50, 1617–1624 (2017).

[45] X. PAN, T. KORTEMME. Recent advances in de novo protein design: Principles, methods, and applications. *Journal of Biological Chemistry* 296, 100558 (2021).

[46] S. GP. Filamentous fusion phage: novel expression vectors that display cloned antigens on the virion surface. *Science* 228, 1315–1317 (1985).

[47] S. BROWN. Metal-recognition by repeating polypeptides. *Nature Biotechnology* 15, 269–272 (1997).

[48] S. BROWN. Engineered iron oxide-adhesion mutants of the Escherichia coli phage λ receptor. *Proceedings of the National Academy of Sciences of the United States of America* 89, 8651–8655 (1992).

[49] G. P. SMITH, V. A. PETRENKO. Phage Display. *Chemical Reviews* 97, 391–410 (1997).

[50] R. LIU, A. M. ENSTROM, K. S. LAM. Combinatorial peptide library methods for immunobiology research. *Experimental Hematology* 31, 11–30 (2003).

[51] J. GUO, J. M. CATCHMARK, M. N. A. MOHAMED *ET AL.* Identification and characterization of a cellulose binding heptapeptide revealed by phage display. *Biomacromolecules* 14, 1795–1805 (2013).

[52] D. ROTHENSTEIN, B. CLAASEN, B. OMIECIENSKI, P. LAMMEL, J. BILL. Isolation of ZnO-binding 12-mer peptides and determination of their binding epitopes by NMR spectroscopy. *Journal of the American Chemical Society* 134, 12547–12556 (2012).

[53] T. SCHWEMMER, J. BAUMGARTNER, D. FAIVRE, H. G. BÖRNER. Peptide-mediated nanoengineering of inorganic particle surfaces: A General route toward surface functionalization via peptide adhesion domains. *Journal of the American Chemical Society* 134, 2385–2391 (2012).

[54] K. I. SANO, K. SHIBA. A Hexapeptide Motif that Electrostatically Binds to the Surface of Titanium. *Journal of the American Chemical Society* 125, 14234–14235 (2003).

[55] M. GUNGORMUS, H. FONG, I. W. KIM *ET AL.* Regulation of in vitro calcium phosphate

mineralization by combinatorially selected hydroxyapatite-binding peptides. *Biomacromolecules* 9, 966–973 (2008).

[56] W. J. CHUNG, K. Y. KWON, J. SONG, S. W. LEE. Evolutionary screening of collagen-like peptides that nucleate hydroxyapatite crystals. *Langmuir* 27, 7620–7628 (2011).

[57] C. Y. CHIU, Y. LI, Y. HUANG. Size-controlled synthesis of Pd nanocrystals using a specific multifunctional peptide. *Nanoscale* 2, 927–930 (2010).

[58] H. HEINZ, B. L. FARMER, R. B. PANDEY *ET AL.* Nature of molecular interactions of peptides with gold, palladium, and Pd-Au bimetal surfaces in aqueous solution. *Journal of the American Chemical Society* 131, 9704–9714 (2009).

[59] C. JUDS, J. SCHMIDT, M. G. WELLER *ET AL.* Combining Phage Display and Next-Generation Sequencing for Materials Sciences: A Case Study on Probing Polypropylene Surfaces. *Journal of the American Chemical Society* 142, 10624–10628 (2020).

[60] H. EJIMA, H. MATSUNO, T. SERIZAWA. Biological identification of peptides that specifically bind to poly(phenylene vinylene) surfaces: Recognition of the branched or linear structure of the conjugated polymer. *Langmuir* 26, 17278–17285 (2010).

[61] Y. KUMADA, Y. TOKUNAGA, H. IMANAKA *ET AL.* Screening and characterization of affinity peptide tags specific to polystyrene supports for the orientated immobilization of proteins. *Biotechnology Progress* 22, 401–405 (2006).

[62] N. B. ADEY, A. H. MATARAGNON, J. E. RIDER, J. M. CARTER, B. K. KAY. Characterization of phage that bind plastic from phage-displayed random peptide libraries. *Gene* 156, 27–31 (1995).

[63] S. JU, K. Y. LEE, S. J. MIN *ET AL.* Single-carbon discrimination by selected peptides for individual detection of volatile organic compounds. *Scientific Reports* 5, 1–6 (2015).

[64] S. SWAMINATHAN, M. BULLOUGH, Q. LI, A. ZHOU, Y. CUI. Non-lithographic patterning of phage-displayed peptides with wrinkled elastomers. *Journal of the Royal Society Interface* 11, (2014).

[65] S. R. WHALEY, D. S. ENGLISH, E. L. HU, P. F. BARBARA, A. M. BELCHER. Selection of peptides with semiconductor binding specificity for directed nanocrystal assembly. *Nature* 405, 665–668 (2000).

[66] D. GEBAUER, A. VERCH, H. G. BÖRNER, H. CÖLFEN. Influence of selected artificial peptides on calcium carbonate precipitation - A quantitative studyp. *Crystal Growth and Design* 9, 2398–2403 (2009).

[67] U. O. S. SEKER, H. V. DEMIR. Material binding peptides for nanotechnology. *Molecules* 16, 1426–1451 (2011).

[68] F. BREITLING, A. NESTEROV, V. STADLER, T. FELGENHAUER, F. R. BISCHOFF. High-density peptide arrays. *Molecular BioSystems* 5, 224–234 (2009).

[69] K. RÜBSAM, L. WEBER, F. JAKOB, U. SCHWANEBERG. Directed evolution of polypropylene and polystyrene binding peptides. *Biotechnology and Bioengineering* 115, 321–330 (2018).

[70] Y. WANG, X. YU, H. ZHAO. Biosystems design by directed evolution. *AIChE Journal* 66, 1–10 (2020).

[71] S. DEDISCH, A. WIENS, M. D. DAVARI *ET AL.* Matter-tag: A universal immobilization platform for enzymes on polymers, metals, and silicon-based materials. *Biotechnology and Bioengineering* 117, 49–61 (2020).

[72] K. RÜBSAM, M. D. DAVARI, F. JAKOB, U. SCHWANEBERG. KnowVolution of the polymer-binding peptide LCI for improved polypropylene binding. *Polymers* 10, 1–12 (2018).

[73] G. GÜVEN, R. PRODANOVIC, U. SCHWANEBERG. Protein engineering - an option for

enzymatic biofuel cell design. *Electroanalysis* 22, 765–775 (2010).

[74] R. BANSAL, A. CARE, M. S. LORD, T. R. WALSH, A. SUNNA. Experimental and theoretical tools to elucidate the binding mechanisms of solid-binding peptides. *New Biotechnology* 52, 9–18 (2019).

[75] N. ALVISI, F. A. GUTIÉRREZ-MEJÍA, M. LOKKER *ET AL.* Self-assembly of elastin-like polypeptide brushes on silica surfaces and nanoparticles. *Biomacromolecules* 22, 1966–1979 (2021).

[76] C. R. SO, C. TAMERLER, M. SARIKAYA. Adsorption, diffusion, and self-assembly of an engineered goldbinding peptide on Au(111) investigated by atomic force microscopy. *Angewandte Chemie - International Edition* 48, 5174–5177 (2009).

[77] A. M. SULTAN, Z. C. WESTCOTT, Z. E. HUGHES *ET AL.* Aqueous Peptide-TiO2 Interfaces: Isoenergetic Binding via Either Entropically or Enthalpically Driven Mechanisms. *ACS Applied Materials and Interfaces* 8, 18620–18630 (2016).

[78] A. GLADYTZ, T. JOHN, T. GLADYTZ *ET AL.* Peptides@mica: from affinity to adhesion mechanism. *Phys. Chem. Chem. Phys.* 18, 23516–23527 (2016).

[79] E. NAKOUZI, S. YADAV, B. A. LEGG *ET AL.* Visualizing Solution Structure at Solid-Liquid Interfaces using Three-Dimensional Fast Force Mapping. *Journal of visualized experiments : JoVE* (2021) doi:10.3791/62585.

[80] X. MA, S. ZHANG, F. JIAO *ET AL.* Tuning crystallization pathways through sequence engineering of biomimetic polymers. *Nature Materials* 16, 767–774 (2017).

[81] K. C. NEUMAN, A. NAGY. Single-molecule force spectroscopy: Optical tweezers, magnetic tweezers and atomic force microscopy. *Nature Methods* 5, 491–505 (2008).

[82] A. LEADER, D. MANDLER, M. RECHES. The role of hydrophobic, aromatic and electrostatic interactions between amino acid residues and a titanium dioxide surface. *Physical Chemistry Chemical Physics* 20, 29811–29816 (2018).

[83] Z. KUANG, S. N. KIM, W. J. CROOKES-GOODSON, B. L. FARMER, R. R. NAIK. Biomimetic chemosensor: Designing peptide recognition elements for surface functionalization of carbon nanotube field effect transistors. *ACS Nano* 4, 452–458 (2010).

[84] A. S. OUDE VRIELINK, A. ALOI, L. L. C. OLIJVE, I. K. VOETS. Interaction of ice binding proteins with ice, water and ions. *Biointerphases* 11, 018906 (2016).

[85] S. KASUGAI, T. NAGATA, J. SODEK. Temporal studies on the tissue compartmentalization of bone sialoprotein (BSP), osteopontin (OPN), and SPARC protein during bone formation In Vitro. *Journal of Cellular Physiology* 152, 467–477 (1992).

[86] K. L. MORRISON, G. A. WEISS. Combinatorial alanine-scanning. *Current Opinion in Chemical Biology* 5, 302–307 (2001).

[87] A. D. J. HAYMET, L. G. WARD, M. M. HARDING, C. A. KNIGHT. Valine substituted winter flounder 'antifreeze': Preservation of ice growth hysteresis. *FEBS Letters* 430, 301–306 (1998).

[88] M. A. A. ABDELHAMID, T. IKEDA, K. MOTOMURA *ET AL.* Application of volcanic ash particles for protein affinity purification with a minimized silica-binding tag. *Journal of Bioscience and Bioengineering* 122, 633–638 (2016).

[89] H. CHEN, X. SU, K. G. NEOH, W. S. CHOE. Probing the interaction between peptides and metal oxides using point mutants of a TiO2-binding peptide. *Langmuir* 24, 6852–6857 (2008).

[90] C. LIU, D. L. STEER, H. SONG, L. HE. Superior Binding of Proteins on a Silica Surface: Physical Insight into the Synergetic Contribution of Polyhistidine and a Silica-Binding Peptide. *Journal of Physical Chemistry Letters* 13, 1609–1616 (2022).

[91] A. H. MAO, S. L. CRICK, A. VITALIS, C. L. CHICOINE, R. V. PAPPU. Net charge per residue modulates conformational ensembles of intrinsically disordered proteins. *Proceedings of the National Academy of Sciences of the United States of America* 107, 8183–8188 (2010).

[92] T. IKEDA, K. MOTOMURA, Y. AGOU *ET AL.* The silica-binding Si-tag functions as an affinity tag even under denaturing conditions. *Protein Expression and Purification* 77, 173–177 (2011).

[93] R. VAN DER LEE, M. BULJAN, B. LANG *ET AL.* Classification of intrinsically disordered regions and proteins. *Chemical Reviews* 114, 6589–6631 (2014).

[94] T. IKEDA, A. KURODA. Why does the silica-binding protein ' Si-tag' bind strongly to silica surfaces? Implications of conformational adaptation of the intrinsically disordered polypeptide to solid surfaces. *Colloids and Surfaces B: Biointerfaces* 86, 359–363 (2011).

[95] K. RÜBSAM, B. STOMPS, A. BÖKER, F. JAKOB, U. SCHWANEBERG. Anchor peptides: A green and versatile method for polypropylene functionalization. *Polymer* 116, 124–132 (2017).

[96] A. L. BOSKEY, E. VILLARREAL-RAMIREZ. Intrinsically disordered proteins and biomineralization. *Matrix Biology* 52–54, 43–59 (2016).

[97] S. P. GRAETHERT, M. J. KULPER, S. M. GAGNÉ *ET AL.* β-Helix structure and ice-binding properties of a hyperactive antifreeze protein from an insect. *Nature* 406, 325–328 (2000).

[98] R. HASSERT, M. PAGEL, Z. MING *ET AL.* Biocompatible silicon surfaces through orthogonal click chemistries and a high affinity silicon oxide binding peptide. *Bioconjugate Chemistry* 23, 2129–2137 (2012).

[99] N. H. CHO, T. C. CHEONG, J. H. MIN *ET AL.* A multifunctional core-shell nanoparticle for dendritic cell-based cancer immunotherapy. *Nature Nanotechnology* 6, 675–682 (2011).

[100] R. BANSAL, Z. ELGUNDI, S. C. GOODCHILD *ET AL.* The effect of oligomerization on a solid-binding peptide binding to silica-based materials. *Nanomaterials* 10, 1–17 (2020).

[101] U. O. S. SEKER, B. WILSON, D. SAHIN, C. TAMERLER, M. SARIKAYA. Quantitative affinity of genetically engineered repeating polypeptides to inorganic surfaces. *Biomacromolecules* 10, 250–257 (2009).

[102] C. FASTING, C. A. SCHALLEY, M. WEBER *ET AL.* Multivalency as a chemical organization and action principle. *Angewandte Chemie - International Edition* 51, 10472–10498 (2012).

[103] B. GABRYELCZYK, G. R. SZILVAY, V. K. SINGH *ET AL.* Engineering of the function of diamond-like carbon binding peptides through structural design. *Biomacromolecules* 16, 476–482 (2015).

[104] W. TANG, Y. MA, S. XIE *ET AL.* Valency-dependent affinity of bioactive hydroxyapatite-binding dendrons. *Biomacromolecules* 14, 3304–3313 (2013).

[105] B. A. HELMS, S. W. A. REULEN, S. NIJHUIS *ET AL.* High-affinity peptide-based collagen targeting using synthetic phage mimics: From phage display to dendrimer display. *Journal of the American Chemical Society* 131, 11683–11685 (2009).

[106] K. I. SANO, K. AJIMA, K. IWAHORI *ET AL.* Endowing a ferritin-like cage protein with high affinity and selectivity for certain inorganic materials. *Small* 1, 826–832 (2005).

[107] A. V. TERSKIKH, J. M. LE DOUSSAL, R. CRAMERI *ET AL.* 'Peptabody': A new type of high avidity binding protein. *Proceedings of the National Academy of Sciences of the*

United States of America 94, 1663–1668 (1997).

[108] R. Z. LEGEROS. Calcium phosphate-based osteoinductive materials. *Chemical Reviews* 108, 4742–4753 (2008).

[109] A. AKESON, A. HERMAN, D. WIGINTON, J. GREENBERG. Endothelial cell activation in a VEGF-A gradient: Relevance to cell fate decisions. *Microvascular Research* 80, 65–74 (2010).

[110] R. R. CHEN, E. A. SILVA, W. W. YUEN, D. J. MOONEY. Spatio-temporal VEGF and PDGF delivery patterns blood vessel formation and maturation. *Pharmaceutical Research* 24, 258–264 (2007).

[111] F. BORCARD, D. STAEDLER, H. COMAS *ET AL.* Chemical functionalization of bioceramics to enhance endothelial cells adhesion for tissue engineering. *Journal of Medicinal Chemistry* 55, 7988–7997 (2012).

[112] R. FUJISAWA, M. MIZUNO, Y. NODASAKA, K. YOSHINORI. Attachment of osteoblastic cells to hydroxyapatite crystals by a synthetic peptide (Glu7-Pro-Arg-Gly-Asp-Thr) containing two functional sequences of bone sialoprotein. *Matrix Biology* 16, 21–28 (1997).

[113] D. ITOH, S. YONEDA, S. KURODA *ET AL.* Enhancement of osteogenesis on hydroxyapatite surface coated with synthetic peptide (EEEEEEEPRGDT) in vitro. *Journal of Biomedical Materials Research* 62, 292–298 (2002).

[114] B. K. CULPEPPER, W. M. WEBB, P. P. BONVALLET, S. L. BELLIS. Tunable delivery of bioactive peptides from hydroxyapatite biomaterials and allograft bone using variable-length polyglutamate domains. *Journal of Biomedical Materials Research - Part A* 102, 1008–1016 (2014).

[115] A. A. SAWYER, K. M. HENNESSY, S. L. BELLIS. The effect of adsorbed serum proteins, RGD and proteoglycan-binding peptides on the adhesion of mesenchymal stem cells to hydroxyapatite. *Biomaterials* 28, 383–392 (2007).

[116] J. BAIN, B. CULPEPPER, M. REDDY, S. BELLIS. Comparing Variable-Length Polyglutamate Domains to Anchor an Osteoinductive Collagen-Mimetic Peptide to Diverse Bone Grafting Materials. *The International Journal of Oral & Maxillofacial Implants* 29, 1437–1445 (2014).

[117] B. K. CULPEPPER, P. P. BONVALLET, M. S. REDDY, S. PONNAZHAGAN, S. L. BELLIS. Polyglutamate directed coupling of bioactive peptides for the delivery of osteoinductive signals on allograft bone. *Biomaterials* 34, 1506–1513 (2013).

[118] J. L. BAIN, P. P. BONVALLET, R. V. ABOU-ARRAJ *ET AL.* Enhancement of the Regenerative Potential of Anorganic Bovine Bone Graft Utilizing a Polyglutamate-Modified BMP2 Peptide with Improved Binding to Calcium-Containing Materials. *Tissue Engineering - Part A* 21, 2426–2436 (2015).

[119] Y. XI, X. MIAO, Y. LI *ET AL.* BMP2-mimicking peptide modified with E7 coupling to calcined bovine bone enhanced bone regeneration associating with activation of the Runx2/SP7 signaling axis. *Journal of Biomedical Materials Research - Part B Applied Biomaterials* 108, 80–93 (2020).

[120] W. CUI, Q. LIU, L. YANG *ET AL.* Sustained Delivery of BMP-2-Related Peptide from the True Bone Ceramics/Hollow Mesoporous Silica Nanoparticles Scaffold for Bone Tissue Regeneration. *ACS Biomaterials Science and Engineering* 4, 211–221 (2018).

[121] J. LUO, H. ZHANG, J. ZHU *ET AL.* 3-D mineralized silk fibroin/polycaprolactone composite scaffold modified with polyglutamate conjugated with BMP-2 peptide for bone tissue engineering. *Colloids and Surfaces B: Biointerfaces* 163, 369–378 (2018).

[122] L. WENG, S. K. BODA, H. WANG *ET AL.* Novel 3D Hybrid Nanofiber Aerogels Coupled with

BMP-2 Peptides for Cranial Bone Regeneration. *Advanced Healthcare Materials* 7, 1–16 (2018).

[123] A. POLINI, J. WANG, H. BAI *ET AL.* Stable biofunctionalization of hydroxyapatite (HA) surfaces by HA-binding/osteogenic modular peptides for inducing osteogenic differentiation of mesenchymal stem cells. *Biomaterials Science* 2, 1779–1786 (2014).

[124] N. W. PENSA, A. S. CURRY, M. S. REDDY, S. L. BELLIS. The addition of a polyglutamate domain to the angiogenic QK peptide improves peptide coupling to bone graft materials leading to enhanced endothelial cell activation. *PLoS ONE* 14, 1–15 (2019).

[125] N. W. PENSA, A. S. CURRY, M. S. REDDY, S. L. BELLIS. Sustained delivery of the angiogenic QK peptide through the use of polyglutamate domains to control peptide release from bone graft materials. *Journal of Biomedical Materials Research - Part A* 107, 2764–2773 (2019).

[126] A. S. CURRY, D. T. MCPHERSON, A. M. BARLOW *ET AL.* Addition of an oligoglutamate domain to bone morphogenic protein 2 confers binding to hydroxyapatite materials and induces osteoblastic signaling. *PLoS ONE* 14, 1–15 (2019).

[127] T. SUN, K. ZHOU, M. LIU *ET AL.* Loading of BMP-2-related peptide onto three-dimensional nano-hydroxyapatite scaffolds accelerates mineralization in critical-sized cranial bone defects. *Journal of Tissue Engineering and Regenerative Medicine* 12, 864–877 (2018).

[128] C. MENG, W. SU, M. LIU *ET AL.* Controlled delivery of bone morphogenic protein-2-related peptide from mineralised extracellular matrix-based scaffold induces bone regeneration. *Materials Science and Engineering C* 126, 112182 (2021).

[129] T. SUN, Y. QU, W. CUI *ET AL.* Evaluation of osteogenic inductivity of a novel BMP2-mimicking peptide P28 and P28-containing bone composite. *Journal of Biomedical Materials Research - Part A* 106, 210–220 (2018).

[130] L. YANG, J. HUANG, S. YANG *ET AL.* Bone Regeneration Induced by Local Delivery of a Modified PTH-Derived Peptide from Nanohydroxyapatite/Chitosan Coated True Bone Ceramics. *ACS Biomaterials Science and Engineering* 4, 3246–3258 (2018).

[131] M. GILBERT, W. J. SHAW, J. R. LONG *ET AL.* Chimeric peptides of statherin and osteopontin that bind hydroxyapatite and mediate cell adhesion. *Journal of Biological Chemistry* 275, 16213–16218 (2000).

[132] J. S. LEE, J. S. LEE, A. WAGONER-JOHNSON, W. L. MURPHY. Modular Peptide Growth Factors for Substrate-Mediated Stem Cell Differentiation. *Angewandte Chemie* 121, 6384–6387 (2009).

[133] S. H. BROUNTS, J. S. LEE, S. WEINBERG *ET AL.* High affinity binding of an engineered, modular peptide to bone tissue. *Molecular Pharmaceutics* 10, 2086–2090 (2013).

[134] J. S. LEE, J. S. LEE, W. L. MURPHY. Modular peptides promote human mesenchymal stem cell differentiation on biomaterial surfaces. *Acta Biomaterialia* 6, 21–28 (2010).

[135] Y. LU, J. S. LEE, B. NEMKE *ET AL.* Coating with a Modular Bone Morphogenetic Peptide Promotes Healing of a Bone-Implant Gap in an Ovine Model. *PLoS ONE* 7, 1–7 (2012).

[136] J. S. LEE, A. J. WAGONER JOHNSON, W. L. MURPHY. A modular, hydroxyapatite-binding version of vascular endothelial growth factor. *Advanced Materials* 22, 5494–5498 (2010).

[137] D. SUÁREZ-GONZÁLEZ, J. S. LEE, S. K. LAN LEVENGOOD, R. VANDERBY, W. L. MURPHY. Mineral coatings modulate β-TCP stability and enable growth factor binding and release. *Acta Biomaterialia* 8, 1117–1124 (2012).

[138] H. RAMARAJU, S. J. MILLER, D. H. KOHN. Dual-functioning phage-derived peptides

encourage human bone marrow cell-specific attachment to mineralized biomaterials. *Connective Tissue Research* 55, 160–163 (2014).

[139] J. RAMASWAMY, H. K. NAM, H. RAMARAJU, N. E. HATCH, D. H. KOHN. Inhibition of osteoblast mineralization by phosphorylated phage-derived apatite-specific peptide. *Biomaterials* 73, 120–130 (2015).

[140] H. RAMARAJU, S. J. MILLER, D. H. KOHN. Dual-functioning peptides discovered by phage display increase the magnitude and specificity of BMSC attachment to mineralized biomaterials. *Biomaterials* 134, 1–12 (2017).

[141] N. DINJASKI, R. PLOWRIGHT, S. ZHOU *ET AL.* Osteoinductive recombinant silk fusion proteins for bone regeneration. *Acta Biomaterialia* 49, 127–139 (2017).

[142] H. RAMARAJU, D. H. KOHN. Cell and Material-Specific Phage Display Peptides Increase iPS-MSC Mediated Bone and Vasculature Formation In Vivo. *Advanced Healthcare Materials* 8, 1–11 (2019).

[143] W. N. ADDISON, S. J. MILLER, J. RAMASWAMY *ET AL.* Phosphorylation-dependent mineral-type specificity for apatite-binding peptide sequences. *Biomaterials* 31, 9422–9430 (2010).

[144] S. HAN, Y. FAN, Z. ZHOU *ET AL.* Promotion of enamel caries remineralization by an amelogenin-derived peptide in a rat model. *Archives of Oral Biology* 73, 66–71 (2017).

[145] S. DOGAN, H. FONG, D. T. YUCESOY *ET AL.* Biomimetic Tooth Repair: Amelogenin-Derived Peptide Enables in Vitro Remineralization of Human Enamel. *ACS Biomaterials Science and Engineering* 4, 1788–1796 (2018).

[146] X. PENG, S. HAN, K. WANG *ET AL.* The amelogenin-derived peptide TVH-19 promotes dentinal tubule occlusion and mineralization. *Polymers* 13, (2021).

[147] L. DING, S. HAN, X. PENG *ET AL.* Tuftelin-derived peptide facilitates remineralization of initial enamel caries in vitro. *Journal of Biomedical Materials Research - Part B Applied Biomaterials* 108, 3261–3269 (2020).

[148] Y. S. LEE, Y. H. PARK, D. S. LEE *ET AL.* Tubular dentin regeneration using a cpne7-derived functional peptide. *Materials* 13, 1–21 (2020).

[149] K. WANG, X. WANG, H. LI *ET AL.* A statherin-derived peptide promotes hydroxyapatite crystallization and in situ remineralization of artificial enamel caries. *RSC Advances* 8, 1647–1655 (2018).

[150] Q. YE, P. SPENCER, E. YUCA, C. TAMERLER. Engineered Peptide Repairs Defective Adhesive–Dentin Interface. *Macromolecular Materials and Engineering* 302, 1–6 (2017).

[151] E. WANG, S. H. LEE, S. W. LEE. Elastin-like polypeptide based hydroxyapatite bionanocomposites. *Biomacromolecules* 12, 672–680 (2011).

[152] H. J. KIM, D. LEE, S. CHO *ET AL.* Improvement of the Bonding Properties of Mineral Trioxide Aggregate by Elastin-Like Polypeptide Supplementation. *Scanning* 2019, (2019).

[153] H. J. KIM, W. S. LEE, J. JEONG *ET AL.* Effect of elastin-like polypeptide incorporation on the adhesion maturation of mineral trioxide aggregates. *Journal of Biomedical Materials Research - Part B Applied Biomaterials* 108, 2847–2856 (2020).

[154] J. H. JANG, S. SHIN, H. J. KIM *ET AL.* Improvement of physical properties of calcium phosphate cement by elastin-like polypeptide supplementation. *Scientific Reports* 8, 1–11 (2018).

[155] V. J. NEUBAUER, T. SCHEIBEL. Spider Silk Fusion Proteins for Controlled Collagen Binding and Biomineralization. *ACS Biomaterials Science and Engineering* 6, 5599–

5608 (2020).

[156] K. IIJIMA, H. NAGAHAMA, A. TAKADA *ET AL.* Surface functionalization of polymer substrates with hydroxyapatite using polymer-binding peptides. *Journal of Materials Chemistry B* 4, 3651–3659 (2016).

[157] E. YUCA, S. X. XIE, L. SONG *ET AL.* Reconfigurable dual peptide tethered polymer system offers a synergistic solution for next generation dental adhesives. *International Journal of Molecular Sciences* 22, (2021).

[158] X. WU, S. MAHALINGAM, S. K. VANOOSTEN *ET AL.* New Generation of Tunable Bioactive Shape Memory Mats Integrated with Genetically Engineered Proteins. *Macromolecular Bioscience* 17, 1–8 (2017).

[159] I. LAURIA, C. DICKMEIS, J. RÖDER *ET AL.* Engineered Potato virus X nanoparticles support hydroxyapatite nucleation for improved bone tissue replacement. *Acta Biomaterialia* 62, 317–327 (2017).

[160] Y. Y. LIN, J. SCHUPHAN, C. DICKMEIS *ET AL.* Attachment of Ultralow Amount of Engineered Plant Viral Nanoparticles to Mesenchymal Stem Cells Enhances Osteogenesis and Mineralization. *Advanced Healthcare Materials* 9, 1–13 (2020).

[161] Z. BIN HUANG, X. SHI, J. MAO, S. Q. GONG. Design of a hydroxyapatite-binding antimicrobial peptide with improved retention and antibacterial efficacy for oral pathogen control. *Scientific Reports* 6, 1–11 (2016).

[162] H. YAZICI, G. HABIB, K. BOONE *ET AL.* Self-assembling antimicrobial peptides on nanotubular titanium surfaces coated with calcium phosphate for local therapy. *Materials Science and Engineering C* 94, 333–343 (2019).

[163] R. FATEME, G. FATEMEH, S. SIMA, A. MOSHAVERINIA, S. HASANNIA. New Engineered Fusion Peptide with Dual Functionality: Antibacterial and Strong Binding to Hydroxyapatite. *International Journal of Peptide Research and Therapeutics* 1629–1639 (2020) doi:10.1007/s10989-019-09963-8.

[164] X. WANG, Y. WANG, K. WANG *ET AL.* Bifunctional anticaries peptides with antibacterial and remineralizing effects. *Oral Diseases* 25, 488–496 (2019).

[165] I. MCCARTHY. The Physiology of Bone Blood Flow: A Review. *Journal of Bone and Joint Surgery* 88, 4–9 (2006).

[166] K. YOKOGAWA, K. MIYA, T. SEKIDO *ET AL.* Selective delivery of estradiol to bone by aspartic acid oligopeptide and its effects on ovariectomized mice. *Endocrinology* 142, 1228–1233 (2001).

[167] L. OUYANG, J. ZHANG, J. PAN, L. YAN, L. GUO. Synthesis and preliminary evaluation in vitro of novel naproxen-dendritic peptide conjugates Synthesis and preliminary evaluation in vitro of novel naproxen-dendritic peptide conjugates L. Ouyang et al. *Drug Delivery* 16, 348–356 (2009).

[168] J. PAN, L. MA, B. LI, Y. LI, L. GUO. Novel dendritic naproxen prodrugs with poly(aspartic Acid) Oligopeptide: Synthesis and hydroxyapatite binding in vitro. *Synthetic Communications* 42, 3441–3454 (2012).

[169] J. L. MILLÁN, S. NARISAWA, I. LEMIRE *ET AL.* Enzyme replacement therapy for murine hypophosphatasia. *Journal of Bone and Mineral Research* 23, 777–787 (2008).

[170] S. TOMATSU, A. M. MONTÃO, V. C. DUNG *ET AL.* Enhancement of drug delivery: Enzyme-replacement therapy for murine morquio a syndrome. *Molecular Therapy* 18, 1094–1102 (2010).

[171] G. ZHANG, B. GUO, H. WU *ET AL.* A delivery system targeting bone formation surfaces to facilitate RNAi-based anabolic therapy. *Nature Medicine* 18, 307–314 (2012).

[172] T. JIANG, X. YU, E. J. CARBONE *ET AL.* Poly aspartic acid peptide-linked PLGA based nanoscale particles: Potential for bone-targeting drug delivery applications. *International Journal of Pharmaceutics* 475, 547–557 (2014).

[173] L. ZHANG, H. CAO, J. ZHANG *ET AL.* Comparative study of (Asp)7-CHOL-modified liposome prepared using pre-insertion and post-insertion methods for bone targeting in vivo. *Journal of Drug Targeting* 25, 149–155 (2017).

[174] X. KE, W. LIN, X. LI *ET AL.* Synergistic dual-modified liposome improves targeting and therapeutic efficacy of bone metastasis from breast cancer. *Drug Delivery* 24, 1680–1689 (2017).

[175] H. YANG, Z. YU, S. JI *ET AL.* Construction and evaluation of detachable bone-targeting MOF carriers for the delivery of proteasome inhibitors. *RSC Advances* 12, 14707–14715 (2022).

[176] T. MATSUMOTO, K. MIYAKE, S. YAMAMOTO *ET AL.* Rescue of severe infantile hypophosphatasia mice by AAV-mediated sustained expression of soluble alkaline phosphatase. *Human Gene Therapy* 22, 1355–1364 (2011).

[177] C. J. ALMÉCIGA-DÍAZ, A. M. MONTAÑO, L. A. BARRERA, S. TOMATSU. Tailoring the AAV2 capsid vector for bone-targeting. *Pediatric Research* 84, 545–551 (2018).

[178] M. REN, Y. LI, H. ZHANG *ET AL.* An oligopeptide/aptamer-conjugated dendrimer-based nanocarrier for dual-targeting delivery to bone. *Journal of Materials Chemistry B* 9, 2831–2844 (2021).

[179] E. YUCA, A. Y. KARATAS, U. O. S. SEKER *ET AL.* In vitro labeling of hydroxyapatite minerals by an engineered protein. *Biotechnology and Bioengineering* 108, 1021–1030 (2011).

[180] J. BANG, H. PARK, J. YOO *ET AL.* Selection and identification of a novel bone-targeting peptide for biomedical imaging of bone. *Scientific Reports* 10, 1–10 (2020).

[181] K. OGAWA, A. ISHIZAKI, K. TAKAI *ET AL.* Evaluation of Ga-DOTA-(D-Asp)n as bone imaging agents: D-aspartic acid peptides as carriers to bone. *Scientific Reports* 7, 1–11 (2017).

[182] X. WANG, Y. DENG, S. LI *ET AL.* Biomineralization-based virus shell-engineering: Towards neutralization escape and tropism expansion. *Advanced Healthcare Materials* 1, 443–449 (2012).

[183] X. WANG, C. SUN, P. LI *ET AL.* Vaccine Engineering with Dual-Functional Mineral Shell: A Promising Strategy to Overcome Preexisting Immunity. *Advanced Materials* 28, 694–700 (2016).

[184] S. LUO, P. ZHANG, P. ZOU *ET AL.* A Self-Biomineralized Novel Adenovirus Vectored COVID-19 Vaccine for Boosting Immunization of Mice. *Virologica Sinica* 36, 1113–1123 (2021).

[185] M. GUO, J. LI, Z. TENG *ET AL.* Article four simple biomimetic mineralization methods to improve the thermostability and immunogenicity of virus-like particles as a vaccine against foot-and-mouth disease. *Vaccines* 9, 1–15 (2021).

[186] G. WANG, R. Y. CAO, R. CHEN *ET AL.* Rational design of thermostable vaccines by engineered peptide-induced virus selfbiomineralization under physiological conditions. *Proceedings of the National Academy of Sciences of the United States of America* 110, 7619–7624 (2013).

[187] Y. LIN, X. WANG, X. HUANG *ET AL.* Calcium phosphate nanoparticles as a new generation vaccine adjuvant. *Expert Review of Vaccines* 16, 895–906 (2017).

[188] D. CHIU, W. ZHOU, S. KITAYAPORN *ET AL.* Biomineralization and size control of stable calcium phosphate core-protein shell nanoparticles: Potential for vaccine applications. *Bioconjugate Chemistry* 23, 610–617 (2012).

[189] W. ZHOU, A. O. MOGUCHE, D. CHIU, K. MURALI-KRISHNA, F. BANEYX. Just-in-time vaccines: Biomineralized calcium phosphate core-immunogen shell nanoparticles induce long-lasting CD8+ T cell responses in mice. *Nanomedicine: Nanotechnology, Biology, and Medicine* 10, 571–578 (2014).

[190] P. TREGUER, P. TRÉGUER, D. M. NELSON *ET AL.* The silica balance in the world ocean: a reestimate. *Science* 268, 375–379 (1995).

[191] K. ALBERT, X. C. HUANG, H. Y. HSU. Bio-templated silica composites for next-generation biomedical applications. *Advances in Colloid and Interface Science* 249, 272–289 (2017).

[192] M. A. A. ABDELHAMID, S. P. PACK. Biomimetic and bioinspired silicifications: Recent advances for biomaterial design and applications. *Acta Biomaterialia* 120, 38–56 (2021).

[193] C. C. LECHNER, C. F. W. BECKER. Modified silaffin R5 peptides enable encapsulation and release of cargo molecules from biomimetic silica particles. *Bioorganic and Medicinal Chemistry* 21, 3533–3541 (2013).

[194] C. C. LECHNER, C. F. W. BECKER. Immobilising proteins on silica with site-specifically attached modified silaffin peptides. *Biomaterials Science* 3, 288–297 (2015).

[195] M. A. A. ABDELHAMID, K. B. YEO, M. R. KI, S. P. PACK. Self-encapsulation and controlled release of recombinant proteins using novel silica-forming peptides as fusion linkers. *International Journal of Biological Macromolecules* 125, 1175–1183 (2019).

[196] E. M. CARLISLE. Silicon: A Possible Factor in Bone Calcification. *Science* 167, 279–280 (1970).

[197] W. WANG, K. W. K. YEUNG. Bone grafts and biomaterials substitutes for bone defect repair: A review. *Bioactive Materials* 2, 224–247 (2017).

[198] A. J. MIESZAWSKA, L. D. NADKARNI, C. C. PERRY, D. L. KAPLAN. Nanoscale control of silica particle formation via silk-silica fusion proteins for bone regeneration. *Chemistry of Materials* 22, 5780–5785 (2010).

[199] L. L. S. CANABADY-ROCHELLE, D. J. BELTON, O. DESCHAUME *ET AL.* Bioinspired silicification of silica-binding peptide-silk protein chimeras: Comparison of chemically and genetically produced proteins. *Biomacromolecules* 13, 683–690 (2012).

[200] J. GUO, C. LI, S. LING *ET AL.* Multiscale design and synthesis of biomimetic gradient protein/biosilica composites for interfacial tissue engineering. *Biomaterials* 145, 44–55 (2017).

[201] J. GUO, S. LING, W. LI *ET AL.* Coding Cell Micropatterns Through Peptide Inkjet Printing for Arbitrary Biomineralized Architectures. *Advanced Functional Materials* 28, 1–9 (2018).

[202] Y. K. JO, B. H. CHOI, C. S. KIM, H. J. CHA. Diatom-Inspired Silica Nanostructure Coatings with Controllable Microroughness Using an Engineered Mussel Protein Glue to Accelerate Bone Growth on Titanium-Based Implants. *Advanced Materials* 29, 1–9 (2017).

[203] J. YUN, Y. JEONG, O. NAM *ET AL.* Bone Graft Biomineral Complex Coderived from Marine Biocalcification and Biosilicification. *ACS Applied Bio Materials* 4, 6046–6055 (2021).

[204] X. WU, K. FRASER, J. ZHA, J. S. DORDICK. Flexible Peptide Linkers Enhance the Antimicrobial Activity of Surface-Immobilized Bacteriolytic Enzymes. *ACS Applied Materials and Interfaces* 10, 36746–36756 (2018).

[205] W. YANG, V. S. GONDIL, D. LUO *ET AL.* Optimized silica-binding peptide-mediated delivery of bactericidal lysin efficiently prevents staphylococcus aureus from adhering to

device surfaces. *International Journal of Molecular Sciences* 22, (2021).

[206] K. BRAUN, A. POCHERT, M. LINDÉN *ET AL.* Membrane interactions of mesoporous silica nanoparticles as carriers of antimicrobial peptides. *Journal of Colloid and Interface Science* 475, 161–170 (2016).

[207] J. LU, H. H. SHEN, Z. WU *ET AL.* Self-assembly of bi-functional peptides on large-pore mesoporous silica nanoparticles for miRNA binding and delivery. *Journal of Materials Chemistry B* 3, 7653–7657 (2015).

[208] G. DEL FAVERO, F. BIALAS, S. GRABHER *ET AL.* Silica particles with a quercetin-R5 peptide conjugate are taken up into HT-29 cells and translocate into the nucleus. *Chemical Communications* 55, 9649–9652 (2019).

[209] L. LIANG, A. CARE, R. ZHANG *ET AL.* Facile Assembly of Functional Upconversion Nanoparticles for Targeted Cancer Imaging and Photodynamic Therapy. *ACS Applied Materials and Interfaces* 8, 11945–11953 (2016).

[210] D. POLIKARPOV, L. LIANG, A. CARE *ET AL.* Functionalized upconversion nanoparticles for targeted labelling of bladder cancer cells. *Biomolecules* 9, 1–12 (2019).

[211] T. T. OLMEZ, E. YUCA, E. EYUPOGLU *ET AL.* Autonomous synthesis of fluorescent silica biodots using engineered fusion proteins. *ACS Omega* 3, 585–594 (2018).

[212] J. H. PARK, I. S. CHOI, S. H. YANG. Peptide-catalyzed, bioinspired silicification for single-cell encapsulation in the imidazole-buffered system. *Chemical Communications* 51, 5523–5525 (2015).

[213] G. WANG, H. J. WANG, H. ZHOU *ET AL.* Hydrated silica exterior produced by biomimetic silicification confers viral vaccine heat-resistance. *ACS Nano* 9, 799–808 (2015).

[214] F. BIALAS, C. F. W. BECKER. Biomimetic Silica Encapsulation of Lipid Nanodiscs and β-Sheet-Stabilized Diacylglycerol Kinase. *Bioconjugate Chemistry* 32, 1742–1752 (2021).

[215] W. HAN, A. CHILKOTI, G. P. LÓPEZ. Self-assembled hybrid elastin-like polypeptide/silica nanoparticles enable triggered drug release. *Nanoscale* 9, 6178–6186 (2017).

[216] G. YANG, Y. LIU, H. WANG *ET AL.* Bioinspired Core–Shell Nanoparticles for Hydrophobic Drug Delivery. *Angewandte Chemie - International Edition* 58, 14357–14364 (2019).

[217] M. R. KI, T. K. M. NGUYEN, H. S. JUN, S. P. PACK. Biosilica-enveloped ferritin cage for more efficient drug deliveries. *Process Biochemistry* 68, 182–189 (2018).

[218] M. R. KI, J. K. KIM, S. H. KIM *ET AL.* Compartment-restricted and rate-controlled dual drug delivery system using a biosilica-enveloped ferritin cage. *Journal of Industrial and Engineering Chemistry* 81, 367–374 (2020).

[219] T. K. M. NGUYEN, M. R. KI, R. G. SON *ET AL.* Synthesis of sub-50 nm bio-inspired silica particles using a C-terminal-modified ferritin template with a silica-forming peptide. *Journal of Industrial and Engineering Chemistry* 101, 262–269 (2021).

[220] B. DELALAT, V. C. SHEPPARD, S. RASI GHAEMI *ET AL.* Targeted drug delivery using genetically engineered diatom biosilica. *Nature Communications* 6, (2015).

[221] F. T. C. MOREIRA, A. P. MOREIRA-TAVARES, M. GORETI, F. SALES. Send Orders for Reprints to reprints@benthamscience.ae Sol-Gel-Based Biosensing Applied to Medicinal Science. *Current Topics in Medicinal Chemistry* 15, 245–255 (2015).

[222] T. IKEDA, Y. HATA, K. ICHI NINOMIYA *ET AL.* Oriented immobilization of antibodies on a silicon wafer using Si-tagged protein A. *Analytical Biochemistry* 385, 132–137 (2009).

[223] M. FUKUYAMA, S. YAMATOGI, H. DING *ET AL.* Selective detection of antigen-antibody reaction using si ring optical resonators. *Japanese Journal of Applied Physics* 49, (2010).

[224] M. FUKUYAMA, Y. AMEMIYA, Y. ABE *ET AL.* Sensitivity improvement of biosensors using si ring optical resonators. *Japanese Journal of Applied Physics* 50, (2011).

[225] A. SUNNA, F. CHI, P. L. BERGQUIST. Efficient capture of pathogens with a zeolite matrix. *Parasitology Research* 112, 2441–2452 (2013).

[226] A. CARE, F. CHI, P. L. BERGQUIST, A. SUNNA. Biofunctionalization of silica-coated magnetic particles mediated by a peptide. *Journal of Nanoparticle Research* 16, (2014).

[227] N. SAYYADI, A. CARE, R. E. CONNALLY *ET AL.* A novel universal detection agent for time-gated luminescence bioimaging. *Scientific Reports* 6, 1–9 (2016).

[228] O. CHOI, B. C. KIM, J. H. AN *ET AL.* A biosensor based on the self-entrapment of glucose oxidase within biomimetic silica nanoparticles induced by a fusion enzyme. *Enzyme and Microbial Technology* 49, 441–445 (2011).

[229] K. S. PARK, M. R. KI, K. B. YEO, J. H. CHOI, S. P. PACK. Design of bio-inspired silica-encapsulated protein A for improved immunoprecipitation assays. *Biochemical Engineering Journal* 128, 12–18 (2017).

[230] B. J. F. SWIFT, J. A. SHADISH, C. A. DEFOREST, F. BANEYX. Streamlined Synthesis and Assembly of a Hybrid Sensing Architecture with Solid Binding Proteins and Click Chemistry. *Journal of the American Chemical Society* 139, 3958–3961 (2017).

[231] T. ISHIDA, N. FUJIHARA, T. NISHIMURA *ET AL.* Live-cell imaging of macrophage phagocytosis of asbestos fibers under fluorescence microscopy. *Genes and Environment* 41, 1–3 (2019).

[232] C. J. HENDERSON, E. PUMFORD, D. J. SEEVARATNAM, R. DALY, E. A. H. HALL. Gene to diagnostic: Self immobilizing protein for silica microparticle biosensor, modelled with sarcosine oxidase. *Biomaterials* 193, 58–70 (2019).

[233] N. JORNET-MARTÍNEZ, C. J. HENDERSON, P. CAMPÍNS-FALCÓ, R. DALY, E. A. H. HALL. Towards sarcosine determination in urine for prostatic carcinoma detection. *Sensors and Actuators, B: Chemical* 287, 380–389 (2019).

[234] C. J. HENDERSON, E. ROGNIN, E. A. HALL, R. DALY. Design and model for 'falling particle' biosensors. *Sensors and Actuators, B: Chemical* 329, (2021).

[235] D. SEEVARATNAM, F. ANSAH, Y. ANIWEH, G. A. AWANDARE, E. A. H. HALL. Analysis and validation of silica-immobilised BST polymerase in loop-mediated isothermal amplification (LAMP) for malaria diagnosis. *Analytical and Bioanalytical Chemistry* (2022) doi:10.1007/s00216-022-04131-2.

[236] A. L. DEVRIES, D. E. WOHLSCHLAG. Freezing resistance in some antarctic fishes. *Science* 163, 1073–1075 (1969).

[237] T. CHANG, G. ZHAO. Ice Inhibition for Cryopreservation: Materials, Strategies, and Challenges. *Advanced Science* 8, 1–34 (2021).

[238] H. J. KIM, J. H. LEE, Y. B. HUR *ET AL.* Marine antifreeze proteins: Structure, function, and application to cryopreservation as a potential cryoprotectant. *Marine Drugs* 15, (2017).

[239] Z. LIU, X. ZHENG, J. WANG. Bioinspired Ice-Binding Materials for Tissue and Organ Cryopreservation. *Journal of the American Chemical Society* 144, 5685–5701 (2022).

[240] R. P. TAS, V. SAMPAIO-PINTO, T. WENNEKES, L. W. VAN LAAKE, I. K. VOETS. From the freezer to the clinic. *EMBO reports* 22, 1–7 (2021).

[241] L. F. L. CORREIA, B. R. C. ALVES, R. I. T. P. BATISTA, P. MERMILLOD, J. M. G. SOUZA-FABJAN. Antifreeze proteins for low-temperature preservation in reproductive medicine: A systematic review over the last three decades. *Theriogenology* 176, 94–103 (2021).

[242] H. HUANG, W. FENG, Y. CHEN, J. SHI. Inorganic nanoparticles in clinical trials and

translations. *Nano Today* 35, 100972 (2020).

[243] M. C. DANIEL, D. ASTRUC. Gold Nanoparticles: Assembly, Supramolecular Chemistry, Quantum-Size-Related Properties, and Applications Toward Biology, Catalysis, and Nanotechnology. *Chemical Reviews* 104, 293–346 (2004).

[244] X. YANG, M. YANG, B. PANG, M. VARA, Y. XIA. Gold Nanomaterials at Work in Biomedicine. *Chemical Reviews* 115, 10410–10488 (2015).

[245] J. FORESTIER. Rheumatoid Arthritis and Its Treatment By Gold Salts. *The Lancet* 224, 646–648 (1934).

[246] J. W. LEE, S. R. CHOI, J. H. HEO. Simultaneous Stabilization and Functionalization of Gold Nanoparticles via Biomolecule Conjugation: Progress and Perspectives. *ACS Applied Materials and Interfaces* (2021) doi:10.1021/acsami.1c10436.

[247] Y. WU, M. R. K. ALI, K. CHEN, N. FANG, M. A. EL-SAYED. Gold nanoparticles in biological optical imaging. *Nano Today* 24, 120–140 (2019).

[248] S. M. VAN DE LOOIJ, E. R. HEBELS, M. VIOLA *ET AL.* Gold Nanoclusters: Imaging, Therapy, and Theranostic Roles in Biomedical Applications. *Bioconjugate Chemistry* 33, 4–23 (2022).

[249] Y. ZHENG, J. WU, H. JIANG, X. WANG. Gold nanoclusters for theranostic applications. *Coordination Chemistry Reviews* 431, 213689 (2021).

[250] M. HNILOVA, C. R. SO, E. E. OREN *ET AL.* Peptide-directed co-assembly of nanoprobes on multimaterial patterned solid surfaces. *Soft Matter* 8, 4327–4334 (2012).

[251] M. H. OH, J. H. YU, I. KIM, Y. S. NAM. Genetically Programmed Clusters of Gold Nanoparticles for Cancer Cell-Targeted Photothermal Therapy. *ACS Applied Materials and Interfaces* 7, 22578–22586 (2015).

[252] Y. GAO, Y. LIU, R. YAN *ET AL.* Bifunctional Peptide-Conjugated Gold Nanoparticles for Precise and Efficient Nucleus-Targeting Bioimaging in Live Cells. *Analytical Chemistry* 92, 13595–13603 (2020).

[253] M. OZAKI, S. YOSHIDA, T. TSURUOKA, K. USUI. Intracellular mineralization of gold nanoparticles using gold ion-binding peptides with cell-penetrating ability. *Chemical Communications* 57, 725–728 (2021).

[254] N. S. HEO, S. ZHENG, M. H. YANG *ET AL.* Label-free electrochemical diagnosis of viral antigens with genetically engineered fusion protein. *Sensors (Switzerland)* 12, 10097–10108 (2012).

[255] A. G. VENKATESH, H. BRICKNER, D. LOONEY, D. A. HALL, E. ARONOFF-SPENCER. Clinical detection of Hepatitis C viral infection by yeast-secreted HCV-core:Gold-binding-peptide. *Biosensors and Bioelectronics* 119, 230–236 (2018).

[256] H. LEE, Y. S. LEE, S. S. REGINALD *ET AL.* Biosensing and electrochemical properties of flavin adenine dinucleotide (FAD)-Dependent glucose dehydrogenase (GDH) fused to a gold binding peptide. *Biosensors and Bioelectronics* 165, (2020).

[257] H. LEE, E. M. LEE, S. S. REGINALD, I. S. CHANG. Peptide sequence-driven direct electron transfer properties and binding behaviors of gold-binding peptide-fused glucose dehydrogenase on electrode. *iScience* 24, 103373 (2021).

[258] Y. S. LEE, S. BAEK, H. LEE *ET AL.* Construction of Uniform Monolayer- and Orientation-Tunable Enzyme Electrode by a Synthetic Glucose Dehydrogenase without Electron-Transfer Subunit via Optimized Site-Specific Gold-Binding Peptide Capable of Direct Electron Transfer. *ACS Applied Materials and Interfaces* 10, 28615–28626 (2018).

[259] T. J. PARK, M. S. HYUN, H. J. LEE, S. Y. LEE, S. KO. A self-assembled fusion protein-based surface plasmon resonance biosensor for rapid diagnosis of severe acute respiratory

syndrome. *Talanta* 79, 295–301 (2009).

[260] S. ZHENG, D. K. KIM, T. J. PARK, S. J. LEE, S. Y. LEE. Label-free optical diagnosis of hepatitis B virus with genetically engineered fusion proteins. *Talanta* 82, 803–809 (2010).

[261] K. G. LEE, T. J. LEE, S. W. JEONG *ET AL.* Development of a plastic-based microfluidic immunosensor chip for detection of H1N1 influenza. *Sensors (Switzerland)* 12, 10810–10819 (2012).

[262] T. J. PARK, S. J. LEE, D. K. KIM *ET AL.* Development of label-free optical diagnosis for sensitive detection of influenza virus with genetically engineered fusion protein. *Talanta* 89, 246–252 (2012).

[263] K. C. KO, M. H. CHOI, J. K. RHO, S. H. PARK. A facile method for detecting calcium/calmodulin-dependent protein kinase using radio phosphorylation of a GBP-fused enzyme substrate in a lab-on-a-chip. *Sensors and Actuators, B: Chemical* 178, 434–442 (2013).

[264] F. FATEMI, S. M. AMINI, S. KHARRAZI *ET AL.* Construction of genetically engineered M13K07 helper phage for simultaneous phage display of gold binding peptide 1 and nuclear matrix protein 22 ScFv antibody. *Colloids and Surfaces B: Biointerfaces* 159, 770–780 (2017).

[265] R. V. LEE, H. M. ZAREIE, M. SARIKAYA. Chimeric Peptide-Based Biomolecular Constructs for Versatile Nucleic Acid Biosensing. *ACS Applied Materials and Interfaces* 14, 23164–23181 (2022).

[266] E. J. KIM, E. B. KIM, S. W. LEE *ET AL.* An easy and sensitive sandwich assay for detection of Mycobacterium tuberculosis Ag85B antigen using quantum dots and gold nanorods. *Biosensors and Bioelectronics* 87, 150–156 (2017).

[267] S. K. GURMESSA, L. T. TUFA, J. KIM *ET AL.* Colorimetric Detection of Mycobacterium tuberculosis ESX-1 Substrate Protein in Clinical Samples Using Au@Pd Nanoparticle-Based Magnetic Enzyme-Linked Immunosorbent Assay. *ACS Applied Nano Materials* 4, 539–549 (2021).

[268] J. S. MÖHLER, W. SIM, M. A. T. BLASKOVICH, M. A. COOPER, Z. M. ZIORA. Silver bullets: A new lustre on an old antimicrobial agent. *Biotechnology Advances* 36, 1391–1411 (2018).

[269] H. A. CURRIE, O. DESCHAUME, R. R. NAIK, C. C. PERRY, D. L. KAPLAN. Genetically engineered chimeric silk-silver binding proteins. *Advanced Functional Materials* 21, 2889–2895 (2011).

[270] A. D'SOUZA, J. H. YOON, H. BEAMAN *ET AL.* Nine-Residue Peptide Self-Assembles in the Presence of Silver to Produce a Self-Healing, Cytocompatible, Antimicrobial Hydrogel. *ACS Applied Materials and Interfaces* 12, 17091–17099 (2020).

[271] R. R. NAIK, S. E. JONES, C. J. MURRAY *ET AL.* Peptide templates for nanoparticle synthesis derived from polymerase chain reaction-driven phage display. *Advanced Functional Materials* 14, 25–30 (2004).

[272] R. R. NAIK, S. J. STRINGER, G. AGARWAL, S. E. JONES, M. O. STONE. Biomimetic synthesis and patterning of silver nanoparticles. *Nature Materials* 1, 169–172 (2002).

[273] M. HNILOVA, X. LIU, E. YUCA *ET AL.* Multifunctional protein-enabled patterning on arrayed ferroelectric materials. *ACS Applied Materials and Interfaces* 4, 1865–1871 (2012).

[274] H. POBLETE, A. AGARWAL, S. S. THOMAS *ET AL.* New Insights into Peptide-Silver Nanoparticle Interaction: Deciphering the Role of Cysteine and Lysine in the Peptide Sequence. *Langmuir* 32, 265–273 (2016).

[275] J. P. PALAFOX-HERNANDEZ, Z. TANG, Z. E. HUGHES *ET AL.* Comparative study of materials-binding peptide interactions with gold and silver surfaces and nanostructures: A thermodynamic basis for biological selectivity of inorganic materials. *Chemistry of Materials* 26, 4960–4969 (2014).

[276] T. R. WALSH, M. R. KNECHT. Biointerface Structural Effects on the Properties and Applications of Bioinspired Peptide-Based Nanomaterials. *Chemical Reviews* 117, 12641–12704 (2017).

[277] M. RAI, A. YADAV, A. GADE. Silver nanoparticles as a new generation of antimicrobials. *Biotechnology Advances* 27, 76–83 (2009).

[278] S. PAL, Y. K. TAK, J. M. SONG. Does the antibacterial activity of silver nanoparticles depend on the shape of the nanoparticle? A study of the gram-negative bacterium Escherichia coli. *Applied and Environmental Microbiology* 73, 1712–1720 (2007).

[279] T. W. GIESSEN, P. A. SILVER. Converting a Natural Protein Compartment into a Nanofactory for the Size-Constrained Synthesis of Antimicrobial Silver Nanoparticles. *ACS Synthetic Biology* 5, 1497–1504 (2016).

[280] T. T. H. ANH, M. XING, D. H. T. LE, A. SUGAWARA-NARUTAKI, E. FONG. Elastin-based silver-binding proteins with antibacterial capabilities. *Nanomedicine* 8, 567–575 (2013).

[281] S. K. VANOOSTEN, E. YUCA, B. T. KARACA *ET AL.* Biosilver nanoparticle interface offers improved cell viability. *Surface Innovations* 4, 121–132 (2016).

[282] K. J. CHEN, C. K. LEE. Twofold enhanced dispersin B activity by N-terminal fusion to silver-binding peptide for biofilm eradication. *International Journal of Biological Macromolecules* 118, 419–426 (2018).

[283] D. KIM, S. J. KWON, X. WU *ET AL.* Selective Killing of Pathogenic Bacteria by Antimicrobial Silver Nanoparticle - Cell Wall Binding Domain Conjugates. *ACS Applied Materials and Interfaces* 10, 13317–13324 (2018).

[284] S. K. WOOLFOLK, A. K. CLOYD, Q. YE *ET AL.* Peptide-Enabled Nanocomposites Offer Biomimetic Reconstruction of Silver Diamine Fluoride-Treated Dental Tissues. *Polymers* 14, (2022).

[285] A. CIVANTOS, E. MARTÍNEZ-CAMPOS, V. RAMOS *ET AL.* Titanium Coatings and Surface Modifications: Toward Clinically Useful Bioactive Implants. *ACS Biomaterials Science and Engineering* 3, 1245–1261 (2017).

[286] J. SAMPATH, A. KULLMAN, R. GEBHART, G. DROBNY, J. PFAENDTNER. Molecular recognition and specificity of biomolecules to titanium dioxide from molecular dynamics simulations. *npj Computational Materials* 6, 1–8 (2020).

[287] J. KANG, S. TADA, M. SAKURAGI *ET AL.* An epidermal growth factor derivative with binding affinity for hydroxyapatite and titanium surfaces. *Biomaterials* 34, 9747–9753 (2013).

[288] H. YAZICI, H. FONG, B. WILSON *ET AL.* Biological response on a titanium implant-grade surface functionalized with modular peptides. *Acta Biomaterialia* 9, 5341–5352 (2013).

[289] Y. ZHOU, M. L. SNEAD, C. TAMERLER. Bio-inspired hard-to-soft interface for implant integration to bone. *Nanomedicine: Nanotechnology, Biology, and Medicine* 11, 431–434 (2015).

[290] Z. LIU, S. MA, X. LU *ET AL.* Reinforcement of epithelial sealing around titanium dental implants by chimeric peptides. *Chemical Engineering Journal* 356, 117–129 (2019).

[291] G. VIDAL, T. BLANCHI, A. J. MIESZAWSKA *ET AL.* Enhanced cellular adhesion on titanium by silk functionalized with titanium binding and RGD peptides. *Acta Biomaterialia* 9, 4935–4943 (2013).

[292] K. YUASA, E. KOKUBU, K. KOKUBUN *ET AL.* An artificial fusion protein between bone

morphogenetic protein 2 and titanium-binding peptide is functional in vivo. *Journal of Biomedical Materials Research - Part A* 102, 1180–1186 (2014).

[293] Z. ZHAO, S. MA, C. WU *ET AL.* Chimeric Peptides Quickly Modify the Surface of Personalized 3D Printing Titanium Implants to Promote Osseointegration. *ACS Applied Materials and Interfaces* 13, 33981–33994 (2021).

[294] M. YOSHINARI, T. KATO, K. MATSUZAKA, T. HAYAKAWA, K. SHIBA. Prevention of biofilm formation on titanium surfaces modified with conjugated molecules comprised of antimicrobial and titanium-binding peptides. *Biofouling* 26, 103–110 (2010).

[295] Z. LIU, S. MA, S. DUAN *ET AL.* Modification of Titanium Substrates with Chimeric Peptides Comprising Antimicrobial and Titanium-Binding Motifs Connected by Linkers to Inhibit Biofilm Formation. *ACS Applied Materials and Interfaces* 8, 5124–5136 (2016).

[296] H. GENG, Y. YUAN, A. ADAYI *ET AL.* Engineered chimeric peptides with antimicrobial and titanium-binding functions to inhibit biofilm formation on Ti implants. *Materials Science and Engineering C* 82, 141–154 (2018).

[297] X. ZHANG, H. GENG, L. GONG *ET AL.* Modification of the surface of titanium with multifunctional chimeric peptides to prevent biofilm formation via inhibition of initial colonizers. *International Journal of Nanomedicine* 13, 5361–5375 (2018).

[298] D. T. YUCESOY, M. HNILOVA, K. BOONE *ET AL.* Chimeric Peptides as Implant Functionalization Agents for Titanium Alloy Implants with Antimicrobial Properties. *Jom* 67, 754–766 (2015).

[299] H. YAZICI, M. B. O'NEILL, T. KACAR *ET AL.* Engineered Chimeric Peptides as Antimicrobial Surface Coating Agents toward Infection-Free Implants. *ACS Applied Materials and Interfaces* 8, 5070–5081 (2016).

[300] C. WISDOM, C. CHEN, E. YUCA *ET AL.* Repeatedly Applied Peptide Film Kills Bacteria on Dental Implants. *Jom* 71, 1271–1280 (2019).

[301] E. C. WISDOM, Y. ZHOU, C. CHEN, C. TAMERLER, M. L. SNEAD. Mitigation of Peri-implantitis by Rational Design of Bifunctional Peptides with Antimicrobial Properties. *ACS Biomaterials Science and Engineering* 6, 2682–2695 (2020).

[302] N. Y. HA, H. M. SHIN, P. SHARMA *ET AL.* Generation of protective immunity against Orientia tsutsugamushi infection by immunization with a zinc oxide nanoparticle combined with ScaA antigen. *Journal of Nanobiotechnology* 14, 1–12 (2016).

[303] L. APITIUS, S. BUSCHMANN, C. BERGS *ET AL.* Biadhesive Peptides for Assembling Stainless Steel and Compound Loaded Micro-Containers. *Macromolecular Bioscience* 19, 1–5 (2019).

[304] M. YAVUZ, M. ÜTKÜR, E. Ş. KEHRIBAR *ET AL.* Engineered Bacteria with Genetic Circuits Accumulating Nanomagnets as MRI Contrast Agents. *Small* 2200537, 1–11 (2022).

[305] B. FREELAND, E. MCCARTHY, R. BALAKRISHNAN *ET AL.* A Review of Polylactic Acid as a Replacement Material for Single-Use Laboratory Components. *Materials* 15, (2022).

[306] A. D. CELIZ, J. G. W. SMITH, R. LANGER *ET AL.* Materials for stem cell factories of the future. *Nature Materials* 13, 570–579 (2014).

[307] M. VODNIK, B. ŠTRUKELJ, M. LUNDER. HWGMWSY, an unanticipated polystyrene binding peptide from random phage display libraries. *Analytical Biochemistry* 424, 83–86 (2012).

[308] T. SERIZAWA, T. SAWADA, T. KITAYAMA. Peptide motifs that recognize differences in polymer-film surfaces. *Angewandte Chemie - International Edition* 46, 723–726 (2007).

[309] T. SERIZAWA, P. TECHAWANITCHAI, H. MATSUNO. Isolation of peptides that can recognize

syndiotactic polystyrene. *ChemBioChem* 8, 989–993 (2007).

[310] S. KONAGAYA, K. KATO, T. NAKAJI-HIRABAYASHI, H. IWATA. Design of culture substrates for large-scale expansion of neural stem cells. *Biomaterials* 32, 992–1001 (2011).

[311] T. WAKU, Y. IMANISHI, Y. YOSHINO *ET AL.* Fusion of polymeric material-binding peptide to cell-adhesion artificial proteins enhances their biological function. *Biointerphases* 12, 021002 (2017).

[312] D. B. GEHLEN, L. C. DE LENCASTRE NOVAES, W. LONG *ET AL.* Rapid and Robust Coating Method to Render Polydimethylsiloxane Surfaces Cell-Adhesive. *ACS Applied Materials and Interfaces* 11, 41091–41099 (2019).

[313] D. CARSON, M. HNILOVA, X. YANG *ET AL.* Nanotopography-Induced Structural Anisotropy and Sarcomere Development in Human Cardiomyocytes Derived from Induced Pluripotent Stem Cells. *ACS Applied Materials and Interfaces* 8, 21923–21932 (2016).

[314] M. GARAY-SARMIENTO, L. WITZDAM, M. VOROBII *ET AL.* Kill&Repel Coatings: The Marriage of Antifouling and Bactericidal Properties to Mitigate and Treat Wound Infections. *Advanced Functional Materials* 32, (2022).

[315] A. HOSSEINNEJAD, T. FISCHER, P. JAIN *ET AL.* Enzyme mimetic microgel coating for endogenous nitric oxide mediated inhibition of platelet activation. *Journal of Colloid and Interface Science* 601, 604–616 (2021).

[316] P. WINNERSBACH, A. HOSSEINNEJAD, T. BREUER *ET AL.* Endogenous Nitric Oxide-Releasing Microgel Coating Prevents Clot Formation on Oxygenator Fibers Exposed to In Vitro Blood Flow. *Membranes* 12, (2022).

[317] K.-W. HINTZEN, C. SIMONS, K. SCHAFFRATH *ET AL.* BioAdhere: tailor-made bioadhesives for epiretinal visual prostheses. *Biomaterials Science* 10, 3282–3295 (2022).

[318] V. GEORGAKILAS, J. N. TIWARI, K. C. KEMP *ET AL.* Noncovalent Functionalization of Graphene and Graphene Oxide for Energy Materials, Biosensing, Catalytic, and Biomedical Applications. *Chemical Reviews* 116, 5464–5519 (2016).

[319] T. R. WALSH, M. R. KNECHT. Biomolecular Material Recognition in Two Dimensions: Peptide Binding to Graphene, h-BN, and MoS2 Nanosheets as Unique Bioconjugates. *Bioconjugate Chemistry* 30, 2727–2750 (2019).

[320] S. N. KIM, Z. KUANG, J. M. SLOCIK *ET AL.* Preferential binding of peptides to graphene edges and planes. *Journal of the American Chemical Society* 133, 14480–14483 (2011).

[321] M. S. MANNOOR, H. TAO, J. D. CLAYTON *ET AL.* Graphene-based wireless bacteria detection on tooth enamel. *Nature Communications* 3, 763–768 (2012).

[322] D. KHATAYEVICH, T. PAGE, C. GRESSWELL *ET AL.* Selective detection of target proteins by peptide-enabled graphene biosensor. *Small* 10, 1505–1513 (2014).

[323] S. KIM, L. XING, A. E. ISLAM *ET AL.* In Operando Observation of Neuropeptide Capture and Release on Graphene Field-Effect Transistor Biosensors with Picomolar Sensitivity. *ACS Applied Materials and Interfaces* 11, 13927–13934 (2019).

[324] A. E. ISLAM, C. M. CRASTO, C. M. CRASTO *ET AL.* Graphene-Based Electrolyte-Gated Field-Effect Transistors for Potentiometrically Sensing Neuropeptide y in Physiologically Relevant Environments. *ACS Applied Nano Materials* 3, 5088–5097 (2020).

[325] E. WANG, M. S. DESAI, K. HEO, S. W. LEE. Graphene-based materials functionalized with elastin-like polypeptides. *Langmuir* 30, 2223–2229 (2014).

[326] M. HNILOVA, E. E. OREN, U. O. S. SEKER *ET AL.* Effect of molecular conformations on the adsorption behavior of gold-binding peptides. *Langmuir* 24, 12440–12445 (2008).

[327] K. T. NAM, D. KIM, P. J. YOO *ET AL.* Virus-Enabled Synthesis and Assembly Battery

Electrodes. *Science* 885–888 (2006).

[328] M. J. PENDER, L. A. SOWARDS, J. D. HARTGERINK, M. O. STONE, R. R. NAIK. Peptide-mediated formation of single-wall carbon nanotube composites. *Nano Letters* 6, 40–44 (2006).

[329] S. WANG, E. S. HUMPHREYS, S.-Y. CHUNG *ET AL.* Peptides with selective affinity for carbon nanotubes. *Nature Materials* 2, 196–200 (2003).

[330] Q. Q. HOANG, F. SICHERI, A. J. HOWARD, D. S. C. YANG. Bone recognition mechanism of porcine osteocalcin from crystal structure. *Nature* 425, 977–980 (2003).

[331] S. J. SEGVICH, H. C. SMITH, D. H. KOHN. The adsorption of preferential binding peptides to apatite-based materials. *Biomaterials* 30, 1287–1298 (2009).

[332] J. MAO, X. SHI, Y. B. WU, S. Q. GONG. Identification of specific hydroxyapatite {001} binding heptapeptide by phage display and its nucleation effect. *Materials* 9, (2016).

[333] D. K. YARBROUGH, E. HAGERMAN, R. ECKERT *ET AL.* Specific binding and mineralization of calcified surfaces by small peptides. *Calcified Tissue International* 86, 58–66 (2010).

[334] W. J. SHAW, K. FERRIS, B. TARASEVICH, J. L. LARSON. The structure and orientation of the C-terminus of LRAP. *Biophysical Journal* 94, 3247–3257 (2008).

[335] W. GONG, J. WANG, Z. CHEN, B. XIA, G. LU. Solution structure of LCI, a novel antimicrobial peptide from bacillus subtilis. *Biochemistry* 50, 3621–3627 (2011).

[336] L. APITIUS, K. RÜBSAM, C. JAKESCH, F. JAKOB, U. SCHWANEBERG. Ultrahigh-throughput screening system for directed polymer binding peptide evolution. *Biotechnology and Bioengineering* 116, 1856–1867 (2019).

[337] M. NOOR, T. DWORECK, A. SCHENK *ET AL.* Polymersome surface decoration by an EGFP fusion protein employing Cecropin A as peptide 'anchor'. *Journal of Biotechnology* 157, 31–37 (2012).

[338] S. DEDISCH, F. OBSTALS, A. DE LOS SANTOS PEREIRA *ET AL.* Turning a Killing Mechanism into an Adhesion and Antifouling Advantage. *Advanced Materials Interfaces* 6, (2019).

[339] T. SERIZAWA, T. SAWADA, H. MATSUNO, T. MATSUBARA, T. SATO. A peptide motif recognizing a polymer stereoregularity. *Journal of the American Chemical Society* 127, 13780–13781 (2005).

[340] Y. KUMADA, Y. SHIRITANI, K. HAMASAKI, T. OHSE, M. KISHIMOTO. High biological activity of a recombinant protein immobilized onto polystyrene. *Biotechnology Journal* 4, 1178–1189 (2009).

[341] R. R. NAIK, L. L. BROTT, S. J. CLARSON, M. O. STONE. Silica-Precipitating Peptides Isolated from a Combinatorial Phage Display Peptide Library. *Journal of Nanoscience and Nanotechnology* 2, 95–100 (2002).

[342] N. KRÖGER, R. DEUTZMANN, M. SUMPER. Polycationic peptides from diatom biosilica that direct silica nanosphere formation. *Science* 286, 1129–1132 (1999).

[343] S. NYGAARD, R. WENDELBO, S. BROWN. Surface-Specific Zeolite-Binding Proteins. *Advanced Materials* 14, 1853–1856 (2002).

[344] D. WIBOWO, C. X. ZHAO, A. P. J. MIDDELBERG. Emulsion-templated silica nanocapsules formed using bio-inspired silicification. *Chemical Communications* 50, 11325–11328 (2014).

[345] M. B. DICKERSON, S. E. JONES, Y. CAI *ET AL.* Identification and design of peptides for the rapid, high-yield formation of nanoparticulate TiO2 from aqueous solutions at room temperature. *Chemistry of Materials* 20, 1578–1584 (2008).

[346] K. B. YEO, M. R. KI, K. S. PARK, S. P. PACK. Novel silica-forming peptides derived from Ectocarpus siliculosus. *Process Biochemistry* 58, 193–198 (2017).

[347] B. L. COYLE, M. ROLANDI, F. BANEYX. Carbon-binding designer proteins that discriminate between sp2- and sp3-hybridized carbon surfaces. *Langmuir* 29, 4839–4846 (2013).

[348] R. H. SEDLAK, M. HNILOVA, C. GROSH *ET AL.* Engineered Escherichia coli silver-binding periplasmic protein that promotes silver tolerance. *Applied and Environmental Microbiology* 78, 2289–2296 (2012).

[349] J. M. GIBSON, V. RAGHUNATHAN, J. M. POPHAM, P. S. STAYTON, G. P. DROBNY. A REDOR NMR study of a phosphorylated statherin fragment bound to hydroxyapatite crystals. *Journal of the American Chemical Society* 127, 9350–9351 (2005).

[350] D. KASE, J. L. KULP, M. YUDASAKA *ET AL.* Affinity selection of peptide phage libraries against single-wall carbon nanohorns identifies a peptide aptamer with conformational variability. *Langmuir* 20, 8939–8941 (2004).

[351] C. STEWART, B. AKHAVAN, S. G. WISE, M. M. M. BILEK. A review of biomimetic surface functionalization for bone-integrating orthopedic implants: Mechanisms, current approaches, and future directions. *Progress in Materials Science* 106, 100588 (2019).

[352] A. CARE, H. NEVALAINEN, P. L. BERGQUIST, A. SUNNA. Effect of Trichoderma reesei proteinases on the affinity of an inorganic-binding peptide. *Applied Biochemistry and Biotechnology* 173, 2225–2240 (2014).

[353] Y. LIU, J. D. ADAMS, K. TURNER *ET AL.* Controlling the selection stringency of phage display using a microfluidic device. *Lab on a Chip* 9, 1033–1036 (2009).

[354] Y. H. HSIAO, C. Y. HUANG, C. Y. HU *ET AL.* Continuous microfluidic assortment of interactive ligands (CMAIL). *Scientific Reports* 6, 1–11 (2016).

[355] D. J. LEE, H. S. PARK, K. KOO *ET AL.* Gold Binding Peptide Identified from Microfluidic Biopanning: An Experimental and Molecular Dynamics Study. *Langmuir* 35, 522–528 (2019).

[356] C. R. SO, Y. HAYAMIZU, H. YAZICI *ET AL.* Controlling self-assembly of engineered peptides on graphite by rational mutation. *ACS Nano* 6, 1648–1656 (2012).

CHAPTER 3

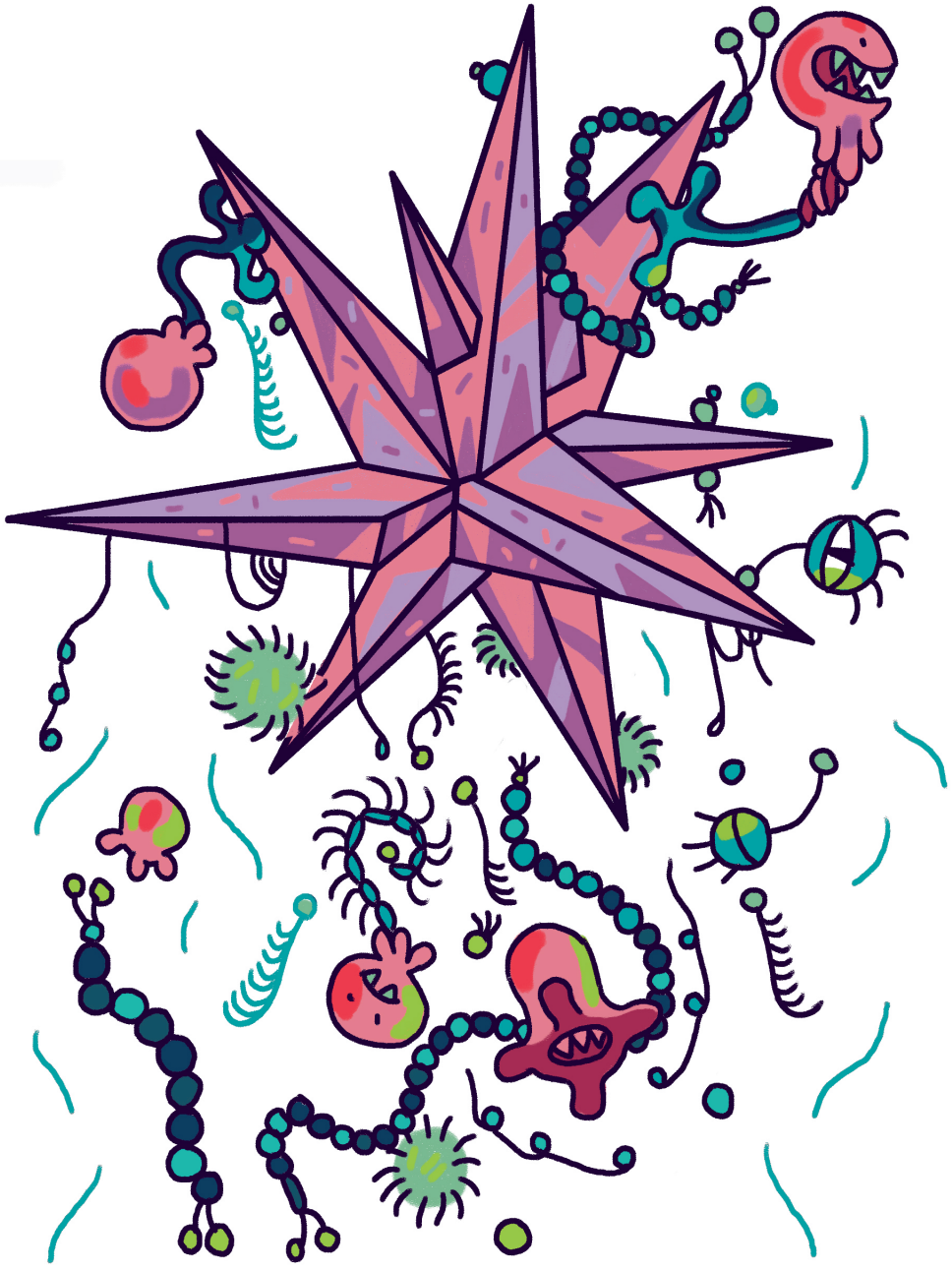

Self-assembly of elastin-like polypeptide brushes on silica surfaces and nanoparticles

Control over the placement and the activity of biomolecules on solid surfaces is a key challenge in bionanotechnology. While covalent approaches excel in performance, physical attachment approaches excel in ease of processing, which is equally important in many applications. In this chapter, we show how the precision of recombinant protein engineering can be harnessed to design and produce protein-based diblock polymers with a silica-binding block and highly hydrophilic elastin-like block. We also show that these diblock polypeptides self-assemble on silica surfaces and nanoparticles to form stable polypeptide brushes, which can be used as a scaffold for later biofunctionalization. From atomic force microscopy-based single-molecule force spectroscopy, we find that individual silica-binding peptides have high unbinding rates. Nevertheless, from quartz crystal microbalance measurements, we find that the self-assembled polypeptide brushes cannot easily be rinsed off. From atomic force microscopy imaging and bulk dynamic light scattering, we find that the binding to silica induces fibrillar self-assembly of the peptides. Hence, we conclude that the unexpected stability of these self-assembled polypeptide brushes is at least in part due to peptide–peptide interactions of the silica-binding blocks at the silica surface.

This chapter is published as:
Nicolò Alvisi[†], Fabiola A. Gutiérrez-Mejía[†], Meike Lokker, Yu-Ting Lin, Arthur M. de Jong, Floris van Delft, Renko de Vries; Self-Assembly of Elastin-like Polypeptide Brushes on Silica Surfaces and Nanoparticles, in *Biomacromolecules* **2021** *22 (5),* 1966-1979

[†] = shared first authorship

3.1. Introduction

A key aspect of bionanotechnology is the control of placement and the activity of biomolecules on solid surfaces. For example, biofunctionalization of solid surfaces is crucial in biosensing and for implanted biomaterials.[1] In the simplest approaches, biomolecules are either directly immobilized on surfaces through often nonspecific covalent bonds or physically adsorbed.[2,3] On the one hand, covalent coupling results in stronger immobilization since bonds are typically irreversible. On the other hand, physical adsorption generates bonds to the surface that are typically reversible, but the process is simpler.

In biosensing, the surface attachment of antibodies used to detect antigens provides a useful example. The direct and nonspecific covalent immobilization of antibodies on solid surfaces may lead to a significant loss of antibody activity, especially at high surface densities.[4] A probable cause for the loss of activity is the misorientation of the antibodies, leading to reduced accessibility of the antigen-binding region. Another cause is the partial or full denaturation of the antibodies, caused by the direct contact with the solid surface (Figure 3-1a). The same mechanisms are operative when antibodies are directly physically adsorbed on surfaces (Figure 3-1b). One solution to avoid misorientation or denaturation is to indirectly attach antibodies, or other bioactive molecules, to the surface via polymer brushes (Figure 3-1c). Following this strategy, the performance of diagnostic devices can be improved using antifouling polymers.[5] The technology for the synthesis and subsequent functionalization of antifouling polymer brushes on solid substrates has reached a sophisticated level.[6,7] However, the required procedures for low-cost, bulk applications are still too complex and too expensive. Therefore, there is continued interest in the development of technologies for the generation of stable polymer brushes via simple adsorption.

The most notable examples of non-covalently immobilized polymer brushes are poly(ethylene glycol) (PEG) copolymers such as PEG-*g*-PLL (poly l-lysine) and PEG-*g*-PEI (polyethylene imine).[8] These have a so-called “bottle-brush” architecture, consisting of a polycationic main chain (PLL or PEI) to which short PEG side chains are grafted. The polycationic main chain adsorbs onto many relevant surfaces, while the PEG side chains extend perpendicularly from the polycationic main chain, thereby forming a brush. PEG is widely used as an antifouling material, while bioactive molecules can

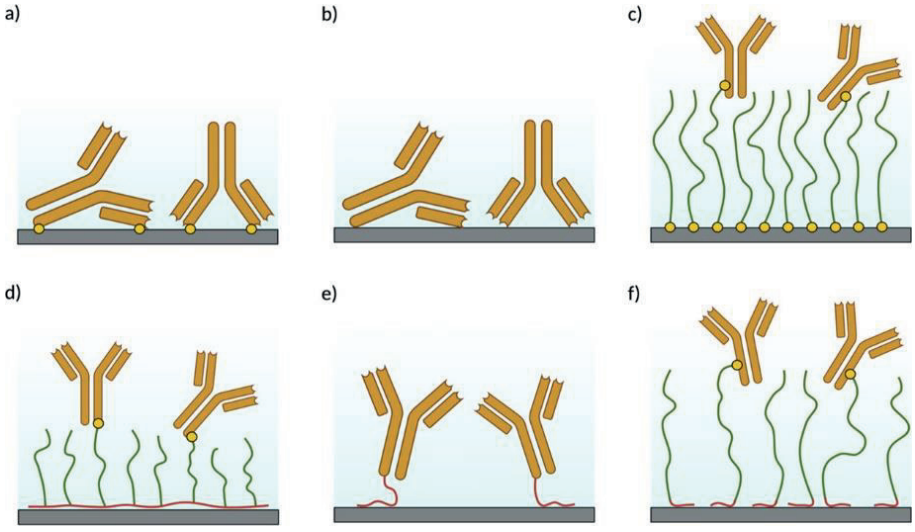

Figure 3-1. Biomolecule immobilization strategies illustrated for the case of antibodies. **(a)** Direct covalent attachment. **(b)** Direct physical adsorption. **(c)** Attachment to a covalently anchored polymer brush. **(d)** Attachment to a physically anchored PLL-*g*-PEG brush. **(e)** Physical immobilization through an SBP immobilization tag. **(f)** Physical immobilization through an SBP immobilization tag and antifouling polypeptide linker.

be readily attached to the PEG side chains by chemical procedures (Figure 3-1d).[6,9–11]

A complementary approach to synthetic polymers is the use of recombinant or synthetic polypeptides. Polypeptides offer the advantage of precise control of polymer chemistry, including the conjugation of bioactive molecules such as antibodies, and the possibility to directly include other functional peptide or protein blocks in the design.[12,13] Another advantage is the possibility to use many extensively studied solid-binding peptides (SBPs) as binding modules for specific surfaces. SBPs are short amino acid sequences that interact non-covalently with solid surfaces with affinities in the micro- to nanomolar range, and they have been widely employed as immobilization tags for the direct immobilization of proteins on various surfaces (Figure 3-1e).[14–17] However, as emphasized before, attachment to an antifouling polymer brush is preferred to prevent loss of activity of sensitive biomolecules such as antibodies.

There is precedent for the use of SBPs as part of genetically engineered polypeptide designs. For example, sequences based on spider silk have been fused to silica-binding domains to synthesize biomimetic coatings for nanoparticles.[18] The chimeric silk proteins form β-sheet-rich fibers on silica surfaces. In a similar strategy, Li *et al.* have used silica-binding domains to immobilize micelles of elastin-like polypeptides (ELPs) on silica nanoparticles and surfaces.[19] Immobilization using a diblock polypeptide with an SBP and an inert hydrophilic domain such as a hydrophilic ELP (Figure 3-1f) is another promising option. This design has recently been explored by Li *et al*.[20] for the immobilization of cells on gold surfaces. Here, we wish to explore a similar diblock design for coating silica surfaces.

Following Li *et al.*, we use ELPs as inert and antifouling polypeptide blocks.[20] ELPs are based on sequence motifs from human tropoelastin characterized by the pentapeptide E^X = VPGXG where X is any amino acid except proline, and they have been extensively characterized.[21,22] ELPs have found applications in biosensing,[23] tissue engineering,[24] nanoparticle coatings,[25] drug delivery systems,[26] biomineralization studies,[27] immunoassays,[28] and molecular switches.[29] To obtain inert and hydrophilic polypeptide brushes, we choose serine as a guest residue in our ELPs (X=S).

The authors have previously developed a diblock polypeptide C–B^{K12} consisting of an oligolysine block B^{K12} = K_{12} and a random coil hydrophilic block with a collagen-like sequence, C = $(GXaaYaa)_{132}$. The C–B^{K12} diblock spontaneously assembles on DNA to form a dense brush.[30] The same diblock polypeptide also assembles into dense hydrophilic brushes on the surface of nanodiamonds, providing the nanodiamonds with colloidal stability and promoting their uptake by cells.[31]

Building on our previous experience with the C-B^{K12} diblock, the basic design that we study here is also a simple diblock. We explore B-$E^S{}_{40}$ diblocks, where E^S = VPGSG and B is a series of silica-binding peptide blocks. First, we characterize in detail the silica-binding properties of the B domains, using quartz crystal microbalance (QCM), atomic force microscopy (AFM), and single molecule force spectroscopy (SMFS).[32–35] Next, we demonstrate that the B-$E^S{}_{40}$ diblocks form dense polymer brushes on silica surfaces and show that the diblocks stabilize silica nanoparticles. We also explore interactions of coated silica nanoparticles with coated silica surfaces using a single-particle surface mobility assay. We find that even prolonged rinsing does not displace the diblocks from silica surfaces, unless high ionic strength buffers are used.

We attribute this feature to strong peptide–peptide interactions of the SBPs on the silica surface, in addition to their inherent affinity to silica surfaces.

3.2. Materials and methods

"Scan-Asyst air" AFM tips were purchased from Bruker (USA). The maleimide-PEG-NHS molecule was purchased from Polypure. QCM-D sensors were purchased from Biolin Scientific (Sweden). A number of peptides were custom ordered from PepScan (Table 3-1), the reported purity is from high-performance liquid chromatography (HPLC) analysis, the reported mass is the experimental mass from mass spectrometry. Peptides were ion-exchanged to Na+ counterions by the manufacturer. Poly(l-lysine)-grafted poly(ethylene glycol) was purchased from SuSoS (Switzerland) with a grafting ratio of 3.5. The molecular weight of the PLL backbone and PEG side chains was 20 and 2 kDa, respectively. All other chemical reagents were purchased from Sigma-Aldrich.

3.2.1. Buffer preparation

10 mM phosphate buffer (PB) pH 7.4 with different amounts of added NaCl is used throughout. Buffer solutions were filtered and degassed before use.

3.2.2. Quartz crystal microbalance with dissipation monitoring

A Q-Sense E4 (Biolin Scientific, Sweden) quartz crystal microbalance with dissipation monitoring (QCM-D) instrument was used to quantify peptide and polypeptide binding to silica. QCM sensors coated with SiO_2 were obtained from the instrument manufacturer and cleaned according to instructions of the manufacturer. Prior to measurements, the instrument was equilibrated with starting buffer (PB with added NaCl as indicated) for at least 20 min at a flow

Table 3-1. Purity and molecular weight of synthetic peptides.

Name	Sequence	MW (Da)	Purity (%)
B^{R14}	R_{14}	2151.6	>96
B^{R13}-*Cys*	$R_{13}C$	2204.7	>99
B^{RT}	$(RTHRK)_4$	2732.3	>98
B^{RT}-*Cys*	$(RTHRK)_4C$	2835.5	>92
B^{RQ}	$(RQSSRGR)_2$	1672.9	>92
B^{RQ}-*Cys*	$(RQSSRGR)_2C$	1776.1	>98
$E^{S}{}_3$	$(VPGSG)_3$	1210.3	>99
$E^{S}{}_3$-*Cys*	$(VPGSG)_3C$	1313.5	>98

rate of 50 µL min^{-1}. Analysis of QCM-D data was done using QSense software (Biolin Scientific). For some measurements a linear filter was applied to correct for a small amount of baseline drift. Experimental observables are the changes in resonance frequency Δf and energy dissipation D. If energy dissipation is small enough, the adsorbed mass Δm per unit area is calculated from the change in resonance frequency through the Sauerbrey equation:

$$\Delta f = -C\frac{\Delta m}{n} \quad (1)$$

The oscillation frequency is an odd multiple (n = 1,3,5,…) of the crystal resonance frequency (5 MHz). The numerical prefactor (for a 5 MHz crystal, per unit area of crystal surface) is C = 17.7 ng cm^{-2} Hz^{-1}. The active area of the crystal was 0.2 cm^2. Adsorbed masses per unit area Γ obtained from the Sauerbrey equation, versus the bulk concentration C were fitted by an effective Langmuir adsorption isotherm:

$$\Gamma = \frac{K_{d,app}c}{1+K_{d,app}c}\Gamma_{max} \quad (2)$$

where Γ_{max} is the limiting adsorption, at high concentrations, and $K_{d,app}$ is an apparent dissociation constant.

3.2.3. Atomic force microscopy tip functionalization

We followed previously published protocols for functionalization of AFM tips for single molecule force measurements.[36] AFM tips (Bruker, USA) were cleaned with chloroform. Amino activation was performed by immersing the AFM tips in 30 µL of (3-aminopropyl-)triethoxysilane (APTES) and 10 µL of triethylamine, in a closed chamber under an argon atmosphere, for 2 h. Next, tips were cleaned again with chloroform and nitrogen gas and 1 mg of a maleimide-PEG-NHS linker was dissolved in 0.5 mL of chloroform and 30 µL of triethylamine. AFM cantilevers were then soaked in this solution in a small Teflon beaker for 3 h. Finally, tips were washed three times with chloroform. Peptides B^{R13}-*Cys*, B^{RT}-*Cys*, B^{RQ}-*Cys* and $E^{S}{}_3$-*Cys* were covalently attached to maleimide groups of the PEG linkers attached to the AFM tips via thiol bonds. To this end, a solution was prepared of 100 µL of peptide (100 µM), 2 µL of EDTA (100 mM, pH7.5), 5 µL of 4-(2-hydroxyethyl)-1-piperazineethanesulfonic acid (HEPES) (1 M, pH 7.5), 2 µL of TCEP (100 mM), and 2 µL of HEPES (1 M, pH 9.6). Tips were immersed in the abovementioned solution for 4 h. Tips were washed with PB and stored at 4 °C in PB for not more than 2 weeks before use.

3.2.4. Atomic force microscopy imaging in air

Atomically flat silica surfaces were obtained using silicon wafers (Siltronic AG) with a 2–3 nm oxide layer due to natural oxidation with oxygen in air. Silica surfaces were cleaned with ultrapure (Milli-Q) water and ethanol and plasma-cleaned for 5 min. For AFM imaging, peptide solutions, at concentrations as indicated, were filtered with a 10 kDa centrifugal filter and sonicated for 30 min to ensure that no peptide aggregates were present prior to imaging. Next, cleaned silica surfaces were immersed in 100 µL of peptide solution for 1 h. Silica samples were gently rinsed with ultrapure water and carefully dried with nitrogen. Samples were imaged with a Multimode Bruker AFM (Bruker, USA) using the automatic ScanAsyst imaging mode. ScanAsyst air tips were used with a nominal radius <10 nm.

3.2.5. Dynamic light scattering

For dynamic light scattering (DLS), a ZS-Nano (Malvern, UK) instrument was used, employing small-volume (20 µL) quartz cuvettes. Light scattering was measured at a scattering angle of 173°, at room temperature, T = 20 °C. Hydrodynamic sizes reported are the average of three measurements, obtained using the Zetasizer software version 7.13 (Malvern, UK). For DLS on peptide solutions, peptide solutions were filtered using a 10 kDa centrifugal filter and sonicated for 30 min to ensure that no peptide aggregates were present prior to the measurement. For each peptide sample, continuous, time-dependent measurements were performed, and each reported hydrodynamic size is the average of three measurements with duration of the measurement being controlled using the instrument. For measurements on silica nanoparticles coated with polypeptides, the polypeptide solution and the silica nanoparticles were sonicated for 15 min. The polypeptide solution was filtered using a 0.22 µm filter. Increasing concentrations of polypeptide were incubated with the silica nanoparticles for 10 min. For each sample, continuous measurements were performed, and each reported hydrodynamic size is the average of three measurements, with duration of the measurement being controlled using the instrument.

3.2.6. Single molecule force microscopy measurements

Silica surfaces were prepared as described for AFM imaging in air. Functionalized tips prepared as described above were used, and experiments

were performed in PB buffer pH 7.4 at the indicated concentration of NaCl. Single-molecule force-extension measurements, in a liquid flow cell, were performed using a ForceRobot 300 instrument (JPK, Germany) which allowed to probe a grid of points (10 μm × 10 μm) on the silica surface for multiple times, to give a total of >2000 measurements per pulling rate. Pulling rates used here were 12, 10, 5, 2.5, 1.25, 0.625, 0.325, and 0.165 μm s^{-1}. A contact time between the tip and the surface of 0.2 s was set to let the peptides bind the surface. The spring constant and sensitivity of the cantilevers used here were calibrated with the contact-free thermal noise routine from the JPK software. The JPKSPM data analysis software, Microsoft Excel (USA), and Matlab (USA) were used to analyze the data and classify events. For each force-extension curve, a baseline was subtracted. Peptides studied here consist of no more than 21 amino acids. The PEG linker has an average number of 27 repeat units. Assuming a 0.4 nm contour length per monomer, we expect forces to vanish at extensions longer than about 20 nm. Data was therefore preclassified using the JPKSPM software, with force–distance curves for which there was still a significant force at extensions >20 nm not being analyzed. The loading rate for each curve was obtained as the slope of the force versus time curves immediately before rupture. To analyze the force extension curves, individual force extension curves were analyzed with a freely jointed chain (FJC) model.[37] For *M* parallel chains:

$$L(f) = L_c\left(coth\left(\frac{Fb}{k_BT}\right) - \frac{k_BT}{Fb}\right) + N_s\frac{F}{MK_s} \quad (3)$$

Where F is the applied force, N_s is the total number of segments, k_B is the Boltzmann constant, and T is the temperature. The contour length L_c determines the overall range of the force extension curve. The Kuhn length $b = 0.7\ nm$ determines the slope in the low-force regime and the curvature in the mid-force regime, while the segment elasticity MK_s determines the slope in the high-force regime. Only single-rupture events were analyzed; a very small subset with multiple smaller rupture events was not considered in the analysis.

The loading rate dependency of the rupture force data was fitted to the Friddle-de Yoreo (FdY) model.[38] This model accounts for the expected transition from a near-equilibrium regime with fast re-bonding at low loading rates (L_r), to a regime of rapid irreversible nonequilibrium detachment at high loading rates, described by the Bell-Evans model. The near-equilibrium regime is characterized by an apparent equilibrium rupture force (f_{eq}), the

nonequilibrium regime by the unbinding rate k_{off} and distance to the transition state x_t:

$$f = f_{eq} + \frac{k_B T}{x_t} e^{\frac{1}{R(feq)}} E_1\left(\frac{1}{R(f_{eq})}\right) \quad (4)$$

where

$$R(f_{eq}) = \frac{L_T \cdot x_t}{k_{off}(f_{eq}) k_B T} \quad (5)$$

This is solved using the approximate relation $e^z E_1(z) \cong \ln(1 + e^{-\frac{\gamma}{z}})$ where γ ≈0.577 is Euler's constant. Furthermore, k_B is the Boltzmann constant and T is the absolute temperature.

To calculate the free energy of binding per unit length ΔG_b, we use the Manohar relationship for pulling polymers away from a surface, where $\Delta G_b = \gamma_{adh} l_{mono}$ and l_{mono} is the length of the monomer.[39] We take l_{mono} = 0.35 nm. The tension γ_{adh} is:

$$\gamma_{adh} = \frac{k_B T}{b} \ln\left(\frac{4\pi \sinh\left(\frac{feqb}{k_B T}\right)}{\frac{feqb}{k_B T}}\right) \quad (6)$$

Where b is the Kuhn length, for which we take *b* ≈ 0.7 nm. The free energy is expressed in thermal energies $k_B T$, where *T* =298K is the temperature of the experiment.

3.2.7. Construction of expression plasmids for polypeptides

To construct expression plasmids for the polypeptides, synthetic genes encoding B^{R9} = R_9, B^{RT} = $(RTHRK)_4$, and B^{RQ} = $(RQSSRGR)_2$ were synthesized by Macrogen (Amsterdam, The Netherlands). A synthetic gene for $E^S{}_{40}$ was designed using the Codon scrambler tool developed by Tang and Chilkoti[40] and synthesized by GenScript Inc. (USA). All the synthetic fragments were designed in order to contain the features necessary for recursive directional ligation by plasmid reconstruction (PRe-RDL) cloning, as described by McDaniel *et al*.[41] Sequences of the DNA fragments used are given in Table A3-1. The fragments were ligated into separate *XbaI*/*EcorI*-digested pET-24a(+) vectors, in order to construct a library of PRe-RDL compatible vectors. A total of 10 ng of plasmid DNA was transformed into *E. coli* BL21 cells by means of electroporation. Colonies containing the correct DNA inserts were selected and confirmed by DNA sequencing. Next, plasmids for expression of

the diblock polypeptides *B*-E^S_{40} were constructed from the PRe-RDL plasmids for the elastin-like protein block E^S_{40} and those for the binding blocks *B*, as described by McDaniel *et al*.[41] Full amino acid sequences for the diblock polypeptides *B*-E^S_{40} are given in Table A3-2.

3.2.8. Protein expression

E. coli BL21 transformed with the expression plasmids for the polypeptides was cultured at 37 ℃ and 200 rpm for 16 h in 10 mL Terrific Broth (TB) medium containing 50 μg mL^{-1} kanamycin. A starter culture was inoculated in 2 L of TB medium containing 50 μg mL^{-1} kanamycin and incubated for 24 h at 37 °C and 200 rpm. After 8 h from the start of the incubation, Isopropyl β- d-1-thiogalactopyranoside (IPTG) was added to a final concentration of 1 mM and cells were grown overnight before harvesting.

3.2.9. Protein isolation and purification

Bacterial cells were centrifuged at 3300 rpm for 10 min at 4 °C and resuspended in 50 mL of cold phosphate-buffered saline (PBS). Cells were lysed using three cycles of a French press (SLM Aminco). Next, 4 mL of 10% (v/v) polyethyleneamine was added to the cell lysates to precipitate DNA. The cell lysate was centrifuged for 15 min at 15,000 rpm at 4 °C to pellet the insoluble fraction. The ELP-containing polypeptides were first purified using inverse transition cycling. Ammonium sulphate was added to the supernatant to a final concentration of 0.5 M. The supernatant was heated to 37 °C and centrifuged for 10 min at 15,000 rpm at 37 °C. The pellet was resuspended in 10 mL of cold 20 mM HEPES pH 8.0 to solubilize the aggregated ELP. The ELP-enriched lysate was centrifuged for 10 min at 15,000 rpm at 4 °C to pellet the remaining insoluble matter. Next, polypeptides were further purified using ion-exchange chromatography. The low ionic strength buffer (buffer A) was 20 mM HEPES pH 8.0. The high ionic strength buffer was 20 mM HEPES pH 8.0 and 1 M NaCl (buffer B). Samples were injected in a cation-exchange column (UNO Q6, Bio-Rad Laboratories, USA) and eluted with a linear gradient from buffer A to buffer B. The polypeptides of interest typically eluted at a salt concentration of 0.7 M, as found by sodium dodecyl sulfate-polyacrylamide gel electrophoresis (SDS-PAGE) analysis. In some cases, SDS-PAGE indicated that a small amount of impurities was still present. These were removed using a mild bake-out procedure: solutions were heated at 60 °C for 15 min, cooled in ice for 10 min, and then centrifuged for 15 min at

15,000 rpm at 4 °C to pellet the insoluble contaminants. The final purity of the polypeptides was assessed by SDS-PAGE.

3.2.10. Mass spectrometry

To confirm the identity of the polypeptides, their molecular weights were determined using matrix-assisted laser desorption/ionization (MALDI) mass spectrometry. Spectra were obtained using a Bruker UltraFlextreme machine (Bruker, USA). Samples were prepared for analysis following the instructions provided by the manufacturer.

3.2.11. N-terminal protein sequencing

N-terminal sequencing was performed by Alphalyse (Odense, Denmark) on an ABI Procise 494 sequencer by Edman degradation chemistry.

3.2.12. Particle mobility assay

For glass substrate functionalization, glass slides (25 × 75 mm, #5, Menzel-Gläser) were precleaned by 30 min of sonication in isopropanol (absolute, VWR) and 10 min of sonication in ultrapure water. After the substrate was dried with a nitrogen stream, 1 min of oxygen plasma was applied to the slides to plasma-oxidize the surface. Custom-made fluid cell stickers (Grace Biolabs) with an approximate volume of 20 µL were then attached to the substrate and 0.5 mg mL^{-1} of PLL-*g*-PEG solution in ultrapure water, respectively 0.5 mg mL^{-1} of B^{RT}-E^{S}_{40} solution in ultrapure water was immediately injected to the flow chamber and incubated for 5 h at room temperature.

For particle functionalization, vials with carboxyl-functionalized silica particles (Bangs Laboratories, 1 µm mean diameter) at a concentration of 1 mg mL^{-1} were incubated with, respectively, 0.9 mg mL^{-1} of B^{RT}-E^{S}_{40} in ultrapure water and 0.9 mg mL^{-1} of PLL-*g*-PEG in ultrapure water and placed on a rotating fin (VWR, The Netherlands) for 3 h at room temperature. Streptavidin-coated polystyrene superparamagnetic particles (10 mg mL^{-1}, Dynabeads MyOne Streptavidin C1, 65001, Thermo Scientific) at a concentration of 1 mg mL^{-1} in PBS (130 mM NaCl, pH 7.4) were incubated with 5 µL of 11 nt ssDNA (5′ TCACGGTACGA 3′ Biotin, Integrated DNA Technologies) at a concentration of 2 µM in PBS and mPEG-Biotin (PG1-BN-1k, Nanocs) at a concentration of 100 µM in PBS buffer for 70 min on a rotating fin. The particle mixtures were washed with 0.05 vol % Tween-20 (Sigma-Aldrich) and reconstituted in 1000 µL of PBS (130 mM NaCl, 7 mM Na_2HPO_4, and 3 mM

NaH_2PO_4 at pH 7.4). Right before injecting particles to the flow chamber, the particle solution was sonicated with 10 pulses at 70% with 0.5 duty cycle (Hielscher, Ultrasound Technology).

For the particle mobility assay, particles with different modifications were added to the variously modified surfaces at a final concentration of 0.01 mg mL^{-1} in PBS. The trajectory of the particles was recorded for 1 and 5 min at a frame rate of 30 and 60 Hz with an integration time of 5 ms in a field of view of 883 × 552 μm2 with the Leica microscope (Dark field microscopy, Leica DMI5000M). By applying a Gaussian fitting over the intensity of pixels around the particle, the center of every particle can be determined to within approx. 20 nm and tracked over all frames.

3.3. Results and discussion

At neutral pH, silica has a weak negative charge.[42] Under these conditions and at low ionic strength, arginine has been found to adsorb most strongly to silica compared to the natural amino acids, at least in part due the high pKa of its side chain.[43] Indeed, in sequences of many silica-binding peptides, arginine is over-represented. While many sequences have been reported as being SBPs, a detailed characterization of their binding to silica has only been carried out for few of them. Here we choose to explore as binding domains *B* the peptide sequences B^{RT} and B^{RQ}, and the oligoarginine control peptides B^{Rn} = R_n. The peptides were fused to ELP (repeat sequence of VPGSG) to generate brush-like diblocks $B\text{-}E^S_{40}$ (Figure 3-2).

The first SBP characterized is the highSP peptide which was engineered from a weaker binding precursor isolated from *E. coli*.[44–46] The sequence of highSP will be referred to as B^{RT} after its first two residues, B^{RT} = $(RTHRK)_4$. B^{RT} shows high affinity to silica, zinc and other oxidized metals and has already been successfully employed as binding tag.[44,47] A second evaluated SBP is SB7, which was isolated from the spore-coat protein CotB1 of *Bacillus cereus.*[43] Its sequence will be referred to as B^{RQ}, again after the first two residues, B^{RQ} = $(RQSSRGR)_2$. This peptide was designed as short affinity purification tag, using silica-based materials.

Representative QCM-D data for the adsorption of the solid-binding peptide B^{RT} in PB to silica are shown in Figure 3-3a. The lowest concentration for which we observe significant binding is slightly below 1 μM. For this concentration, as well as for higher concentrations, adsorbed peptide layers form in less than 10 min. Flushing with PB buffer for 10 min does not lead to

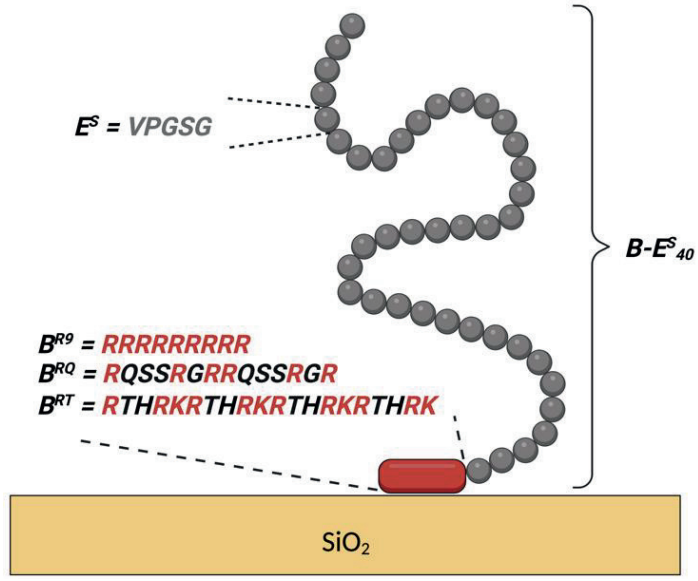

Figure 3-2. Schematic structure of *B*-E^S_{40} diblocks for forming hydrophilic polypeptide brushes on silica surfaces.

significant detachment of the adsorbed peptides. The out-of-phase response, or energy dissipation, is minimal and so is the dispersion between frequency shifts for different harmonics, indicating a rigidly adsorbed peptide layer that co-vibrates with the crystal oscillations.

Since we wish to construct diblock polypeptides *B*-E^S_{40} with solid-binding domains *B* and long hydrophilic ELP domains E^S_{40} (E^S = VPGSG), we also performed QCM-D measurements on the adsorption of a short elastin-like peptide E^S_3 to silica. For efficient brush formation, the longer hydrophilic blocks should not compete with the binding blocks in binding to the silica. For example, it is well-known that PEG has a strong affinity for silica.[48] For PLL-*g*-PEG polymers, this may compete with the PLL backbone in adsorbing to silica surfaces. The results of our measurements are included in Figure 3-3a. Within the accuracy of the instrument, we could not detect any adsorption of E^S_3, suggesting that this ELP is a good choice as a hydrophilic block when aiming to construct self-assembling brushes on silica.

Since the out-of-phase response or dissipation *D* in the QCM-D experiments was shown to be negligible and there was hardly any dispersion

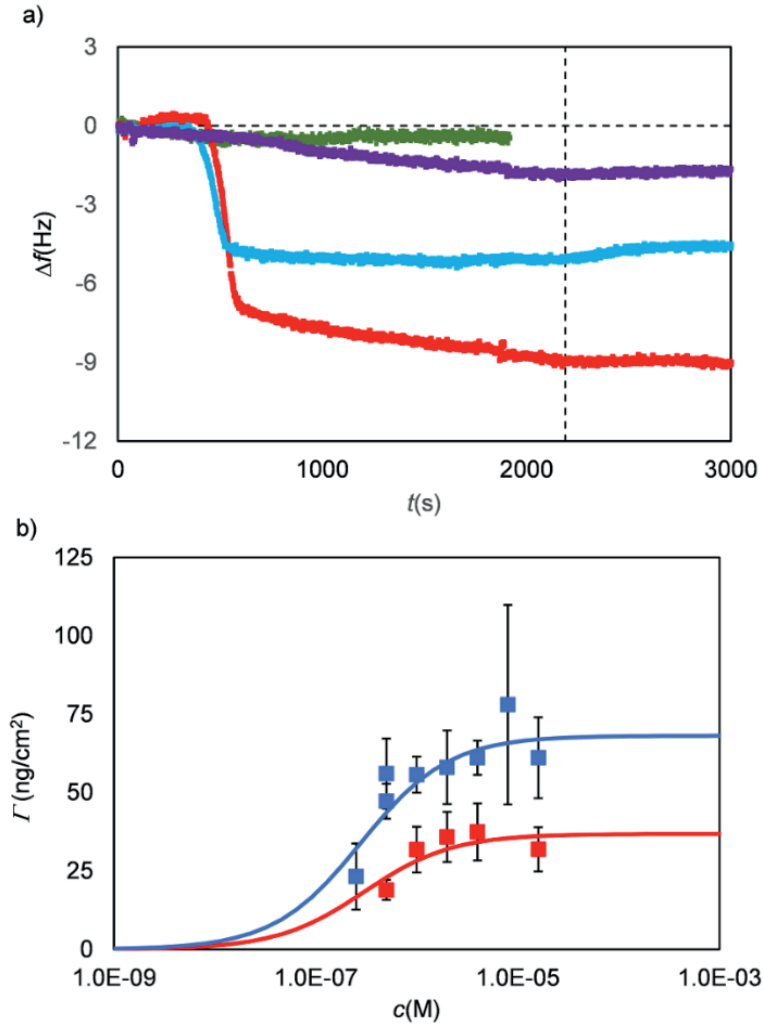

Figure 3-3. Representative QCM-D data for the adsorption of the SBP B^{RT} and the short ELP E^{S}_{3} to silica. **(a)** Frequency Δf (Hz) shift versus time t (s) for B^{RT} at increasing peptide concentrations (purple: 0.175 μM; blue: 5 μM; red: 10 μM), and for E^{S}_{3} (green: 5 μM). The vertical dashed line indicates the start of the buffer wash (PB). **(b)** Representative curve of saturation adsorbed mass Γ (ng cm^{-2}) versus peptide concentration c (M) for the SBP B^{RQ}. Blue filled squares: adsorption in PB buffer; red filled squares: adsorption in PBS buffer. Data were fitted using Langmuir isotherms (solid lines) to obtain apparent dissociation constants $K_{d,app}$ (M^{-1}) and maximum adsorbed masses Γ_{max} (Table 3-2). Error bars are standard deviations for >3 independent measurements.

between frequency shifts for different harmonics, the Sauerbrey equation can be applied to relate the frequency shift to adsorbed mass per unit area.[14] Results for the saturation values of the adsorbed mass per unit area Γ as a function of peptide concentration *c* (M) for B^{RT} are shown in Figure 3-3b. The results for the other SBPs B^{RQ} and B^{R14} were similar, and are shown in Figure A3-1. A Langmuir equation was applied to fit the data to get apparent dissociations constants $K_{d,app}$ and plateau values Γ_{max} for the adsorbed mass per unit area.

Strictly speaking, the validity of the Langmuir equation requires that the peptides are non-interacting on the surface, and that the adsorbed layer is in full equilibrium. For all three peptides (B^{RT}, B^{RQ} and B^{R14}), there are strong indications for irreversible adsorption rather than equilibrium adsorption, and for an important role of peptide–peptide interactions at the solvent–silica interface. Hence, it is unlikely that the peptides satisfy the requirements for the validity of the Langmuir equation. Therefore, we prefer to denote the dissociation constants obtained by the Langmuir fits of the QCM data as apparent dissociation constants $K_{d,app}$.

Values for dissociations constants $K_{d,app}$ and plateau values Γ_{max} are listed in Table 3-2. Within the rather large error of the measurements, there are no significant differences in the apparent dissociation constants of the peptides. Apparent dissociation constants $K_{d,app}$ for all three peptides are in the order of μM. Saturation densities are in the order of 0.5 mg m^{-2}. Both values are fairly typical for adsorbed peptide layers.[14,49,50] The saturation density corresponds to an approximate surface area per peptide in the order of 5 nm^2.

Next, we attempted to image the ultrastructure of the adsorbed peptide layers by performing AFM imaging on dried peptide layers in air. Control measurements of clean silica slides did not show any feature with heights in excess of 200 pm. AFM images show surface features that are strongly dependent on the concentrations at which the layers are formed. For all peptides, at low concentrations, we observe a homogeneous background and small globular features, whereas at higher concentrations, a homogeneous background and surface-bound fibrils are observed. Selected results for the SBP B^{RT} are shown in Figure 3-4a-c; an overview with results for all SBPs and concentrations tested is shown in Figure A3-2.

For the SBPs B^{RT} and B^{RQ}, surface-bound fibrils were observed when adsorption was performed at concentrations above about 5 μM, whereas for the B^{R14} control peptide, surface-bound fibrils were already observed at

Table 3-2. Parameters from Langmuir fits of QCM-D data.

Peptide	PB		PBS	
	$K_{d,app}$ [10^6 M^{-1}]	Γ_{max} [ng cm^{-2}]	$K_{d,app}$ [10^6 M^{-1}]	Γ_{max} [ng cm^{-2}]
B^{R14}	1.4	90	0.7	70
B^{RT}	3.6	70	3.3	40
B^{RQ}	2.5	40	0.5	40

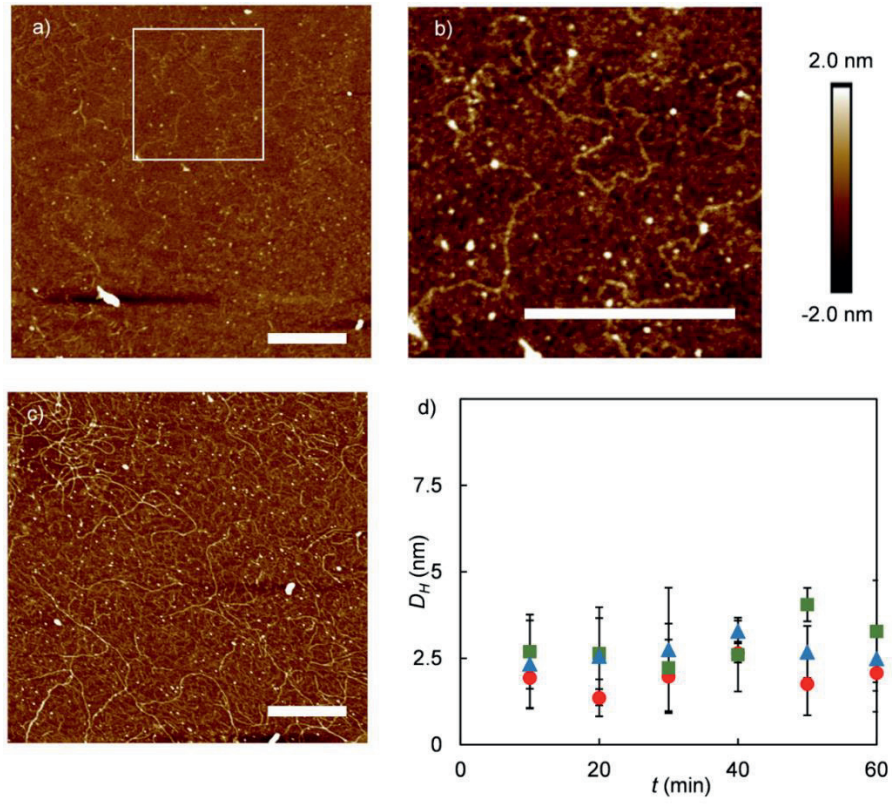

Figure 3-4. Surface-induced fibril formation for SBP B^{RT} on silica. **(a-c)** AFM images of B^{RT} adsorbed onto silica from PB buffer and incubated for 1 h, imaged in air, for different concentrations and magnifications. Scale bars are 200 nm. **(a)** 3.66 μM, **(b)** Zoom-in of region outlined in (a). **(c)** 36.6 μM. **(d)** Hydrodynamic diameter D_H (nm) from DLS of 1 mg mL^{-1} SBP solutions in PB, as a function of time. Red circle: B^{RQ}; green square: B^{RT}; blue triangle: B^{R14}.

concentrations of around 0.5 μM, one order of magnitude lower. For each peptide, cross-sections of multiple fibrils (n = 6) were analyzed and average fibril heights h_{fibril} were calculated. Fibrils heights for different peptides are similar: h_{fibril} = 0.8 ± 0.2 nm for B^{RT}, h_{fibril} = 0.5 ± 0.2 nm for B^{RQ}, and h_{fibril} = 0.9 ± 0.4 nm for B^{R14}. It should be noted that drying may have impacted the final morphology of the fibrils as imaged. This could be checked by complementary AFM imaging experiments in liquid.

To establish whether fibril formation is induced by the silica surface or if fibrils form in solution and subsequently adsorb, we monitored peptide solutions for long periods using DLS. Results are shown in Figure 3-4d. Peptide solutions of 1 mg mL^{-1} were carefully filtered and sonicated to ensure that no aggregates were present at the start of the measurement. The concentration of 1 mg mL^{-1} is well above the concentrations for which fibrils were observed in the AFM images. Hydrodynamic radii were measured for 1 h. During this time, the observed hydrodynamic diameter (D_H) remained small, in the order of 2.5 nm, which is the size expected for monomeric peptides in solution. Samples measured over 3 days and 1 week did not show any noticeable change in hydrodynamic size either (data not shown). Hence, fibril formation of the SBPs appears to be driven by interaction with silica surfaces and not start in the bulk solution. These results confirm that SBPs strongly interact with each other when adsorbed to silica surfaces; clearly, a simple Langmuir adsorption isotherm cannot be used to describe the mechanism of a peptide layer formation on the surface, even though the data of saturation adsorption Γ_{max} versus concentration c can be fitted with a Langmuir isotherm.

To obtain information on the binding of individual SBPs to silica, in the absence of peptide–peptide interactions, we resorted to the measurement of single-molecule force-extension curves using AFM. An AFM tip is functionalized with maleimide-terminated PEG linkers, to which cysteine-terminated SBPs are attached via thiol bonds at a low density, as sketched in Figure A3-3a. As shown in Figure A3-4d-f, there are typically a small number of peptides M <30 that interact simultaneously with the surface when using this procedure.[38] The low density guarantees that peptides do not interact with each other during the experiments.

The peptides studied here consist of no more than 21 amino acids, while the PEG linker has an average number of 27 repeat units; assuming an approximate size of 0.4 nm per monomer, a total contour length for the constructs of approximately 20 nm can be calculated. The absence of

attraction at distances larger than this cutoff was used as a first selection criterion to identify relevant events. Histograms of rupture forces for the SBPs and the negative controls (respectively, the inert ELP peptide $E^S{}_3$ and the non-functionalized PEG linkers) are shown in Figure 3-5a,b. As expected, for the SBPs we find a large number of rupture events and forces at rupture of order 100 pN. In contrast, for the negative controls, the number of events for which a rupture is detected is much lower, and typical rupture forces are lower, thus validating that in our experiment we measure adhesion forces of SBPs for the

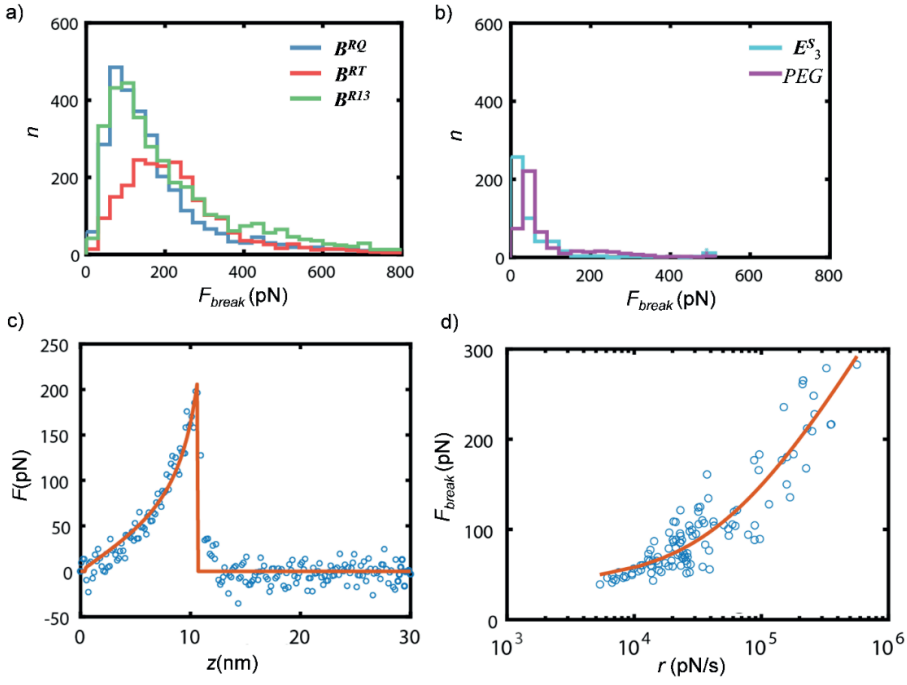

Figure 3-5. Single-molecule AFM based force spectroscopy. **(a)** Histogram of number of events *n* versus breaking force F_{break} (pN) for SBPs B^{RQ}-*Cys*, B^{RT}-*Cys*, B^{R13}-*Cys*. **(b)** Histogram of number of events *n* versus breaking force F_{break} (pN) for negative controls: PEG-linker without conjugated peptide, and the non-adsorbing elastin-like peptide $E_S{}^3$. **(c)** Example fit of single force-curve for B^{R13}-*Cys* with the freely jointed chain model, used to extract approximate numbers of parallel peptides *M* and contour lengths L_c. **(d)** Final result of data analysis, for the case of B^{RT}-*Cys*: breaking force F_{break} (pN) versus loading rate *r* (pN s^{-1}), for selected events with *M* = 1, ..., 7. The red line is the fit with the FdY model, fit parameters for all SBPs are given in Table 3-3.

silica substrate. A typical force-extension curve for the SBP $B^{R13}Cys$ is shown in Figure 3-5c. All similar force-extension curves were fitted with a Freely Jointed Chain (FJC) model for *M* parallel chains, to give the contour-length L_c, breaking force F_{break}, and loading rate *r* at rupture, as well as an estimate of the number *M* of parallel chains in the rupture event. While most force-extension curves showed only a single rupture event and hence could be analyzed as described above, a small number of force-extension curves were also recorded that showed rupture in multiple steps.[51] These rare events were excluded from the analysis. We find that most rupture events have a number of parallel bonds $M < 10$. To ensure that we measure binding and unbinding of individual peptides, we focus on the events corresponding to a low number of parallel bonds, $M = 1, ..., 7$. Histograms of the contour-length L_c and number of parallel bonds *M* are presented in Figure A3-4. For data with $M = 1, \ldots, 7$, rupture force versus loading rate was analyzed using the FdY model for *M* parallel bonds that can detach and reattach.[38,52] The FdY model has been used before to analyze the adhesion of proteins to substrates,[53,54] polymer to minerals,[55] and of peptides to inorganic materials.[56] At low loading rates, the rapid (re)binding and unbinding leads to a constant rupture force, but at higher loading rates, the model recovers the known logarithmic loading-rate dependence for the case in which rebinding is neglected.[38] An example fit for the SBP B^{RT} is shown in Figure 3-5d, fits for the other SBPs are given in Figure A3-3. Fit parameters for all SBPs are listed in Table 3-3. An approximate binding free energy ΔG is calculated from the fitted F_{eq} by using a relation previously derived by Manohar (Table 3-3).[39]

We want to highlight the relatively high off-rates for B^{RT}, for example ($k_{off} \approx 2.9 \cdot 10^2$ s^{-1}), although they are still not as high as for the adhesion of a shorter and more weakly adhering peptide (GCRL) to silica ($k_{off} \approx 2.6 \cdot 10^3$ s^{-1}).[51] Our data demonstrates that single SBPs detach rapidly, thereby supporting the hypothesis that the relative stability of SBP layers is caused by peptide-peptide interactions at the silica surface, which reinforce the surface layers.

Table 3-3. Fit Parameters for FdY Fits of Rupture Force Versus Loading Rate for SBP, Binding to Silica.

SBP	k_{off} (s^{-1})	x_t (Å)	F_{eq} (pN)	ΔG (k_B T)
B^{R13}	145.9	0.6	29.4	2.62
B^{RQ}	246.4	0.3	46.1	3.81
B^{RT}	287.4	0.4	40.0	3.36

After it was established that all SBPs bind with similar affinities, have similar off-rates as individual peptides, but form peptide layers that are not easily detached, *B*-E^S_{40} diblock polypeptides were generated with binding blocks *B* = B^{RT}, B^{RQ} and B^{R9}. A shorter R_n block was used compared to the experiments with synthetic peptides (B^{R9} instead of B^{R14}) since highly cationic polypeptides are often difficult to express because of their possible toxicity to the production host, in our case *E. coli*.

Three fusion proteins were successfully produced and purified from *E. coli*. Representative SDS-PAGE and MALDI coupled to time-of-flight mass spectrometry (MALDI-TOF) results for B^{RT}-E^S_{40} are shown in Figure 3-6. As expected, the overexpressed polypeptides are not found in the insoluble cell pellet (Figure 3-6a) but rather in the soluble extract obtained after cell disruption. The presence of positively charged silica binding domains *B* in the fusion proteins was used for purification via cation-exchange chromatography. This method allowed for a nearly complete purification in one step. A final mild bake-out procedure was sufficient to further purify the desired proteins to an acceptable level (Figure 3-6a). As previously observed, the poor SDS-binding of ELPs leads to anomalously high molecular weights in SDS-PAGE when compared with globular protein molecular weight standards.[57,58] To confirm

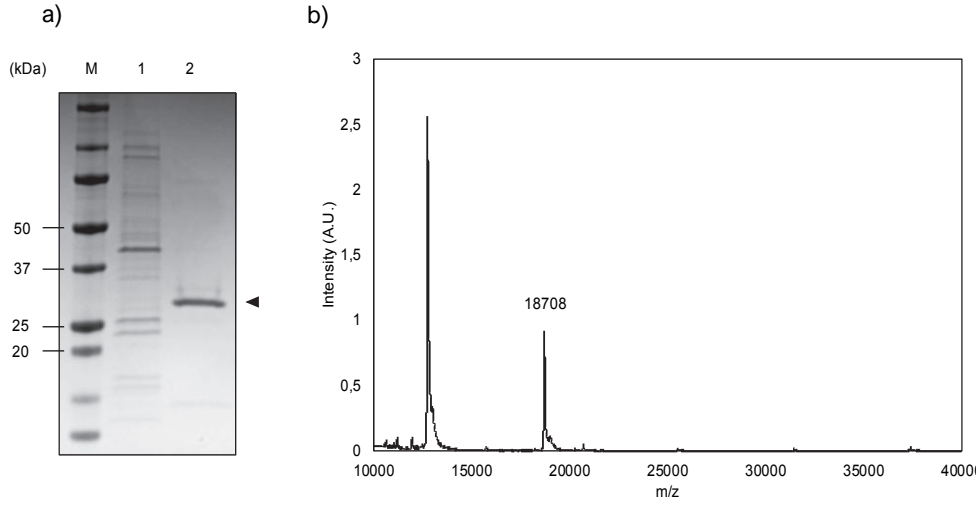

Figure 3-6. Purification and characterization of recombinant *B*-E^S_{40} diblock polypeptides, example data for B^{RT}-E^S_{40}. **(a)** SDS-PAGE analysis. Lane 1: insoluble pellet; lane 2: purified polypeptide; lane M: molecular mass marker. **(b)** MALDI-TOF spectrum.

the identity of the polypeptides, MALDI-TOF spectra were determined for the purified proteins (Figure 3-6b). The experimentally determined masses correspond well with the theoretically expected values, as shown in Table 3-4. A further confirmation was obtained via N-terminal protein sequencing (data not shown).

Next, layer formation on silica surfaces was studied using QCM-D for the B-E^S_{40} diblocks and compared to that of the binding blocks B alone. A representative comparison for 1 μM B^{RT} peptide versus the same molar concentration of B^{RT}-E^S_{40} diblock polypeptide is shown in Figure 3-7. At this concentration, saturated layers were formed for both the SBP and the diblock polypeptide. The curves of the frequency shift Δf and dissipation D versus time are substantially different for the two cases: for the diblock polypeptide, both the frequency shift and the dissipation are higher. This indicates that, due to the E^S_{40} tails, the adsorbed mass per unit area is higher. In addition, the highly hydrated non-adsorbed E^S_{40} tails do not co-vibrate with the quartz crystal, in contrast to the strongly adsorbed B^{RT} domains, leading to high dissipation.[59] Similar results were found for the other diblock polypeptides, B^{RQ}-E^S_{40} and B^{R9}-E^S_{40}. This finding confirms that the diblock polypeptides form self-assembled E^S_{40} brushes as intended.

Given the complexities and uncertainties in precisely fitting QCM-D data for cases when significant dissipation is present, the frequency change Δf was used as a qualitative measure for the adsorbed amount.[3] Limiting values of the frequency change Δf versus concentration are shown in Figure 3-8. Whereas for the individual B blocks we found that saturated layers are formed at concentrations around 1 μM, it seems that for the diblock polypeptides a saturation value for the frequency change is already reached at concentrations below 1 μM. This could be caused by the steric repulsion of the E^S_{40} tails limiting further adsorption, as was also found for similar diblock polypeptides adhering to double stranded DNA.[60]

Table 3-4. Molecular weights of diblock polypeptides B-E^S_{40} as computed from the amino acid sequence and as determined using MALDI-TOF.

Diblock polypeptide	M_{theo} (kg mol^{-1})	M_{exp} (kg mol^{-1})
B^{R9}-E^S_{40}	17.452	17.458
B^{RQ}-E^S_{40}	17.645	17.652
B^{RT}-E^S_{40}	18.704	18.708

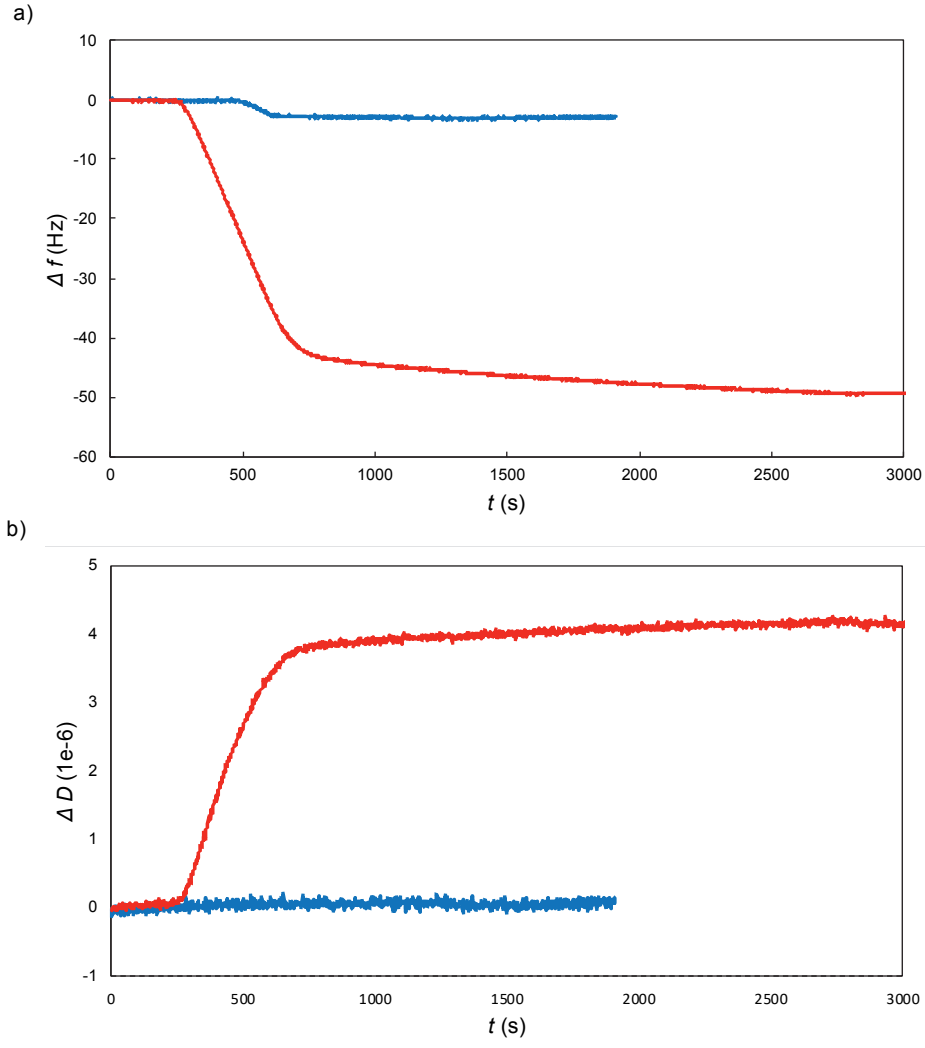

Figure 3-7. Representative comparison of QCM-D data for adsorption to silica for 1μM *B*-E^{S}_{40} diblock polypeptides with corresponding data for the SBP *B*. Red: diblock polypeptides B^{RT}-E^{S}_{40}; blue: SBP B^{RT}. **(a)** Frequency shift versus time. **(b)** Dissipation versus time.

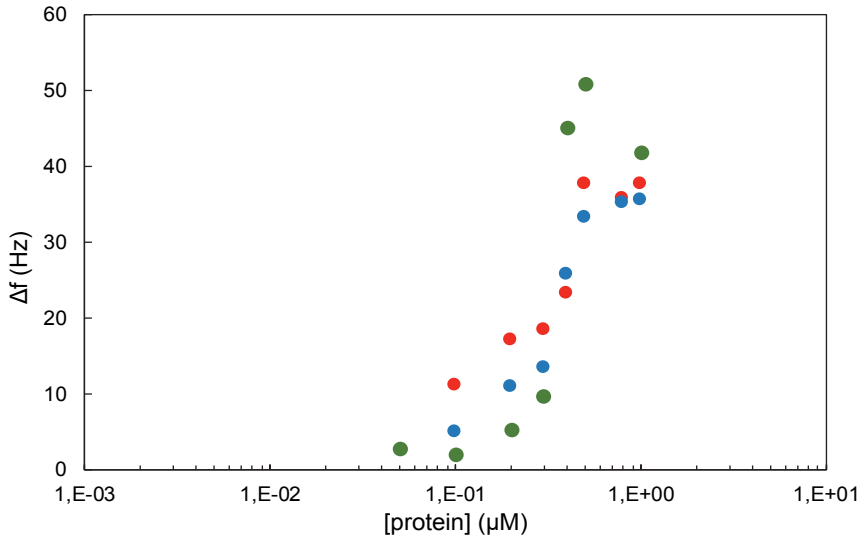

Figure 3-8. Limiting frequency shifts Δf for B-E^S_{40} diblocks, versus polypeptide concentration c (μM). Green: B=B^{RT}; blue: B=B^{RQ}; red: B=B^{R9}.

Other aspects of the polypeptide brushes self-assembled from B-E^S_{40} on silica were investigated for the specific case of B = B^{RT}. First, we considered the dependence of brush formation on solution conditions. Since the adsorption of the cationic binding peptides is largely electrostatically driven, we expect a significant dependence of the layer formation on the ionic strength of the buffer. This expectation is confirmed by the QCM-D results shown in Figure 3-9.

As shown in Figure 3-9a, an adsorbed layer is rapidly formed when flowing a solution of 5 μM of B^{RT}-E^S_{40} in PB over a clean silica surface. Upon rinsing with PB buffer, there is a negligible change in the frequency shift, indicating minimal desorption. This observation is similar to the peptide binding blocks B by themselves. Upon shifting to PBS (=PB + 150 mM NaCl), we observe a significant decrease in the magnitude of the frequency shift. Finally, upon flushing in PB + 500 mM NaCl, the frequency shift drops nearly to the baseline. A separate channel was used to correct for the effect of the buffer on the crystal oscillation frequency. The experiment indicates that the stability of the self-assembled polypeptide brushes is strongly influenced by the ionic strength of the buffer.

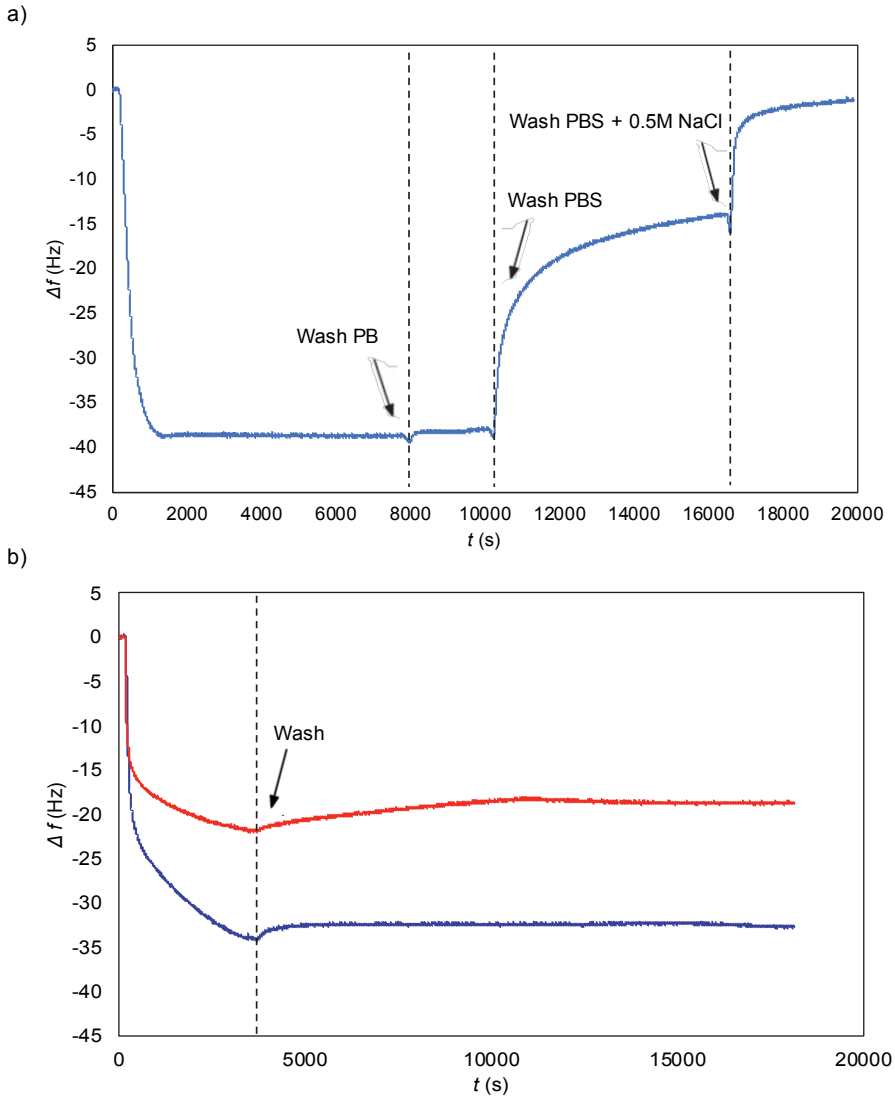

Figure 3-9. Salt-dependence of brush formation for 5 μM B^{RT}-E^{S}_{40} frequency shift Δf versus time *t*. **(a)** Adsorption of B^{RT}-E^{S}_{40} from PB followed by washing with PBS (150 mM NaCl), followed by washing with a high salt buffer (PBS + 0.5 M NaCl). **(b)** Adsorption from PB followed by washing with PB (blue), compared with adsorption from PBS followed by washing with PBS (red).

In another QCM-D experiment, brushes were assembled at different ionic strengths rather than exposed to a higher ionic strength after having been formed at low ionic strength. Results are shown in Figure 3-9b. A 5 μM solution of B^{RT}-E^{S}_{40} in either PB or PBS was flown over a clean silica sensor. After a saturated layer had formed, the sensor was rinsed with either PB or PBS for 4 h and the shift in frequency of the sensor was monitored. We find that the frequency shift for assembly in PBS is similar to the shift when the layer is first formed in PB and subsequently exposed to PBS. Note that for this experiment, we performed prolonged rinsing with buffer and even after many hours of rinsing, there is hardly any shift in frequency. This indicates that for a given buffer composition, there is no polypeptide desorption neither when rinsing with PB for saturated layers formed in PB nor for PBS for saturated layers formed in PBS.

The self-assembled polypeptide brushes can be used to stabilize and functionalize not only macroscopic flat silica surfaces but also silica nano- and microparticles. To investigate brush formation around silica nanoparticles, DLS was performed on nonporous silica particles with a reported hydrodynamic diameter of D_H = 163 nm. A diluted suspension of these particles was incubated for 5 min with increasing concentrations of the diblock polypeptide B^{RT}-E^{S}_{40}. As shown in Figure 3-10, we determine a hydrodynamic diameter of 161 ± 0.8 nm for the bare silica particles, in agreement with the manufacturer specifications. Upon increasing the B^{RT}-E^{S}_{40} diblock concentration, the particle diameter increases until it stabilizes at a final diameter of approximately 189 nm at 0.5 μM B^{RT}-E^{S}_{40}. This implies an approximate hydrodynamic brush height of $h \approx 14$ nm. In a separate DLS experiment, it was found that the hydrodynamic diameter of the free B^{RT}-E^{S}_{40} diblock, which is dominated by the coil size of the E^{S}_{40} block, was D_H = 9 ± 1 nm. This finding suggests that the E^{S}_{40} chains of the adsorbed diblocks are stretched. A similar result was found for polypeptide brushes self-assembled around DNA.[60]

In searching for effective uses of our hydrophilic brush-forming polypeptides, we were inspired by a novel single-molecule biosensing platform in which the mobility of a functionalized micrometer-sized particle tethered to a functionalized surface is modulated by single-molecule interactions.[61–63] This new biosensing platform allows for the continuous monitoring of analytes and is based on affinity interactions, similarly to, for example, an antibody sandwich or competition assay. For such a platform, it is essential to completely block

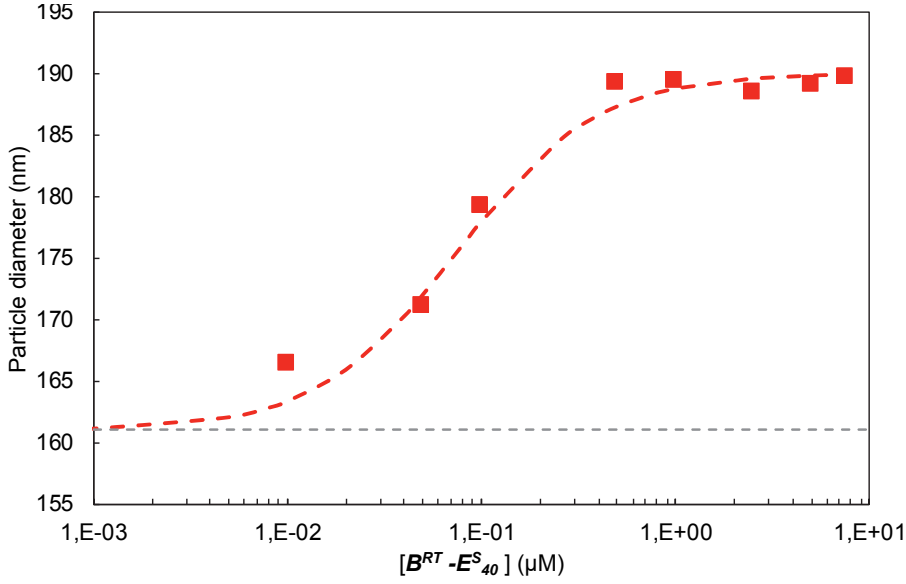

Figure 3-10. Formation of stable polymer brush on silica particles measured with DLS. Particle diameter versus concentration of B^{RT}-E^{S}_{40}. Bare nonporous silica particles were incubated with increasing concentrations of B^{RT}-E^{S}_{40}, and the particle size was measured by means of dynamic light scattering. Each measurement was repeated three times, error bars are contained within the size of the dot. The gray dashed line represents the measured hydrodynamic diameter of bare silica particles.

interaction of the tethered particles with non-functionalized surfaces. As a first demonstration of the functionality of the self-assembled brushes in a biosensing application, we demonstrate the effectiveness of the B^{RT}-E^{S}_{40} diblocks in blocking nonspecific particle–surface interactions. It is nonetheless worth noting that for full functionality of the polypeptides in biosensing, we will also need to show adequate antifouling against smaller biomolecules and long-term stability of the brushes. This aspect will be the subject of later chapters. Blocking of nonspecific interactions by polypeptide brushes formed by B^{RT}-E^{S}_{40} diblocks on silica nanoparticles and glass slides was tested using a particle mobility assay, as illustrated in Figure 3-11. The interactions between particles and surface are directly reflected by the mobility.[64] To record the mobility of micron-sized particles over time, we used dark-field microscopy. The position of every particle at each frame is localized with an accuracy of about 20 nm

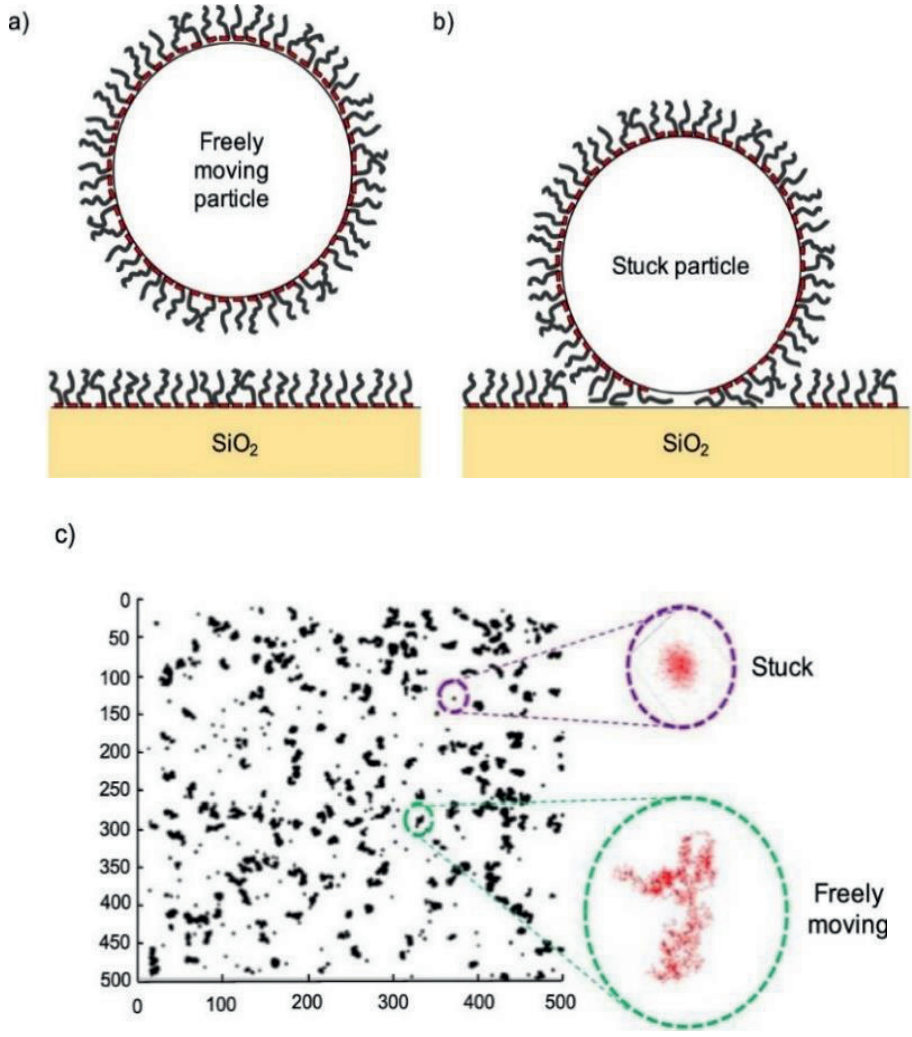

Figure 3-11. Schematic representation of the particle mobility assay. Particles coated with biomolecules such as ssDNA, streptavidin, and B^{RT}-E^{S}_{40} sediment to the surface of the substrate and show Brownian motion. The mobility and fraction of stuck particles is influenced by the interactions between particles and surfaces. **(a)** Schematic of a particle not interacting with the surface and **(b)** a particle strongly interacting. **(c)** Example of particle position trajectories recorded over time for multiple particles. The insets show typical observed trajectories for a stuck and freely moving particle.

and then reconstructed into a trajectory over time. Silica particles and magnetic particles with specific modifications are sedimented onto the surface of coated glass slides and their trajectories are reconstructed. For each particle, a two-dimensional diffusion coefficient D_{2D} is determined from the mean squared displacement, $\langle(\vec{r}(t+\tau)-\vec{r}(t))^2\rangle = 4D_{2D}\tau$. By analyzing the particle trajectories and setting a threshold for the diffusion coefficient, freely moving particles and stuck particles are distinguished, and percentages are obtained for particles that ultimately become stuck. Results are given in Table 3-5, for silica and polystyrene particles with various surface modifications, and for silica surfaces coated with either B^{RT}-E^{S}_{40} diblock polypeptides or PLL-*g*-PEG copolymers, which is the current standard for self-assembled antifouling brushes. While both B^{RT}-E^{S}_{40} and PLL-*g*-PEG coatings are effective in preventing nonspecific interactions if both the particle and the surface are non-functionalized, various functionalized particles with biosensing applications such as ssDNA-, biotin-PEG-, and streptavidin-coated particles stick stronger to PLL-*g*-PEG-coated glass slides. In contrast, minimal nonspecific interactions are found between these functionalized particles and glass slides coated with B^{RT}-E^{S}_{40}, demonstrating the usefulness of B^{RT}-E^{S}_{40} as a blocker of nonspecific particle-surface interactions.

3.4. Concluding remarks

By comparing the surface binding ability of different arginine-rich silica-binding peptides *B*, we have established that in-plane, peptide–peptide interactions play a crucial role in the formation of adsorbed silica-binding peptide layers. Presumably thanks to the cooperative nature of the layer formation by the SBPs *B*, the self-assembled brushes formed by the *B*-E^{S}_{40} diblocks are excellent blockers of various nonspecific interactions.

Table 3-5. Fraction of differently modified particles stuck to differently modified silica surfaces (%), as obtained from a particle mobility assay.

particle type	**modification**	**glass modification**	
		B^{RT}-E^{S}_{40}	**PLL-*g*-PEG**
silica	B^{RT}-E^{S}_{40}	1.3 ± 0.6	3.8 ± 0.9
silica	PLL-*g*-PEG	1.9 ± 0.6	2.5 ± 0.2
polystyrene	ssDNA	1.0 ± 0.7	25.0 ± 14.6
polystyrene	biotin-PEG	1.7 ± 0.8	12.6 ± 6.0
polystyrene	streptavidin	3.2 ± 1.0	80.1 ± 13.0

A possible advantage of these polypeptides over other self-assembling brush systems such as PLL-*g*-PEG is that our diblock polypeptide can directly be used as a recombinant immobilization tag for functional proteins. In addition, we have found that PLL-*g*-PEG does not perform as effectively as B^{RT}-E^{S}_{40} in blocking nonspecific interactions of functionalized particles with glass surfaces. Nonetheless, further testing is necessary to evaluate the antifouling properties of our polymer brush compared to PLL-*g*-PEG. Since SBPs have been investigated for many types of surfaces, such as plastics and metals, the recombinant polypeptide approach also appears to be easier to generalize than the synthetic adsorbing bottle-brush systems.

Our diblocks are also a good starting point for the design of polypeptides that form brushes with improved salt resistance, as it may be required for some applications. Stronger attachment of the brushes to silica could possibly be engineered by arranging for higher binding cooperativity. For example, elaborating on a previous example of silica-binding ELP micelles,[19] one could try designing triblock polypeptides featuring an additional "self-assembly" midblock, which could be a more hydrophobic ELP block. Alternatively, one could try to include multiple binding tags in a linear topology, although the gain in binding strength should be balanced against an inevitable reduction in the grafting density of the polymer brush.

3.5. List of abbreviations

Abbreviation	Meaning
AFM	atomic force microscopy
DLS	dynamic light scattering
ELP	elastin-like polypeptide
FdY	Friddle-de Yoreo
HEPES	4-(2-hydroxyethyl)-1-piperazineethanesulfonic acid
HPLC	high-performance liquid chromatography
MALDI	matrix-assisted laser desorption/ionization
MALDI-TOF	MALDI coupled to time-of-flight mass spectrometry
PB	phosphate buffer
PBS	phosphate-buffered saline
PEG	poly(ethylene glycol)
PEG-*g*-PLL	poly(l-lysine)-grafted poly(ethylene glycol)
PEG-*g*-PEI	polyethylene imine-grafted poly(ethylene glycol)
PRe-RDL	recursive directional ligation by plasmid reconstruction
QCM	quartz crystal microbalance
QCM-D	quartz crystal microbalance with dissipation monitoring
SBP	solid-binding peptide
SDS-PAGE	sodium dodecyl sulfate-polyacrylamide gel electrophoresis
SMFS	single molecule force spectroscopy
TB	Terrific Broth

3.6. Appendix

Table A3-1. Sequences of used synthetic gene fragments

	Nucleotide sequence	**Amino acid sequence**
B^{R9}	cccctctagaaataattttgtttaactttaagaag gaggagtacatatgcgtcgccgtcgacgccg gcgccgtaggtgatgataataattcttcaggatc cgaattc	RRRRRRRRR
B^{RQ}	cccctctagaaataattttgtttaactttaagaag gaggagtacatatgcgccagagcagccgcg gccgccgccagagcagccgcggccgggggg tgatgataataattcttcaggatccgaattc	RQSSRGRRQSSRGR
B^{RT}	cccctctagaaataattttgtttaactttaagaag gaggagtacatatgcgtacccatcggaaacg cactcaccgcaaacgcacacaccggaagcg tacgcatcgcaaggggtgataataataagactt caggatccgaattc	RTHRKRTHRKRTHRKRTHRK
E^{S}_{40}	gaggagatacatatggtcgggagtgcctggat cgggcgttcctgggtccggagtacctggctcg ggagtaccgggttctggcgttccaggtagtgg cgtcccagggagtggggtacctgggtcgggt gtaccgggctctggtgtgcctggttcgggagtc ccaggttccggagtgccaggatcaggcgtac caggctcaggtgtccctggttcaggagtgccg ggaagtggggtccctggatctggtgtcccagg atctggagttccgggatcaggtgtgccaggttc tggagtgcccggatctggggtgcctgggagc ggcgtacctggtagtggggttccaggctccgg tgtacccggatcaggggtaccaggttcaggtgt acctggatcaggagtcccgggtagtggagtac cagggtcaggtgttccagggtctggagtccct ggcagtggtgtaccaggatccggagtccccg gaagcggtgttcccggtagcggagttccagga tcgggggtaccggggtcaggagttcctggatc cggcgtgccaggcagcggggtacccggctc aggagtacccggttcaggggttcctggttctgg tgttcctggctgataataatgatcttcaggaattc	SGVPGSGVPGSGVPGSGVPGSG VPGSGVPGSGVPGSGVPGSGVP GSGVPGSGVPGSGVPGSGVPGS GVPGSGVPGSGVPGSGVPGSGV PGSGVPGSGVPGSGVPGSGVPG SGVPGSGVPGSGVPGSGVPGSG VPGSGVPGSGVPGSGVPGSGVP GSGVPGSGVPGSGVPGSGVPGS GVPGSGVPGSGVPGSGVPGSGV P

*for underlined nucleotides

Table A3-2. Full amino acid sequences of diblock polypeptide

	Amino acid sequence
B^{R9}-E^{S}_{40}	RRRRRRRRRGSGVPGSGVPGSGVPGSGVPGSGVPGSGVPG SGVPGSGVPGSGVPGSGVPGSGVPGSGVPGSGVPGSGVPGSGVPG SGVPGSGVPGSGVPGSGVPGSGVPGSGVPGSGVPGSGVPGSGVPGSGVPG SGVPGSGVPGSGVPGSGVPGSGVPGSGVPGSGVPGSGVPGSGVPGSGVPG SGVPGSGVPGSGVPGSGVPGSGVPGSGVP
B^{RQ}-E^{S}_{40}	RQSSRGRRQSSRGRGSGVPGSGVPGSGVPGSGVPGSGVPGSGVPG SGVPGSGVPGSGVPGSGVPGSGVPGSGVPGSGVPGSGVPGSGVPGSGVPG SGVPGSGVPGSGVPGSGVPGSGVPGSGVPGSGVPGSGVPGSGVPGSGVPG SGVPGSGVPGSGVPGSGVPGSGVPGSGVPGSGVPGSGVPGSGVPGSGVPG SGVPGSGVPGSGVPGSGVPGSGVPGSGVP
B^{RT}-E^{S}_{40}	RTHRKRTHRKRTHRKRTHRKGSGVPGSGVPGSGVPGSGVPGSGVPG SGVPGSGVPGSGVPGSGVPGSGVPGSGVPGSGVPGSGVPGSGVPGSGVPG SGVPGSGVPGSGVPGSGVPGSGVPGSGVPGSGVPGSGVPGSGVPGSGVPG SGVPGSGVPGSGVPGSGVPGSGVPGSGVPGSGVPGSGVPGSGVPGSGVPG SGVPGSGVPGSGVPGSGVPGSGVPGSGVPGSGVPGSGVP

a)

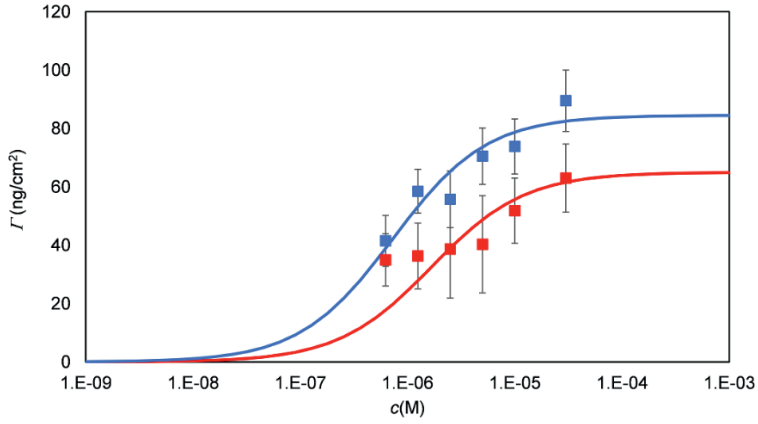

b)

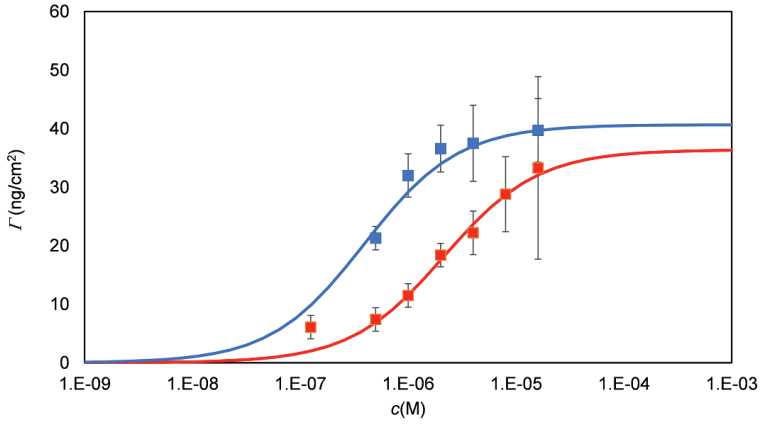

Figure A3-1. QCM-D data for the adsorption of the SBPs **(a)** B^{RQ} and **(b)** B^{R14}. Saturation adsorbed mass Γ(ng cm^{-2}) versus peptide concentration c (M). Blue filled squares: adsorption in PB buffer; red filed squares: adsorption in PBS buffer. Data was fitted using Langmuir isotherms (solid lines) to obtain apparent dissociation constants $K_{d,app}$ (M^{-1}) and maximum adsorbed masses Γ_{max} (Table **3-2**, main text). Error bars are standard deviations for > 3 independent measurements.

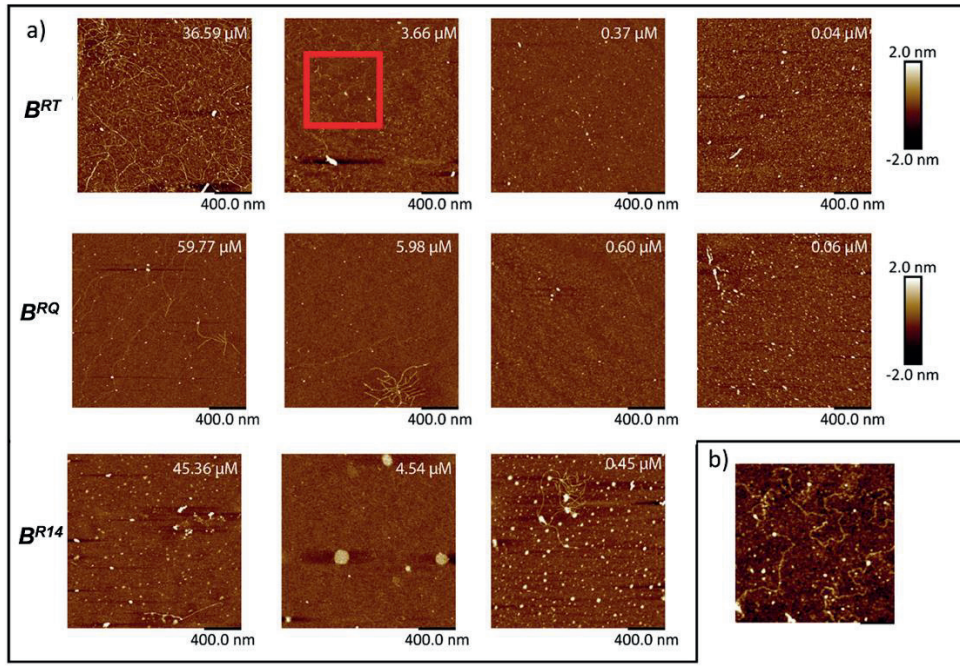

Figure A3-2. AFM images in air for SBPs B^{RT}, B^{RQ}, and B^{R14} deposited on clean silica surfaces from solution (phosphate buffer) at different concentrations. **(a)** Top row B^{RT}; middle row B^{RQ}; bottom row B^{R14}; concentration decreases from left to right. Surface-induced fibril formation is most pronounced at higher concentrations. **(b)** 200×200 nm zoom for B^{RT} at 3.66 mM for region indicated by red square in (a).

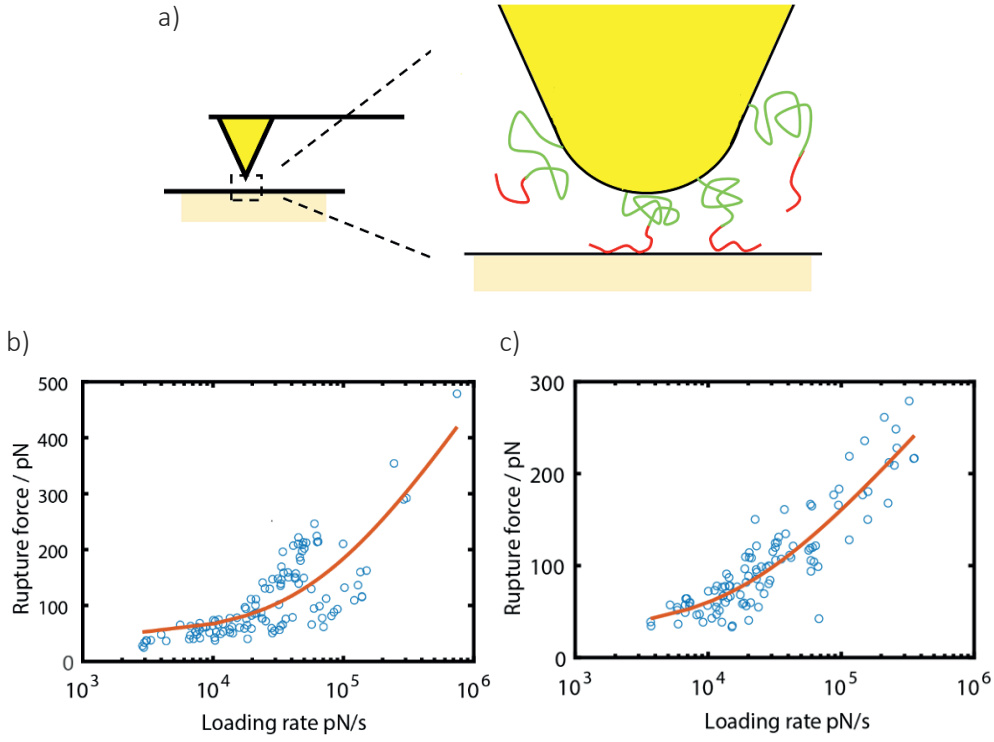

Figure A3-3. (a) Schematic representation of AFM-based force-spectroscopy for SBPs adhering to silica. Peptides are in red, the PEG27 linker is in green, AFM tip is in yellow. **(b)** Average rupture force versus loading rate for all events with < 7 SBPs binding in parallel (open symbols) and fit to Friddle-de Yoreo model for B^{RQ}. **(c)** Average rupture force versus loading rate for all events with < 7 SBPs binding in parallel (open symbols) and fit to Friddle-de Yoreo model for $B^{R13}Cys$. For the fit parameters, see Table 3-2, main text.

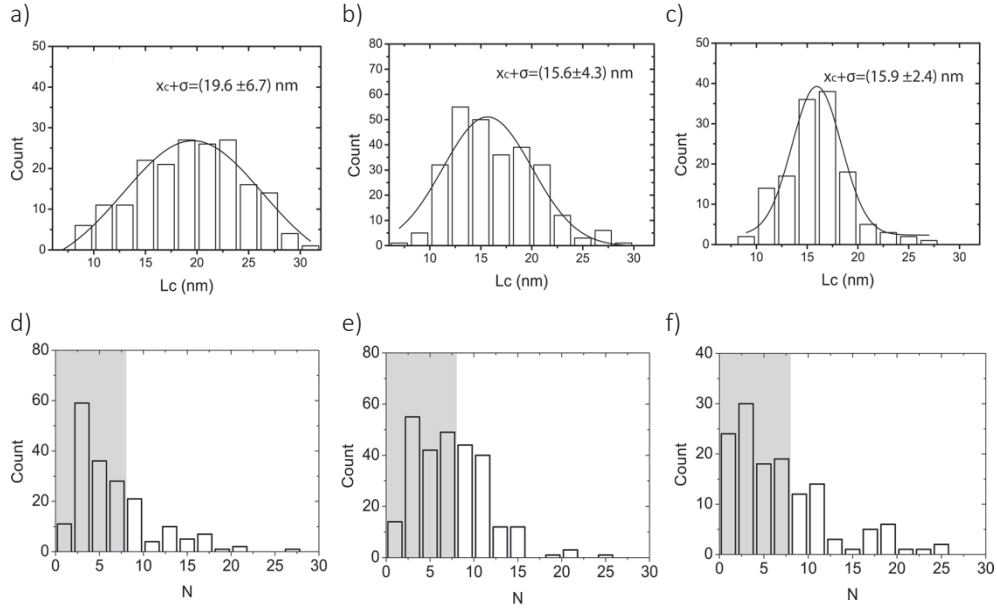

Figure A3-4. Event selection for the measurement of force-extension curves using AFM. All single-rupture events were fitted to a FJC model, to give a contour length Lc and the number N of SBPs binding (in parallel) to the surface. **(a)**-**(c)** Histograms of contour lengths. The average contour length and standard deviation are indicated in the figures. **(a)** B^{RT}; **(b)** B^{RQ}; **(c)** $B^{R13}Cys$. **(d)**-**(f)** Histograms of number N of SBPs binding (in parallel) to the surface. For determining the average rupture force versus loading rate, only events with N < 7 are used, indicated in grey. **(d)** B^{RT}; **(e)** B^{RQ}; **(f)** $B^{R13}Cys$.

3.7. References

[1] K. E. Sapsford, W. R. Algar, L. Berti *et al.* Functionalizing nanoparticles with biological molecules: Developing chemistries that facilitate nanotechnology. *Chemical Reviews* 113, 1904–2074 (2013).

[2] E. A. Vogler. Protein adsorption in three dimensions. *Biomaterials* 33, 1201–1237 (2012).

[3] M. Rabe, D. Verdes, S. Seeger. Understanding protein adsorption phenomena at solid surfaces. *Advances in Colloid and Interface Science* 162, 87–106 (2011).

[4] B. Saha, P. Songe, T. H. Evers, M. W. J. Prins. The influence of covalent immobilization conditions on antibody accessibility on nanoparticles. *Analyst* 142, 4247–4256 (2017).

[5] Q. Yu, Y. Zhang, H. Wang, J. Brash, H. Chen. Anti-fouling bioactive surfaces. *Acta Biomaterialia* 7, 1550–1557 (2011).

[6] S. Lowe, N. M. O'Brien-Simpson, L. A. Connal. Antibiofouling polymer interfaces: Poly(ethylene glycol) and other promising candidates. *Polymer Chemistry* 6, 198–212 (2015).

[7] J. Baggerman, M. M. J. Smulders, H. Zuilhof. Romantic Surfaces: A Systematic Overview of Stable, Biospecific, and Antifouling Zwitterionic Surfaces. *Langmuir* 35, 1072–1084 (2019).

[8] S. Gon, B. Fang, M. M. Santore. Interaction of cationic proteins and polypeptides with biocompatible cationically-anchored PEG brushes. *Macromolecules* 44, 8161–8168 (2011).

[9] L. Zhang, B. D. Klein, C. S. Metcalf *et al.* Incorporation of monodisperse oligoethyleneglycol amino acids into anticonvulsant analogues of galanin and neuropeptide y provides peripherally acting analgesics. *Molecular Pharmaceutics* 10, 574–585 (2013).

[10] Y. Ding, P. Zhang, X. Y. Tang *et al.* PEG prodrug of gambogic acid: Amino acid and dipeptide spacer effects. *Polymer* 53, 1694–1702 (2012).

[11] S. Saxer, C. Portmann, S. Tosatti *et al.* Surface assembly of catechol-functionalized poly(L-lysine)- graftpoly(ethylene glycol) copolymer on titanium exploiting combined electrostatically driven self-organization and biomimetic strong adhesion. *Macromolecules* 43, 1050–1060 (2010).

[12] D. W. W. Urry. Physical chemistry of biological free energy transduction as demonstrated by elastic protein-based polymers. *Journal of Physical Chemistry B* 101, 11007–11028 (1997).

[13] W. Hassouneh, S. R. MacEwan, A. Chilkoti. Fusions of elastin-like polypeptides to pharmaceutical proteins. *Methods in Enzymology* 502, 215–237 (2012).

[14] Z. Tang, J. P. Palafox-Hernandez, W. C. Law *et al.* Biomolecular recognition principles for bionanocombinatorics: An integrated approach to elucidate enthalpic and entropic factors. *ACS Nano* 7, 9632–9646 (2013).

[15] A. Sengupta, C. K. Thai, M. S. R. Sastry *et al.* A genetic approach for controlling the binding and orientation of proteins on nanoparticles. *Langmuir* 24, 2000–2008 (2008).

[16] A. Care, P. L. Bergquist, A. Sunna. Solid-binding peptides: Smart tools for

nanobiotechnology. *Trends in Biotechnology* 33, 259–268 (2015).

[17] A. Care, K. Petroll, E. S. Y. Gibson, P. L. Bergquist, A. Sunna. Solid-binding peptides for immobilisation of thermostable enzymes to hydrolyse biomass polysaccharides. *Biotechnology for Biofuels* 10, 1–16 (2017).

[18] C. W. P. Foo, S. V. Patwardhan, D. J. Belton *et al.* Novel nanocomposites from spider silk-silica fusion (chimeric) proteins. *Proceedings of the National Academy of Sciences of the United States of America* 103, 9428–9433 (2006).

[19] L. Li, N. K. Li, Q. Tu *et al.* Functional Modification of Silica through Enhanced Adsorption of Elastin-Like Polypeptide Block Copolymers. *Biomacromolecules* 19, 298–306 (2018).

[20] L. Li, C.-K. Mo, A. Chilkoti, G. P. Lopez, N. J. Carroll. Creating cellular patterns using genetically engineered, gold- and cell-binding polypeptides. *Biointerphases* 11, 021009 (2016).

[21] M. Shah, P. Y. Hsueh, G. Sun *et al.* Biodegradation of elastin-like polypeptide nanoparticles. *Protein Science* 21, 743–750 (2012).

[22] M. B. Van Eldijk, C. L. McGann, K. L. Kiick, J. C. M. Van Hest. Elastomeric polypeptides. *Topics in Current Chemistry* 310, 71–116 (2012).

[23] L. Li, C. W. Shields, J. Huang *et al.* Rapid capture of biomolecules from blood: Via stimuli-responsive elastomeric particles for acoustofluidic separation. *Analyst* 145, 8087–8096 (2020).

[24] A. Girotti, J. Reguera, J. C. Rodríguez-Cabello *et al.* Design and bioproduction of a recombinant multi(bio)functional elastin-like protein polymer containing cell adhesion sequences for tissue engineering purposes. *Journal of Materials Science: Materials in Medicine* 15, 479–484 (2004).

[25] J. Zong, S. L. Cobb, N. R. Cameron. Short elastin-like peptide-functionalized gold nanoparticles that are temperature responsive under near-physiological conditions. *Journal of Materials Chemistry B* 6, 6667–6674 (2018).

[26] P. Shi, S. Aluri, Y. A. Lin *et al.* Elastin-based protein polymer nanoparticles carrying drug at both corona and core suppress tumor growth in vivo. *Journal of Controlled Release* 171, 330–338 (2013).

[27] W. Han, S. R. MacEwan, A. Chilkoti, G. P. López. Bio-inspired synthesis of hybrid silica nanoparticles templated from elastin-like polypeptide micelles. *Nanoscale* 7, 12038–12044 (2015).

[28] J. Lee, O. Kim, J. Jung *et al.* Simple fabrication of a smart microarray of polystyrene microbeads for immunoassay. *Colloids Surf., B* 72, 173–180 (2009).

[29] J. Lee, J. Jung, K. Na, P. Heo, J. Hyun. Polypeptide-mediated switchable microarray of bacteria. *ACS Applied Materials and Interfaces* 1, 1359–1363 (2009).

[30] A. Hernandez-Garcia, M. W. T. Werten, M. C. Stuart, F. A. De Wolf, R. De Vries. Coating of single DNA molecules by genetically engineered protein diblock copolymers. *Small* 8, 3491–3501 (2012).

[31] T. Zheng, F. Perona Martínez, I. M. Storm *et al.* Recombinant Protein Polymers for Colloidal Stabilization and Improvement of Cellular Uptake of Diamond Nanosensors. *Analytical Chemistry* 89, 12812–12820 (2017).

[32] A. A. Thyparambil, Y. Wei, R. A. Latour. Determination of peptide - Surface adsorption free energy for material surfaces not conducive to SPR or QCM

using AFM. *Langmuir* 28, 5687–5694 (2012).

[33] S. O. Kim, J. A. Jackman, M. Mochizuki *et al.* Correlating single-molecule and ensemble-average measurements of peptide adsorption onto different inorganic materials. *Physical Chemistry Chemical Physics* 18, 14454–14459 (2016).

[34] S. Krysiak, S. Liese, R. R. Netz, T. Hugel. Peptide desorption kinetics from single molecule force spectroscopy studies. *Journal of the American Chemical Society* 136, 688–697 (2014).

[35] C. Tamerler, E. E. Oren, M. Duman, E. Venkatasubramanian, M. Sarikaya. Adsorption kinetics of an engineered gold binding peptide by surface plasmon resonance spectroscopy and a quartz crystal microbalance. *Langmuir* 22, 7712–7718 (2006).

[36] A. Ebner, L. Wildling, H. J. Gruber. Functionalization of AFM tips and supports for molecular recognition force spectroscopy and recognition imaging. in *Methods in Molecular Biology* vol. 1886 117–151 (Humana Press, New York, NY, 2019).

[37] F. Oesterhelt, M. Rief, H. E. Gaub. Single molecule force spectroscopy by AFM indicates helical structure of poly(ethylene-glycol) in water. *New Journal of Physics* 1, 6–6 (1999).

[38] R. W. Friddle, A. Noy, J. J. De Yoreo. Interpreting the widespread nonlinear force spectra of intermolecular bonds. *Proceedings of the National Academy of Sciences of the United States of America* 109, 13573–13578 (2012).

[39] S. Manohar, A. Jagota. Sequence-dependent force response during peeling of single-stranded DNA from graphite. *Physical Review E - Statistical, Nonlinear, and Soft Matter Physics* 81, 021805 (2010).

[40] N. C. Tang, A. Chilkoti. Combinatorial codon scrambling enables scalable gene synthesis and amplification of repetitive proteins. *Nature Materials* 15, 419–424 (2016).

[41] J. R. McDaniel, J. A. MacKay, F. G. Quiroz, A. Chilkoti. Recursive directional ligation by plasmid reconstruction allows rapid and seamless cloning of oligomeric genes. *Biomacromolecules* 11, 944–952 (2010).

[42] Ralph K. Iler. *The Chemistry of Silica: Solubility, Polymerization, Colloid and Surface Properties and Biochemistry of Silica*. (Wiley, 1979).

[43] M. A. A. Abdelhamid, T. Ikeda, K. Motomura *et al.* Application of volcanic ash particles for protein affinity purification with a minimized silica-binding tag. *Journal of Bioscience and Bioengineering* 122, 633–638 (2016).

[44] R. Hassert, M. Pagel, Z. Ming *et al.* Biocompatible silicon surfaces through orthogonal click chemistries and a high affinity silicon oxide binding peptide. *Bioconjugate Chemistry* 23, 2129–2137 (2012).

[45] A. Gladytz, T. John, T. Gladytz *et al.* Peptides@mica: From affinity to adhesion mechanism. *Physical Chemistry Chemical Physics* 18, 23516–23527 (2016).

[46] C. K. Thai, H. Dai, M. S. R. Sastry *et al.* Identification and characterization of Cu2O- and ZnO-binding polypeptides by escherichia coli cell surface display: Toward an understanding of metal oxide binding. *Biotechnology and Bioengineering* 87, 129–137 (2004).

[47] S. Zernia, R. Frank, R. H. J. Weiße *et al.* Surface-Binding Peptide Facilitates Electricity-Driven NADPH-Free Cytochrome P450 Catalysis. *ChemCatChem*

10, 525–530 (2018).

[48] M. Malmsten, P. Linee, T. Cosgrove. Adsorption of PEO-PPO-PEO Block Copolymers at Silica. *Macromolecules* 25, 2474–2481 (1992).

[49] M. Hnilova, C. R. So, E. E. Oren *et al.* Peptide-directed co-assembly of nanoprobes on multimaterial patterned solid surfaces. *Soft Matter* 8, 4327–4334 (2012).

[50] A. Rimola, M. Sodupe, P. Ugliengo. Affinity scale for the interaction of amino acids with silica surfaces. *Journal of Physical Chemistry C* 113, 5741–5750 (2009).

[51] R. H. Meißner, G. Wei, L. C. Ciacchi. Estimation of the free energy of adsorption of a polypeptide on amorphous SiO2 from molecular dynamics simulations and force spectroscopy experiments. *Soft Matter* 11, 6254–6265 (2015).

[52] R. W. Friddle, K. Battle, V. Trubetskoy *et al.* Single-molecule determination of the face-specific adsorption of Amelogenin's C-terminus on hydroxyapatite. *Angewandte Chemie - International Edition* 50, 7541–7545 (2011).

[53] V. Reiter-Scherer, J. L. Cuellar-Camacho, S. Bhatia *et al.* Force Spectroscopy Shows Dynamic Binding of Influenza Hemagglutinin and Neuraminidase to Sialic Acid. *Biophysical Journal* 116, 1037–1048 (2019).

[54] M. Pfreundschuh, D. Alsteens, R. Wieneke *et al.* Identifying and quantifying two ligand-binding sites while imaging native human membrane receptors by AFM. *Nature Communications* 6, 8857 (2015).

[55] K. K. Sand, R. W. Friddle, J. J. Deyoreo. Quantifying the free energy landscape between polymers and minerals. *Scientific Reports* 7, 8663 (2017).

[56] J. Tao, K. C. Battle, H. Pan *et al.* Energetic basis for the molecular-scale organization of bone. *Proceedings of the National Academy of Sciences of the United States of America* 112, 326–331 (2015).

[57] L. Willems, L. Van Westerveld, S. Roberts *et al.* Nature of amorphous hydrophilic block affects self-assembly of an artificial viral coat polypeptide. *Biomacromolecules* 20, 3641–3647 (2019).

[58] L. Willems, S. Roberts, I. Weitzhandler *et al.* Inducible Fibril Formation of Silk-Elastin Diblocks. *ACS Omega* 4, 9135–9143 (2019).

[59] I. Reviakine, D. Johannsmann, R. P. Richter. Hearing what you cannot see and visualizing what you hear: Interpreting quartz crystal microbalance data from solvated interfaces. *Analytical Chemistry* 83, 8838–8848 (2011).

[60] I. M. Storm, M. Kornreich, A. Hernandez-Garcia *et al.* Liquid crystals of self-assembled DNA bottlebrushes. *Journal of Physical Chemistry B* 119, 4084–4092 (2015).

[61] E. W. A. Visser, J. Yan, L. J. Van IJzendoorn, M. W. J. Prins. Continuous biomarker monitoring by particle mobility sensing with single molecule resolution. *Nature Communications* 9, 1–10 (2018).

[62] R. M. Lubken, A. M. De Jong, M. W. J. Prins. Multiplexed Continuous Biosensing by Single-Molecule Encoded Nanoswitches. *Nano Letters* 20, 2296–2302 (2020).

[63] J. Yan, L. Van Smeden, M. Merkx, P. Zijlstra, M. W. J. Prins. Continuous Small-Molecule Monitoring with a Digital Single-Particle Switch. *ACS Sensors* vol. 5 1168–1176 at https://doi.org/10.1021/acssensors.0c00220 (2020).

[64] T. Yanagishima, L. Di Michele, J. Kotar, E. Eiser. Diffusive behaviour of PLL-PEG

coated colloids on λ-DNA brushes - Tuning hydrophobicity. *Soft Matter* 8, 6792–6798 (2012).

CHAPTER 4

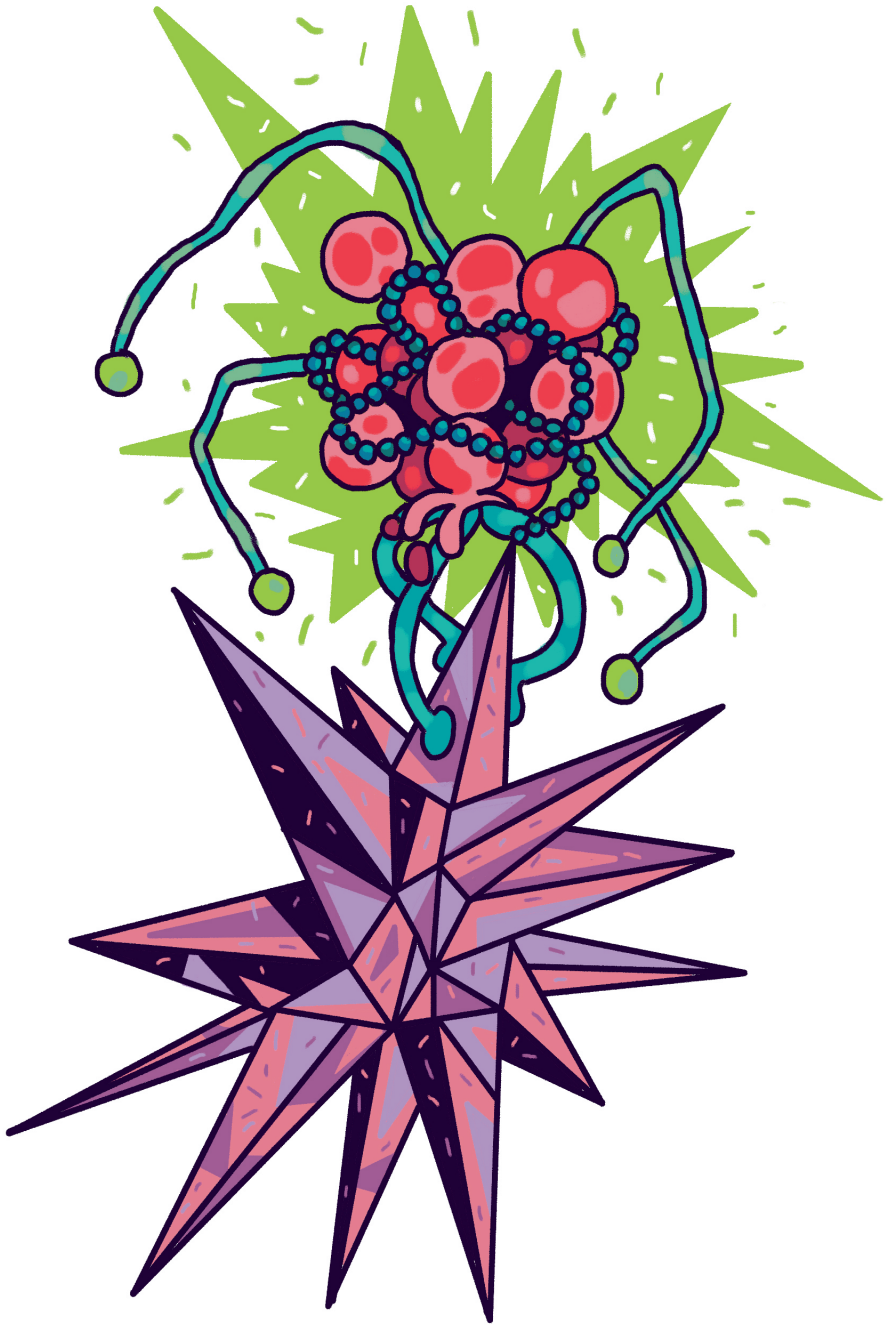

Design of polypeptides self-assembling into antifouling coatings: applying multivalency

In this chapter, we propose to apply multivalent binding of solid-binding peptides (SBPs) for the physical attachment of antifouling polypeptide brushes on solid surfaces. Using a silica-binding peptide as a model SBP, we find that both tandem-repeated SBPs and SBPs repeated in branched architectures implemented via a multimerization domain work well to improve the binding strength of polypeptide brushes, as compared to earlier designs with a single SBP. At the same time, either the solubility or the yield of recombinant production is low for many of the designed sequences. For a single design, with the domain structure *B*-*M*-*E*, both solubility and yield of recombinant production were high. In this design, *B* is a silica-binding peptide, *M* is a highly thermostable, de novo-designed trimerization domain, and *E* is a hydrophilic elastin-like polypeptide. We show that the *B*-*M*-*E* triblock polypeptide rapidly assembles into highly stable polypeptide brushes on silica surfaces, with excellent antifouling properties against high concentrations of serum albumin. Given that SBPs adsorbing to a wide range of materials have been identified, the *B*-*M*-*E* triblock design provides a template for the development of polypeptides for coating other materials such as metals or plastics.

This chapter is published as:
Nicolò Alvisi, Chuanbao Zheng, Meike Lokker, Victor Boekestein, Robbert de Haas, Bauke Albada, Renko de Vries; Design of Polypeptides Self-Assembling into Antifouling Coatings: Exploiting Multivalency in *Biomacromolecules* **2022** *23 (9)*, 3507–3516

4.1. Introduction

A key challenge in designing interfaces between artificial materials and biological materials (foods, body fluids, tissues, microorganisms, etc.) is to prevent unwanted adsorption and accumulation of biological macromolecules and microorganisms at the interface.[1,2] For solid surfaces, coatings with a hydrophilic polymer brush can prevent biofouling to a large degree.[3,4] The brushes can be attached to the surfaces either chemically or via multiple weaker physical bonds, with both approaches having their own advantages and disadvantages.[2,5,6] The best-known examples of physical attachment of antifouling brushes are comb polymers with surface-binding main chains and antifouling side chains, such as the widely used poly(L-lysine)-*g*-poly(ethylene glycol) (PLL-*g*-PEG) graft copolymers with PLL main chains and a high density of short PEG side chains.[6,7] This polymer is particularly effective for negatively charged surfaces such as glass.[6]

For strong physical attachment to a wider range of important solid materials (metals, plastics, and minerals), solid-binding peptides (SBPs) are a useful strategy.[8,9] SBPs are short amino acid sequences selected for binding to solid surfaces, usually with enrichment strategies such as phage display.[10,11] Multiple SBPs have been discovered and developed, with binding affinity for a wide range of materials including oxides,[12,13] metals,[14] and plastics.[15–17] Despite their application potential, their actual use for immobilizing molecular cargo to solids is still limited. In fact, the binding of SBPs to solids is not permanent since their dissociation constants are typically larger than 100 nM, depending on the solution conditions.

An obvious strategy to engineer stronger binding using SBPs is to introduce multivalent binding, displaying multiple SBPs on a scaffold structure (Figure 4-1a, b). A first approach is to use tandem repeated SBPs, connected directly or via spacers (Figure 4-1a). Hassert *et al.* reported the development of a strongly silica-binding peptide (highSP) containing quadruple repeats of the minimal binding motif of a weaker precursor.[18] Cho *et al.* showed that triplicate tandem repeats of a ZnO-binding peptide led to stronger and more stable peptide coatings on ZnO particles than the single SBP.[19] Contrarily, Seker *et al.* showed that the use of multiple SBPs does not necessarily lead to stronger binding.[20] Recent findings by Bansal *et al.* suggest that the lack of

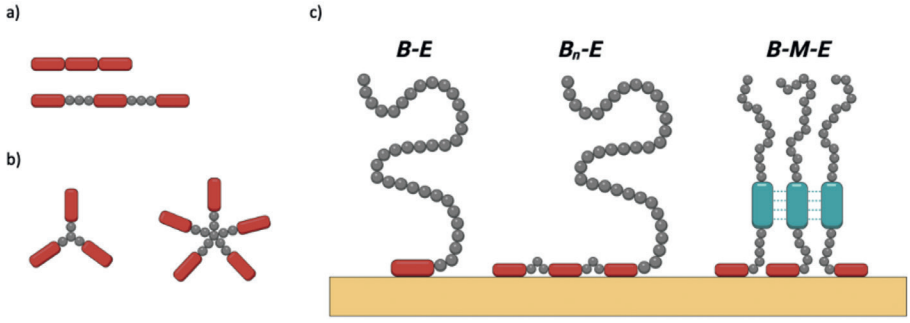

Figure 4-1. Multivalent display of SBPs. **(a)** Linear tandem repeats. **(b)** Star-like architectures on scaffold. **(c)** Brush-forming polypeptides with SBPs as "surface stickers". Left: *B-E* diblock architecture, middle: B_n-*E* diblock architecture with tandem repeated SBPs, right: *B-M-E* star-like architecture, with oligomerizing middle block *M*.

improved binding could be due to the fact that the tandem repeated SBPs cannot simultaneously adopt the optimal spatial conformation for surface binding.[21]

Among the possible scaffold architectures for multivalent display, star-like architectures have been explored for SBPs (Figure 4-1b).[22] Tang *et al.* reported a 100- fold increase in binding affinity for a tetravalent dendron exposing hydroxyapatite-binding peptides compared to the monovalent peptide.[23] Similar results were reported also for trimeric and tetrameric dendrons with diamond-like carbon-binding peptides.[24] Pentameric dendrons were also developed in order to mimic phage display.[25] Protein-based scaffolds have also been explored. For example, Terskikh *et al.* employed the pentameric assembly domain of the cartilage oligomeric matrix protein to increase the binding affinity of a synthetic peptide for cell-type specific surface recognition.[26] Similarly, Sano *et al.* fused a titanium-binding aptamer to the L chain of ferritin, creating a cage architecture of 24 polypeptide chains with a 1000-fold increase in binding affinity compared to the single SBP.[27]

Here, we focus on the physical attachment of antifouling polypeptide brushes to solid surfaces using SBPs as surface stickers, with the potential to design self-assembling brushes suitable for a wide range of solid substrates. Previously, we have reported the design of a protein-based diblock polymer *B-E* comprised of a silica-binding SBP block *B*, and a hydrophilic elastin-like domain *E* (Figure 4-1c, left). We showed that these polymers assemble into

stable hydrophilic brushes on silica surfaces and nanoparticles.[28] While the coatings were relatively stable against prolonged rinsing with phosphate-buffered saline (PBS), solutions with higher ionic strengths (>0.5 M NaCl) were still able to displace the adsorbed polymers.

For the design of polypeptide brushes with good resistance to displacement in a wider range of solvent conditions, we here explore whether we can employ multivalent SBP binding. Based on the literature on multivalent binding of SBPs discussed above, we consider both designs B_n-*E* with tandem-repeated SBPs (Figure 4-1c, middle) and designs *B*-*M*-*E* with star-like architectures, where *M* is an oligomerizing domain (Figure 4-1c, right). Unfortunately, we find that many designs do not satisfy basic prerequisites, such as simple production and purification, and good solubility. However, we find that these prerequisites are satisfied by a specific *B*-*M*-*E* design, where *M* is a highly stable, de novo-designed, trimer-forming domain. For this design, we investigate its self-assembly on silica surfaces, the stability of the brushes it forms, and the antifouling properties of these brushes with respect to bovine serum albumin.

4.2. Materials and methods

4.2.1. Construction of expression plasmids for polypeptides

For the construction of B_n-*E* diblocks with tandem repeated binding blocks B^{RT}, a synthetic gene encoding for B_n -E^S_{20} was synthesized by Twist Bioscience (USA). For n = 1, the block encodes a poly-histidine tag for downstream purification, the B^{RT} = $(RTHRK)_4$ tag, and the linker polypeptide E^S_{20} = $(VPGSG)_{20}$. For n = 2, the block encodes a poly-histidine tag for downstream purification, two B^{RT} = $(RTHRK)_4$ tags interspaced by a linker E^S_3 = $(VPGSG)_3$, and the linker polypeptide E^S_{20} = $(VPGSG)_{20}$. For n = 3, the block encodes a poly-histidine tag for downstream purification, three B^{RT} = $(RTHRK)_4$ tags interspaced by a linker E^S_3 = $(VPGSG)_3$, and the linker polypeptide E^S_{20} = $(VPGSG)_{20}$. The synthetic fragments were designed to contain the features needed for PRe-RDL cloning, as described by McDaniel.[29] The fragment was digested with *BamHI/AcuI* and ligated into a *BamHI/AcuI*-digested pET-24a(+) vector containing the E^S_{20} = $(VPGSG)_{20}$ sequence.

For the construction of *B*-*M*-*E* triblocks, a synthetic gene encoding for the B^{RT}-*M* block was synthesized by Integrated DNA Technologies (Belgium). The block encodes a poly-histidine tag for downstream purification, the B^{RT} =

$(RTHRK)_4$ tag, a linker polypeptide E^S_5 = $(VPGSG)_5$ and the multimerization domains *M*. The synthetic fragment was designed to contain the features needed for PRe-RDL cloning, as described by McDaniel.[29] The fragment was digested with *BamHI/AcuI* and ligated into a *BamHI/AcuI*-digested pET-24a(+) vector containing the E^S_{40}= $(VPGSG)_{40}$ sequence.

For all constructs, plasmid DNA was transformed into *Escherichia coli* DH5α via heat shock. Colonies containing the correct DNA insert were selected and confirmed by DNA sequencing. Then, the plasmid was transformed into *E. coli* T7-Express. The full amino acid sequences of the polypeptides are reported in Table A4-1.

4.2.2. Protein expression

E. coli T7-Express containing the expression plasmids for the polypeptides was cultured at 37 °C and 215 rpm for 16 h in 25 mL terrific broth (TB) medium containing 50 μg mL^{-1} kanamycin. The starter culture was inoculated in 1 L of lysogeny broth (LB) medium containing 50 μg mL^{-1} kanamycin and incubated at 37 °C and 215 rpm until OD_{600} > 0.6. When necessary, 0.5% D-glucose was added. Then, isopropylthio-β-galactoside was added to a final concentration of 1 mM and cells were incubated overnight at 18 °C and 215 rpm before harvesting.

4.2.3. Protein purification

Bacterial cells were centrifuged at 6000 rpm for 30 minutes at 4 °C and resuspended in 30 mL of cold extraction buffer (50 mM Tris pH 8.00, 300 mM NaCl, 30 mM imidazole). Phenylmethylsulfonyl fluoride was added to the cell suspension to a final concentration of 1 mM. Cells were lysed via sonication (Q125 Sonicator, QSonica). The cell lysate was centrifuged for 30 minutes at 30,000 g at 4 °C to pellet the insoluble fraction. Next, the polypeptide was purified using immobilized metal ion affinity chromatography (IMAC). The sample was injected in an IMAC column (Bio-Scale Mini Profinity IMAC cartridge, Bio-Rad Laboratories, USA) and washed with extraction buffer containing 2 M NaCl to remove DNA contamination. The polypeptide was eluted with a linear gradient from extraction buffer to elution buffer (50 mM Tris pH 8.00, 300 mM NaCl, 300 mM imidazole). The purity of the polypeptides was assessed by sodium dodecyl sulfate-polyacrylamide gel electrophoresis (SDS-PAGE).

4.2.4. Matrix-assisted laser desorption/ionization-time of flight analysis

To confirm the size of the polypeptide, its molecular weight was determined using matrix-assisted laser desorption/ionization mass spectrometry coupled to time-of-flight mass spectrometry (MALDI-TOF). The spectrum was obtained using a Bruker UltraFlextreme machine. The sample was prepared following the instructions provided by the manufacturer.

4.2.5. Circular dichroism

For the circular dichroism measurements, a Jasco Spectropolarimeter J-715 was used. Data were collected and analyzed with Jasco software. For the sample preparation, the protein was dissolved at a concentration of 0.1 mg mL^{-1} in PBS pH. 7.4. The solution was sonicated for 10 min to reduce the presence of aggregates before the measurement. A quartz cuvette with a 1 mm path was used. For the spectrum measurements, the instrument was set to continuous scanning mode, with a data pitch of 0.1 nm, a scanning speed of 50 nm min^{-1} and a band width of 2 nm. Each spectrum was accumulated 20 times. For the temperature ramp, the ellipticity was measured at 222 nm while increasing the temperature of the sample from 20 °C to 95 °C, at 1 °C min^{-1}.

4.2.6. Dynamic light scattering

For the dynamic light scattering (DLS) measurements, a ZS-Nano (Malvern, U.K.) instrument was used. Light scattering was measured at a scattering angle of 173°, at a temperature of 20 °C. The reported hydrodynamic sizes were obtained using the Zetasizer software version 7.13 (Malvern). Nonfunctionalized silica microspheres with a diameter of 163 nm were purchased from Bangs Laboratories (USA). For DLS on *B-M-E* solutions, the protein was dissolved in the appropriate buffer (phosphate buffer PB with increasing concentrations of NaCl). The solutions were filtered using a 0.22 µm filter and sonicated for 10 min to reduce the presence of aggregates before the measurement. For each sample, continuous measurements were performed, with the duration of each measurement defined by the instrument. Each reported hydrodynamic size is the average of 10 measurements. For measurements on silica nanoparticles coated with B_n-*E* or *B-M-E*, the polypeptide solution and the silica nanoparticles (50 µL, 0.01% v/v) were sonicated for 10 min. The polypeptide solution was filtered using a 0.22 µm

filter. Increasing concentrations of protein were incubated with the nanoparticle solution (total volume 100 µL) for 10 min. For each sample, continuous measurements were done, each reported hydrodynamic size is the average of 10 measurements, with the duration of the measurement defined by the instrument. For the ζ-potential measurements, the samples were prepared following the same procedure. A dip cell (Malvern) was used. Each reported ζ-potential value is the average of 15 measurements.

4.2.7. Quartz crystal microbalance with dissipation monitoring

The binding of polypeptide to silica was quantified with a quartz crystal microbalance with dissipation monitoring (QCM-D), using a QSense E4 instrument (Biolin Scientific, Sweden). QCM sensors coated with SiO2 were obtained from Biolin Scientific and cleaned according to the provided instructions. For the salt dependency measurements, each sensor was equilibrated with the appropriate buffer (PB, PBS 150 mM NaCl, PBS + 0.5 M NaCl, PBS + 1 M NaCl) at a flow rate of 50 µL min^{-1} until a stable baseline was reached. Bn-E or B-M-E were dissolved to a final concentration of 10 µM and dialyzed in the previously mentioned buffers. The protein solutions were sonicated for 10 minutes prior to the measurement. Analysis of QCM-D data was performed using QSense software (Biolin Scientific). For the antifouling test, each sensor was equilibrated with PBS at a flow rate of 50 µL min^{-1} until a stable baseline was reached. The SiO_2 sensors were coated with PLL-*g*-PEG (1 mg mL^{-1}), the diblock polypeptide *B-E* (5 µM) and *B-M-E* (5 µM) until a stable value of frequency shift (*Δf*) was reached. Coated and uncoated sensors were then flushed with a solution of bovine serum albumin (2 mg mL^{-1}). Analysis of QCM-D data was performed using QSense software.

4.2.8. Atomic force microscopy imaging in air

Atomically flat silica surfaces were obtained by using silicon wafers (Siltronic AG) with a 2-3 nm oxide layer due to natural oxidation with oxygen in air. Silica surfaces were cleaned with ultrapure water (MilliQ) and ethanol, and plasma-cleaned for 5 min. For atomic force microscopy (AFM) imaging, 30 µL of protein solution were deposited on a cleaned silica surface and incubated for 1 min. After that, samples were gently rinsed with MilliQ water and carefully dried with nitrogen. Samples were imaged with a Multimode Bruker AFM (Bruker, USA) using the automatic ScanAsyst imaging mode. ScanAsyst air tips with a nominal radius <10 nm were used.

4.3. Results and discussion

In Chapter 3, we found that *B-E* diblocks with silica-binding blocks B^{RT}= $(RTHRK)_4$ and elastin-like hydrophilic blocks $E^S{}_{40}$ = $(VPGSG)_{40}$ satisfy the prerequisites of simple production and purification, as well as good solubility and silica binding.[18,28] Therefore, our current designs still employ B^{RT} as binding block for silica surfaces and $E^S{}_{40}$ as hydrophilic brush-forming block. We designed both B_n-*E* diblocks with tandem repeated binding blocks B^{RT} (up to three repeats) and *B-M-E* triblocks, with oligomerizing mid-blocks *M* of different valences *m*. As oligomerizing blocks *M*, we selected four naturally occurring[30–33] and three highly stable, de-novo computationally designed oligomerizing domains.[34] In some cases, the N-terminal of the oligomerization blocks did not allow for suitable display of the binding block. For these cases, we used *M-B-E* triblock designs instead. Finally, we used short $E^S{}_n$ sequences (*n* = 3-5) as linkers for connecting oligomerization and binding blocks to form tandem repeats. Designs are listed in Table 4-1. They all feature N-terminal poly-histidine-tags, were recombinantly produced in *Escherichia coli,* and purified using IMAC affinity chromatography. For full protein sequences, see Table A4-1.

Table 4-1. Overview of tested designs.

oligomerization block M			***protein design***	
name	origin	*m*	type	Sequence
N/A			B_n-*E*	B^{RT}- $E^S{}_{40}$
			B_n-*E*	B^{RT}-$E^S{}_3$ -B^{RT} -$E^S{}_{40}$
			B_n-*E*	B^{RT}-$E^S{}_3$-B^{RT}-$E^S{}_3$ -B^{RT}-$E^S{}_{40}$
Foldon[30]	*natural*	3	*B-M-E*	B^{RT}- M^{foldon}-$E^S{}_{40}$
I53.50A[33]		3	*B-M-E*	B^{RT}- $E^S{}_5$-$M^{I53.50A}$-$E^S{}_{40}$
LSM-α[31]		7	*B-M-E*	B^{RT}- $E^S{}_3$-$M^{LSM-\alpha}$-$E^S{}_{40}$
TRAP[32]		11	*M-B-E*	M^{TRAP}-$E^S{}_3$-B^{RT}-$E^S{}_{40}$
HR00C3_2[34]	*de novo*	3	*B-M-E*	B^{RT}-$E^S{}_3$-M^{HR00C3_2}-$E^S{}_{40}$
HR00C3_2[34]		3	*B-M*	B^{RT}-$E^S{}_3$-M^{HR00C3_2}
ank1C4_2[34]		4	*M-B-E*	M^{ank1C4_2}-$E^S{}_3$-B^{RT}-$E^S{}_{40}$
1na0C3_3[34]		3	*M-B-E*	M^{1na0C3_3}-$E^S{}_3$-B^{RT}-$E^S{}_{40}$

SDS-PAGE analysis of the expression and purification of the tandem-repeat designs B_n-*E* (*n* = 1-3) is shown in Figure A4-1. We found that the expression of the tandem-repeat designs decreases rapidly with increasing *n*. Some improvement in expression for *n* = 2 and 3 was found using LB medium containing 0.5% D-glucose (Figure A4-1b,d,f), suggesting that the expression at higher *n* is limited by the toxicity of the polypeptide.[35] QCM-D analysis of brush formation by B_n-*E* diblocks with *n* = 1, 2 on silica-coated quartz sensors showed that the tandem-repeat strategy is effective in improving brush stability against displacement by high ionic strength solutions (Figure A4-2). Nonetheless, the tandem repeat designs will not be further explored because of the problems in the production of these polymers. Instead, we will focus on employing oligomerizing mid-blocks *M* with star-like display of the SBPs (Figure 4-1c, right).

While all designs containing natural oligomerization domains could be expressed (Figure A4-3), the expression of the constructs with de-novo designed oligomerization domains was found to be higher (Figure A4-3e, f). However, preliminary investigations showed that the proteins with the de-novo designed oligomerization domains 1na0C3_3 and ank1C4_2 had lower solubility than the construct with the HR00C3_2 oligomerization domain. Therefore, we focus our attention on the design B^{RT}-E^{S}_{3}-M^{HR00C3_2}-E^{S}_{40}, containing the trimerization domain HR00C3_2 (PDB 5K7V) designed by Fallas *et al.*.[34] We will subsequently refer to this construct as *B-M-E*, with the implicit understanding that the binding block is $B = B^{RT}$-E^{S}_{3}, the multimerization block is $M = M^{HR0032\_2}$ and the hydrophilic random coil block is $E = E^{S}_{40}$.

A schematic representation of the *B-M-E* triblocks adhering to a silica surface is shown in Figure 4-2a, with Figure 4-2b showing the experimental crystal structure of the trimer of *M*.[34] Representative SDS-PAGE results for the purification process and MALDI-TOF results for the purified triblock are shown in Figure 4-3. Although a fraction of *B-M-E* did not bind to the IMAC column, the protein could be eluted with high purity (Figure 4-3a). To confirm the correct size of the polypeptide, the purified protein was analyzed using MALDI-TOF mass spectrometry (Figure 4-3b). We found that the experimentally determined mass (51.370 kg mol^{-1}) is equal to the theoretically expected value (51.363 kg mol^{-1}) within the error of the measurement.

First, we investigated whether the trimerization domain *M* still folds correctly when included in the *B-M-E* triblock. The domain is extremely stable

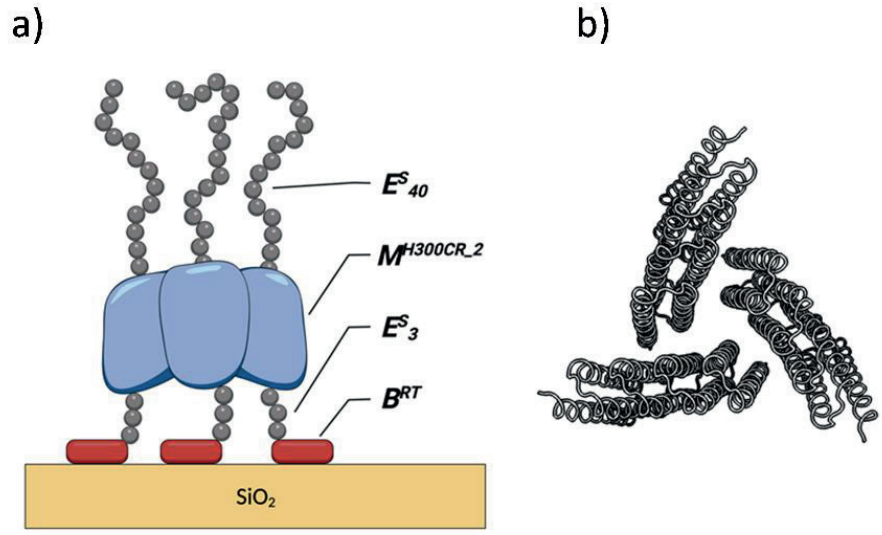

Figure 4-2. (a) Schematic representation of the structure of a trimer of the *B-M-E* triblock, with $B = B^{RT}\text{-}E^S_3$, $M = M^{HR00C3\_2}$ and $E = E^S_{40}$, adsorbed to a silica surface. **(b)** Crystal structure of the trimer of M^{HR00C3_2} (PDB 5K7V), corresponding to a view from the top (C-terminal side) for the adsorbed *B-M-E* trimer.

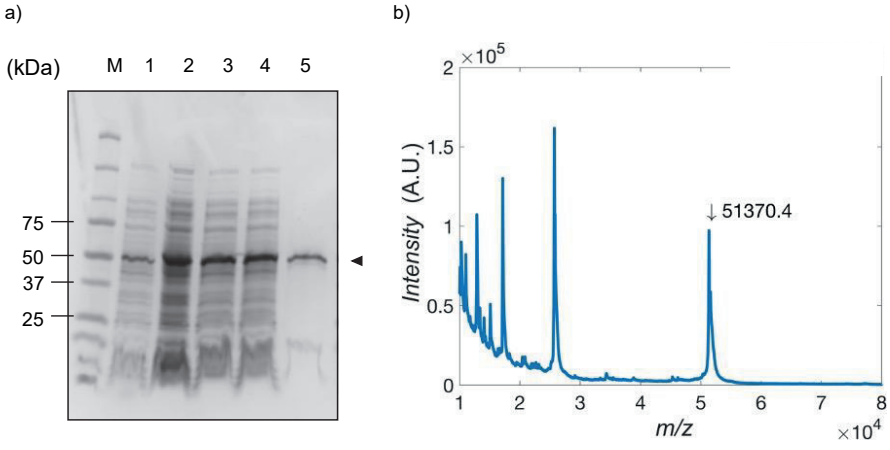

Figure 4-3. Purification and characterization of *B-M-E* triblock. **(a)** SDS-PAGE analysis. Lane 1: intact cells; lane 2: cell lysate; lane 3: soluble lysate; lane 4: IMAC flow-through; lane 5: IMAC fractions; lane M: molecular marker. **(b)** MALDI-TOF spectrum.

in solution, both at high temperature and in presence of denaturants.[34] Furthermore, the secondary structure of the *M* domain is exclusively α-helical (Figure 4-2b), even though a large portion of the *B-M-E* triblock has a disordered structure. For this reason, if the circular dichroism spectrum of the *B-M-E* triblock shows features that are distinctive for α-helical proteins, we can assume that the trimerization domain *M* is correctly folded. CD spectra for the triblock are shown in Figure 4-4a. At 20 °C, the spectrum clearly shows two negative bands at 222 nm and 210 nm, characteristic of α-helical proteins.[36] We conclude that the trimerization domain *M* is still correctly folded when included in the *B-M-E* triblock.

Next, we investigated the thermal stability of the trimerization domain in the *B-M-E* triblock. As shown in Figure 4-4a, heating the protein solution to 95 °C does not drastically affect the features of the spectrum. After cooling back to 20 °C, the spectrum is similar to the measurement before heating, indicating a fully reversible behavior and no significant unfolding. The upward shift could be caused by the partial evaporation of the sample during the heating phase, with a consequent increase in the protein concentration. As shown in Figure 4-4b, the measured ellipticity at 222 nm increases slightly and monotonically

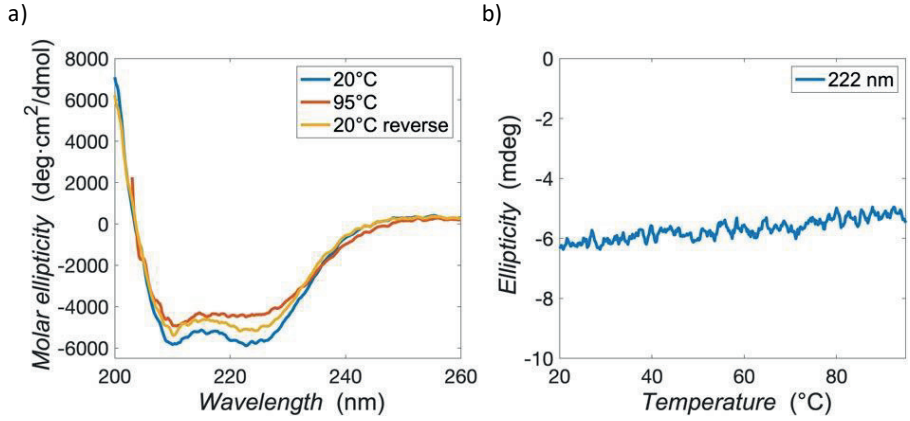

Figure 4-4. Analysis of the secondary structure of the *B-M-E* triblock with circular dichroism spectroscopy. **(a)** Molar ellipticity vs wavelength. Spectra were recorded at 20 °C, at 95 °C and again at 20 °C. Solution conditions: 0.1 mg mL^{-1} of protein in PBS, pH 7.4. Data were collected in a cell with a 1 mm path length. **(b)** Ellipticity at 222 nm plotted as a function of temperature during a heating ramp (1 °C min^{-1}).

during a temperature ramp from 20 °C to 95 °C, clearly indicating that there is no unfolding before 95 °C within the timescale of the measurement.

Possibly, the trimerization of the *M* block could be affected by the presence of the binding block *B* at the N-terminus or the random coil block *E* at the C-terminus. To investigate this, we first evaluated if the presence of the binding blocks affects trimerization. To this end, we expressed and purified the diblock *B-M* (Figure A4-4). We found that this polypeptide quickly aggregated in solution after purification. Since the *M* block, the *B* block, and the *B-M-E* triblocks are soluble in PBS pH 7.4, we conclude that the *B* and *M* blocks co-precipitate in our *B-M* diblock design. We hypothesize that since the binding block *B* is highly cationic (+12) and the trimerization domain *M* has a high net negative charge (-24), the observed co-precipitation is likely caused by strong electrostatic interactions between *B* and *M* blocks (see schematic in Figure A4-5c).

Next, we explored the consequences of electrostatic interactions between *B* and *M* blocks for the self-assembly in solution of the *B-M-E* triblocks. Theoretically, the long hydrophilic random coil blocks *E* should solubilize the *B-M* precipitates, in line with previous observations regarding the use of hydrophilic ELPs for the stabilization and solubilization of macromolecules.[37] Nevertheless, the *E* blocks may not be able to completely prevent association of *B-M-E* trimers in solution. The sizes for *B-M-E* triblocks in solution were determined using DLS. Since we hypothesized that *B-M* interactions are electrostatically driven, we varied the salt concentration to establish whether they can be screened by the addition of salt. As shown in Figure 4-5a, we find that the scattering intensity for *B-M-E* solutions is highly salt-dependent, showing a sharp decrease beyond a salt concentration *[NaCl]* ≈ 400 mM. As shown in Figure 4-5b, below *[NaCl]* ≈ 400 mM, using a distribution analysis of the autocorrelation function, we only detect assemblies with hydrodynamic diameters D_H ≈ 250 nm. Above *[NaCl]* ≈ 400 mM, we observe a slight decrease of the size of the large assemblies. Additionally, we observe assemblies with a much smaller hydrodynamic diameters D_H ≈ 22 nm at *[NaCl]* = 400 mM. For *[NaCl]* > 400 mM, the scattering intensities corresponding to the large and small assemblies are similar. Given the strong dependence of scattering intensity on particle size, this finding implies that at least at *[NaCl]* > 400 mM, most of the *B-M-E* proteins is part of the small assemblies.

A trimer of the *M* block has a height of 5 nm and a diameter of 7 nm.

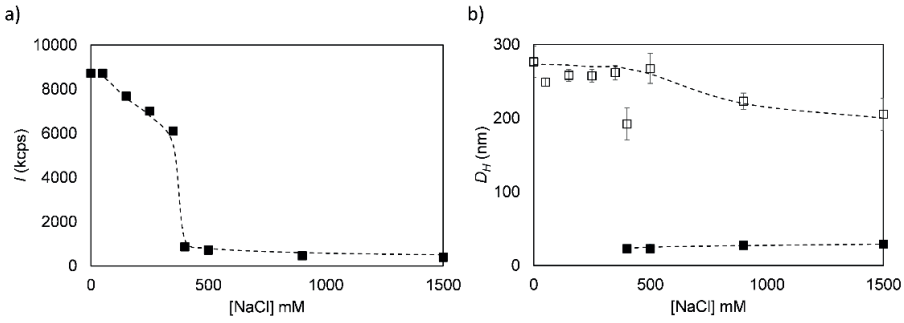

Figure 4-5. Salt-dependence of self-assembly of *B-M-E* triblocks in solution. **(a)** Light scattering intensity (scattering angle 173°) versus concentration NaCl added to PB buffer *[NaCl]* (mM). **(b)** Distribution analysis of dynamic light scattering data. Open symbols: hydrodynamic diameter $D_{H,\,eff}$ (nm) for major peak; closed symbols: hydrodynamic diameter $D_{H,\,eff}$ (nm) for minor peak. Solution conditions: 1 mg mL^{-1} protein, dissolved in 10 mM PB pH 7.4 with the indicated amount of NaCl. Dashed lines are guides to the eye.

The hydrodynamic diameter of a single *E* block is 9 nm.[28] Hence, the observed assemblies with a hydrodynamic diameter $D_H \approx 22$ nm could likely correspond to the *B-M-E* trimers, although this cannot be established with certainty from the DLS measurements alone. We attempted to separate the putative trimers from the larger assemblies using size exclusion chromatography (SEC) at a salt concentration *[NaCl]* = 500 mM to establish their precise solution stoichiometry. Unfortunately, we found that the proteins eluted as a single broad peak covering a range of hydrodynamic sizes (Figure A4-5a). At the same time, SDS-PAGE indicated that the peak fractions only consisted of the *B-M-E* protein (Figure A4-5b). This observation likely indicates that the trimers are in fast equilibrium with the larger assemblies. Indeed, all SEC fractions showed the presence of both the larger and the smaller assemblies in DLS.

The interaction of the *B-M-E* triblocks with silica surfaces was investigated using monodisperse non-porous silica nanoparticles with a hydrodynamic diameter D_H =163 nm. As we have shown for the *B-E* diblocks, this DLS-based method allows for a straightforward determination of both the concentration of protein required for a stable adsorbed polypeptide brush and the brush height.[28] Results are shown in Figure 4-6a. The results show that a protein concentration of ~1 μM is required for the formation of a stable brush. At lower concentrations, bridging interactions lead to particle aggregation, resulting in very high scattering intensities and large effective particle radii. At

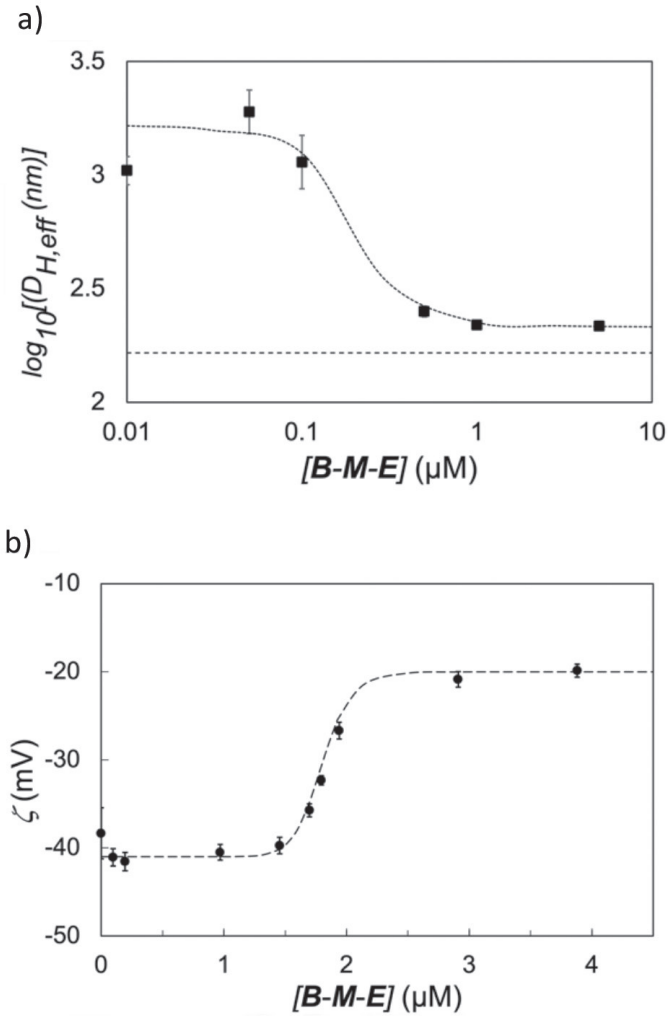

Figure 4-6. Interaction of *B-M-E* triblocks with 163 nm silica particles. **(a)** Effective hydrodynamic radius $D_{H,eff}$ (nm) of the particles as determined using dynamic light scattering, versus concentration of added protein *B-M-E* (μM). Long-dashed line represents the diameter (D_H =163 nm) of the bare silica particles, short-dashed line is a guide for the eye. Solution conditions: silica particles were dissolved in 10 mM PB pH 7.4 at a concentration of 0.01% v/v. Protein was dissolved in 10 mM PB pH 7.4. **(b)** Zeta potential ζ (mV) of the particles versus concentration of added protein *B-M-E* (μM). Solution conditions: silica particles were dissolved in 10 mM PB pH 7.4 at a concentration of 0.01% v/v. Protein was dissolved in 10 mM PB pH 7.4.

higher concentrations the bridging interactions disappear, and we measured a particle diameter of D_H = 220 nm, leading to an estimated brush height $h \approx$ 28 nm.

Electrophoretic Light Scattering was used to determine the change in ζ-potential of the silica particles coated with the *B-M-E* triblocks. Results are shown in Figure 4-6b. Consistently with the DLS results, we found that a concentration of *B-M-E* of a few μM is required to give rise to a significant change of the ζ-potential, due to self-assembly of a polypeptide brush on the surface of the silica particles. The coating makes the ζ-potential less negative, increasing from around -40 mV to around -20mV.

In Chapter 3, we found that binding with a single solid-binding peptide is not strong enough to resist displacement at higher salt concentrations.[28] This finding was part of the motivation to investigate multivalent SBP binding. We used a QCM to investigate whether the *B-M-E* triblocks can still form stable brushes on silica surfaces at high concentrations of NaCl. The triblock polypeptide was dissolved at a concentration of 10 μM in PB, PBS, PBS with 0.5 M NaCl and PBS with 1 M NaCl. The kinetics of adsorption of the *B-M-E* triblocks at these different salt concentrations on silica were followed via QCM. Polypeptide solutions were flushed over the silica sensors and after a stable layer had formed, sensors were rinsed with the various buffers used for layer formation. Results are shown in Figure 4-7. As expected, a lower ionic strength of the buffer leads to a stronger QCM signal, but the influence of ionic strength is not very large: even at 1M NaCl, the QCM signal at saturation for PBS + 1 M NaCl is still ≈ 70% of that for the PB. In addition, prolonged rinsing with PBS + 1 M NaCl does not remove the layers formed in the same buffer.

According to the QCM measurements, the *B-M-E* trimers form stable layers on silica surfaces, with good resistance against rinsing with both low and high salt buffers. This observation, however, does not necessarily imply that the proteins adsorb as expected, with their binding domains *B* facing the silica and the elastin-like blocks *E* facing the solution. One possibility is that the larger assemblies observed in DLS for bulk solutions adsorb on the silica and form inhomogeneous layers. To exclude this possibility, we performed AFM of *B-M-E* layers adsorbed on silica. Imaging was done in air; the results are shown in Figure 4-8. We found that after drying, *B-M-E* layers are very thin (<10 nm) and homogeneous over large areas of 2 μm × 2 μm. The surface morphology of the *B-M-E* layers as observed in AFM is that of densely packed dots, which we tentatively identify with the trimers. Hence, AFM rules out the

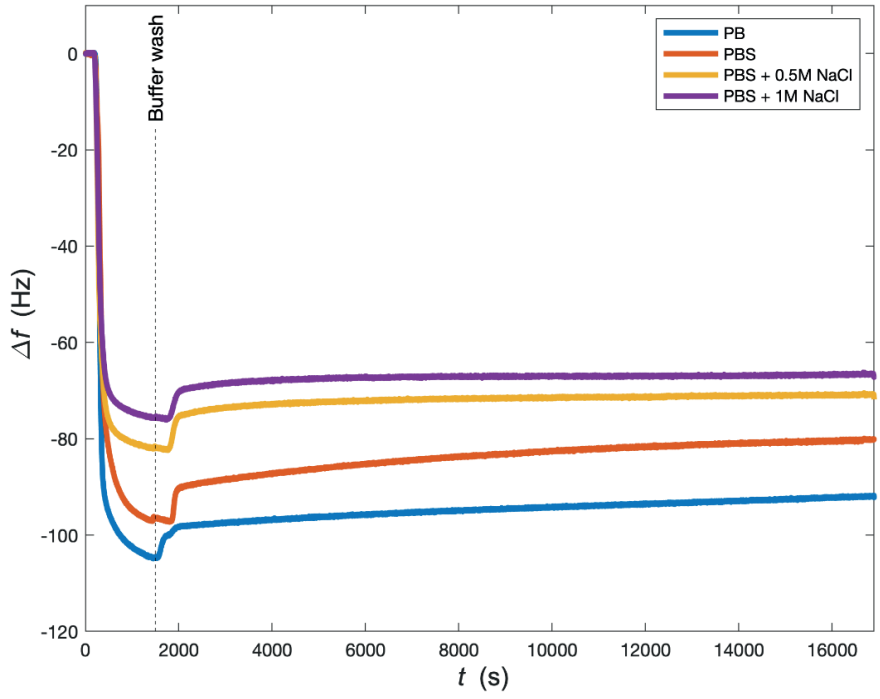

Figure 4-7. Salt dependence of brush formation on silica for 10 μM *B-M-E* measured with quartz crystal microbalance. Frequency shift Δ*f* (Hz) versus time *t* (s) after the start of injection of 10 μM *B-M-E*. Buffers used for brush formation and consecutive rinsing are the following: PB (blue); phosphate-buffered saline (PBS, 150 mM NaCl, orange); PBS + 0.5 M NaCl (yellow); PBS + 1 M NaCl (purple). Rinsing with buffer starts at the change in QCM signal following the vertical dashed line.

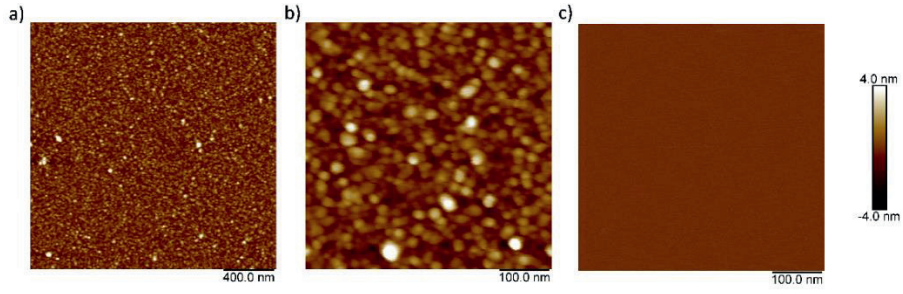

Figure 4-8. Surface morphology of *B-M-E* coated silica from AFM in air. Silica surfaces were coated for 1 min with solutions of 2 mg mL^{-1} of *B-M-E* in PBS, rinsed, dried, and imaged in air. **(a)** 2μm × 2 μm; **(b)** 0.5μm × 0.5 μm; **(c)** 0.5μm × 0.5μm silica only (control).

possibility that the larger dynamic assemblies observed using DLS in solution lead to inhomogeneous coatings.

Next to brush stability, the prevention of biological fouling is a key property for the successful application of adsorbed brushes. As a first step, we tested the antifouling ability against high concentrations of serum albumin in PBS pH 7.4. We used PLL-*g*-PEG polymers as a positive control for self-assembled antifouling brushes, and we also tested our previously designed *B*-*E* diblock polypeptides. QCM was used to follow the kinetics of brush assembly on silica-coated quartz sensors. After brush formation, a high concentration of bovine serum albumin (BSA, 2 mg mL^{-1}) was flushed on the sensor, followed by rinsing with PBS. As a negative control, we used a bare silica sensor. QCM results are shown in Figure 4-9.

For the negative control on bare silica, a strong QCM signal is observed upon injecting BSA. Only a small part of the adsorbed BSA is removed in the PBS rinsing step that follows, demonstrating the BSA has adsorbed irreversibly. The results for the PLL-*g*-PEG-coated silica sensors are as expected: the self-assembled PLL-*g*-PEG brushes effectively prevent the adsorption of BSA on the silica surface (Figure 4-9a). During BSA injection, a small decrease in frequency shift is recorded, indicating a small amount of BSA adsorption on the PEG tails. However, BSA is weakly bound and is removed again in the subsequent rinsing step. The results for silica sensors coated with the *B*-*E* diblock show that brushes are gradually rinsed off by PBS (Figure 4-9b). Upon injecting BSA, only a very small amount of BSA adsorbs, which is removed during the subsequent rinsing step. However, a fair amount of brush desorption takes place during the BSA injection step. The *B*-*E* brushes are considerably less stable than the PLL-*g*-PEG brushes with respect to rinsing with both PBS and BSA in PBS.

Finally, the results for sensors coated with the *B*-*M*-*E* triblock are shown in Figure 4-9c. At least for this assay, this polymer seems to perform better in terms of both stability and antifouling properties: changing from PBS to 2 mg mL^{-1} BSA in PBS hardly influences the QCM signal. Since we do not observe changes in the signal upon flushing with concentrated BSA, we can also conclude that all binding blocks *B* in the *B*-*M*-*E* coatings are properly oriented toward the silica surface, as designed. In fact, for the weakly bound *B*-*E* diblocks, we observe strong displacement caused by BSA, indicating that the negatively charged BSA molecules compete effectively with the negatively

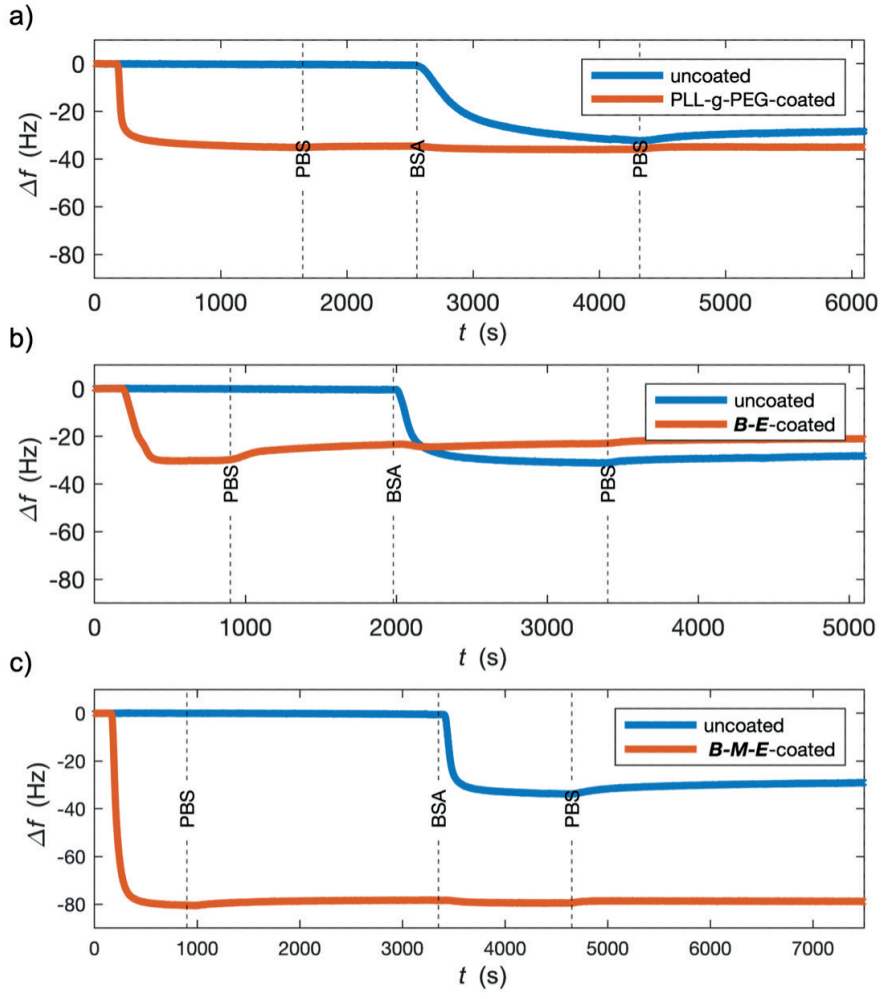

Figure 4-9. Antifouling properties of PLL-*g*-PEG, *B-E* and *B-M-E* polymer brushes adsorbed on silica surface. QCM frequency shift Δf (Hz) versus time t (s) after starting the injection of the brush forming polymer. At the first dashed vertical lines, we switch to rinsing with PBS. At the second vertical dashed lines, we inject 2 mg mL^{-1} BSA in PBS. At the third dashed vertical lines, we switch back to rinsing with PBS. Blue lines: bare silica negative control; orange lines: with pre-adsorbed polymer brush. **(a)** PLL-*g*-PEG brush, **(b)** *B-E* brush, **(c)** *B-M-E* brush.

charged silica. This also indicates a strong interaction between the *B* block and BSA. In the *B-M-E* coatings, any exposed binding blocks *B* would have also led to strong interactions with BSA, which we did not observe.

4.4. Concluding remarks

Our work shows that it is possible to design, produce, and purify self-assembling polypeptide brushes that harness multivalent binding of SBPs for attachment to solid surfaces. The number of successful designs is strongly limited by practical constraints such as polypeptide toxicity, low expression levels, and low solubility. However, we also show that the design with sequence B^{RT}-$E^{S}{}_{3}$-M^{HR00C3_2}-$E^{S}{}_{40}$ has very promising properties, forming highly stable and antifouling polypeptide brushes on silica surfaces.

Given the initial success of our *B-M-E* design as antifoulant against concentrated solutions of BSA in PBS, the following step would be to evaluate complex biological fluids such as diluted serum. In fact, antifouling behavior against a single prominent serum protein such as BSA does not guarantee similar results with a complex mixture of biomolecules.[38,39] Hence, further changes to our original design may still be necessary. These modifications could include changing the length or nature of the *E* block.

While PLL-*g*-PEG brushes are already adequate for many applications, we believe that recombinant antifouling polypeptides may offer advantages for specific cases. In particular, the *B-M-E* triblock sequence can be directly used as a combined adhesion and antifouling tag for displaying proteins on surfaces. Also, given the wealth of data on SBPs suitable for other surfaces, we expect it will be relatively straightforward to develop *B-M-E* triblocks that strongly adhere to metals and plastics.

4.5. List of abbreviations

Abbreviation	Meaning
AFM	atomic force microscopy
DLS	dynamic light scattering
IMAC	immobilized metal ion affinity chromatography
LB	lysogeny broth
MALDI-TOF	matrix-assisted laser desorption/ionization coupled to time-of-flight mass spectrometry
PB	phosphate buffer
PBS	phosphate-buffered saline
PEG	poly(ethylene glycol)
PEG-*g*-PLL	poly(l-lysine)-grafted poly(ethylene glycol)
PEG-*g*-PEI	polyethylene imine-grafted poly(ethylene glycol)
QCM	quartz crystal microbalance
QCM-D	quartz crystal microbalance with dissipation monitoring
SBP	solid-binding peptide
SDS-PAGE	sodium dodecyl sulfate-polyacrylamide gel electrophoresis
SEC	size exclusion chromatography
TB	Terrific Broth

4.6. Appendix

Table A4-1. Amino acid sequences of all constructs

	Amino acid sequence
B^{RT}-E^{S}_{40}	MGSSHHHHHHSSGGSGVPGSGVPGSGVPRTHRKRTHRKRTHRKRT HRKGSGVPGSGVPGSGVPGSGVPGSGVPGSGVPGSGVPGSGVPGSGVPGS GVPGSGVPGSGVPGSGVPGSGVPGSGVPGSGVPGSGVPGSGVPGSGVPGS GVPGSGVPGSGVPGSGVPGSGVPGSGVPGSGVPGSGVPGSGVPGSGVPGS GVPGSGVPGSGVPGSGVPGSGVPGSGVPGSGVPGSGVPGSGVPGSGVPGS GVPGSGVPGSGVPGSGVPGSGVPGC
B^{RT}-E^{S}_{3}-	MGSSHHHHHHSSGGSGVPGSGVPGSGVPRTHRKRTHRKRTHRKRT
B^{RT}-E^{S}_{40}	HRKGSGVPGSGVPGSGVPRTHRKRTHRKRTHRKRTHRKGSGVPGSG VPGSGVPGSGVPGSGVPGSGVPGSGVPGSGVPGSGVPGSGVPGSGVPGSG VPGSGVPGSGVPGSGVPGSGVPGSGVPGSGVPGSGVPGSGVPGSGVPGSG VPGSGVPGSGVPGSGVPGSGVPGSGVPGSGVPGSGVPGSGVPGSGVPGSG VPGSGVPGSGVPGSGVPGSGVPGSGVPGSGVPGSGVPGSGVPGSGVPGSG VPGSGVPGSGVPGC
B^{RT}-E^{S}_{3}-	MGSSHHHHHHSSGGSGVPGSGVPGSGVPRTHRKRTHRKRTHRKRT
B^{RT}-E^{S}_{3}-	HRKGSGVPGSGVPGSGVPRTHRKRTHRKRTHRKRTHRKGSGVPGSG
B^{RT}-E^{S}_{40}	VPGSGVPRTHRKRTHRKRTHRKRTHRKGSGVPGSGVPGSGVPGSGV PGSGVPGSGVPGSGVPGSGVPGSGVPGSGVPGSGVPGSGVPGSGVPGSGV PGSGVPGSGVPGSGVPGSGVPGSGVPGSGVPGSGVPGSGVPGSGVPGSGV PGSGVPGSGVPGSGVPGSGVPGSGVPGSGVPGSGVPGSGVPGSGVPGSGV PGSGVPGSGVPGSGVPGSGVPGSGVPGSGVPGSGVPGSGVPGSGVPGSGV PGC
B^{RT}-	MGHHHHHHGGSRTHRKRTHRKRTHRKRTHRKGYIPEAPRDGQAYVR
M^{foldon}-	KDGEWVLLSTFLSGVPGSGVPGSGVPGSGVPGSGVPGSGVPGSGVP
E^{S}_{40}	GSGVPGSGVPGSGVPGSGVPGSGVPGSGVPGSGVPGSGVPGSGVPGSGVP GSGVPGSGVPGSGVPGSGVPGSGVPGSGVPGSGVPGSGVPGSGVPGSGVP GSGVPGSGVPGSGVPGSGVPGSGVPGSGVPGSGVPGSGVPGSGVPGSGVP GSGVPGSGVPGSGVPGSGVPGSGVPGSGVPG
B^{RT}-E^{S}_{5}-	MGHHHHHHGGSRTHRKRTHRKRTHRKRTHRKSGVPGSGVPGSGVP
$M^{I53.50A}$-	GSGVPGSGVPGMKMEELFKKHKIVAVLRANSVEEAIEKAVAVFAGGVH
E^{S}_{40}	LIEITFTVPDADTVIKALSVLKEKGAIIGAGTVTSVEQARKAVESGAEFIV SPHLDEEISQFAKEKGVFYMPGVMTPTELVKAMKLGHDILLLFPGEVV GPQFVKAMKGPFPNVKFVPTGGVNLDNVAKWFKAGVLAVGVGKALV KGKPDEVREKAKKFVKKIRGATEGSLEGSGVPGSGVPGSGVPGSGVP GSGVPGSGVPGSGVPGSGVPGSGVPGSGVPGSGVPGSGVPGSGVPGSGVP GSGVPGSGVPGSGVPGSGVPGSGVPGSGVPGSGVPGSGVPGSGVPGSGVP GSGVPGSGVPGSGVPGSGVPGSGVPGSGVPGSGVPGSGVPGSGVPGSGVP

	GSGVPGSGVPGSGVPGSGVPGSGVPGSGVPGSGVPGSGVPGSGVP G
B^{RT}-E^{S}_{3}-	MGHHHHHHGGSRTHRKRTHRKRTHRKRTHRKGSGVPGSGVPGSGV
$M^{LSM\text{-}\alpha}$-	PSQRVNVQRPLDALGNSLNSPVIIKLKGDREFRGVLKSFDLHMNLVLN
E^{S}_{40}	DAEELEDGEVTRRLGTVLIRGDNIVYISPSGVPGSGVPGSGVPGSGVP GSGVPGSGVPGSGVPGSGVPGSGVPGSGVPGSGVPGSGVPGSGVP GSGVPGSGVPGSGVPGSGVPGSGVPGSGVPGSGVPGSGVPGSGVP GSGVPGSGVPGSGVPGSGVPGSGVPGSGVPGSGVPGSGVPGSGVP GSGVPGSGVPGSGVPGSGVPGSGVPGSGVPGSGVPGSGVPGSGVP G
M^{TRAP}-	MGHHHHHHGGSYTNSDFVVIKALEDGVNVIGLTRGADTRFHHSEKLD
E^{S}_{3}-B^{RT}-	KGEVLIAQFTEHTSAIKVRGKAYIQTRHGVIESEGKKSGVPGSGVPGSG
E^{S}_{40}	VPGSGVPGSGVPGRTHRKRTHRKRTHRKRTHRKSGVPGSGVPGSGV PGSGVPGSGVPGSGVPGSGVPGSGVPGSGVPGSGVPGSGVPGSGV PGSGVPGSGVPGSGVPGSGVPGSGVPGSGVPGSGVPGSGVPGSGV PGSGVPGSGVPGSGVPGSGVPGSGVPGSGVPGSGVPGSGVPGSGV PGSGVPGSGVPGSGVPGSGVPGSGVPGSGVPGSGVPGSGVPGSGV PGSGVPG
M^{1na0C3_3}-	MGSSHHHHHHSSGMNLAEKMYKAGNAMYRKGQYTIAIIAYTLALLKD
E^{S}_{3}-B^{RT}-	PNNAEAWYNLGNAAYKKGEYDEAIEAYQKALELDPNNAEAWYNLGN
E^{S}_{40}	AYYKQGDYDEAIEYYQKALELDPNNAEAKQNLGNAKQKQGLGSGVP GSGVPGSGVPRTHRKRTHRKRTHRKRTHRKGSGVPGSGVPGSGVPG SGVPGSGVPGSGVPGSGVPGSGVPGSGVPGSGVPGSGVPGSGVPGSGVPG SGVPGSGVPGSGVPGSGVPGSGVPGSGVPGSGVPGSGVPGSGVPGSGVPG SGVPGSGVPGSGVPGSGVPGSGVPGSGVPGSGVPGSGVPGSGVPGSGVPG SGVPGSGVPGSGVPGSGVPGSGVPGSGVPGSGVPGSGVPGSGVPG
B^{RT}-E^{S}_{3}-	MGSSHHHHHHSSGRTHRKRTHRKRTHRKRTHRKGSGVPGSGVPGS
M^{HR00C3_2} -E^{S}_{40}	GVPMIEEVVAEMIDILAESSKKSIEELARAADNKTTEKAVAEAIEEIARLA TAAIQLIEALAKNLASEEFMARAISAIAELAKKAIEAIYRLADNHTTDTFM ARAIAAIANLAVTAILAIAALASNHTTEEFMARAISAIAELAKKAIEAIYRL ADNHTTDKFMAAAIEAIALLATLAILAIALLASNHTTEEFMAKAISAIAEL AKKAIEAIYRLADNHTSPTYIEKAIEAIEKIARKAIKAIEMLAKNITTEEYKE KAKSAIDEIREKAKEAIKRLEDNRTGSGVPGSGVPGSGVPGSGVPGSG VPGSGVPGSGVPGSGVPGSGVPGSGVPGSGVPGSGVPGSGVPGSGVPGSG VPGSGVPGSGVPGSGVPGSGVPGSGVPGSGVPGSGVPGSGVPGSGVPGSG VPGSGVPGSGVPGSGVPGSGVPGSGVPGSGVPGSGVPGSGVPGSGVPGSG VPGSGVPGSGVPGSGVPGSGVPGSGVPGSGVPGSGVPGSGVPGSGVPGSG VPGSGVPG
M^{ank1C4_2}-	MGSSHHHHHHSSGMSEDGELLILAAELGIAEAVRMLIEQGADVNASD
E^{S}_{3}-B^{RT}-	DDGRTPLHHAAENGHLAVVLLLLLKGADVNAKDSDGRTPLHHAAENG
E^{S}_{40}	HKTVVLLLILMGADVNAKDSDGRTPLHHAAENGHKEVVKLLIRKGADV

NTSDSDGRTPLDLAREHGNEEVVKLLEKQLGSGVPGSGVPGSGVPRT
HRKRTHRKRTHRKRTHRKGSGVPGSGVPGSGVPGSGVPGSGVPGSG
VPGSGVPGSGVPGSGVPGSGVPGSGVPGSGVPGSGVPGSGVPGSG
VPGSGVPGSGVPGSGVPGSGVPGSGVPGSGVPGSGVPGSGVPGSG
VPGSGVPGSGVPGSGVPGSGVPGSGVPGSGVPGSGVPGSGVPGSG
VPGSGVPGSGVPGSGVPGSGVPGSGVPGSGVPGSGVPG

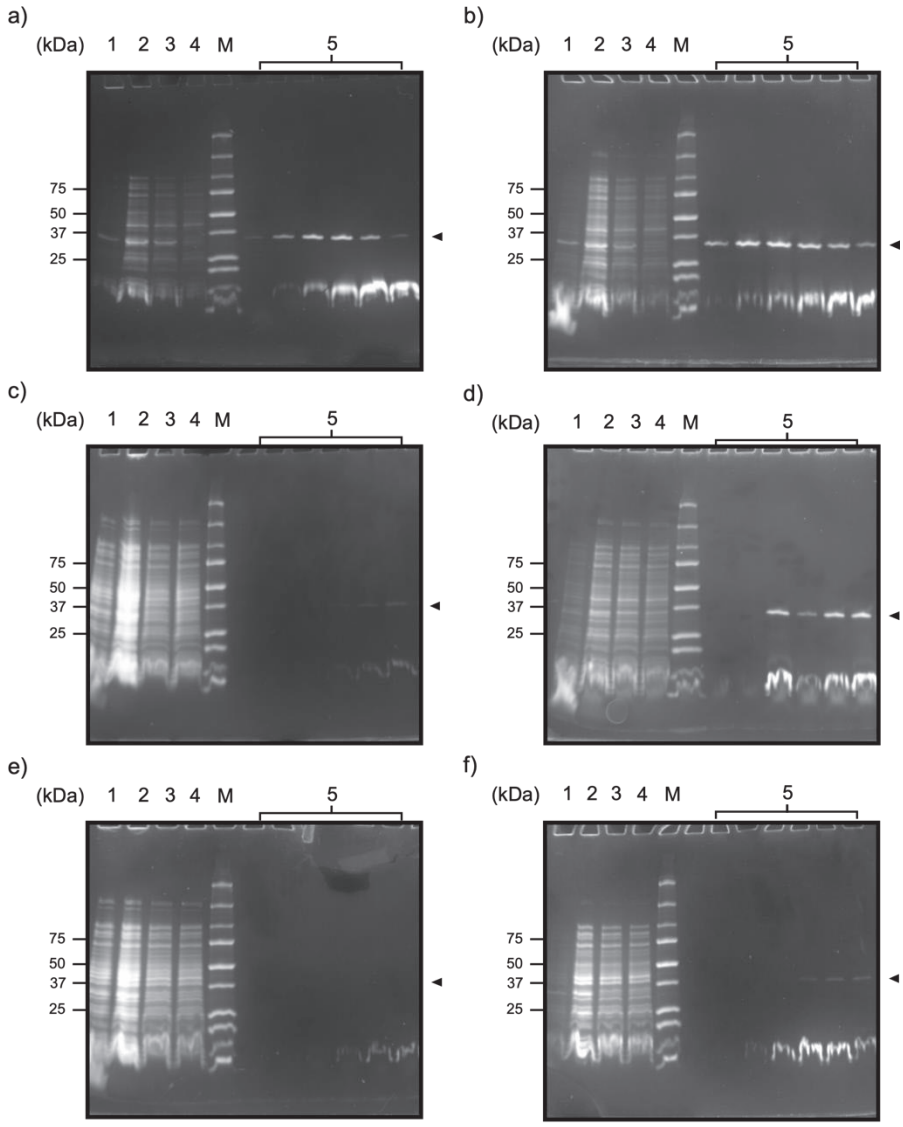

Figure A4-1. Expression and purification of polypeptides B_n-*E* with tandem repeated SBPs: B^{RT}-E^{S}_{40} (*n* = 1), B^{RT}-E^{S}_{3} -B^{RT} -E^{S}_{40} (*n* = 2) and B^{RT}-E^{S}_{3}-B^{RT}-E^{S}_{3}-B^{RT}-E^{S}_{40} (*n* = 3). SDS-PAGE analysis. Lane 1: intact cells; lane 2: cell lysate; lane 3: insoluble lysate; lane 4: soluble lysate; lane 5: IMAC fractions; lane M: molecular marker. **(a)** *n* = 1, LB medium; **(b)** *n* = 1, LB medium + 0.5% D-glucose; **(c)** *n* = 2, LB medium, **(d)** *n* = 2, LB medium + 0.5% D-glucose; **(e)** *n* = 3, LB medium; **(f)** *n* = 3, LB medium + 0.5% D-glucose.

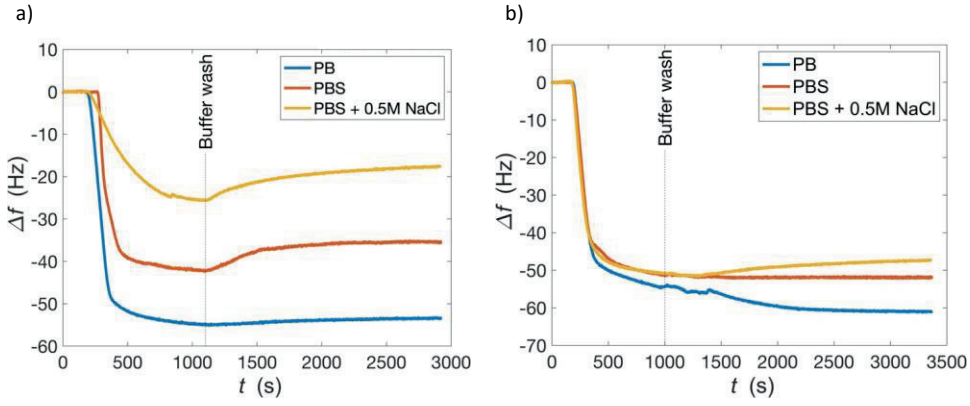

Figure A4-2. Stability of brushes formed on silica surfaces by B_n-E polymers with n = 1 and 2 (B^{RT}-E^{S}_{40} and B^{RT}-E^{S}_{3}-B^{RT}-E^{S}_{40}). Frequency change Δf (Hz) as measured by QCM, versus time t (s) after injection of polypeptide solutions at a concentration of 5 μM. Buffers used for brush formation and consecutive rinsing are phosphate buffer (PB, blue), phosphate buffer saline (PBS, 150 mM NaCl, orange), and PBS + 0.5 M NaCl (yellow). Rinsing with buffer starts at the change in QCM signal following the vertical dashed line. **(a)** B^{RT}-E^{S}_{40}; **(b)** B^{RT}-E^{S}_{3}-B^{RT}-E^{S}_{40}.

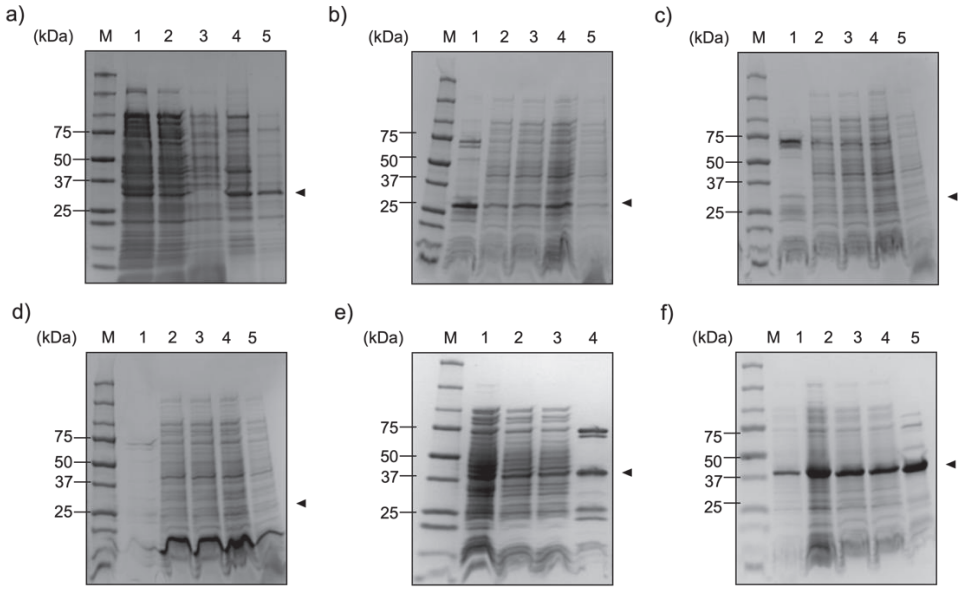

Figure A4-3. Expression and purification of triblock constructs *B-M-E*. **(a)** SDS-PAGE analysis of B^{RT}- M^{foldon}-E^{S}_{40}. Lane 1: intact cells; lane 2: cell lysate; lane 3: insoluble lysate; lane 4: soluble lysate; lane 5: IMAC fractions; lane M: molecular marker. **(b)** SDS-PAGE analysis of B^{RT}- E^{S}_{5}-$M^{I53.50A}$-E^{S}_{40}. Lane 1: IMAC fractions; lane 2: IMAC flow-through; lane 3: soluble lysate; lane 4: cell lysate; lane 5: intact cells; lane M: molecular marker. **(c)** SDS-PAGE analysis of B^{RT}- E^{S}_{3}-$M^{LSM-α}$-E^{S}_{40}. Lane 1: IMAC fractions; lane 2: IMAC flow-through; lane 3: soluble lysate; lane 4: cell lysate; lane 5: intact cells; lane M: molecular marker. **(d)** SDS-PAGE analysis of M^{TRAP}-E^{S}_{3}-B^{RT}-E^{S}_{40}. Lane 1: intact cells; lane 2: cell lysate; lane 3: soluble lysate; lane 4: IMAC flow-through; lane 5: IMAC fractions; lane M: molecular marker. **(e)** SDS-PAGE analysis of M^{1na0C3_3}-E^{S}_{3}-B^{RT}-E^{S}_{40}. Lane 1: intact cells; lane 2: cell lysate; lane 3: soluble lysate; lane 4: IMAC fractions; lane M: molecular marker. **(f)** SDS-PAGE analysis of M^{ank1C4_2}-E^{S}_{3}-B^{RT}-E^{S}_{40}. Lane 1: intact cells; lane 2: cell lysate; lane 3: soluble lysate; lane 4: IMAC flow-through; lane 5: IMAC fractions; lane M: molecular marker.

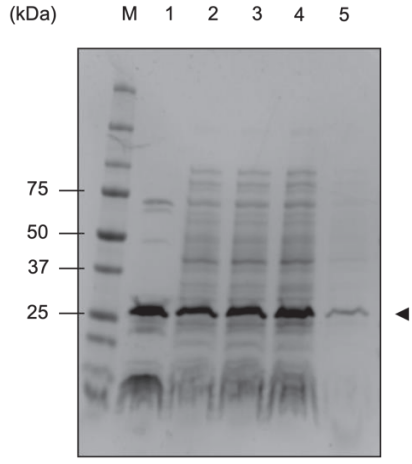

Figure A4-4. Expression and purification of *B-M* di-block construct (B^{RT}-$E^{S}{}_{3}$-M^{HR00C3_2}). SDS-PAGE analysis. Lane 1: IMAC eluate; lane 2: IMAC flow-through; lane 3: soluble lysate; lane 4: cell lysate; lane 5: intact cells; lane M: molecular weight marker.

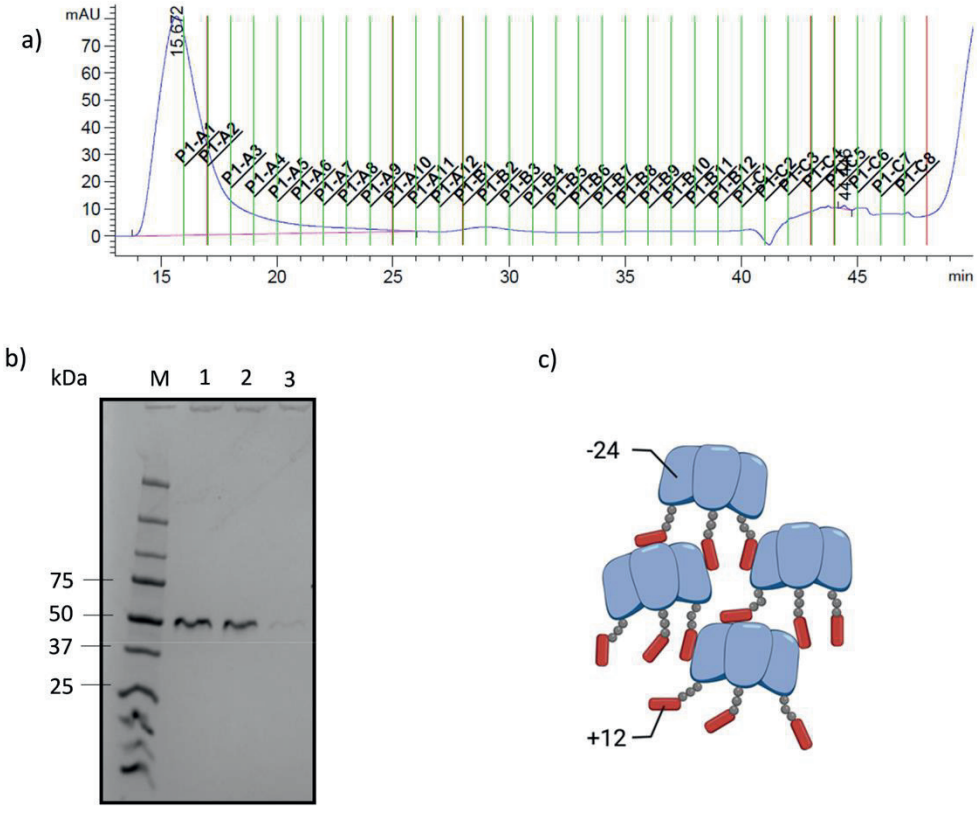

Figure A4-5. Size exclusion chromatography of triblock construct *B-M-E* (B^{RT}-E^{S}_{3}-M^{HR00C3_2}-E^{S}_{40}) at high salt. **(a)** Chromatogram, absorbance at 280 nm versus elution time. Superose 6 Increase 10/300 GL column; buffer is PBS + 500 mM NaCl pH 7.4; flow rate: 0.5 mL min^{-1}; fraction size: 0.5 mL. **(b)** SDS-PAGE of fractions P1-A1 (lane 1), P1-A2 (lane 2) and P1-A3 (lane 3). **(c)** Schematic illustration of the possible electrostatic driving force for insolubility of *B-M* diblocks and salt-dependent bulk self-assembly of *B-M-E*. Only the *B-M* part of the triblock is illustrated. Experimentally observed insolubility of the *B-M* diblock is likely due to electrostatic association of the positively charged binding blocks *B* (charge +12) with the negatively charged trimerization blocks *M* (charge -24). In the context of the trimer *B-M-E* we hypothesize that the same interaction causes the experimentally observed salt-dependent reversible formation of higher order self-assemblies in solution.

4.7. References

[1] J. L. HARDING, M. M. REYNOLDS. Combating medical device fouling. *Trends in Biotechnology* 32, 140–146 (2014).

[2] Q. YU, Y. ZHANG, H. WANG, J. BRASH, H. CHEN. Anti-fouling bioactive surfaces. *Acta Biomaterialia* 7, 1550–1557 (2011).

[3] N. LIU, N. HUI, J. J. DAVIS, X. LUO. Low Fouling Protein Detection in Complex Biological Media Supported by a Designed Multifunctional Peptide. *ACS Sensors* 3, 1210–1216 (2018).

[4] H. VAISOCHEROVÁ, E. BRYNDA, J. HOMOLA. Functionalizable low-fouling coatings for label-free biosensing in complex biological media: advances and applications. *Analytical and Bioanalytical Chemistry* 407, 3927–3953 (2015).

[5] J. BAGGERMAN, M. M. J. SMULDERS, H. ZUILHOF. Romantic Surfaces: A Systematic Overview of Stable, Biospecific, and Antifouling Zwitterionic Surfaces. *Langmuir* 35, 1072–1084 (2019).

[6] S. LOWE, N. M. O'BRIEN-SIMPSON, L. A. CONNAL. Antibiofouling polymer interfaces: Poly(ethylene glycol) and other promising candidates. *Polymer Chemistry* 6, 198–212 (2015).

[7] S. GON, B. FANG, M. M. SANTORE. Interaction of cationic proteins and polypeptides with biocompatible cationically-anchored PEG brushes. *Macromolecules* 44, 8161–8168 (2011).

[8] A. CARE, P. L. BERGQUIST, A. SUNNA. Solid-binding peptides: Smart tools for nanobiotechnology. *Trends in Biotechnology* 33, 259–268 (2015).

[9] D. T. YUCESOY, D. KHATAYEVICH, C. TAMERLER, M. SARIKAYA. Rationally designed chimeric solid-binding peptides for tailoring solid interfaces. *Medical Devices & Sensors* 3, 1–12 (2020).

[10] S. R. WHALEY, D. S. ENGLISH, E. L. HU, P. F. BARBARA, A. M. BELCHER. Selection of peptides with semiconductor binding specificity for directed nanocrystal assembly. *Nature* 405, 665–668 (2000).

[11] C. TAMERLER, D. KHATAYEVICH, M. GUNGORMUS *ET AL.* Molecular biomimetics: GEPI-based biological routes to technology. *Biopolymers* 94, 78–94 (2010).

[12] R. R. NAIK, L. L. BROTT, S. J. CLARSON, M. O. STONE. Silica-Precipitating Peptides Isolated from a Combinatorial Phage Display Peptide Library. *Journal of Nanoscience and Nanotechnology* 2, 95–100 (2002).

[13] C. K. THAI, H. DAI, M. S. R. SASTRY *ET AL.* Identification and characterization of Cu2O- and ZnO-binding polypeptides by escherichia coli cell surface display: Toward an understanding of metal oxide binding. *Biotechnology and Bioengineering* 87, 129–137 (2004).

[14] D. KHATAYEVICH, M. GUNGORMUS, H. YAZICI *ET AL.* Biofunctionalization of materials for implants using engineered peptides. *Acta Biomaterialia* 6, 4634–4641 (2010).

[15] D. B. GEHLEN, L. C. DE LENCASTRE NOVAES, W. LONG *ET AL.* Rapid and Robust Coating Method to Render Polydimethylsiloxane Surfaces Cell-Adhesive. *ACS Applied Materials and Interfaces* 11, 41091–41099 (2019).

[16] K. RÜBSAM, B. STOMPS, A. BÖKER, F. JAKOB, U. SCHWANEBERG. Anchor peptides: A green and versatile method for polypropylene functionalization. *Polymer* 116, 124–132 (2017).

[17] T. Waku, Y. Imanishi, Y. Yoshino *et al.* Fusion of polymeric material-binding peptide to cell-adhesion artificial proteins enhances their biological function. *Biointerphases* 12, 021002 (2017).

[18] R. Hassert, M. Pagel, Z. Ming *et al.* Biocompatible silicon surfaces through orthogonal click chemistries and a high affinity silicon oxide binding peptide. *Bioconjugate Chemistry* 23, 2129–2137 (2012).

[19] N. H. Cho, T. C. Cheong, J. H. Min *et al.* A multifunctional core-shell nanoparticle for dendritic cell-based cancer immunotherapy. *Nature Nanotechnology* 6, 675–682 (2011).

[20] U. O. S. Seker, B. Wilson, D. Sahin, C. Tamerler, M. Sarikaya. Quantitative affinity of genetically engineered repeating polypeptides to inorganic surfaces. *Biomacromolecules* 10, 250–257 (2009).

[21] R. Bansal, Z. Elgundi, S. C. Goodchild *et al.* The effect of oligomerization on a solid-binding peptide binding to silica-based materials. *Nanomaterials* 10, 1–17 (2020).

[22] C. Fasting, C. A. Schalley, M. Weber *et al.* Multivalency as a chemical organization and action principle. *Angewandte Chemie - International Edition* 51, 10472–10498 (2012).

[23] W. Tang, Y. Ma, S. Xie *et al.* Valency-dependent affinity of bioactive hydroxyapatite-binding dendrons. *Biomacromolecules* 14, 3304–3313 (2013).

[24] B. Gabryelczyk, G. R. Szilvay, V. K. Singh *et al.* Engineering of the function of diamond-like carbon binding peptides through structural design. *Biomacromolecules* 16, 476–482 (2015).

[25] B. A. Helms, S. W. A. Reulen, S. Nijhuis *et al.* High-affinity peptide-based collagen targeting using synthetic phage mimics: From phage display to dendrimer display. *Journal of the American Chemical Society* 131, 11683–11685 (2009).

[26] A. V. Terskikh, J. M. Le Doussal, R. Crameri *et al.* 'Peptabody': A new type of high avidity binding protein. *Proceedings of the National Academy of Sciences of the United States of America* 94, 1663–1668 (1997).

[27] K. I. Sano, K. Ajima, K. Iwahori *et al.* Endowing a ferritin-like cage protein with high affinity and selectivity for certain inorganic materials. *Small* 1, 826–832 (2005).

[28] N. Alvisi, F. A. Gutiérrez-Mejía, M. Lokker *et al.* Self-assembly of elastin-like polypeptide brushes on silica surfaces and nanoparticles. *Biomacromolecules* 22, 1966–1979 (2021).

[29] J. R. McDaniel, J. A. MacKay, F. G. Quiroz, A. Chilkoti. Recursive directional ligation by plasmid reconstruction allows rapid and seamless cloning of oligomeric genes. *Biomacromolecules* 11, 944–952 (2010).

[30] J. Stetefeld, S. Frank, M. Jenny *et al.* Collagen stabilization at atomic level: Crystal structure of designed (GlyProPro)10foldon. *Structure* 11, 339–346 (2003).

[31] A. Wason, F. G. Pearce, J. A. Gerrard, B. C. Mabbutt. Archaeal Lsm rings as stable self-assembling tectons for protein nanofabrication. *Biochemical and Biophysical Research Communications* 489, 326–331 (2017).

[32] A. D. Malay, M. Watanabe, J. G. Heddle, J. R. H. Tame. Crystal structure of unliganded TRAP: Implications for dynamic allostery. *Biochemical Journal* 434,

427–434 (2011).

[33] T. G. W. EDWARDSON, D. HILVERT. Virus-Inspired Function in Engineered Protein Cages. *Journal of the American Chemical Society* 141, 9432–9443 (2019).

[34] J. A. FALLAS, G. UEDA, W. SHEFFLER *ET AL.* Computational design of self-assembling cyclic protein homo-oligomers. *Nature Chemistry* 9, 353–360 (2017).

[35] R. NOVY. Use of glucose to control basal expression in the pET System. *Innovations* 13, 13–15 (2001).

[36] G. HOLZWARTH, P. DOTY. The Ultraviolet Circular Dichroism of Polypeptides. *Journal of the American Chemical Society* 87, 218–228 (1965).

[37] S. R. MACEWAN, A. CHILKOTI. Applications of elastin-like polypeptides in drug delivery. *Journal of Controlled Release* 190, 314–330 (2014).

[38] C. R. EMMENEGGER, E. BRYNDA, T. RIEDEL *ET AL.* Interaction of blood plasma with antifouling surfaces. *Langmuir* 25, 6328–6333 (2009).

[39] H. VAISOCHEROVÁ, W. YANG, Z. ZHANG *ET AL.* Ultralow fouling and functionalizable surface chemistry based on a zwitterionic polymer enabling sensitive and specific protein detection in undiluted blood plasma. *Analytical Chemistry* 80, 7894–7901 (2008).

CHAPTER 5

Design of antifouling polypeptides self-assembling on gold surfaces: applying modularity

One of the advantages offered by protein-based coatings is the ability to precisely control the chemistry and the functionalities included in larger designs. In this chapter, we explore the modularity of our *B*-*M*-*E* triblock design regarding both the binding block *B* and the polymer block *E*. Using a solid-binding peptide (SBP) with affinity for gold as a *B* block, our design can be adapted for the functionalization of gold surfaces. At the same time, we replace the polymer block *E* with a zwitterionic elastin-like polypeptide to tentatively improve the antifouling properties of the protein-coating. We find that the new gold-coating *B*-*M*-*E* proteins can be recombinantly produced with high solubility and high yield. Similarly to our previous silica-binding design, these proteins retain the thermal stability granted by the trimerization domain *M*. Our preliminary results also show that the two proteins can form stable coatings on gold surfaces, with excellent antifouling properties against high concentrations of bovine serum albumin. Although more thorough testing and characterization are still needed, our preliminary work proves the modularity of the *B*-*M*-*E* triblock design.

5.1. Introduction

In Chapter 3, we compared the surface binding capabilities of three solid-binding peptides (SBPs) when included in recombinant *B-E* diblocks. We selected the B^{RT}-tag as a silica binder for our following designs, aiming to improve the salt resistance of the polymer brush by increasing the binding cooperativity. In Chapter 4, we showed how multivalent binding of SBPs can be effectively harnessed for the functionalization of silica surfaces. Whereas multivalency via tandem repeats revealed many practical constraints, the design of star-like structures proved to be an effective strategy. Unlike many tested designs, the polypeptide B^{RT}-$E^{S}{}_{3}$-M^{HR00C3_2}-$E^{S}{}_{40}$ could be easily produced and purified, with good expression levels and high solubility. Measurements performed via Dynamic Light Scattering and a Quartz Crystal Microbalance revealed that the polypeptide forms brushes on silica surfaces, resisting displacement at high concentrations of NaCl. Furthermore, the adsorbed brush displays good antifouling properties against bovine serum albumin (BSA), comparably to poly(l-lysine)-grafted poly(ethylene glycol) (PLL-*g*-PEG) brushes.

In Chapters 3 and 4, the production and screening of different polypeptides was performed using recombinant DNA technology. We engineered recombinant polypeptides to include either more functional peptides at specific locations (SBPs in tandem), or entire protein blocks (multimerization domain *M*). In previous chapters, we have suggested that the design, because of its modular nature, could be exploited for the functionalization of surfaces other than silica. Since SBPs have been developed for a multitude of solid surfaces (plastics, metals, etc.), they could be explored as *B* blocks for the design of a new recombinant *B-M-E* triblock. Thus, to test the modularity of the design with respect to the *B* block, we here investigate a recombinant *B-M-E* triblock adapted for coating gold surfaces.

Gold surfaces are becoming increasingly relevant both in the fields of biosensing and in biomedical research.[1–4] In particular, gold nanoparticles have been extensively explored due to their biocompatibility, inertness and tunable chemical and optical properties.[5,6] Gold nanoparticles have been extensively investigated in plasmon-based sensing, such as label-free single molecule detection.[7] Gold is also extensively studied and used in electrochemical sensing, mostly for the fabrication of nanoengineered surfaces for electrodes.[1] Additionally, gold nanoparticles are widely used in therapy and diagnostic applications, for drug delivery, *in vivo* imaging

(computer tomography, photoacoustic imaging) and photothermal therapy.[3,8] Many diagnostic kits already available on the market make use of gold nanoparticles, including rapid diagnostic kits for SARS-CoV-2.[9]

Gold nanoparticles can be functionalized both via covalent and non-covalent ligands. In covalent bindings, thiol-mediated interactions are the most common. The sulfur of thiols and thiolated ligands forms a covalent bond with the gold surface.[3] This stable, irreversible interaction is often used for the protection, stabilization and functionalization of gold nanoparticles.[4] Not all applications may benefit from covalent bindings, however. A more tunable and biocompatible alternative is provided by non-covalent interactions, for example via solid-binding peptides.

Many sequences for SBPs binding to gold have been reported, although not all of them have been thoroughly characterized. As a model gold-binding peptide, we focus on the peptide GBP-1 (MHGKTQATSGTIQS). Its physical and chemical characteristics are well known.[10] Unlike many proteins and self-assembled monolayers on gold, GBP-1 does not contain cysteine residues and thus cannot covalently bind the gold surface via a thiol link. Nonetheless, the reported binding strengths are comparable to other thiol-based systems in aqueous environments, even at high salt concentrations.[11,12] Probable binding mechanisms seem to involve the polar groups of glutamines, serines and threonines.[13,14] GBP-1 has already been used as a fusion tag in many protein designs: GBP-1 was included in different biosensor designs for the detection of hepatitis,[15,16] influenza[17] and SARS,[18] but also for enzyme immobilization,[19–21] nanoparticle delivery[22,23] and immunological essays.[24] Nevertheless, our experience with *B-E* diblocks featuring a single SBP suggests that the stability of the adhering layers might be suboptimal in many of these applications. The designs could therefore benefit from increasing the binding valency. Interestingly, Braun *et al*. reported that a tandem repeat of 3 GBP-1 sequences shows a much increased binding strength and surface coverage compared to a single GBP-1.[13,25]

In our original triblock design adapted for silica, we selected a hydrophilic polymer chain *E* to evaluate its antifouling properties. This block showed good antifouling properties against concentrated BSA. Nonetheless, we anticipate that improved antifouling properties might be necessary in real life applications and different environmental conditions. For this reason, we test the modularity of the design with respect to the *E* block by replacing the antifouling polymer chain *E*.

A successful strategy for the creation of antifouling surfaces involves zwitterionic polymer brushes. Zwitterionic polymers are electrically neutral materials that alternate positive and negative charges along their chains. They have recently been proven to be excellent polymers for reducing non-specific adsorption at sensing interfaces.[26–28] Zwitterionic protein polymers are also used in biosensing and nanoparticle coatings.[29,30] Common zwitterionic antifouling peptides consist of short repeats of the amino acids glutamic acid (E) and lysine (K).[1] EK peptides have been successfully introduced into existing proteins without altering their functionality, improving their stability.[31] In addition, alternated or mixed EK sequences could confer antifouling properties to solid surfaces and particles.[32]

In our previous design, the polymer block *E* was based on the pentameric motif VPGXG from elastin, in which X can be any amino acid except proline. In the original *E* block, the uncharged and hydrophilic amino acid serine was chosen (X=S). To explore the antifouling properties of zwitterionic protein brushes, we redesign the *E* block to contain alternating positive and negative guest residues X. In our new *E* block design, aspartic acid (X=D) and lysine (X=K) are chosen as alternating guest residues, resulting in the final *E* block sequence E^{Z}_{40} = (VPGDG-VPGKG)$_{20}$. Lysine was selected, since the other positively charged amino acids (histidine and arginine) have a higher affinity for gold and could compete with GBP-1 for surface binding. The use of aspartic acid was inspired by the zwitterionic polypeptide (ZIPP) designs synthesized by Banskota *et al*.[33]

In this chapter, we test two proteins to evaluate the modularity of our design towards both the *B* and the *E* block. The domain structure of the two new proteins is $B^{GBP\text{-}1}$-E^{S}_{3}-M^{HR00C3_2}-E^{X}_{40}, where $B^{GBP\text{-}1}$ is the gold-binding peptide GBP-1, and X = S (serine, uncharged) or Z (zwitterionic). The star-shaped architecture is maintained in both designs, to introduce multivalent binding on gold surfaces. We perform a preliminary assessment of the antifouling properties of the zwitterionic polymer brush compared to the original *E* block. Our results confirm our expectations regarding the modularity of our protein design, with respect to exchanging both the *B* block and the *E* block.

5.2. Materials and methods

5.2.1. Construction of expression plasmids for polypeptides

For the construction of *B-M-E* triblocks, a synthetic gene encoding for the $B^{GBP\text{-}1}$-E^{S}_{3}-M^{HR00C3_2} block was purchased from Integrated DNA Technologies (Leuven, Belgium). The block encodes a poly-histidine tag for downstream purification, the $B^{GBP\text{-}1}$ = (MHGKTQATSGTIQS) tag, a linker polypeptide E^{S}_{3} = $(VPGSG)_3$ and the multimerization domains M^{HR00C3_2}. The synthetic fragment was designed to contain the features needed for recursive directional ligation by plasmid reconstruction (PRe-RDL) cloning, as described by McDaniel *et al*.[34] For our first polypeptide design ($B^{GBP\text{-}1}$-E^{S}_{3}-M^{HR00C3_2}-E^{S}_{40}), the $B^{GBP\text{-}1}$-E^{S}_{3}-M^{HR00C3_2} block was digested with *BamHI/AcuI* and ligated into a *BamHI/AcuI*-digested pET-24a(+) vector containing the E^{S}_{40} = $(VPGSG)_{40}$ sequence. Four our second polypeptide design ($B^{GBP\text{-}1}$-E^{S}_{3}-M^{HR00C3_2}-E^{Z}_{40}), a second synthetic gene encoding for part of the antifouling E^{Z}_{20} = $(VPGDG\text{-}VPGKG)_{10}$ block was purchased from Twist Bioscience. The synthetic fragment was designed to contain the features needed for PRe-RDL cloning, as described by McDaniel *et al*.[34] Following the PRe-RDL method, the $B^{GBP\text{-}1}$-E^{S}_{3}-M^{HR00C3_2} block was digested with *BamHI/AcuI* and ligated into a *Bam*HI*/Acu*I-digested pET-24a(+) vector containing the E^{Z}_{20} = $(VPGDG\text{-}VPGKG)_{10}$ sequence. The resulting construct was once again digested with *BamHI/AcuI* and ligated into a *BamHI/AcuI*-digested pET-24a(+) vector containing the E^{Z}_{20} block to construct the complete *B-M-E* triblock. For both constructs, plasmid DNA was transformed into *Escherichia coli* DH5α via heat shock. Colonies containing the correct DNA insert were selected and confirmed by DNA sequencing. Then, the plasmid was transformed into *E. coli* T7-Express.

5.2.2. Protein expression.

E. coli T7-Express containing the expression plasmids for the polypeptides was cultured at 37 °C and 215 rpm for 16 hours in 25 mL Terrific Broth medium containing 50 μg mL^{-1} kanamycin. The starter culture was inoculated in 1 L of lysogeny broth medium containing 50 μg mL^{-1} kanamycin and incubated at 37 °C and 215 rpm until OD_{600} > 0.6. Then, isopropylthio-β-galactoside was added to a final concentration of 1 mM and cells were incubated overnight at 18 °C and 215 rpm before harvesting.

5.2.3. Protein purification

Bacterial cells were centrifuged at 6000 rpm for 30 minutes at 4 °C and resuspended in 30 mL of cold extraction buffer (50 mM Tris pH 8.00, 300 mM NaCl, 30 mM imidazole). Phenylmethylsulfonyl fluoride was added to the cell suspension to a final concentration of 1 mM. Cells were lysed via sonication (Q125 Sonicator, QSonica). The cell lysate was centrifuged for 30 minutes at 30,000 x *g* at 4 °C to pellet the insoluble fraction. Next, the polypeptide was purified using immobilized metal ion affinity chromatography (IMAC). The sample was injected in an IMAC column (Bio-Scale Mini Profinity IMAC cartridge, Bio-Rad Laboratories) and washed with extraction buffer. The polypeptide was eluted with a linear gradient from extraction buffer to elution buffer (50 mM Tris pH 8.00, 300 mM NaCl, 300 mM imidazole). The purity of the polypeptides was assessed by sodium dodecyl sulfate-polyacrylamide gel electrophoresis (SDS-PAGE).

5.2.4. Matrix-assisted laser desorption/ionization time-of-flight analysis

To confirm the size of the polypeptide, its molecular weight was determined using matrix-assisted laser desorption/ionization (MALDI) mass spectrometry coupled to time-of-flight mass spectrometry (MALDI-TOF). The spectrum was obtained using a Bruker UltraFlextreme machine. The sample was prepared following the instructions provided by the manufacturer. Data was processed with the software package FlexAnalysis v3.4.

5.2.5. Circular dichroism

For the circular dichroism measurements, a Jasco Spectropolarimeter J-715 was used. Data was collected and analyzed with Jasco software. For the sample preparation, the protein was dissolved at a concentration of 0.1 mg mL^{-1} in phosphate buffered saline (PBS) pH 7.4. The solution was sonicated for 10 min to reduce the presence of aggregates before the measurement. A quartz cuvette with a 1 mm path was used. For the spectrum measurements, the instrument was set to continuous scanning mode, with a data pitch of 0.1 nm, a scanning speed of 50 nm min^{-1} and a band width of 2 nm. Each spectrum was accumulated 20 times.

5.2.6. Quartz crystal microbalance with dissipation monitoring

A Q-Sense E4 Quartz crystal microbalance with dissipation monitoring (QCM-D) instrument (Biolin Scientific, Sweden) was used to quantify polypeptide binding to silica. Gold-coated QCM sensors coated with Au were obtained from Biolin Scientific and cleaned according to the provided instructions. Each sensor was equilibrated with PBS at a flow rate of 50 µL min^{-1} until a stable baseline was reached. The Au sensors were coated with B^{GBP-1}-E^{S}_{3}-M^{HR00C3_2}-E^{S}_{40} and B^{GBP-1}-E^{S}_{3}-M^{HR00C3_2}-E^{Z}_{40} (10 µM) until a stable value of Δf was reached (35 mins). Coated and uncoated sensors were then flushed with a solution of BSA (1 mg mL^{-1}). Analysis of QCM-D data was performed using QSense Dfind software v1.2.7.

5.3. Results

Representative SDS-PAGE results for the purification process of the two triblocks are shown in Figure 5-1. For simplicity, we will refer to our two polypeptides as B^{GBP-1}-*M*-E^{S} and B^{GBP-1}-*M*-E^{Z}. In both cases, a fraction of the target protein did not bind to the IMAC column, similarly to previous observations regarding the silica-binding *B*-*M*-*E* triblock. Nonetheless, B^{GBP-1}-*M*-E^{S} could be eluted with high purity, while B^{GBP-1}-*M*-E^{Z} showed the presence of a few impurities.

To confirm the correct size and purity of the polypeptide B^{GBP-1}-*M*-E^{Z}, the purified protein was analyzed using MALDI-TOF mass spectrometry (Figure 5-2). We found that the experimentally determined mass (51.712 kg mol^{-1}) is comparable to the theoretically expected value (51.704 kg mol^{-1}) within the error of the measurement. Furthermore, no contaminants could be detected.

We then investigated if the trimerization domain *M* can still correctly fold in the new B^{GBP-1}-*M*-E^{Z} triblock. As mentioned in Chapter 4, the trimerization domain is extremely stable and exclusively α-helical, even though the gold-binding B^{GBP-1}-*M*-E^{Z} triblock is mostly composed of disordered structure.[35] For this analysis, we recorded the circular dichroism spectrum of a version of the B^{GBP-1}-*M*-E^{Z} triblock in which the E^{Z} block was truncated to only half of its length (B^{GBP-1}-E^{S}_{3}-M^{HR00C3_2}-E^{Z}_{20}). A preliminary measurement with this truncated protein would allow us to evaluate the effect of both the gold-binding B^{GBP-1} block and the E^{Z} block on protein folding, reducing the influence of the unfolded E^{Z} block on the circular dichroism spectrum. Like in Chapter 4, we assume a correctly folded *M* domain will yield a circular dichroism spectrum

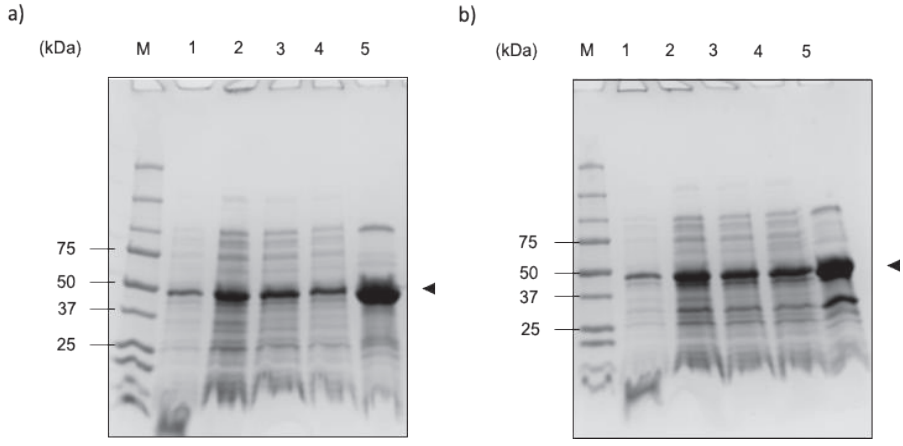

Figure 5-1. Purification of gold-binding *B-M-E* triblocks with SDS-PAGE analysis. Lane 1: intact cells; lane 2: cell lysate; lane 3: soluble lysate; lane 4: IMAC flow-through; lane 5: IMAC fractions; lane M: molecular marker. **(a)** $B^{GBP\text{-}1}$-*M*-E^{S}; **(b)** $B^{GBP\text{-}1}$-*M*-E^{Z}.

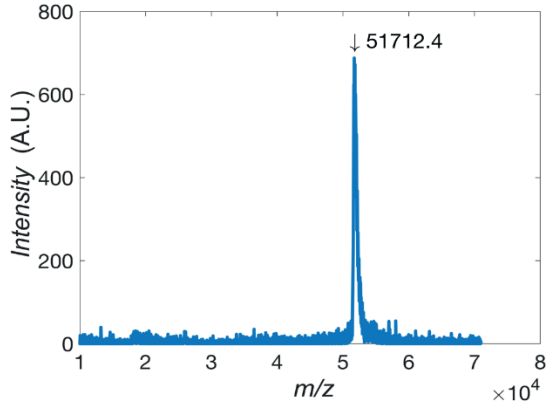

Figure 5-2. MALDI-TOF spectrum of $B^{GBP\text{-}1}$-*M*-E^{Z} protein.

with features that are distinctive for α-helical proteins. CD spectra for the truncated the $B^{GBP\text{-}1}$-*M*-E^{Z} triblock are shown in Figure 5-3. At room temperature (20 °C), the spectrum shows two clear negative bands at 210 nm and 222 nm, typical of α-helical proteins.[36] Increasing the temperature of the sample to 95 °C causes a mild change at the 222 nm band. After cooling down to room temperature, the measurement is identical to the spectrum before

heating, indicating full thermal stability and suggesting no significant unfolding. Similar results were found also for the $B^{GBP\text{-}1}$-*M*-E^{S} triblock (data not shown).

We tested the ability of the two *B*-*M*-*E* blocks to adhere to gold surfaces and prevent biological fouling. QCM was used to assess both the assembly of polymer brushes on gold-coated quartz sensors and the ability to prevent the unspecific adhesion of BSA in PBS buffer, pH 7.4. The QCM sensors were first coated with the gold-binding triblocks and, after brush formation, a high concentration of BSA (1 mg mL^{-1}) was flushed on the sensors. The sensors were then rinsed with PBS buffer. A bare gold sensor was used as negative control. The results of this preliminary experiment are shown in Figure 5-4.

For the negative control on bare gold, QCM signal is recorded after the injection of BSA. Rinsing the sensor with PBS does not result in a change in QCM signal, showing that BSA has adsorbed irreversibly on the sensor. Gold sensors can be stably coated with both $B^{GBP\text{-}1}$-*M*-E^{S} and $B^{GBP\text{-}1}$-*M*-E^{Z}, as shown in the first part of the graph: after injection of the protein solutions, the sensors

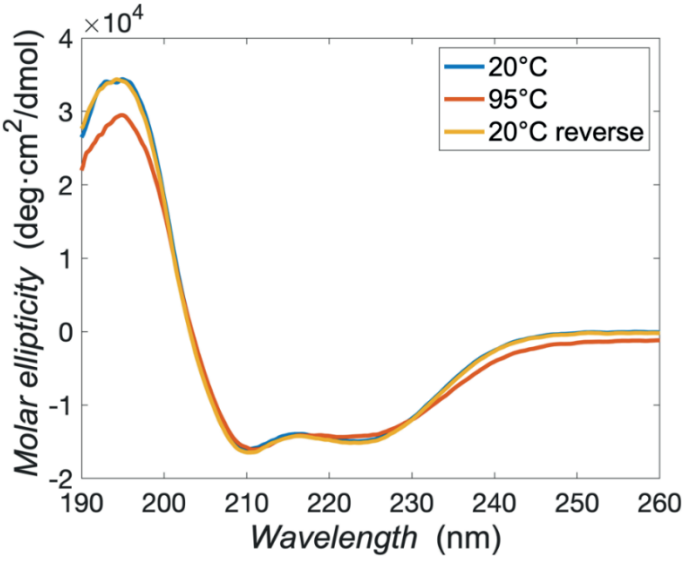

Figure 5-3. Analysis of the secondary structure of a gold-binding $B^{GBP\text{-}1}$-*M*-E^{Z} triblock with circular dichroism spectroscopy. Molar ellipticity is plotted versus wavelength. Spectra were recorded at 20 °C, at 95 °C and again at 20 °C. Solution conditions: 0.1 mg mL^{-1} of protein in PBS, pH 7.4. Data were collected in a cell with a 1 mm path length.

are quickly coated and reach a stable QCM signal. No desorption seems to take place when the sensors are flushed with PBS solution. These results show that the B^{GBP-1} block can confer gold-binding abilities to our proteins, with good and stable coverage. It can also be noted that the B^{GBP-1}-*M*-E^Z coating causes a larger frequency shift compared to B^{GBP-1}-*M*-E^S. Since the two proteins have a comparable molecular mass, the recorded difference suggests that the B^{GBP-1}-*M*-E^Z coating binds with a higher protein density. This hypothesis is confirmed by the similar energy dissipation recorded for the two coatings, indicating that the coating hydration is not responsible for the mass difference (data not shown).

Finally, the assay shows that both E^S and E^Z blocks retain excellent antifouling properties. Upon injecting the BSA solution, the QCM signals for both proteins are hardly influenced. The small variations in the recorded frequency shift can be attributed to the expected signal drift of the QCM sensor over long measurements.

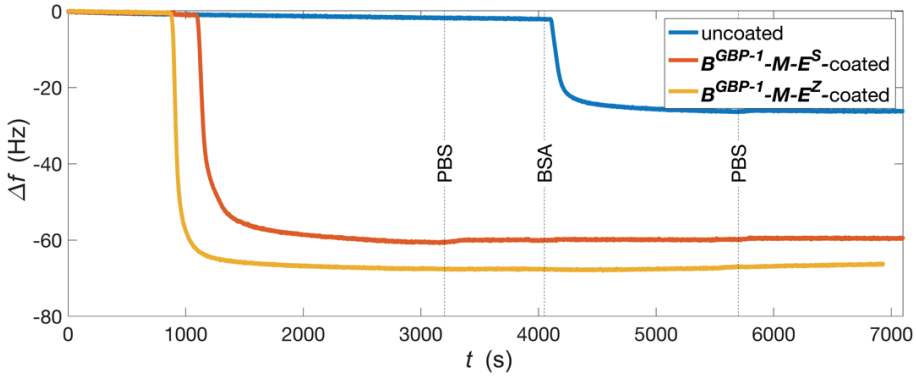

Figure 5-4. Antifouling properties of gold-binding *B-M-E* polymer brushes adsorbed on Au surface. QCM frequency shift Δf (Hz) versus time t (s) after starting the injection of the brush-forming polymer. At the first dashed vertical lines we switch to rinsing with PBS, at the second vertical dashed lines we switch to injecting 1 mg mL^{-1} BSA in PBS, and at the third dashed vertical lines we switch back to rinsing with PBS. Blue line: bare gold negative control, orange line: B^{GBP-1}-*M*-E^S, yellow line: B^{GBP-1}-*M*-E^Z.

5.4. Concluding remarks

Our preliminary work proves the modularity of our *B-M-E* triblock design, towards both the *B* block and the *E* block. While gold surfaces can be functionalized after replacing the silica-binding SBP with the gold-binding peptide GBP-1, the hydrophilic *E* block can also be easily replaced with a zwitterionic *E* block. In both cases, exchanging blocks does not negatively impact the folding and stability of the *M* block. Furthermore, the antifouling properties of the polypeptide are maintained with the use of a zwitterionic protein polymer.

These promising preliminary results are in line with research on zwitterionic polymers, even though further research is required to evaluate their antifouling behavior with complex biological fluids (diluted serum or blood). Changes in the length of the E^Z block might be necessary to meet these conditions and grant sufficient antifouling properties.

The functionalization of gold nanoparticles requires both a highly antifouling coating and the precise exposition of bioactive moieties in most applications (theranostics, drug delivery, and photothermal therapy). These results can be achieved only with good coverage of the gold surface. For this reason, the coverage and formation of a polymer brush should be better investigated using Quartz Crystal Microbalance. A thorough analysis is also necessary to confirm the higher protein density of $B^{GBP\text{-}1}$-*M*-E^Z coatings.

The modularity of the triblock design can also be further explored by adding more functionalities to the protein. For example, proteins tags for the attachment of cargos (antibodies, probes, and drugs) could be placed at the C-terminal of the protein to ensure their correct exposition on the surface. Alternatively, a different set of SBPs could be tested to develop *B-M-E* triblocks suitable for other relevant surfaces (plastics and metals). Although different multimerization domains (*M* blocks) could be explored in the future, the results collected in Chapter 4 clearly indicate that finding a suitable replacement is not a trivial task. Given the positive results obtained with the current *M* block, we therefore gauge it unnecessary, albeit technically feasible, to investigate different molecular architectures.

5.5. List of abbreviations

Abbreviation	Meaning
BSA	bovine serum albumin
MALDI-TOF	matrix-assisted laser desorption/ionization coupled to time-of-flight mass spectrometry
PBS	phosphate-buffered saline
PEG-*g*-PLL	poly(l-lysine)-grafted poly(ethylene glycol)
QCM	quartz crystal microbalance
QCM-D	quartz crystal microbalance with dissipation monitoring
SBP	solid-binding peptide
SDS-PAGE	sodium dodecyl sulfate-polyacrylamide gel electrophoresis

5.6. References

[1] M. J. Russo, M. Han, P. E. Desroches *et al.* Antifouling Strategies for Electrochemical Biosensing: Mechanisms and Performance toward Point of Care Based Diagnostic Applications. *ACS Sensors* 6, 1482–1507 (2021).

[2] H. Lee, Y. S. Lee, S. S. Reginald *et al.* Biosensing and electrochemical properties of flavin adenine dinucleotide (FAD)-Dependent glucose dehydrogenase (GDH) fused to a gold binding peptide. *Biosensors and Bioelectronics* 165, (2020).

[3] J.-H. Lee, J.-W. Choi. Application of Plasmonic Gold Nanoparticle for Drug Delivery System. *Current Drug Targets* 19, 271–278 (2017).

[4] K. Saha, S. S. Agasti, C. Kim, X. Li, V. M. Rotello. Gold nanoparticles in chemical and biological sensing. *Chemical Reviews* 112, 2739–2779 (2012).

[5] H. H. Jeong, E. Choi, E. Ellis, T. C. Lee. Recent advances in gold nanoparticles for biomedical applications: From hybrid structures to multi-functionality. *Journal of Materials Chemistry B* 7, 3480–3496 (2019).

[6] W. jin Jeong, J. Bu, L. J. Kubiatowicz *et al.* Peptide–nanoparticle conjugates: a next generation of diagnostic and therapeutic platforms? *Nano Convergence* 5, 1–18 (2018).

[7] A. B. Taylor, P. Zijlstra. Single-Molecule Plasmon Sensing: Current Status and Future Prospects. *ACS Sensors* 2, 1103–1122 (2017).

[8] J. Conde, A. Ambrosone, V. Sanz *et al.* Design of multifunctional gold nanoparticles for in vitro and in vivo gene silencing. *ACS Nano* 6, 8316–8324 (2012).

[9] Y. Zhou, Y. Wu, L. Ding, X. Huang, Y. Xiong. Point-of-care COVID-19 diagnostics powered by lateral flow assay. *TrAC - Trends in Analytical Chemistry* 145, 116452 (2021).

[10] S. Brown. Metal-recognition by repeating polypeptides. *Nature Biotechnology* 15, 269–272 (1997).

[11] C. Tamerler, E. E. Oren, M. Duman, E. Venkatasubramanian, M. Sarikaya. Adsorption kinetics of an engineered gold binding peptide by surface plasmon resonance spectroscopy and a quartz crystal microbalance. *Langmuir* 22, 7712–7718 (2006).

[12] M. Sarikaya, C. Tamerler, A. Jen, K. Schulten, F. Baneyx. Molecular biomimetics: nanotechnology through biology. *Nature materials* 2, 577–585 (2003).

[13] S. Kanata, T. Nishino, R. Makiura, S. Saiki, N. Hayashi. Single-molecule imaging of gold-binding peptide adsorbed on au(111). *Analytical Sciences* 29, 405–409 (2013).

[14] C. R. So, J. L. Kulp, E. E. Oren *et al.* Molecular recognition and supramolecular self-assembly of a genetically engineered gold binding peptide on Au{111}. *ACS Nano* 3, 1525–1531 (2009).

[15] N. S. Heo, S. Zheng, M. H. Yang *et al.* Label-free electrochemical diagnosis of viral antigens with genetically engineered fusion protein. *Sensors (Switzerland)* 12, 10097–10108 (2012).

[16] S. Zheng, D. K. Kim, T. J. Park, S. J. Lee, S. Y. Lee. Label-free optical diagnosis of

hepatitis B virus with genetically engineered fusion proteins. *Talanta* 82, 803–809 (2010).

[17] K. G. Lee, T. J. Lee, S. W. Jeong *et al.* Development of a plastic-based microfluidic immunosensor chip for detection of H1N1 influenza. *Sensors (Switzerland)* 12, 10810–10819 (2012).

[18] T. J. Park, M. S. Hyun, H. J. Lee, S. Y. Lee, S. Ko. A self-assembled fusion protein-based surface plasmon resonance biosensor for rapid diagnosis of severe acute respiratory syndrome. *Talanta* 79, 295–301 (2009).

[19] J. W. Lee, S. R. Choi, J. H. Heo. Simultaneous Stabilization and Functionalization of Gold Nanoparticles via Biomolecule Conjugation: Progress and Perspectives. *ACS Applied Materials and Interfaces* (2021) doi:10.1021/acsami.1c10436.

[20] K. C. Ko, M. H. Choi, J. K. Rho, S. H. Park. A facile method for detecting calcium/calmodulin-dependent protein kinase using radio phosphorylation of a GBP-fused enzyme substrate in a lab-on-a-chip. *Sensors and Actuators, B: Chemical* 178, 434–442 (2013).

[21] T. Kacar, M. T. Zin, C. So *et al.* Directed self-immobilization of alkaline phosphatase on micro-patterned substrates via genetically fused metal-binding peptide. *Biotechnology and Bioengineering* 103, 696–705 (2009).

[22] M. H. Oh, J. H. Yu, I. Kim, Y. S. Nam. Genetically Programmed Clusters of Gold Nanoparticles for Cancer Cell-Targeted Photothermal Therapy. *ACS Applied Materials and Interfaces* 7, 22578–22586 (2015).

[23] B. Zheng, I. Yamashita, M. Uenuma *et al.* Site-directed delivery of ferritin-encapsulated gold nanoparticles. *Nanotechnology* 21, (2010).

[24] F. Fatemi, S. M. Amini, S. Kharrazi *et al.* Construction of genetically engineered M13K07 helper phage for simultaneous phage display of gold binding peptide 1 and nuclear matrix protein 22 ScFv antibody. *Colloids and Surfaces B: Biointerfaces* 159, 770–780 (2017).

[25] R. Braun, M. Sarikaya, K. Schulten. Genetically engineered gold-binding polypeptides: Structure prediction and molecular dynamics. *Journal of Biomaterials Science, Polymer Edition* 13, 747–757 (2002).

[26] J. Baggerman, M. M. J. Smulders, H. Zuilhof. Romantic Surfaces: A Systematic Overview of Stable, Biospecific, and Antifouling Zwitterionic Surfaces. *Langmuir* 35, 1072–1084 (2019).

[27] S. Lowe, N. M. O'Brien-Simpson, L. A. Connal. Antibiofouling polymer interfaces: Poly(ethylene glycol) and other promising candidates. *Polymer Chemistry* 6, 198–212 (2015).

[28] J. Ladd, Z. Zhang, S. Chen, J. C. Hower, S. Jiang. Zwitterionic polymers exhibiting high resistance to nonspecific protein adsorption from human serum and plasma. *Biomacromolecules* 9, 1357–1361 (2008).

[29] L. Wu, B. Lin, H. Yang *et al.* Enzyme-responsive multifunctional peptide coating of gold nanorods improves tumor targeting and photothermal therapy efficacy. *Acta Biomaterialia* 86, 363–372 (2019).

[30] M. Cui, Y. Wang, M. Jiao *et al.* Mixed Self-Assembled Aptamer and Newly Designed Zwitterionic Peptide as Antifouling Biosensing Interface for Electrochemical Detection of alpha-Fetoprotein. *ACS Sensors* 2, 490–494 (2017).

[31] E. J. Liu, A. Sinclair, A. J. Keefe *et al.* EKylation: Addition of an Alternating-Charge Peptide Stabilizes Proteins. *Biomacromolecules* 16, 3357–3361 (2015).

[32] A. J. Keefe, K. B. Caldwell, A. K. Nowinski *et al.* Screening nonspecific interactions of peptides without background interference. *Biomaterials* 34, 1871–1877 (2013).

[33] S. Banskota, P. Yousefpour, N. Kirmani, X. Li, A. Chilkoti. Long circulating genetically encoded intrinsically disordered zwitterionic polypeptides for drug delivery. *Biomaterials* 192, 475–485 (2019).

[34] J. R. McDaniel, J. A. MacKay, F. G. Quiroz, A. Chilkoti. Recursive directional ligation by plasmid reconstruction allows rapid and seamless cloning of oligomeric genes. *Biomacromolecules* 11, 944–952 (2010).

[35] J. A. Fallas, G. Ueda, W. Sheffler *et al.* Computational design of self-assembling cyclic protein homo-oligomers. *Nature Chemistry* 9, 353–360 (2017).

[36] G. Holzwarth, P. Doty. The Ultraviolet Circular Dichroism of Polypeptides. *Journal of the American Chemical Society* 87, 218–228 (1965).

CHAPTER 6

General discussion

6.1. Introduction

In the Introduction, we described a strategy for the design of a protein-based molecular architecture for the stable functionalization of biomedically relevant surfaces. We also introduced the requirements for functionalization, each presenting their own underlying challenges. Firstly, the architecture should allow the immobilization of sensing/reactive moieties on the surface of interest. This requirement is obviously crucial for the development of any surface functionalization strategy. Secondly, the architecture should allow the proper orientation of the reactive moieties, and, by consequence, the coating should properly orient itself on the surface. Proper orientation is necessary to ensure both retention of functionality and proper surface coverage. Thirdly, the process should be simple and fast, comprising only a few steps. Ideally, the surface functionalization does not require pre-treatments, necessitating short incubation times and no toxic compounds. Finally, the production process should be scalable in a manner compatible with current technology.

In Chapters 3, 4, and 5, we showed how polypeptide-based brushes can be effectively used for the functionalization of solid surfaces. In Chapter 3, we focused on silica surfaces and, upon finding promising yet unsatisfactory results, we showed how multivalency can be harnessed to increase binding strength in Chapter 4. The increase in binding strength allowed the stabilization of the protein coating at high salt concentrations. We showed that the architecture can be engineered to present antifouling properties comparable with synthetic polymers within the tested settings. In Chapter 5, we showed how our multimeric design can be effectively adapted for gold surfaces while retaining its antifouling properties. Although these results provide a promising groundwork for the assembly of antifouling protein coatings on solid surfaces, we did not yet fully reach our aims. In the following sections, we offer a critical evaluation of the achieved goals in relation to our proposed strategy, and we discuss possible future developments.

6.2. A ready-to-use antifouling coating

In Chapter 2, we provided an extensive overview on the biomedical applications of solid-binding peptides (SBPs). Although SBPs have been included in complex designs in many instances, simple designs featuring an SBP and a functional domain were tested both *in vitro* and *in vivo* with similar rates of success. However, most designs fail to address a crucial aspect in any surface functionalization strategy: it is a rather enticing misconception that

SBPs alone can confer antifouling properties to coated surfaces. As discussed in section 2.4, the Vroman effect describes the constant competitive replacement of any adsorbed biomolecule by the proteins contained in biological fluids. This effect is more marked for non-specifically adsorbed proteins, but SBP coatings are also subject to this intrinsically inescapable physical process. Moreover, SBPs might directly interact with the proteins contained in complex media, resulting in non-specific adsorption. It is therefore paramount that any adsorption-based coating strategy take these issues into account, especially for long term and therapeutic applications.

The unwanted adsorption of proteins can be prevented with the addition of antifouling polymers. For this reason, in Chapter 3 we introduced a hydrophilic elastin-like polypeptide (block *E*) to our design. The results of Chapter 3 and 4 show that this block can impart antifouling properties to coated silica surfaces against nanoparticles and serum proteins. Similarly, in Chapter 5, preliminary results show that a *B*-*M*-*E* triblock featuring a gold-binding *B* block and a modified *E* block can form an antifouling coating on gold surfaces. These proof-of-concept results alone provide sufficient evidence for the use of our *B*-*M*-*E* design as a protein-based antifoulant. Nevertheless, further tests are necessary to evaluate possible *in vitro* and *in vivo* applications.

Our diblock polypeptide *B*-*E* showed remarkable antifouling properties in the particle mobility assay described in Chapter 3. In Chapter 4, however, the same diblock could not prevent the adsorption of bovine serum albumin on the silica-coated sensors of a quartz-crystal microbalance. The results of Chapters 3 and 4 highlight a fundamental aspect in the evaluation of antifouling properties: the testing conditions must resemble the application conditions as closely as possible. Our tests were conducted in environments that do not resemble the physiological conditions in which a biosensing platform might perform. In particular, our coating should be evaluated at different values of pH (such as those found in saliva and sweat) and in the presence of more complex solutions (such as diluted serum, whole serum, and whole blood). Combined with the new antifouling *E* block introduced in Chapter 5, these tests could expand the range of possible applications of our antifouling coating. Moreover, recently designed zwitterionic elastin-like polypeptides might grant even better antifouling properties under more challenging conditions.[1]

The preliminary results of Chapter 5 strongly indicate that the assembly of antifouling polypeptide coatings based on the *B-M-E* design is not restricted only to silica surfaces. On the contrary, the proper choice of one of the many available SBP sequences may allow for the functionalization of other biomedically relevant surfaces. The novelty of a modular design that can be easily adapted for surfaces with substantially different surface chemistries cannot be overstated. While our *B-M-E* design can already be used as antifouling coating for silica and gold surfaces, future tests should expand the pool of treatable materials. As previously mentioned in section 2.4, new and relatively unexplored and important materials such as biodegradable plastics, nitrocellulose, and absorbable polymers could provide a proof-of-concept for interesting and farsighted applications. Biodegradable plastics will eventually need to find a prominent role in laboratory practices given the increasing amount of evidence against the use of petroleum-derived plastic materials, the devastating effects of their release in the environment, the growing debate around restrictions on their use, and the remarkable weight of single-use laboratory consumables.[2–5] The implementation of functionalization techniques for biodegradable materials will help define their possible uses and promote their widespread adoption. Furthermore, adsorption-driven biofunctionalization could find interesting applications for absorbable polymers such as surgical sutures. For these intrinsically transient and short-lived materials, the improved biocompatibility of protein coatings may greatly outweigh the concerns around their long-term stability.

As a final discussion point, we should evaluate the introduction of additional functionalities to our current *B-M-E* design to improve its biocompatibility. The use of antifouling coatings in biosensing is strictly linked to better functionality and sensitivity. Additionally, antifouling coatings prevent the unwanted adsorption of proteins and the formation of pathogenic biofilms on implanted biomaterials to increase the chance of successful integration. Since tissue inflammation is linked to implant rejection, our protein coating could include functionalities that locally reduce the host immune response. For example, immunoregulatory proteins secreted by parasitic helminths are known to possess anti-inflammatory properties.[6] These extraordinary mechanisms of immune evasion could be integrated into our existing designs through genetic engineering.

6.3. The next step: biofunctionalization

In the previous section, we argued that our *B-M-E* triblock possesses the necessary features to be used directly as antifouling agent. Such antifouling coating would already provide sufficient functionalization for a few applications in biomedicine (such as catheters and bandages) and industrial equipment. The ability to include more functionalities is therefore crucial for other biomedical applications such as biosensing. Our protein-based coating offers three alternative strategies for the controlled addition of biomolecules on coated surfaces, which are schematically depicted in Figure 6-1: chemical attachment to unique reactive residues, fusion of polypeptides via genetic engineering, and attachment via protein tags, either covalent or non-covalent.

The first strategy involves the addition of a unique chemically reactive terminal amino acid, either natural or unnatural (Figure 6-1a). Cysteine and tyrosine, among others, can specifically react with various linker molecules, usually via click reactions. The use of an intermediate linker would allow for the attachment of various functional compounds, such as other polypeptides, nucleic acids, and drugs. Given the degree of flexibility granted by this approach, we have tentatively explored chemical functionalization for our *B-E* diblock protein. Our diblock designs from Chapter 3 provide a straightforward approach for the chemical conjugation of cargo molecules. In fact, the protein C-terminal is theoretically available for the conjugation of linkers with a precise stoichiometry (one linker per polypeptide). For this reason, we included a terminal cysteine in our *B-E* diblock designs, providing a single reactive sulfhydryl group in a highly accessible position (Appendix Chapter 4). Sulfhydryl groups are commonly used in many bioconjugation approaches, because of their reactivity and stability.[7]

A common protein labelling strategy is maleimide modification, with the formation of a thioether bond that is stable at physiological pH.[8,9] As a proof-of-concept, we first confirmed that the terminal cysteine in the diblock polypeptide is accessible for functionalization with a methoxy-PEG2000-maleimide (mPEG2K-MAL, Sigma-Aldrich) polymer, as shown in Figure 6-2. We then tested a series of linkers for the site-specific conjugation of our diblock polypeptide to monoclonal antibodies (mAbs). The functionalization of antibodies often requires site-specific mutations for the addition of unnatural amino acids or peptide tags.[10] Since genetic engineering of mAbs is a costly procedure, we instead explored a bioconjugation strategy that can be readily

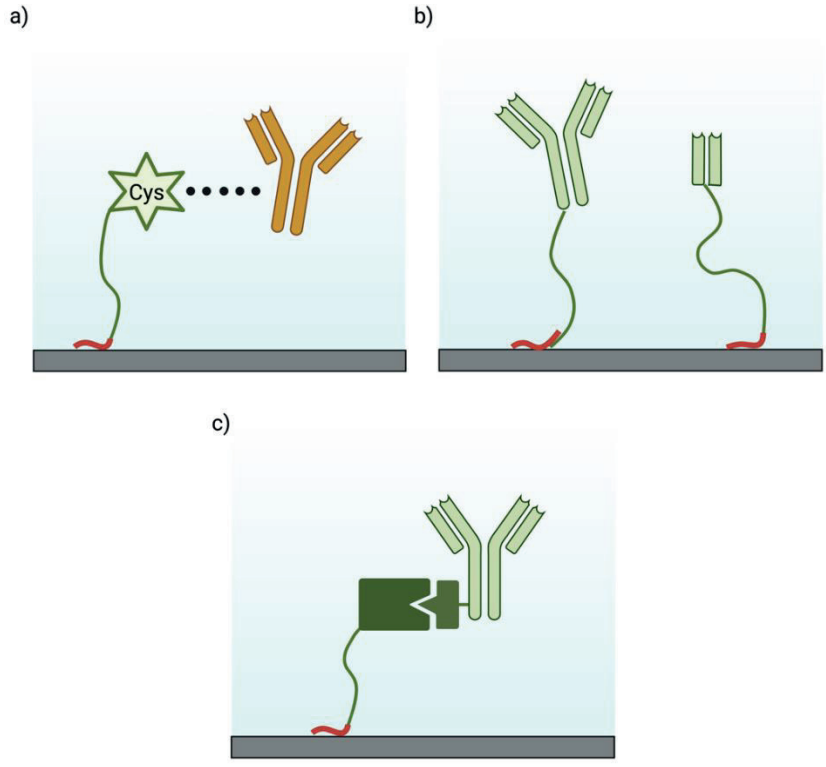

Figure 6-1. Schematic depiction of the proposed biofunctionalization strategies using a polypeptide-based coating. **(a)** The addition of a reactive amino acid can be used for the conjugation of an intermediate linker molecule. The linker can be attached to any biomolecule of interest. **(b)** Polypeptides could be directly fused to the coating via genetic engineering. In this case, entire polypeptide chains (left) or functional domains (right) can be used. **(c)** Protein-based fusion tags could be added to the polypeptide via genetic engineering. Both covalent (SpyTag/SpyCatcher) and non-covalent (protein G) peptides can be used.

applied to any mAb. As shown by van Geel *et al*., the globally conserved glycosylation site on the Fc domain of antibodies can be enzymatically trimmed and functionalized with an azido-modified sugar, thus enabling site-specific click reactions (see Figure 6-3a).[11]

To preliminarily test the bioconjugation efficiency of an azido-modified model mAb (trastuzumab), we evaluated if the modified glycan can be conjugated with a bicyclononyne-PEG2000 polymer (BCN-PEG2K) through a

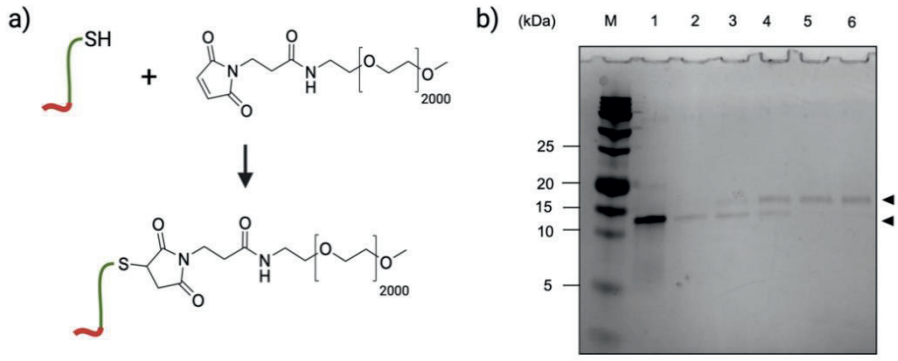

Figure 6-2. Bioconjugation of methoxy-PEG2000 (mPEG2K) polymer with diblock protein. **(a)** Schematic representation of the bioconjugation reaction between our *B-E* diblock featuring a terminal cysteine and mPEG2K. **(b)** Sodium dodecyl sulfate-polyacrylamide gel electrophoresis (SDS-PAGE) analysis of mPEG2K-maleimide conjugated to *B-E* diblock featuring a terminal cysteine. The protein solution was incubated with an excess of tris(2-carboxyethyl)phosphine (TCEP) to reduce disulfide bridges for 2 hours at 4°C. The protein was then incubated with 2, 4, 10, 20, and 30 molar equivalents of mPEG2K-maleimide at room temperature overnight. Lane 1: *B-E* diblock; lane 2: 2 equivalents mPEG2K-MAL; lane 3: 4 equivalents mPEG2K-MAL; lane 4: 10 equivalents mPEG2K-MAL; lane 5: 20 equivalents mPEG2K-MAL; lane 6: 30 equivalents mPEG2K-MAL. The two black arrows indicate the band shift resulting from the conjugation.

click reaction. These results are shown in Figure 6-3b. In our bioconjugation strategy, we tested a series of bifunctional linkers that could react with the azido-modified sugars on the mAb and the C-terminal cysteine of our diblock polypeptides (see Figure 6-3c). Since dibenzoannulated cyclooctyne (DBCO) and BCN probes were successfully tested in antibody-drug conjugates, they were both evaluated for the reaction with the azido-modified sugar.[11,12] Furthermore, we evaluated the use of 3-arylpropionitriles (APN) instead of maleimide for cysteine coupling, given their increased selectivity and stability to hydrolysis in biological environments. [13]

Unfortunately, various initial attempts at bioconjugation of mAb and diblock polypeptide via the aforementioned bifunctional linkers were not successful. The reasons for the unsuccess are hard to pinpoint. Elastin-like polypeptides, named block *E* in our designs, have been extensively used in similar bioconjugation strategies with a wide range of payloads.[14–16] It is therefore reasonable to assume that the chemical composition of the *E* block

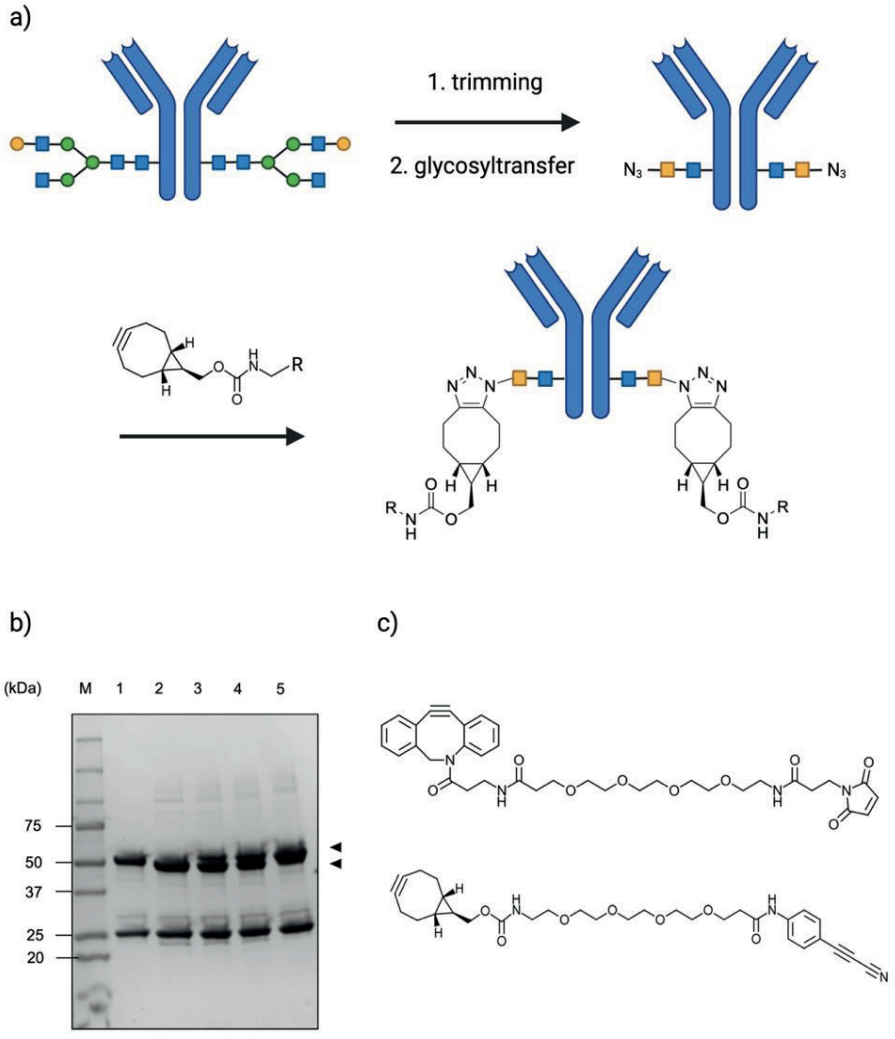

Figure 6-3. Bioconjugation of BCN-PEG2000 (BCN-PEG2K) polymer with remodeled mAb. **(a)** Schematic representation of glycan remodeling of trastuzumab: the native Ab is trimmed by an endoglycosidase; next, an azido-modified sugar is attached using a glycosyl transferase. The azido-modified Ab is then attached to the BCN-PEG2K polymer via click conjugation. **(b)** SDS-PAGE analysis in reducing conditions of BCN-PEG2K conjugated to azido-trastuzumab. Glycan remodeling was performed on trastuzumab with materials and protocol kindly provided by Synaffix (The Netherlands). The remodeled trastuzumab was then purified with protein A and incubated with 2, 5, and 20 molar

equivalents of BCN-PEG2K overnight at 4°C. Lane 1: native trastuzumab; lane 2: azido-trastuzumab; lane 3: 2 equivalents BCN-PEG2K; lane 4: 5 equivalents BCN-PEG2K; lane 5: 20 equivalents BCN-PEG2K. The two black arrows indicated the minor shift of the band corresponding to the heavy chain of trastuzumab between native and remodeled mAb. A small upward shift is visible after bioconjugation. **(c)** Chemical structure of the bifunctional linkers tested for the conjugation of our *B-E* diblock and azido-modified trastuzumab: DBCO-PEG4-maleimide (top, purchased from Creative Biolabs, USA) and BCN-PEG4-APN (bottom, purchased from Conju-Probe, USA).

and the size of the antibody conjugate should not be limiting factors for the conjugation efficiency. We can nonetheless recognize the solubility of the polypeptide-linker conjugate as a probable point of attention, especially during downstream processing. The preliminary results reported here show that further research might have yielded a successful outcome, particularly since positive results were achieved by our colleagues in this research project using the same reaction to couple ssDNA and mAbs.[17] In our case, progress was deemed too slow to justify further research efforts, and we instead focused our attention on improving the binding affinity of the polypeptide via multivalency (Chapter 4). We still believe that this strategy should be investigated, alongside other promising alternatives.

A second possible strategy for cargo attachment would involve the direct fusion of the peptides or proteins of interest via genetic engineering (Figure 6-1b). As amply described in Chapter 2, this strategy was successfully explored with cell-adhesion motifs, antimicrobial peptides, and enzymes used as payload for SBP "stickers". The same microbial production host (*Escherichia coli*) can be used, granting ease of manipulation, fast growth, and low costs. In the specific case of therapeutic immunoglobulin G (IgG) antibodies, bacterial cells lack the molecular machinery required for the glycosylation of the Fc region. However, especially for biosensing applications, bacteria could be utilized for the recombinant production of antigen-binding fragments, aglycosylated IgG variants, and non IgG antibody formats.[18] While engineering therapeutic mAbs requires substantial economic investments, our proposed solution would be cheaper, scalable, and applicable in smaller enterprises of low- and middle-income countries. However, it is worth mentioning that, unlike the previously described strategy, this method is restricted to peptides and proteins.

A third strategy for the immobilization of relevant biomolecules would entail the addition of protein-based fusion tags (Figure 6-1c). Unlike chemically

synthesized linkers, protein-based tags can be included in our polypeptide designs at the genetic level with no repercussions on protein production and purification. These tags could then be used for the selective conjugation of target biomolecules, either in bulk or on coated surfaces. For example, an increasingly popular tag system is the SpyCatcher/SpyTag system, in which a 13 amino acid peptide (SpyTag) spontaneously forms an irreversible isopeptide bond with its 15kDa partner (SpyCatcher).[19] This system has been successfully applied in the synthesis of antibody-enzyme complexes and in combination with elastin-like polypeptides, suggesting its compatibility with our protein designs.[20,21] A major shortcoming of this approach is the required engineering of both protein conjugates with either SpyTag or SpyCatcher, which would greatly hinder the use of commercially available mAbs. Fortunately, in our review in Chapter 2, we reported a system for the capture of IgGs based on the antibody-binding protein G. Proteins G, A, and L are bacterial proteins that can strongly and non-covalently bind the Fc region of antibodies and they are routinely used in affinity chromatographic purification techniques. These proteins could provide a universal tag for the bioconjugation of antibodies to our protein designs. Alternatively, shorter peptides derived from protein A, for example, could be used.[22,23] To summarize, the use of protein-based tags would introduce a second reaction step in our functionalization strategy while expanding the repertoire of polypeptides available for bioconjugation.

Finally, although our diblock *B-E* designs could be used as anchors, the results of Chapters 3 and 4 highlight that these designs underperform with regards to binding strength and antifouling properties. Our trimeric *B-M-E* design improved both these features, but it does not grant the same precise control over surface geometry. In fact, while the stoichiometry of a diblock-conjugate reaction is well-defined, each *B-M-E* design provides three possible reactive groups. Hence, the conjugation of a single cargo molecule to a *B-M-E* trimer is difficult. In this case, the use of reactive terminal amino acids or protein tags would nonetheless be a preferrable option in combination with longer *E* blocks that could provide sufficient spacing and reduce steric hindrance. We also believe that the improved stability and antifouling properties of the *B-M-E* design certainly outweigh the reduced control over payload conjugation.

6.4. The promise of scalability

The design, production, and purification of recombinant proteins is one of the fundamental aspects of biotechnology. Most biotechnological efforts, however, are focused on therapeutic compounds, with a clear bias in the destination of molecular tools, techniques, and funding. Therefore, the needs of materials science must be met within the boundaries of current biotechnological knowledge. The polypeptides introduced in the Chapters 3, 4, and 5 presented us with practical challenges that should be taken into consideration, both in the design of different polypeptides and in relation to future scalability.

A first point of attention revolves around the synthesis of long DNA fragments encoding repeated amino acid sequences. Although the redundancy of the genetic code grants a certain degree of exploitable flexibility (e.g., Codon Scrambler), this feature is directly at odds with the need to optimize the codon frequency for increased production yield.[24] Furthermore, the recognition of unique DNA sequences is a key aspect in most molecular biology tools (PCR, restriction enzymes, recombination-based assembly techniques). Fortunately, most hurdles can be effectively tackled thanks to advanced tools for cloning strategies *in silico* and molecular techniques tailored for tandem-repetitive amino acid sequences.[25] In addition, the synthetic manufacturing of DNA sequences has greatly improved in recent years. For these reasons, the synthesis, replacement, and cloning of new DNA fragments is not a limitation for the modularity of our *B-M-E* design. As proven by the preliminary results in Chapter 5, we can safely assume that our cloning strategy is compatible with the suggestions highlighted in the previous sections.

The recombinant production of synthetic proteins constitutes another important step with a significant impact on the scalability of the process. The scalability of a fermentation process is critical for successful large-scale, industrial implementations. Industrial scale-up is usually developed starting with small volumes in a laboratory setting, followed by the stepwise transferring to larger volumes in industrial bioreactors. The optimization of technical parameters such as mass transfer, oxygen transfer rate, reactor geometry, and agitation speed, is studied in bioprocess engineering, and is thus not in the scope of this thesis. It should nevertheless be remembered that the production of recombinant proteins with bacterial hosts is a highly successful and widely adopted strategy with almost 40 years of market

expertise.[26] For the sake of easy scalability, we adopted *E. coli* as our expression system.

Aside from the *E. coli* strain that we utilized in Chapters 3, 4, and 5, we could consider using different production hosts. For example, *E. coli* strains have been engineered to improve the secretion efficiency of overexpressed proteins and reduce misfolding and protease degradation.[27,28] The secretion of recombinant proteins could also positively influence the cytotoxic effect of our tandem designs described in Chapter 4. Alternatively, other *E. coli* strains have been mutated to create oxidative conditions in the cytoplasm, allowing for the formation of disulfide bonds required for protein folding.[29,30] Finally, eukaryotic expression systems such as yeasts (*Saccharomyces cerevisiae* and *Pichia pastoris*)[31,32] and plants (*Nicotiana benthamiana*)[33] would provide yet another cheap and attractive alternative with improved control on glycosylation.

In Chapters 3 and 4, all the described protein designs could be produced using *E. coli* as a host. Still, the ability to produce purifiable amounts of protein was not deemed as a sufficient prerequisite for production scale-up. For subsequent physical characterization, we focused on designs with a consistent protein yield. For both our *B-E* and *B-M-E* designs, we could achieve stable yields of 2-3 mg L^{-1} growth medium. The results of Chapter 4 highlight that the net charge of the expressed protein can increase cytotoxic effects with an obvious influence on the production yield. Our preliminary results from Chapter 5 indicate that the non-cytotoxic variant of our *B-M-E* design adapted for gold surfaces could be produced with yields of 8-10 mg L^{-1} growth medium. Luckily, the optimization of the fermentation process can attain higher and stable yields even for cytotoxic proteins via different *E. coli* strains and improved culture conditions.[26] Given the wealth of available biotechnological tools in this regard, we can assume that our protein designs are compatible with standardized industrial scale-up processes.

The scalability of protein production is linked to the effective surface area that can be coated by our polypeptide. During our Dynamic Light Scattering measurements in Chapter 4, non-porous silica particles could be stably coated with a concentration of *B-M-E* polypeptide in the µM scale (see Figure 4-6). A quick calculation reveals that the total surface area of the silica particles is $\approx 1.2 \cdot 10^{-3}$ m^2. Although full coverage was achieved at a protein concentration between 1 and 10 µM, we will assume for our calculations that a 10 µM concentration of *B-M-E* is needed to fully coat the area. If we assume

the optimization of the production can ultimately yield 1 g of polypeptide (10 mg L^{-1} yield, 100 L reactor), the amount would be sufficient to coat a silica surface of ≈ 24 m^2. We can therefore conclude that 1 g of our protein coating would be ideal for applications that do not require the functionalization of large surfaces, such as biosensing cartridges.

The purification of recombinant proteins from the bacterial cytoplasm is the last relevant step in our production strategy. Based on the necessary level of purity, protein purification generally relies on a series of chromatographic techniques applicable both at small and large scale.[26] In Chapter 3, proteins were purified via ion exchange chromatography, while we chose immobilized metal affinity chromatography (IMAC) for the purification in Chapters 4 and 5. Although ion exchange chromatography provides greater freedom in the optimization of its parameters, we opted for the addition of an IMAC-compatible poly-histidine tag to our designs instead of exploiting the positive charges on the silica-binding peptides. A poly-histidine tag allowed us to reliably streamline the purification process for different proteins without relying on the physical properties of solid-binding peptides. In this way, protein designs with different solid-binding peptides could be purified without altering the method used (Chapter 5). This design choice relies on the premise that the IMAC-tag does not negatively influence surface binding nor the functionality of the surface coating. In the case of our *B*-*M*-E designs for silica and gold surfaces, this premise was experimentally proved to be correct. Preventively, the addition of a cleavable peptide sequence could be considered, to enable the removal of the poly-histidine tag after product recovery.

The estimation of the costs of recombinantly produced proteins is heavily dependent on the intended final use. In general, proteins for industrial use (enzymes for food, cleaning products, and waste management) and proteins for pharmaceutical use (antibodies, hormones, and vaccines) have similar manufacturing techniques. Although the production and purity requirements are more stringent for pharmaceutical proteins, the costs of production do not account for the drastic difference in retail pricing. In fact, the difference in price is driven by clinical trials, research and development, patent constraints, marketing, liability, and return on investment to shareholders. Proteins for pharmaceutical use have a retail cost on the order of 10^7-10^9 US dollars per kg: since lengthy clinical trials are needed for commercialization, the time to recoup the initial investment under patent

protection is short.[34] On the contrary, proteins for industrial use have a retail cost on the order of 10 US dollars per kg.[34] It is therefore clear that our *B-M-E* triblock could provide cheap coating only for uses that do not require clinical trials such as *in vitro* biosensing systems. As a measure of comparison, the retail price range for a synthetic antifouling polymer such as PEG spans from 10 to 10^6 US dollars per kg for long polymer chains or additional reactive moieties.[35,36]

6.5. A hopeful outlook: new designs, new sources

The considerations laid out in sections 6.2-6.4 collect and organize most of the practical output that, by lack of space or relevance, we could not organically present in the previous chapters. We can now conclude that we have partially reached our goal and that further research may bridge the current gap. We have detailed the many possible ways forward, both in biosensing applications and, more broadly, for surface coatings. We will now focus our attention on the prospects of this technology in relation to the advancements in the field of materials science.

The number of architectures studied in this thesis is as limited as it is serendipitously sufficient to find successful designs. It is therefore desirable that other protein-based molecular architectures be explored for the self-assembly of coatings on solid surfaces. While we relied on multivalent display of solid-binding peptides via multimeric protein blocks, the use of different protein blocks can provide higher control over the assembly of uniform coatings. For example, the addition of crosslinking moieties (e.g., tyrosine) interspersed in the *E* block could enable the formation of highly stable and uniform antifouling coatings. Since elastin-like polypeptides present customizable physical properties and excellent biocompatibility, the rational manipulation of our *E* block can open new applications in tissue engineering and drug delivery.[37] Alternatively, the multimerization *M* block can be replaced or engineered for the self-assembly of larger structures. Given the exceptional wealth of protein nanomaterials capable of self-assembling in 1D and 2D structures, these strategies could be implemented in our *B-M-E* designs.[38]

The wealth of data on protein nanomaterials conceals two structural problems that are delaying the widespread application of such materials. Firstly, the absence of a database dedicated to protein nanomaterials is a major obstacle in the design of polypeptides based on previously characterized architectures or domains. In Chapter 2, we attempted to

describe an updated and comprehensive overview of the biomedical applications of solid-binding peptides, including amino acid sequences and tested applications. Although we hope to have provided a valuable tool for present and future material scientists, it is obvious that solid-binding peptides and biomedicine represent but a fraction of the multifaceted and intrinsically multidisciplinary field of protein design. Many databases are already collecting data about protein structures (Protein Data Bank) and sequence and functions (Expasy), while others focus on materials properties (SpringerMaterials).[39,40] The creation of a database dedicated to proteins as molecular building blocks would introduce a flexible toolbox in the rational design of functional nanomaterials.

The second challenge lies in current technological limitations. As this thesis amply demonstrates, the interaction between functional building blocks is hard to predict in terms of production, purification, yield, folding, stability, and overall functionality of the resulting polypeptide. The lack of reliable predictive tools for the abovementioned factors results in a "trial and error" approach to protein design rather than a rational one. In the short term, increasing the number of tested designs is the most logical option. As testified by the success of the biotech company Ginkgo Bioworks, automation of cell programming accompanied by high-throughput genome engineering will allow the screening of an increasing number of protein designs in shorter times. Concurrently, the improvements in computational power and neural networks will contribute to the development of reliable software for the *in silico* screening of new protein materials.

In conclusion, the increasing role of biotechnology in materials science will provide valuable tools for the synthesis of innovative protein nanomaterials for the biofunctionalization of solid surfaces. We hope that the findings of this thesis represent one of the many incremental steps towards reaching that goal.

6.6. List of abbreviations

Abbreviation	Meaning
APN	3-arylpropionitriles
BCN	bicyclononyne
BCN-PEG2K	bicyclononyne-PEG2000
DBCO	dibenzoannulated cyclooctyne
IgG	immunoglobulin G
IMAC	immobilized metal affinity chromatography
mAb	monoclonal antibody
mPEG2K	methoxy-PEG2000
mPEG2K-MAL	methoxy-PEG2000-maleimide
PCR	polymerase chain reaction
PEG	poly(ethylene glycol)
SDS-PAGE	sodium dodecyl sulfate-polyacrylamide gel electrophoresis
ssDNA	single strand DNA
TCEP	tris(2-carboxyethyl)phosphine

6.7. Reference list

[1] S. Banskota, P. Yousefpour, N. Kirmani, X. Li, A. Chilkoti. Long circulating genetically encoded intrinsically disordered zwitterionic polypeptides for drug delivery. *Biomaterials* 192, 475–485 (2019).

[2] T. van Emmerik, A. Schwarz. Plastic debris in rivers. *Wiley Interdisciplinary Reviews: Water* 7, 1–24 (2020).

[3] C. T. J. Roebroek, S. Harrigan, T. H. M. Van Emmerik *et al.* Plastic in global rivers: Are floods making it worse? *Environmental Research Letters* 16, (2021).

[4] W. C. Li, H. F. Tse, L. Fok. Plastic waste in the marine environment: A review of sources, occurrence and effects. *Science of the Total Environment* 566–567, 333–349 (2016).

[5] B. Freeland, E. McCarthy, R. Balakrishnan *et al.* A Review of Polylactic Acid as a Replacement Material for Single-Use Laboratory Components. *Materials* 15, (2022).

[6] J. Sabaté del Río, O. Y. F. Henry, P. Jolly, D. E. Ingber. An antifouling coating that enables affinity-based electrochemical biosensing in complex biological fluids. *Nature Nanotechnology* 14, 1143–1149 (2019).

[7] J. M. Chalker, G. J. L. Bernardes, Y. A. Lin, B. G. Davis. Chemical modification of proteins at cysteine: Opportunities in chemistry and biology. *Chemistry - An Asian Journal* 4, 630–640 (2009).

[8] A. Hosseinnejad, T. Fischer, P. Jain *et al.* Enzyme mimetic microgel coating for endogenous nitric oxide mediated inhibition of platelet activation. *Journal of Colloid and Interface Science* 601, 604–616 (2021).

[9] P. Winnersbach, A. Hosseinnejad, T. Breuer *et al.* Endogenous Nitric Oxide-Releasing Microgel Coating Prevents Clot Formation on Oxygenator Fibers Exposed to In Vitro Blood Flow. *Membranes* 12, (2022).

[10] Y. Jung, J. Y. Jeong, B. H. Chung. Recent advances in immobilization methods of antibodies on solid supports. *Analyst* 133, 697–701 (2008).

[11] R. Van Geel, M. A. Wijdeven, R. Heesbeen *et al.* Chemoenzymatic Conjugation of Toxic Payloads to the Globally Conserved N-Glycan of Native mAbs Provides Homogeneous and Highly Efficacious Antibody-Drug Conjugates. *Bioconjugate Chemistry* 26, 2233–2242 (2015).

[12] J. M. M. Verkade, M. A. Wijdeven, R. van Geel *et al.* A polar sulfamide spacer significantly enhances the manufacturability, stability, and therapeutic index of antibody–drug conjugates. *Antibodies* 7, 7–9 (2018).

[13] O. Koniev, G. Leriche, M. Nothisen *et al.* Selective irreversible chemical tagging of cysteine with 3-arylpropiolonitriles. *Bioconjugate Chemistry* 25, 202–206 (2014).

[14] J. M. Malho, J. Brand, G. Pecastaings *et al.* Multifunctional Stimuli-Responsive Cellulose Nanocrystals via Dual Surface Modification with Genetically Engineered Elastin-Like Polypeptides and Poly(acrylic acid). *ACS Macro Letters* 7, 646–650 (2018).

[15] J. F. Nawroth, J. R. McDaniel, A. Chilkoti, R. Jordan, R. Luxenhofer. Maleimide-Functionalized Poly(2-Oxazoline)s and Their Conjugation to Elastin-Like Polypeptides. *Macromolecular Bioscience* 16, 322–333 (2016).

[16] M. R. Dreher, D. Raucher, N. Balu *et al.* Evaluation of an elastin-like polypeptide-doxorubicin conjugate for cancer therapy. *Journal of Controlled Release* 91, 31–43 (2003).

[17] Y.-T. Lin. Biofunctionalization strategies for continuous monitoring biosensors. *Eindhoven University of Technology* (2022).

[18] Y. J. Lee, K. J. Jeong. Challenges to production of antibodies in bacteria and yeast. *Journal of Bioscience and Bioengineering* 120, 483–490 (2015).

[19] B. Zakeri, J. O. Fierer, E. Celik *et al.* Peptide tag forming a rapid covalent bond to a protein, through engineering a bacterial adhesin. *Proceedings of the National Academy of Sciences of the United States of America* 109, (2012).

[20] A. R. Swartz, W. Chen. SpyTag/SpyCatcher Functionalization of E2 Nanocages with Stimuli-Responsive Z-ELP Affinity Domains for Tunable Monoclonal Antibody Binding and Precipitation Properties. *Bioconjugate Chemistry* 29, 3113–3120 (2018).

[21] H. Kimura, R. Asano, N. Tsukamoto, W. Tsugawa, K. Sode. Convenient and Universal Fabrication Method for Antibody-Enzyme Complexes as Sensing Elements Using the SpyCatcher/SpyTag System. *Analytical Chemistry* 90, 14500–14506 (2018).

[22] B. Madan, G. Chaudhary, S. M. Cramer, W. Chen. ELP-z and ELP-zz capturing scaffolds for the purification of immunoglobulins by affinity precipitation. *Journal of Biotechnology* 163, 10–16 (2013).

[23] A. R. Swartz, Q. Sun, W. Chen. Ligand-Induced Cross-Linking of Z-Elastin-like Polypeptide-Functionalized E2 Protein Nanoparticles for Enhanced Affinity Precipitation of Antibodies. *Biomacromolecules* 18, 1654–1659 (2017).

[24] N. C. Tang, A. Chilkoti. Combinatorial codon scrambling enables scalable gene synthesis and amplification of repetitive proteins. *Nature Materials* 15, 419–424 (2016).

[25] J. R. McDaniel, J. A. MacKay, F. G. Quiroz, A. Chilkoti. Recursive directional ligation by plasmid reconstruction allows rapid and seamless cloning of oligomeric genes. *Biomacromolecules* 11, 944–952 (2010).

[26] N. K. Tripathi. Production and purification of recombinant proteins from Escherichia coli. *ChemBioEng Reviews* 3, 116–133 (2016).

[27] B. L. Nannenga, F. Baneyx. Reprogramming chaperone pathways to improve membrane protein expression in Escherichia coli. *Protein Science* 20, 1411–1420 (2011).

[28] H. Sonoda, Y. Kumada, T. Katsuda, H. Yamaji. Effects of cytoplasmic and periplasmic chaperones on secretory production of single-chain Fv antibody in Escherichia coli. *Journal of Bioscience and Bioengineering* 111, 465–470 (2011).

[29] H. Sonoda, Y. Kumada, T. Katsuda, H. Yamaji. Functional expression of single-chain Fv antibody in the cytoplasm of Escherichia coli by thioredoxin fusion and co-expression of molecular chaperones. *Protein Expression and Purification* 70, 248–253 (2010).

[30] R. Levy, R. Weiss, G. Chen, B. L. Iverson, G. Georgiou. Production of correctly folded fab antibody fragment in the cytoplasm of Escherichia coli trxB gor mutants via the coexpression of molecular chaperones. *Protein Expression and Purification* 23, 338–347 (2001).

[31] G. WANG, M. HUANG, J. NIELSEN. Exploring the potential of Saccharomyces cerevisiae for biopharmaceutical protein production. *Current Opinion in Biotechnology* 48, 77–84 (2017).

[32] M. KARBALAEI, S. A. REZAEE, H. FARSIANI. Pichia pastoris: A highly successful expression system for optimal synthesis of heterologous proteins. *Journal of Cellular Physiology* 235, 5867–5881 (2020).

[33] J. BALLY, H. JUNG, C. MORTIMER *ET AL.* The rise and rise of nicotiana benthamiana: A plant for all reasons. *Annual Review of Phytopathology* 56, 405–426 (2018).

[34] J. PUETZ, F. M. WURM. Recombinant Proteins for Industrial versus Pharmaceutical Purposes: A Review of Process and Pricing. *Processes* 7, 476 (2019).

[35] Sigma Aldrich. https://www.sigmaaldrich.com/NL/en/product/sigma/81255 (2022).

[36] NanoSoft Polymers. https://www.nanosoftpolymers.com/product-category/functional-pegs/ (2022).

[37] A. K. VARANKO, J. C. SU, A. CHILKOTI. Elastin-Like Polypeptides for Biomedical Applications. *Annual Review of Biomedical Engineering* 22, 343–369 (2020).

[38] R. ZENG, C. LV, C. WANG, G. ZHAO. Bionanomaterials based on protein self-assembly: Design and applications in biotechnology. *Biotechnology Advances* 52, 107835 (2021).

[39] S. K. BURLEY, C. BHIKADIYA, C. BI *ET AL.* RCSB Protein Data Bank: Powerful new tools for exploring 3D structures of biological macromolecules for basic and applied research and education in fundamental biology, biomedicine, biotechnology, bioengineering and energy sciences. *Nucleic Acids Research* 49, D437–D451 (2021).

[40] S. DUVAUD, C. GABELLA, F. LISACEK *ET AL.* Expasy, the Swiss Bioinformatics Resource Portal, as designed by its users. *Nucleic Acids Research* 49, W216–W227 (2021).

THE MAIN BLOB, ALSO KNOWN AS STICKER, IS BORN FROM A E-COWLI FARM IN THE PLAIN REGION OF THE STICKYVERSE.

IT STEALS FROM SURROUNDING FAUNA AND FLORA TO BUILD ITS BODY UNTILL IT REACHES MAXIMUM STICKINESS.

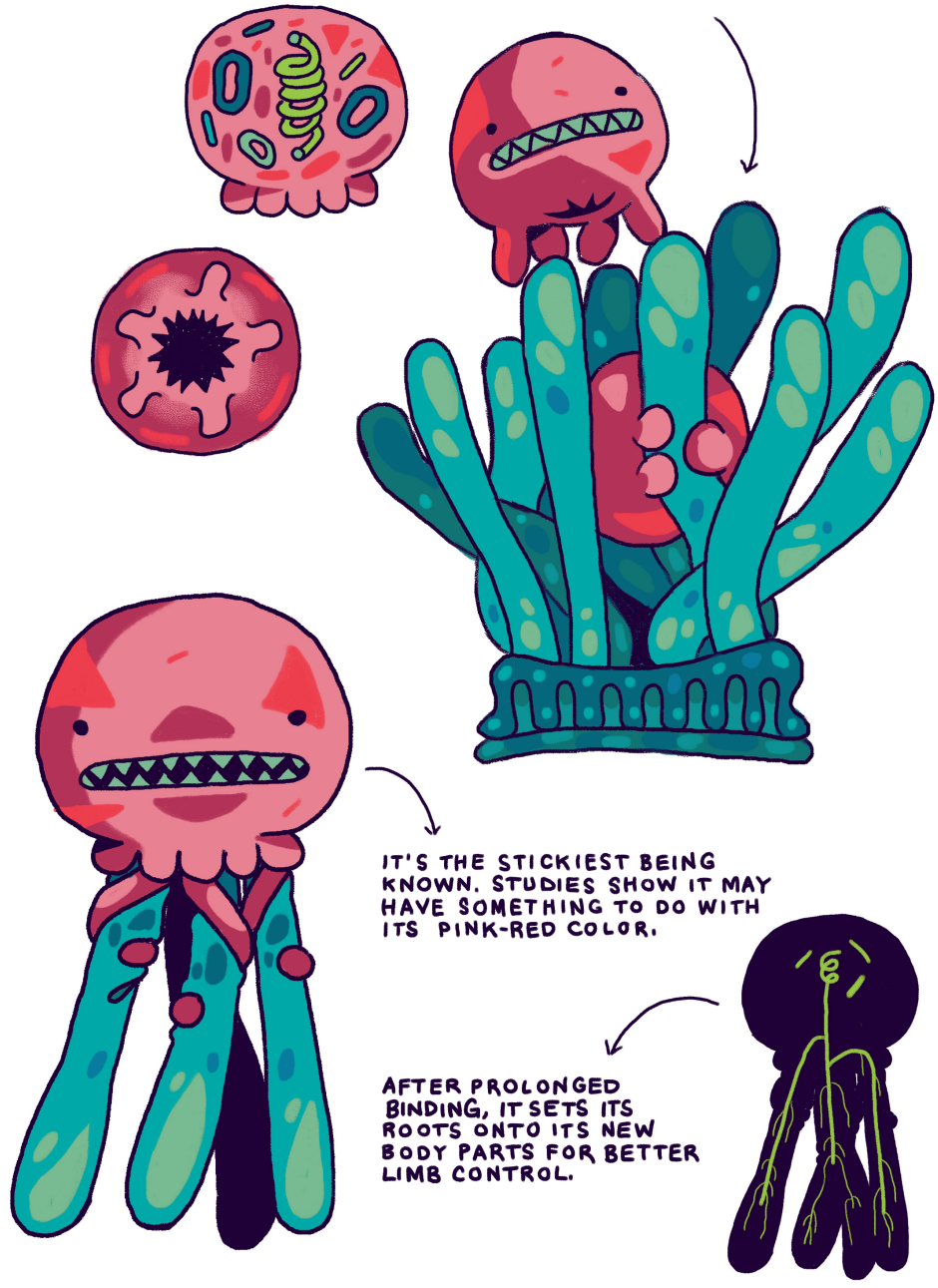

IT'S THE STICKIEST BEING KNOWN. STUDIES SHOW IT MAY HAVE SOMETHING TO DO WITH ITS PINK-RED COLOR.

AFTER PROLONGED BINDING, IT SETS ITS ROOTS ONTO ITS NEW BODY PARTS FOR BETTER LIMB CONTROL.

Summary

A biomaterial, in its broadest definition, is any synthetic, nonviable material intended to interact with biological systems. Although rudimentary biomaterials have existed for centuries as replacements for damaged tissues, scientists and engineers have only recently unravelled the molecular requirements for novel biomaterials. In particular, it has become clear that the interface between solid materials and biological systems plays a fundamental role in the design of information-rich and dynamic materials. The functionalization of solid surfaces allows for the creation of biomaterials that can actively participate and improve the interplay with living components, drastically expanding the possible applications from implants to diagnostic and therapeutic tools. As we detail in **Chapter 1**, however, the modification of solid surfaces with biocompatible functionalities presents two challenges: the coating must resist unwanted adsorption of proteins and cells (biofouling), while maintaining its structural integrity and desired functions. To overcome these challenges, we explore the potential of polypeptide-based coatings as molecular tools for the design of novel biomaterial surfaces, focusing on biosensing applications.

The synthesis of a protein-based coating relies on the use of functional polypeptide blocks. In our designs, we want to make use of solid-binding peptides as anchors for the non-covalent adsorption of our protein coating. Solid-binding peptides have been successfully applied in materials science in the past decades, as evidenced by the multiple examples in the use of solid-binding peptides for biomedical applications. In **Chapter 2**, we first describe how solid-binding peptides are developed and how they bind to solid surfaces. We then analyze a selection of successfully implemented molecular architectures for the functionalization of both naturally occurring (calcium phosphate, silicates, and ice crystals) and synthetic surfaces (metals, plastics, and graphene). Although the use of solid-binding peptides still presents practical constraints, we conclude the chapter with an outlook on possible advancements and new applications.

In **Chapter 3**, we assess in detail the silica binding ability of a series of solid-binding peptides. We then explore the recombinant production of simple polypeptide diblocks named *B*-*E*, where the *B* block is a series of silica-binding peptides, and the *E* block is a hydrophilic elastin-like polypeptide. We show that the microbial production platform *Escherichia coli* can be used for the recombinant production of the designed protein diblocks. We focus on one

B-E diblock and demonstrate that it can form dense polymer brushes on silica surfaces and stabilize silica nanoparticles. With a quartz crystal microbalance, we show that the polypeptide brush can withstand prolonged rinsing, but that high ionic strength buffers quickly displace the protein diblocks. Finally, we show that the *B-E* diblock prevents non-specific interactions between functionalized particles and polypeptide-coated glass slides.

The concept of multivalent binding for the physical attachment of self-assembling polypeptide brushes is explored in **Chapter 4**. To increase the resistance to displacement in a wider range of solvent conditions, we evaluate the introduction of multiple silica-binding *B* blocks both as tandem repeats and in star-like architectures via an oligomerizing domain *M*. We find that a trimer-forming *M* domain satisfies our production and purification requisites, while tandem repeats show cytotoxic effects in *E. coli*. We then proceed with the characterization of the trimer-forming triblock polypeptide *B-M-E*. We show that this protein can self-assemble in stable and homogenous coatings both on flat silica surfaces and on silica nanoparticles. Finally, we demonstrate the improved salt resistance and antifouling properties of the resulting polypeptide brush via QCM.

In **Chapter 5**, we expand our work on the silica-binding *B-M-E* polypeptide by testing the modularity of the design for the functionalization of gold surfaces. Thanks to recombinant DNA technology, we engineer new *B-M-E* polypeptides featuring a gold-binding peptide as *B* block and a zwitterionic, antifouling *E* block. We find that both polypeptides can be produced and purified similarly to our previous silica-binding *B-M-E* design. A preliminary characterization of the triblock reveals that both polypeptides can stably coat gold surfaces while maintaining excellent antifouling properties in the tested setting.

This thesis concludes with a general discussion in **Chapter 6**, where we present an overview of the findings of this work, including preliminary results on a click chemistry-based bioconjugation strategy that were not included in the previous chapters. We first evaluate the potential of our multifunctional and modular design as antifoulant agent, suggesting further improvements. We then discuss our strategy for the bioconjugation of antibodies to diblock polypeptides, with a focus on alternative recombinant methods for future applications. Successively, we highlight the features of our production strategy that can warrant the possible scalability of the process. We conclude by giving a broader overview on the role of biotechnology in materials science.

HAIR BALLS MAKE UP 70% OF THE STICKYVERSE'S ORGANIC MATERIAL. SOME HAIRBALLS STICK TO EACHOTHERS CREATING SENTIENT MASSES OF FUR.

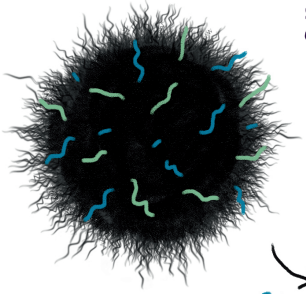

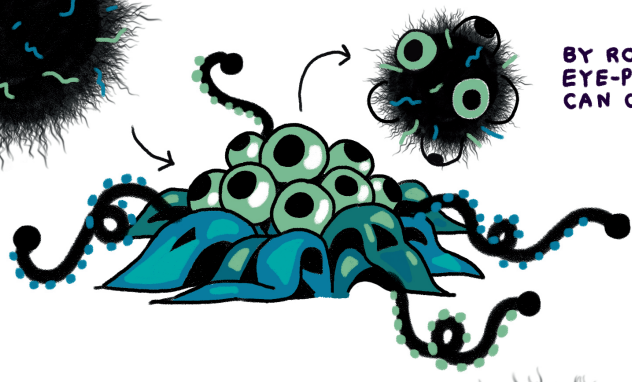

BY ROLLING ON AN EYE-PLANT THEY CAN OBTAIN SIGHT.

THEY CAN GROW UP TO BE COLLOSSAL TENTACLED HAIRBALLS ALMOST 10 METERS IN HEIGHT.

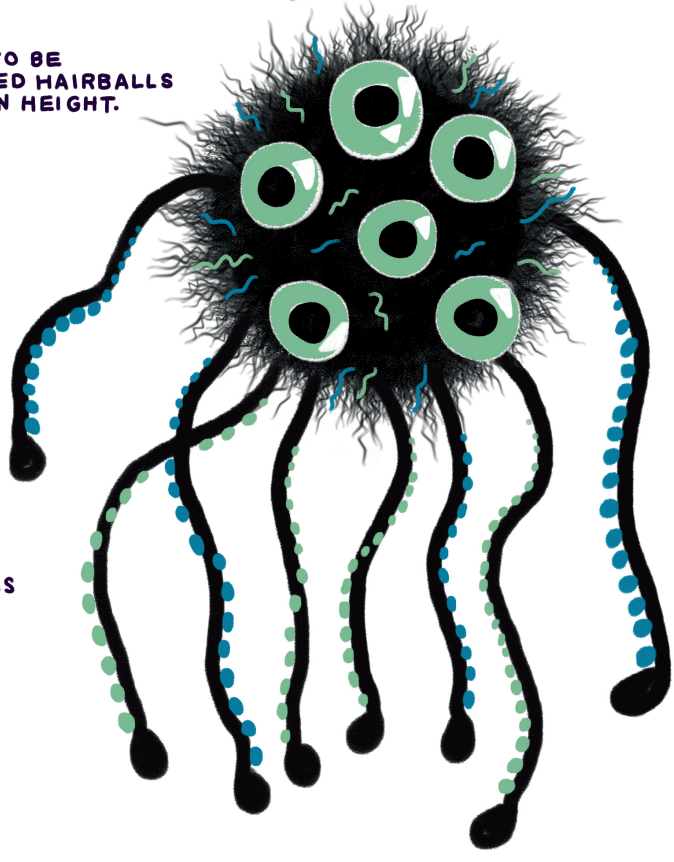

THANKFULLY, THE COLOSSAL HAIR BALLS ARE FILTER FEEDERS AND ONLY EAT THE MICRO-PARTICLES THAT GET STUCK IN THEIR HAIR.

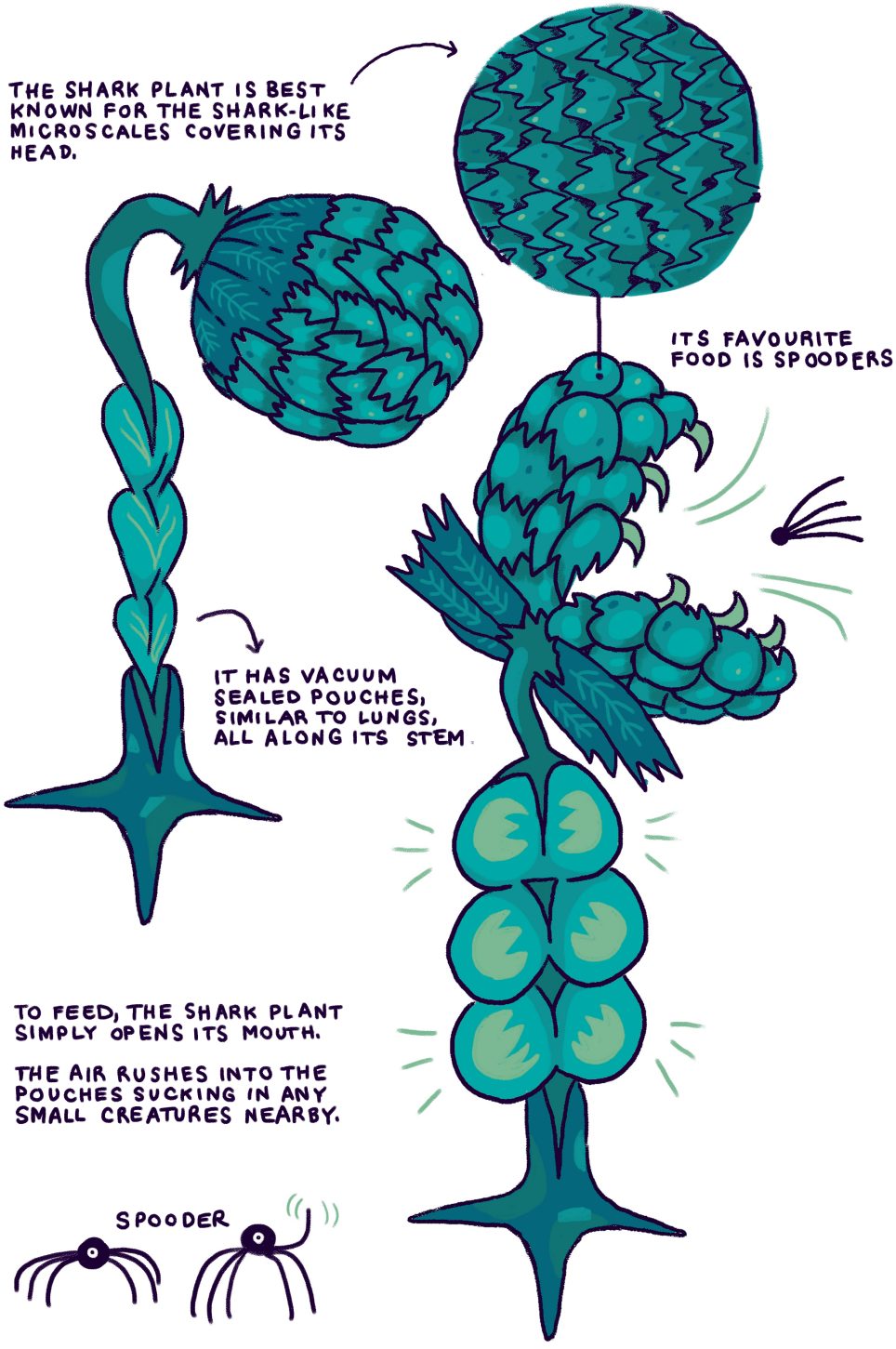
THE SHARK PLANT IS BEST KNOWN FOR THE SHARK-LIKE MICROSCALES COVERING ITS HEAD.
ITS FAVOURITE FOOD IS SPOODERS
IT HAS VACUUM SEALED POUCHES, SIMILAR TO LUNGS, ALL ALONG ITS STEM
TO FEED, THE SHARK PLANT SIMPLY OPENS ITS MOUTH.
THE AIR RUSHES INTO THE POUCHES SUCKING IN ANY SMALL CREATURES NEARBY.
SPOODER

List of Publications

This thesis

- Nicolò Alvisi & Renko de Vries, Biomedical Applications of Solid-Binding Peptides and Proteins, (*submitted*) **2022**. **(Chapter 2)**;
- Nicolò Alvisi[†], Fabiola A. Gutiérrez-Mejía[†], Meike Lokker, Yu-Ting Lin, Arthur M. de Jong, Floris van Delft, Renko de Vries; Self-Assembly of Elastin-like Polypeptide Brushes on Silica Surfaces and Nanoparticles, in *Biomacromolecules* **2021** *22 (5)*, 1966-1979. **(Chapter 3)**;
- Nicolò Alvisi, Chuanbao Zheng, Meike Lokker, Victor Boekestein, Robbert de Haas, Bauke Albada, Renko de Vries; Design of Polypeptides Self-Assembling into Antifouling Coatings: Exploiting Multivalency, in *Biomacromolecules* **2022** *23 (9)*, 3507–3516. **(Chapter 4)**.

[†] = shared first authorship

Other work

- Nicolò Alvisi, Kim van Noort, Sarlita Dwiani, Nathan Geschiere, Octavina Sukarta, Koen Varossieau, Dieu-Linh Nguyen, Richard Strasser, Cornelis H. Hokke, Arjen Schots and Ruud H. P. Wilbers; β-Hexosaminidases Along the Secretory Pathway of *Nicotiana benthamiana* Have Distinct Specificities Toward Engineered Helminth N-Glycans on Recombinant Glycoproteins, in *Frontiers in Plant Science* **2021** 12:638454

THE LAMPLANT IS ONE OF THE FEW ORGANIC LIGHT SOURCES IN THE STICKYVERSE.

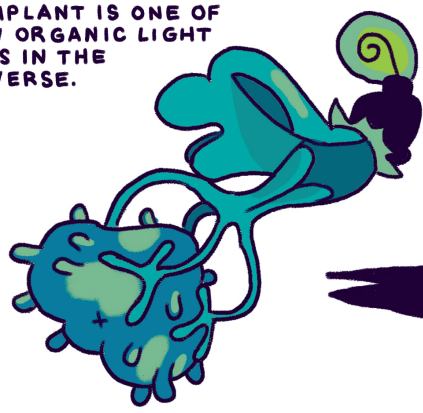

IT LIKES REARRANGING THE LANDSCAPE BY FLYING AROUND CARRYING ROCKS, BLOBS AND HAIRBALLS.

IT GROWS IN DARK CAVES, HANGING UPSIDE-DOWN. IT SLOWLY OPENS, MUCH LIKE A FLOWER, UNTIL IT REACHES MATURITY.

THE FLAPS ARE MADE OF THE SAME MATERIAL AS BUTTERFLY WINGS.

THE FEET RESEMBLE THOSE OF A GECKO AND GET COMMONLY STOLEN BY MAIN BLOBS AND SPOODER FRUITS DUE TO THEIR TOP-NOTCH STICKINESS.

Acknowledgements

"Please, be kind. Especially when we don't know what's going on"
These are the words that Waymond Wang tenderly delivers to his wife Evelyn Wang in one of the most heartfelt scenes of the movie *"Everything everywhere all at once".* Although simple, those words are meaningful. Being kind when facing unknown and challenging situations, being kind regardless of our preconceptions, being kind without having any clue what the result will be. These words resonate for the power of their simplicity. I am writing these words for both of us, dear reader, to remind us that kindness is a responsibility.

In the past seven years, I have met and said goodbye to countless people. During the five years in pursuit of a PhD, I was confronted even more strongly with the reality of working in a liminal space: the luck of meeting wonderful and engaging people was relentlessly counterbalanced by the letdown of having to, sooner or later, watch them leave. My first and possibly unheard words of gratitude are to all of you who made this liminal space feel more like a living room. Looking back at the years spent in Wageningen, I will always be grateful for having had the opportunity of meeting all of you, and I hope you will treasure those memories as jealously as I will.

The past five years, and the pages you're now reading, would not have been possible without the trust that Renko, my daily supervisor, placed in me a long time ago. It was a leap of faith, for both of us. I am grateful for the support you gave me and for your unshakeable belief that this booklet would see the light of day. I would also like to thank my co-supervisors from ORC Bauke and Floris, who endured my talks about bacteria and tried to teach me how to think like an organic chemist. Thank you also to Jasper for making my work at PCC possible.

A huge thank you also to our collaborators Yu-Ting Lin and Arthur de Jong from the Eindhoven University of Technology for their work featured in Chapter 3.

An immense thank you to Alexandra Elbakyan, the creator of Sci-Hub, for making scientific knowledge accessible to everyone, everywhere, free of charge. The second chapter of this thesis would have been impossible to write without your help! An equally immense acknowledgement of unforgivable uselessness goes to Elsevier, for actively trying to stop Alexandra Elbakyan in the name of greed.

Luckily, the opposite of greed was shown to me every day by Mara and Leonie. Thanks to both of you for always being available, kind, and helpful. Mara, although I was sad to see you leave PCC, it's great to see that your path continues toward even more happiness and fulfillment.

When I started five years ago, PCC looked very different. I was placed in my first office simply because that's where all the other Italians were (thanks Mara) and it turned out to be a great decision. You guys made me feel welcome from the very first day. Slav, thanks for being always cheerful and supportive, but most importantly for bullying Aljosha. Aljosha, I cherished our conversations and the dinners together, you're a great scientist and artist; thank you for challenging my beliefs and I wish you all the happiness a Russian is allowed to feel. Simone, what an inspiration you are; I miss the *"Baglioni?"* resonating at 5 PM sharp in the office. I wish all the best to you, your wife Jessi and your son Federico. Marco, my first office and house mate! The time spent with you was a blast and I will forever hold dear all your stories, the jokes, the evenings spent together, the talks about movies and comics, the dinners. Thank you for inviting me at your wedding, and I wish you and Letizia a bright and happy future.

As the years went by, Marco and Simone left the office. Before the empty space was occupied by a pandemic, I had the luck of briefly sharing the office with Chandan and Larry. Thanks to both of you! A special thanks to Larry, who devoted his precious free time to the editing and proof-reading of this manuscript. If you spot any tyopos, you can blame him. Thanks also for being an all-around great dude, really.

In the search for an office closer to my lab, I stranded in my second office one floor below. Thank you, guys, for making the second half of my PhD as great as the first half. Vahid, sorry for kicking you out of the office and keeping your plant barely alive, as we all know it was Martijn's fault; as next in line at PCC to defend your PhD thesis, I wish you all the luck, and see you on the other side. Martijn, you're a horrible human being but I still like you; I'm happy to see that you found your infectious passion for science again, and I wish you all the best for your career. Rob, signore del prosciutto, cinque di maggio, thank you for agreeing to be my paranymph and for being a great inspiration in the past years. This thesis would have been half as long and twice as hard without your help, so a huge thank you for your contributions. Also, setting up a lab from scratch and moving cabinets around was lots of fun. Finally, Riccardo, my second office and house mate! Thank you as well for agreeing

to be my paranymph. Since you moved in to replace Marco right before the pandemic, I enjoyed you more as a housemate than as an officemate, and I could have never wished for a better quarantine buddy. Your attitude towards life is an inspiration, and I wish you all the best in Rome!

Aside from great office mates, I was also blessed with great colleagues. I want to first thank all the members, past and present, of the Biopolymer Materials group, for their help during our meetings and their constructive feedback. I would like to thank a few members in particular. Lione, thank you for being my fairy god mother and teaching me the ins and outs of protein purification, but also for the great trip to Mexico together with Dana, who I thank for her support, kindness, and for always being available for a chat. Fabiola, your work for our publication was fantastic and it was great having you as my "boss", thanks to you and your husband Victor for inviting me to your wedding and giving me an excuse to visit Yucatán, but also thank you for being a big nerd. Huy, signore, you too are an absolute inspiration, I miss your positive spirit and incredible love for falafel, thank you for your kindness and I truly hope that our paths can cross again in the future. Chuanbao, my hero, an immense thank you for your great work, two chapters of this thesis exist only thanks to you, thank you also for all the delicious food you prepared and your incredible gifts, you're an amazing guy and I wish you all the best with your PhD.

Obviously, PCC was not a great working place only because of the people I thanked above! I want to thank Akankshya, Ketan, Ellard, Sophie, Zohreh, Richard, Ralph, Leonardo, Julian, Kasper, Chang, Maarten, Senna, and Nirzar for making the working days less boring, in the labs, in the corridors or while teaching the practicals. I also want to thank all the amazing colleagues who made the PCC o' yore such a welcoming and fun place to work at: Ruben, Sven, Niek, Raisa, Jessica, Qimeng, Justin, Jochem, Riahna, I wish you all the best, wherever you are now and whatever your plans are. A special thanks also to all the people of the staff that I bothered at some point with questions, maybe about DLS (thanks Remco and Tom!) or about the consumables (thanks Diane and Raoul!). A final thanks to René, Lennart, Bart, Dirk, and Peter, the teaching staff of PCC: thanks for allowing me to cultivate my newly found passion and giving me the opportunity to work as teacher. I am blessed to be working with such passionate and enlightened educators.

Thanks to my two lovely students Meike and Victor. I hope I was as good a supervisor as you deserved. Your names featured in our publications testify

better than anything else that you did a great job. I also want to thank all the other students who worked at the Biopolymer Materials group for making the lab hilariously chaotic and all the other students at PCC for making coffee breaks chaotically hilarious.

Thank you to Irene Shajan from ORC for always being helpful in my bioconjugation endeavors. A collective thanks to all the people at the Laboratory of Biochemistry for kindly having me as a guest in their lab during my first year.

A huge thank you to my new colleagues in Team-1 Marijn, Karolina, Minke, Bart, and Mattia. You are the loveliest bunch of people I have met in a long time and I honestly do not know what kind of lottery I won to have you all as colleagues. Although we worked together only for one year, I enjoyed every moment of our tiring, tiring job. Thanks for all your support, your understanding, and kind words.

A special thanks to Ruud Wilbers; although our plans didn't go as expected, I owe you more than you can imagine.

Thank you to The Silent Scalpel for their amazing job with the copyediting of this manuscript.

A final, oversized, and colorized thank you to Louseen Smith for designing all the fantastic art that adorns this booklet. Working with you was a light of hope in the desperate days spent frantically writing this thesis! I had an immeasurable amount of fun and I hope you did too, you turned this rag into a fancy dress and it's so pretty I never want to look away!

Aside from the huge professional debt that I futilely tried to acknowledge in the previous part, I owe a great deal also to many people outside of the campus in Wageningen. Starting with Eleni, Raul, and Jaap-Jan, the people who, just like me, were adopted by this sleepy town seven years ago. We started this journey together and, although we all took different paths, we are still walking in the same direction. There are too many memories to put on paper and I definitely do not know the right words to express what an honor it is to know such brilliant and kind-hearted people. I know you will all be great and do great, thank you for being my friends.

Thanks to my friend Ben, even though you live on the wrong side of the Channel. The times spent with you are the ones I treasure most dearly; you are truly an inspiration and a person I'm proud to call friend. To more times with Bugles and Malteser's, you absolute wa*ker.

A huge *grazie* to all the wonderful Italians who made Wageningen feel closer to the Mediterranean Sea: Fabian, Camilla, Francio, Enrico, Stefano, Lavinia, Giulia, Erika, Nicola, Clementina and all the guests of *la Casa del Popolo*, siete meravigliosi.

Thanks to Henry, for being the eclectic and moderately pessimist spice to my routine. It is only thanks to you that I could realize one of my lifelong dreams and eat a slice of Sachertorte in Vienna.

Thanks to Louise, you've been a great housemate and I truly enjoyed our walks and talks. I have not forgotten that you still need to cook me pasta.

I also want to thank the staff at Heerenstraat Theater in Wageningen, for being the attentive hosts of one of the coziest cinemas I have ever visited. Your movies have kept me sane in the past years, I owe you all a lot.

Sono passati ormai sette anni dalla mia partenza. In questi anni, tante sono le persone che ho perso di vista mentre cercavo di costruirmi un angolo di casa qui, in Olanda. Lorenzo e Lorenzo, grazie per tutti i momenti passati assieme, anche se ormai le nostre strade si sono separate molto tempo fa. Vi auguro il meglio per il vostro futuro.

Alberto, sei l'amico che conosco da più tempo, migliore amico dal primo giorno di prima elementare. Sono molto orgoglioso dei traguardi che hai superato. Mi manchi molto.

Un grazie alla mia famiglia, a cui questo libro è interamente dedicato. So che non ne capirete molto, ma se posso scrivere queste righe è solamente grazie a voi. Vi sono eternamente grato per l'amore e la premura con cui mi avete cresciuto e per l'infinito ed indiscutibile supporto con cui mi avete permesso di compiere questo viaggio. Un grazie alle mie nonne Bruna ed Elena, per avermi insegnato tutto. Grazie ai miei zii Valter e Patrizio e alle mie zie Maura e Patrizia, per l'affetto e la gentilezza di chi dona senza mai voler nulla in cambio. Grazie ai miei cugini Leonardo, Matteo e Davide. Un grazie al babbo, che fin da piccolo ha nutrito la mia curiosità, e a Roberta, per il suo supporto. Un grazie a mia mamma, che oggi sarebbe orgogliosa. Un grazie a mia sorella Alice, ti voglio bene.

Finally, the biggest thank you goes to Violet. You know better than I that without you this booklet wouldn't even exist. Thank you for your endless emotional support. Wherever we end up, may there always be laughter, spirit, and love.

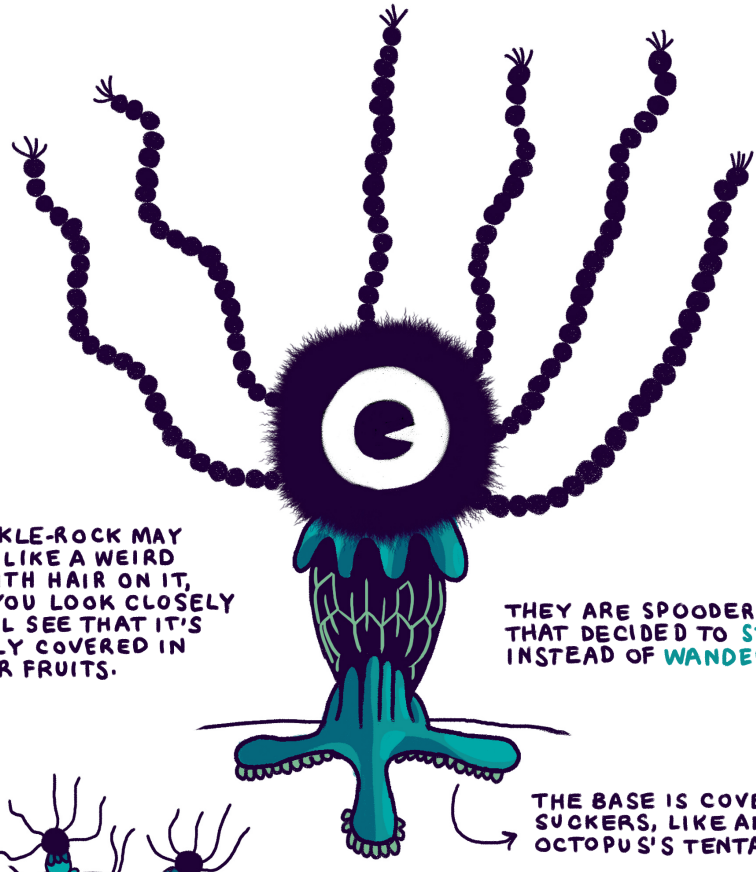

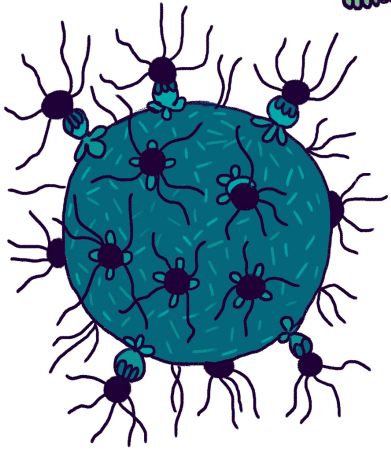

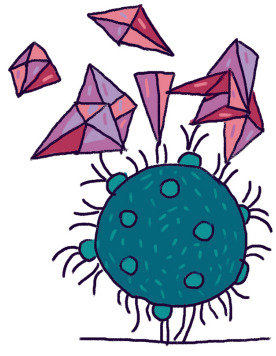

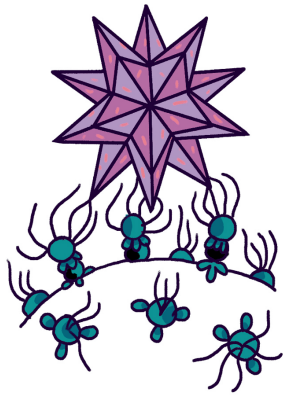

THEY CAN BE FOUND TRYING TO CATCH CRYSTALS FOR FUN OR JUST FLOATING ABOUT PEACEFULLY.

About the author

Nicolò Alvisi was born on 22nd June 1993 in Bologna, Italy. He grew up in the small town of Budrio, the birthplace of the modern classical ocarina. He obtained a double high school diploma/French baccalauréat, with a specialization in languages, in July 2012 from the Liceo Ginnasio Statale "L. Galvani" in Bologna.

While his love for the French language inexplicably faded, Nicolò found a growing interest in the scientific subjects. He went on to study Biotechnology at the Alma Mater Studiorum - University of Bologna (Italy). During his bachelor thesis, he worked under the supervision of prof. Dondini at the department of Agricultural Sciences. He obtained his B.Sc. degree *cum laude* in July 2015.

In September 2015, he started a master's in Plant Biotechnology at Wageningen University & Research (The Netherlands), with a specialization in Plants for Human and Animal Health. During his master's thesis, he worked under the supervision of dr. Ruud Wilbers at the Laboratory of Nematology. He obtained his M.Sc. degree *cum laude* in August 2017.

Since flat landscapes and questionable weather reminded him of home, Nicolò decided to stay in Wageningen. He joined the Laboratory of Physical Chemistry and Soft Matter as a PhD candidate in October 2017. During the following 5 years he worked under the supervision of prof. Renko de Vries from the Laboratory of Physical Chemistry and Soft Matter, and prof. Bauke Albada from the Laboratory of Organic Chemistry. This thesis is the result of the research project.

During his years as a PhD candidate, Nicolò found a new passion in teaching chemistry. Since January 2022, he has been employed as a teacher at the Laboratory of Physical Chemistry and Soft Matter.

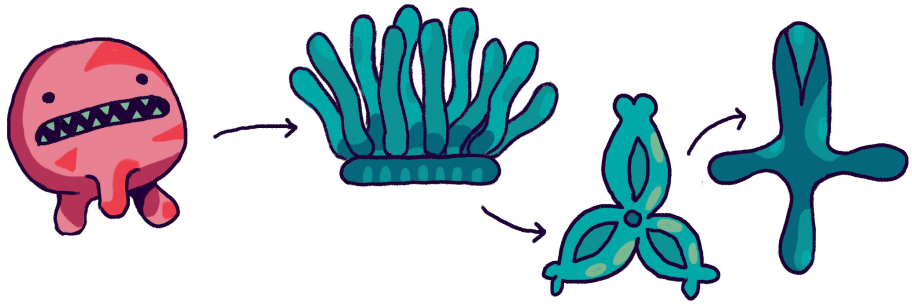

THE STARBLOB IS ONE OF THE MANY EVOLUTIONS OF THE MAIN BLOB. IT'S NORMALLY FOUND IN THE STARFLOWER FOREST, WHERE IT GETS ITS ICONINC TRIANGULAR EARS.

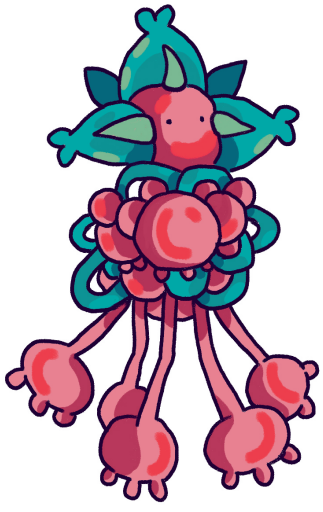

STARBLOBS ARE VERY SOCIAL CREATURES THAT TEND TO STICK TOGETHER NO MATTER WHAT.

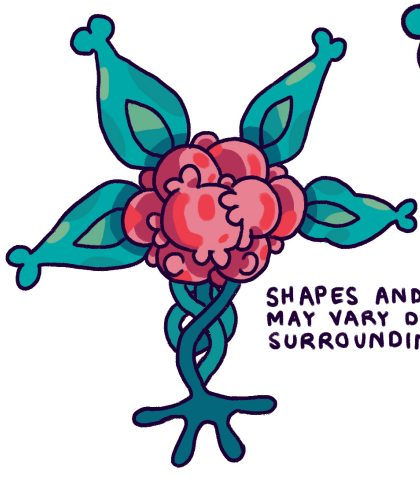

SHAPES AND COMBINATIONS MAY VARY DEPENING ON SURROUNDING FLORA.

Overview of completed training activities

Discipline-specific activities

- CHAINS, NWO (Veldhoven, 2017)
- CHAINS, NWO (Veldhoven, 2018)*
- DutchBiophysics, NWO (Veldhoven, 2018)*
- Brightlands Polymer Days, NWO (Veldhoven, 2021)*
- Teknowlogy, NWO (online, 2021)
- CHAINS, NWO (online, 2021)*
- Physical Methods in Inorganic Chemistry, HRSMC (Leiden/Amsterdam, 2022)
- Microstructural Evolution of Materials: Surface and Surface-Driven Reactions, EdX (MITx) (online, 2022)

  * poster or oral presentation

General courses

- VLAG PhD week, VLAG (Baarlo, 2018)
- Supervising BSc and MSc thesis students, WGS (Wageningen, 2019)
- Efficient Writing Strategies, WiL (Wageningen, 2020)
- Cultural anthropology, Università di Reggio Calabria (online, 2020)
- Psychology of learning processes, Università di Reggio Calabria (online, 2020)
- Theory and methods of didactics, Università di Reggio Calabria (online, 2020)

Assisting in teaching and supervision

- General Chemistry (2018-2020)
- Supervision of MSc and BSc students

Other activities

- Preparation of research proposal, PCC (Wageningen, 2018)
- Weekly Group Meetings, PCC (Wageningen, 2018-2021)
- Journal Club, PCC (Wageningen, 2018-2021)
- PhD weekends, PCC (2018, 2019)

The research described in this thesis was financially supported by the Dutch Research Council, domain Applied and Engineering Sciences (NWO-TTW), with project number 15481.

Financial support from Wageningen University for printing this thesis is gratefully acknowledged.

Cover design and decorative illustrations by Louseen Smith

Printed by ProefschriftMaken on FSC-certified paper